STOCHASTIC DYNAMIC RESPONSE OF A TENSION LEG PLATFORM

OYEJOBI DAMILOLA OYEWUMI

FACULTY OF ENGINEERING
UNIVERSITY OF MALAYA
KUALA LUMPUR

2017

University of Malaya

STOCHASTIC DYNAMIC RESPONSE OF A TENSION LEG PLATFORM

OYEJOBI DAMILOLA OYEWUMI

THESIS SUBMITTED IN FULFILMENT
OF THE REQUIREMENTS
FOR THE DEGREE OF DOCTOR OF PHILOSOPHY

FACULTY OF ENGINEERING
UNIVERSITY OF MALAYA
KUALA LUMPUR

2017

University of Malaya

ORIGINAL LITERARY WORK DECLARATION

Name of Candidate: **OYEJOBI DAMILOLA OYEWUMI**

Registration/ Matric No: **KHA130140**

Name of Degree: **Doctor of Philosophy**

Title of Thesis: **Stochastic Dynamic Response of A Tension Leg Platform**

Field of Study: **Structural Engineering**

I do solemnly and sincerely declare that:

(1) I am the sole author/ writer of this work;
(2) This work is original;
(3) Any use of any work in which copyright exists was done by way of fair dealing and for permitted purposes and any excerpt or extract from, or reference to or reproduction of any copyright work has been disclosed expressly and sufficiently and the title of the work and its authorship have been acknowledged in this work;
(4) I do not have any actual knowledge nor do ought I reasonably to know that the making of this work constitutes an infringement of any copyright work;
(5) I hereby assign that all and every rights in the copyright to this work to the University of Malaya (UM), who henceforth shall be owner of the copyright of this work and that any reproduction or any use any form or by any means whatsoever is prohibited without the written consent of UM having been first had and obtained.
(6) I am fully aware that if in the course of making this work I have infringed any copy right whether intentionally or otherwise, I may be subject to legal action or any other action as may be determined by UM.

Candidate's Signature Date

Subscribed and solemnly declared before,

Witness's Signature Date
Name:
Designation

University of Malaya

ABSTRACT

A systematic formulation program for the computation of stochastic dynamic response of a tension leg platform (TLP) was developed and solved for the uncoupled TLP. The effect of tendon dynamics was incorporated into a coupled TLP and was discretized using the finite element method. The platform was idealized as a rigid body and the matrices of equation of motions were formulated and solved by numerical time integration. The TLP response was characterized for regular, unidirectional and directional random waves, as well as for current and wind forces. The ocean waves were simulated using the small amplitude wave theory for regular wave and the Pierson Moskowitz wave spectrum for unidirectional and directional ocean waves. The hydrodynamic forces on the TLP were calculated by modified Morison equation while the wind-drift current on the TLP was modelled with linear profile model. The aerodynamic loadings were computed by the logarithmic wind speed profile for the mean wind speed and the Simiu- Leigh and American Petroleum Institute (API) spectra were used for fluctuating wind component in uncoupled and coupled TLP models respectively. The associated nonlinearity and response-dependent nature of the TLP made the computation of equation of motions time consuming. The results of the TLP responses were reported in time history, power spectrum and statistical values. For regular wave characterization, the results revealed that the platform amplified at the wave frequency only. In contrast with regular wave modelling, the platform amplification in all degrees of freedom occurred predominantly at the surge natural degree of freedom as well as at the wave frequency for unidirectional and directional random waves. Current and wind drag forces caused steady offset displacements in all degrees of freedoms. The motion and tendon tension responses in coupled TLP were lower in magnitude compared to the uncoupled TLP except for surge response. The

University of Malaya

behaviour of TLP in parametric studies of varying wave heights, wave periods, different sea states, loss of tendon from a group of tendon legs were analysed and reported for the purpose of decision making.

This work avoided solving separate equations of motions for the platform model and the tendon leg system but simultaneously coupled it together. This was accomplished by coding the mathematical derivations in a high-level programming language and commercial finite element tool. The finite element tool was not originally designed for the solution of offshore platforms but was adapted for model discretization and the application of hydrodynamic and aerodynamic loadings on the platform. The result of this research was that offshore problem with high level complexities was solved using the knowledge of Civil Engineering.

University of Malaya

ABSTRAK

Satu program penggubalan sistematik untuk pengiraan sambutan dinamik stokastik platform ketegangan kaki (PKK) telah dibangunkan dan diselesaikan untuk PKK terlerai. Kesan dinamik tendon telah digabungkan ke dalam PKK terganding dan di terdiskret menggunakan kaedah unsur terhingga. Platform ini telah diunggulkan sebagai badan tegar dan matriks persamaan gerakan telah dirangka dan diselesaikan dengan integrasi masa berangka. Sambutan PKK dicirikan untuk gelombang rawak biasa, searah dan berarah, dan juga kuasa arus dan angin. Ombak lautan telah di simulasi menggunakan teori gelombang amplitud kecil untuk gelombang biasa dan gelombang spektrum Pierson Moskowitz bagi ombak lautan searah dan berarah. Kuasa hidrodinamik ke atas PKK telah dikira dengan persamaan Morison yang diubahsuai, sementara arus aliran angin ke atas PKK telah dimodelkan dengan model profil linear. Bebanan aerodinamik telah dikira dengan profil kelajuan angin logaritma untuk kelajuan min angin dan Simiu-Leigh serta spektrum API (Institut Petroleum Amerika) masing-masing digunakan untuk komponen turun naik angin dalam model PKK terlerai dan terganding. Sifat PKK berkaitan ketaklelurusan dan yang bersandarkan tindakbalas menjadikan pengiraan persamaan pergerakan satu proses yang memakan masa. Hasil tindakbalas PKK dilaporkan dalam sejarah masa, spektrum kuasa dan nilai statistik. Untuk pencirian gelombang biasa, hasil dapatan menunjukkan bahawa platform dikuatkan pada frekuensi gelombang sahaja. Berbeza dengan model gelombang biasa, penguatan platform bagi semua darjah kebebasan berlaku lebih kerap pada darjah kebebasan semulajadi pusuan serta pada frekuensi gelombang bagi gelombang rawak searah dan berarah. Kuasa seretan arus dan angin menyebabkan pengubahan pengimbangan yang stabil dalam semua darjah kebebasan. Tindakbalas pergerakan dan ketegangan tendon bagi PKK terganding adalah pada magnitud yang lebih rendah berbanding dengan PKK terlerai kecuali dalam tindakbalas

University of Malaya

lonjakan. Kelakuan PKK dalam kajian parametrik ketinggian ombak berbeza-beza, tempoh gelombang, keadaan laut yang berbeza, kehilangan tendon daripada sekumpulan kaki tendon dianalisis dan dilaporkan untuk proses membuat keputusan.

Kajian ini telah mengelak dari menyelesaikan persamaan pergerakan berasingan bagi model platform dan sistem tendon kaki tetapi telah mengandingkannya bersama secara serentak. Ini telah dicapai dengan pengekodan pemerolehan matematik dalam bahasa pengaturan komputer peringkat tinggi dan alat unsur terhingga komersial. Alat unsur terhingga tidak pada asalnya direka bagi penyelesaian platform luar pesisir pantai tetapi telah disesuaikan untuk pendiskretan model dan penggunaan bebanan hidrodinamik dan aerodinamik keatas platform. Hasil kajian ini adalah bahawa masalah luar pesisir pantai dengan kerumitan peringkat tinggi telah diselesaikan dengan menggunakan pengetahuan Kejuruteraan Awam.

University of Malaya

ACKNOWLEDGEMENTS

Giving thanks to the LORD, the maker of heaven and earth and everything within universe including me for he is good and his mercies endure forever.

It is my pleasure to extend my unreserved gratitude and sincere appreciation to my academic professors in person of Dr. Mohammed Jameel and Associate Prof. Dr. Nor Hafizah Binti Ramli @ Sulong of Department of Civil Engineering, University of Malaya for their contribution in making this research a huge success.

I would like to thank Dr Lanre, Dr Dupe and Dr Taofeeq, it is very difficult to express my gratitude in words for your respective roles. I am indebted to my amiable family, Beatrice, Damilola and Damilare Oyejobi for your understanding and cooperation. I equally thank my parents and siblings you have proved to me in several ways that blood is thicker than water. To my late big cousin Bukola Ajayi, even in your death, you live every day in my heart, love you and love your family.

Personal relationship with Damilola, Elizabeth, Hussein and Haider made a huge difference to the success of this program. Thanks to my FORTRAN coach and thesis editor in persons of Mr. Elliot Chandler and Dr (Mrs) Jawakhir Mior Jaafar that painfully went through my FORTRAN codes and thesis respectively, you are very inspiring.

This acknowledgment would be incomplete if University of Malaya is not appreciated for their financial supports from the University grants numbers RP004E-13AET and PB225-2014B. To my spiritual fathers, Pastor (Dr) Gideon Iselewa and Bishop (Dr) Charles Popson, thank you for your enthusiasm in my progress and unwavering belief in me during the programme. It is very difficult to continue mentioning names, friends and well-wishers, specifically, reader of this thesis, I thank you all.

To God immortal, invisible and eternal, be all the glory and bless this work in my hands, Amen.

University of Malaya

TABLE OF CONTENTS

University of Malaya

University of Malaya

University of Malaya

University of Malaya

University of Malaya

University of Malaya

University of Malaya

LIST OF FIGURES

University of Malaya

University of Malaya

University of Malaya

University of Malaya

University of Malaya

LIST OF TABLES

University of Malaya

University of Malaya

LIST OF SYMBOLS AND ABBREVIATIONS

a1	Lower limit of integration
2a	Length of TLP
2b	breadth of TLP
a_n	Acceleration of the structure
a_x, a_y	horizontal and vertical water accelerations
A	Total cross-sectional area of tendons in one column
A_a	Projected area above water part of the platform
A_i	Amplitude of the i^{th} wave component
API	American Petroleum Institute
C	Reference point at centre of mass
$[\mathbf{C}]$	Damping matrix
C_a	Wind drag coefficient
C_D	Sea Drag coefficient
C_M	Inertia coefficient
c_x	Sin phi Cos theta
c_y	Cos phi
c_z	Sin phi Sin theta
COG	Centre of Gravity
CNAP-TLP-2016	Coupled Nonlinear Program
D	Diameter of cylinder
d	Water depth
e_{04}	Perpendicular distance of new centre of buoyancy from x-axis through COG
e_{05}	Perpendicular distance of new centre of buoyancy from y-axis through COG

University of Malaya

E	Modulus of elasticity
EA/L	Vertical stiffness of combined tethers
EI/L	Roll and Pitch effetive stiffness
{**F** }	Force column vector
{F (t)}	Modified force vector in transformed coordinate
F_B	Total upward buoyant force
F_D (k), F_I (k)	Total drag and inertia forces on k^{th} column
F_d, F_i	Total drag and inertia force on the pontoon
F_v	Total vertical dynamic pressure force on the column bottom
FORTRAN	Formulation Translation
FPS	Floating Production System
FPSO	Floating Production, Storage and Offloading System
g	Acceleration due to gravity
GOM	Gulf of Mexico
h	Distance between Centre of Gravity (C.G.) to the bottom of the platform
H	Wave height
I	Moment of inertia matrix
ISSC	International Ship and Offshore Structures Congress
JONSWAP	Joint North Sea Wave Project spectrum
[K]	Stiffness matrix
K_{ij}	Stiffness coefficients.
K	is the Von Karman's constant
L	Length of tendon
LRFD	Load and Resistance Factor Design

University of Malaya

M	Total Mass
[**M**]	Mass matrix
M_a	Added mass
M_{11}	Mass along surge direction
M_{22}	Mass along sway direction
M_{33}	Mass along heave direction
M_{44}	Mass along roll direction
M_{55}	Mass along pitch direction
M_{66}	Mass along yaw direction
MDOF	Multi-Degree of Freedom
MWL	Mean water level
n	Constant
N	Number of wave components
P	Dynamic pressure
PM	Pierson Moskowitz spectrum
PSD	Power spectral density
RMS	Root mean square
r_x	Radius of gyration along x-direction
r_y	Radius of gyration along y-direction
r_z	Radius of gyration along z-direction
t	Time
T	Wave period
TLP	Tension Leg Platform
u, v	Horizontal and vertical water velocities

University of Malaya

UNAP-TLP-2016 Uncoupled Nonlinear Analysis Program

x	x-coordinate of the point along wave direction
x_1, x_2, x_3	Displacements in positive surge, sway and heave directions
x_4, x_5, x_6	Rotational displacement about x-y and z-axis
z_{ref}	Reference elevation which is considered as 10 m.
z_o	Terrain roughness parameter over the sea surface
α, β	Alpha and Beta Rayleigh constants
$\{\xi_j\}$	Displacement of the structure in the transformed coordinate
ζ	Damping ratio in uncoupled mode
ω	Natural frequency of the structure
α	Constant
$\vec{i}, \vec{j}, \vec{k}$	Unit base vectors
θ	Elementary wave angle
θ_p	Main wave direction
γ	Angle of tendon with the vertical axis
ρ_a	Mass density of the air
ρ, ρ_w	Density of water
λ	Wave length
η	Wave profile
k_i	Wave number of the i^{th} wave component
$\emptyset_i$	Wave Phase angle
β	Direction of propagation
ΔT	Change in tendon tension

University of Malaya

ΔL	Change in tendon length
Δn_i	Width of frequency division
Δt	time step
$D(\theta, w)$, $D(\theta)$	Directionality functions
T_0	Initial pretension in the tendons
$\{U\}$	Column vector of displacements at centre of mass
$\{\dot{U}\}$	Column vector of velocity at centre of mass
$\{\ddot{U}\}$	Column vector of acceleration at centre of mass
$S_{PM}(w)$	Pierson-Moskowitz (P M)
$S_u(z, n_i)$	Wind Spectrum
$\bar{u}(z)$	Mean wind speed
$u'(y, z, t)$	Fluctuating wind velocity
$\bar{u}(z)$	Mean wind speed
$U_{eq}'(t)$	Fluctuating wind component
$\dot{U}_c$	Current velocity
$\dot{U}_{c,tide}(0)$	Tidal current velocity at the SWL
v	Magnitude of normal velocity
$\dot{x}$	Structural velocity
$\ddot{x}$	Structural acceleration

University of Malaya

LIST OF APPENDICES

University of Malaya

CHAPTER 1: INTRODUCTION

1.1 Background

Hydrocarbon is important to the human society development ranging from its role in providing electric and heat energies to running the transportation system, among many others. One of the most important events of the nineteenth century was the discovery of these natural resources due to the fact that the world economy was built on these resources and the industry would continue to thrive even with the increase in renewable energy. This would be so on the account that large consumption of energy still rely on oil and gas supply since the percentage of influx of renewable energy is very low and might not be sustainable if not properly subsidized by government policies coupled with nature restrictions.

A primary concern is that exploration and production of oil and gas require technologies that are safe for easy delivery to the end users. Fixed offshore platforms have been used for extraction of hydrocarbons on onshore and in shallow waters. The main challenge encountered by fixed platform was the depletion of oil and gas in shallow waters and this resulted in the search in deep and ultra-deep waters. As a result, the existing technical know-how became unsuitable for deep water mineral exploration. In addition, installation of the fixed platforms became uneconomical and highly challenging in deep waters. Most importantly, there was an increase in the platform dynamics due to the frequency closeness between the natural frequency of the fixed structures and the ocean wave frequency. This poses a risk for deep and ultra-deep waters hence a dynamic analysis of the structure is indispensable. In light of this development, there is a need for floating offshore platforms in deep waters. A well-known example includes Tension leg platform (TLP), Floating production storage and offloading (FPSO), Spar, Semi-submersible and

University of Malaya

Floating production system (FPS). A quick alternative to fixed marine structures was exemplified by the installation of the Lena guyed tower in 1983 in 305 metres water depth as reported in Chakrabarti (2005).

A group of engineers in California, Horton, Brewer, Silcox, and Hudson (1976) as reported in Chakrabarti (2005) invented the concept of tension leg platform that could be tethered to the seabed. This technology, known as Conoco Hutton TLP was first installed in 1984 in the United Kingdom for the North Sea. Adrezin, Bar-Avi, and Benaroya (1996) reviewed literature for over two decades on compliant structures; their work concluded that TLP is well suited for deep water operations of all the classes considered. Salpukas (1994) and Bar-Avi (1999) also reported that TLP is suitable for oil and gas production facility in deep water operations. This concept, tension leg platform was defined according to Veritas (2012) and Veritas (2008) as floating offshore structure connected to the sea bed through the pre-tensioned tendons.

A schematic TLP is illustrated in Figure 1.1 with the structural supporting components classified as the TLP deck, hull, tendon leg system and foundation. The TLP deck area supports the working area, production facilities, accommodation and other purposes. The deck unit is correspondingly being supported by the hull (vertical columns and horizontal pontoons) that provides adequate buoyancy to the deck for it to remain above ocean waves at all times. This buoyancy force also builds up tension in the tendon leg system. The Tendon leg system consists of tendon; and top and bottom connectors. The Veritas (2008) described the tendons as normally parallel, near vertical elements and acting in tension. They usually restrain the rigid motions of the TLP in heave, roll and pitch motions to very small amplitude. The cross-section of such mooring system can be solid or hollow steel pipes and also cables of high strength. The foundation serves as the means of anchoring tendons and the medium for transferring the tension load to the foundation soil.

University of Malaya

The riser system is optional and can be used for drilling, production, export or other purposes.

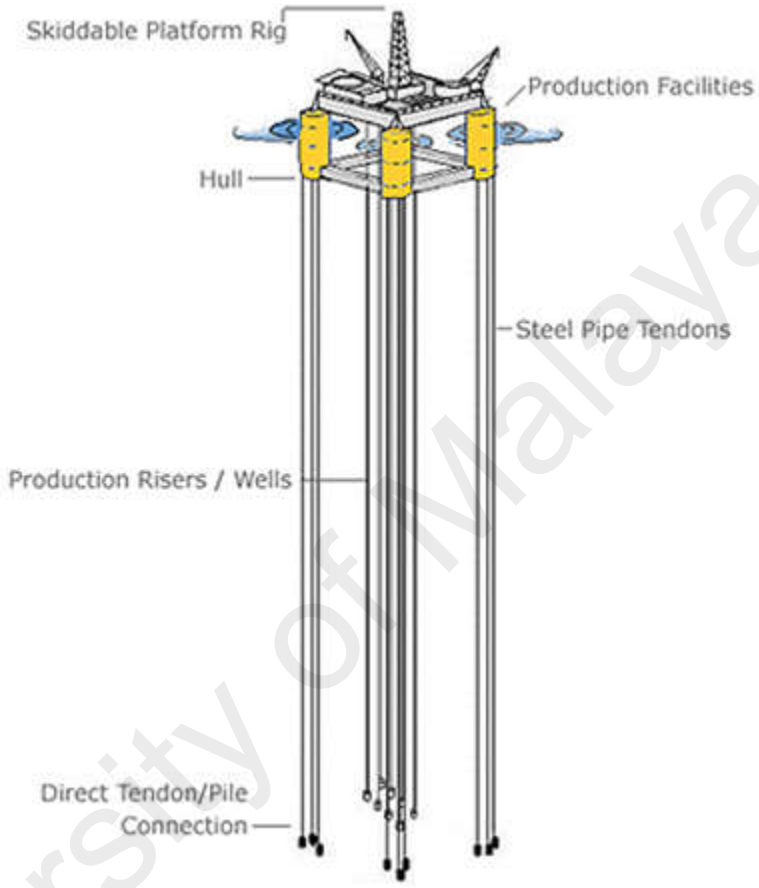

Figure 1.1: Main components of TLP

Chandrasekaran and Jain (2002a) and Yilmaz and Incecik (1996a) outlined the advantages of TLP for oil and gas production facility. It was reported that wave impact on the facility is less due to the compliant nature of TLP. This is made possible as a result of high natural periods of surge, sway and yaw degree of freedoms that are far above periods of exciting wave and also due to the natural periods of heave, pitch and roll that are also lower than the wave exciting frequency. TLP is time and cost effective, especially in deep

University of Malaya

waters when compared to fixed offshore structures. The transportation, fabrication, installation and de-commission of TLP are easy and efficient.

TLP is a Multiple Degree of Freedoms (MDOF) structure with translation (Surge, Sway and Heave) along x, y and z directions and rotational (Roll, Pitch and Yaw) motions about x, y and z directions. The platform is compliant in surge, sway and yaw motions due to the very high natural period that is well above the periods of the oceanic waves and at the same time stiff due to the low natural period of pitch, roll and heave motions, hence it is being regarded as a hybrid structure. These two sets of degrees of freedoms can withstand the broad band frequency of environmental loadings that can occur on the TLP.

A TLP operates in deep water condition coupled with harsh environment. According to Chakrabarti (2005), water depths that are greater than 305 metres (1000 feet) are classified as deep water and those above 1524 metres (5000 feet) as ultra-deep water respectively.

Additionally, the stochastic response of the TLP depends on the environmental loads on the platform. This ranges from wave, wind, current, tides among others. Most importantly, wave frequency forces; steady and fluctuating wind forces; high and low frequency forces; and current drag force must be considered during the analysis stage in order to predict the platform global motion and tension variation in the tendons accurately. These loadings are stochastic in nature and changes over time. As a result of this random phenomenon, the corresponding response of the platform is also nonlinear and stochastic.

The choice of TLP for this study is as a result of its reduced dynamic response in deep waters. Besides, it is heave-restrained and compliant with wave force, is cost effective, requiring less laborious installation and decommission procedures and has advanced buoyancy that exceed the platform weight which keeps the tendons tensioned in all weathers. Moreover, the analysis of the TLP can be undertaken either in frequency or

University of Malaya

time-domain. In the frequency domain, the nonlinear terms are linearized and results are presented in steady state form. Taylor and Jefferys (1986); Kareem and Li (1993); Low and Langley (2006); Low (2009) carried out TLP analysis in the frequency domain. The transient and time effects are normally ignored in the frequency method. The time domain method, on the other hand, includes the problem's nonlinear terms in the equation of motion. In spite of the high computational time in the time domain method, the method had been widely used because its output is accurate. Ahmad (1996), Adrezin and Benaroya (1999a), Chandrasekaran and Jain (2002b), Zou (2003), Siddiqui and Ahmad (2003) carried out dynamic analysis of the TLP in systematic time domain. In this study, the time domain approach is employed for the stochastic response of the TLP. This is done so as to include associated nonlinearity such as relative velocity squared drag forces on the platform hull and tendons, large displacement, variable submergence as a result of variable added mass, variations of tendon tension in tendon into the dynamic equation of motion.

1.2 Present state of the problem

The field of compliant offshore structures is not completely new due to numerous works that have been carried. However, due to emerging new concepts, search for novel approach of analysis and lessons learnt from the existing TLP, there is need for enhanced method of analysis. Several studies on the TLP model had often been carried out in an uncoupled form which simply implies that dynamics and environmental loads on the tendons are ignored. For instance, Jain (1997), Chandrasekaran and Jain (2002a), Chandrasekaran, Jain, and Chandak (2004), Zeng, Shen, and Wu (2007), Kim, Lee, and Goo (2007), Gao, Li, and Cheng (2013), Chen, Kong, and Sun (2013), Refat and El-gamal (2014), El-gamal, Essa, and Ismail (2014), Liu (2014), had studied response of an uncoupled TLP in regular waves and arrived at different submissions due to varied TLP

University of Malaya

geometry and hydrodynamic loadings. In a similar vein, Ahmad (1996), Chandrasekaran and Jain (2002b), Kurian, Gasim, Narayanan, and Kalaikumar (2008), Abou-rayan and Hussein (2014) had carried out response of uncoupled TLP in random seas.

The need for coupled formulation has been identified by Paulling and Webster (1986), Correa, Senra, Jacob, Masetti, and Mourelle (2002) and Chakrabarti (2008). The coupled model implies that hydrodynamic forces on the floating structure is coupled to finite element model of mooring and riser lines with their inertia and damping forces included. Thus, the equations of motion can then be solved iteratively. Chatterjee, Das, and Faulkner (1996), Natvig and Johnsen (2000), Bhattacharyya, Sreekumar, and Idichandy (2003) put forward that, motion characteristics and structural response of compliant structures can be better idealized as a coupled model using finite element method. Limited reports such as Adrezin and Benaroya (1999a), Jayalekshmi, Sundaravadivelu, and Idichandy (2010), Masciola, Nahon, and Driscoll (2013) had considered analysis of coupled TLP in random waves. Zou (2003) carried out coupled dynamic analysis of the hull, tendon and riser.

On the other hand, the joint occurrence of stochastic waves, wind and current forces on the platform has not been fully reported. Hence, without considering possibilities of all possible loadings on the platform, the behaviour of the TLP may not be fully understood. Lastly and most importantly, quite numbers of present specialized hydrodynamic software are in de-coupled form. The platform motions are normally calculated in the software model whereas tendons are considered as weightless spring, Demirbilek (1990). The platform motions will subsequently be used as forced displacements on the tendon during stress analysis. The calculated tendon forces in the platform model and that of stress analysis model has been identified to prone to deviation according to Demirbilek (1990). Therefore, the need for this work is to fully couple platform model with tendons so as to

University of Malaya

incorporate the nonlinearities interaction together with tendon dynamics. This is achieved by writing single mathematical code for the platform and solved the problem in time-domain using finite element technique for different ocean characterization and in different load combinations.

1.3 Aim and objectives of the study

The hydrodynamic analysis of TLP has come a long way with different methods for the representation and analysis of the problem as earlier explained. The aim of this research is to develop a systematic formulation program for the purpose of investigating nonlinear response of TLP to the stochastic wave and wind fields. In line with this aim, the following objectives have been highlighted for the present study:

1. To develop and solve non-linear second-order differential equations of motion of TLP numerically.
2. To investigate response of uncoupled TLP under the action of regular, unidirectional and directional random waves, current and wind forces.
3. To study behaviour of coupled TLP to hydrodynamic and aerodynamic loadings.
4. To investigate significance of tendon dynamics on the platform response.
5. To analyze time histories, power spectral and statistics of TLP's motion and variations in tendon forces.

1.4 Scope of the research

This thesis is limited to the investigation of the nonlinear dynamic response of the tension leg platform to first order wave forces in regular and irregular seas. The components of an equation of motion were formulated using deterministic approach in the time domain, hence, frequency and statistical domain approaches were not employed.

University of Malaya

Besides, due to the time constraint, the scope of the study would be too broad if second order wave forces and potential theory were included. Having defined the scope, the response of dynamic behaviour of four-legged symmetrical TLP in a wave-structure interaction was studied. The International Ship and Offshore Structures Congress, (ISSC TLP) was used for this study. This was chosen due to the fact that ISSC platform does not represent any existing TLP or company.

Moreover, due to the lack of experimental laboratory and possibility of loss of accuracy in scaling down the model in the limited wave tank, a numerical approach was adopted for the solution of the TLP problem. This type of problem is a highly nonlinear and response-dependent problem, which cannot be solved by analytical method. In order to include the associated nonlinearity, the analysis was carried out in the time domain. For the first approach, the Newmark-βeta numerical method, after the work of Bathe (1982), was adopted in FORTRAN coding. The Abaqus finite element method used implicit time integration scheme to solve the nonlinear problems. Both methods are stable and accurate as it had been widely used in other manuscripts such as Islam, Jameel, and Jumaat (2012), Jameel, Ahmad, Islam, and Jumaat (2013), (Islam, Soeb, & Jumaat, 2016). Some of the sources of the nonlinearity considered in this study include wave kinematics with a modification by stretching wave kinematics to the wave free surface. Viscous drag forces of the Morison equation and the interaction between waves and current. Variable submergence of TLP with respect to waves and motion, tension fluctuation in the tendons, and large displacement were also investigated. The above-mentioned points made the equation of motion highly computational expensive and time consuming.

University of Malaya

1.5 Structure of the thesis

This thesis is divided into five different chapters for easy flow and better understanding of the nonlinear dynamic analysis of tension leg platform. Chapter One deals with the historical background of offshore structure with the emphasis on current need and status of the compliant tension leg platform. This is further expatiated with a discussion on the purpose and scope of the research. The second Chapter focuses on the review of relevant literature, covering theories, models and analysis techniques that have been previously used by other authors. Also, the Chapter discusses the general field of offshore structures and classified TLP as a floating offshore structure. Different available wave theories are described and environmental loadings on the structure are also reported. Chapter Three outlines the methodology and materials employed for the dynamic analysis of the TLP. In summary, model discretization and assumptions are stated as well as the procedures for the mathematical formulation of equations of motion in FORTRAN. Also, steps adopted for the finite element discretization of the TLP problem in Abaqus and Aqua software are reported, including the modelling of environmental loadings and method of numerical integration. Consequently, results of the analysis are presented in Chapter Four for logical discussion. The obtained results from the dynamic analysis of the TLP are validated with previous published results. From this, response behaviour in regular and irregular waves are reported and interpreted when TLP was under the action of waves, waves and current forces, and simultaneous occurrence of waves, wind and current forces for uncoupled and coupled TLP models. Chapter Five is concerned with the conclusion from the results of stochastic response of TLP. Lastly, useful recommendation and contribution of the work are discussed.

University of Malaya

CHAPTER 2: LITERATURE REVIEW

2.1 Introduction

Sequel to the historical background in the previous chapter, classification of offshore structures into fixed and floating platform, different wave theories as well as the advantages of the TLP are discussed in this Chapter. Also, environmental forces acting on the platform together with the available analysis methods and load combination by earlier researchers are presented. The present state of the art on dynamic analysis of coupled and uncoupled TLP is reviewed.

2.2 Description of offshore structures

Tension leg platform (TLP) belongs to the field of offshore structures. Offshore structures can be of any structural form depending on water depth; environmental loadings and function of the structures. The offshore structures can be used to explore, drill, store and transport oil and gas resources. Chakrabarti (2005) defined offshore structure as having no fixed access to dry land and may be required to stay in position in all weather conditions. It may be fixed to the seabed or floating.

2.2.1 Fixed offshore structures

Mao, Zhong, Zhang, and Chu (2015) reported that since around 1940s, fixed offshore structures have been thriving. However, as a result of increase in water depth, the field has continued to explore the latest modelling techniques that is economically suitable for deep water conditions, Adrezin et al. (1996). Some of the types of fixed offshore structure in the ocean are explained in the following section.

University of Malaya

2.2.1.1 Jacket/Steel template structures

Jacket structures have been identified as the commonest type of offshore structures used for drilling and production. It is built up with tubular members interconnected to form a three - dimensional space frame and is being limited to (150 – 180 m) water depth in the harsh North Sea environment, Chakrabarti (2005). The steel members of offshore structures are supported by piles driven into the sea bed, with a deck placed on top for providing space for crew quarters, a drilling rig, and production facilities. A typical example of Jacket structure is illustrated in Figure 2.1. In another development, Nallayarasu (2008) reported that fixed platform is economically feasible for installation in water depths up to 500 m. This template type structure is fixed to the seabed by means of tubular piles either driven through legs of the jacket (main piles) or through skirt sleeves attached to the bottom of the jacket. Sannasiraj, Sundar, and Sundaravadivelu (1995) and Jia (2008) studied the dynamic response of fixed jacket offshore in the frequency and the time domains in their respective studies. Mao et al. (2015) carried out scale model experiment for the assessment of foundation degrading on the dynamic response of fixed jacket structure. A similar scaled model in random waves was undertaken theoretically and experimentally by Elshafey, Haddara, and Marzouk (2009). The tension leg platform adopted in this research used lesser steel materials compared to jacket structure.

University of Malaya

Figure 2.1: Steel template platform

2.2.1.2 Gravity base structures

This is another type of fixed platform shown in Figure 2.2 and is limited by water depth up to the 350 metres and is viable for places where pile installation is unsuitable and not feasible according to Nallayarasu (2008). Concrete gravity platforms are mostly used where there is sandy formation or places with strong seabed geological conditions. Chakrabarti (2005) reported that gravity base structures are placed on the seafloor and held in place by their weight. The structures are quite suited for production and storage of oil. Gravity base structures are not suitable for deep water depths and may be uneconomical.

University of Malaya

Figure 2.2: Gravity base structure

2.2.1.3 Jack-up structure

Wilson (2003) defined a jack-up structure as a mobile structure often used for exploratory oil-drilling operations and is a self-elevating platform. This normally consists between three to six legs that support the platform and is attached to a steel mat resting on the floor. Figure 2.3 shows atypical example of Jack-up platform. In Chakrabarti (2005), the legs are made of tubular truss members and the deck is typically buoyant. They are referred to as jack-up because once at the drilling site, the legs are set on the ocean bottom and the deck is jacked up on these legs above the waterline. Kang, Zhang, and Yu (2016) assessed the hydrodynamic performance of a jack-up offshore platform during wet towing using reliability based stochastic method. On the other hand, Vlahos, Cassidy, and Martin (2008) carried out an experimental analysis of three legged jack-up model. Jensen and Capul (2006) employed theories of random vibration and first order reliability method for second order stochastic waves for the assessment of jack-up unit.

University of Ma

Figure 2.3: Jack-up platform

2.2.2 Compliant structures

Nallayarasu (2008) confirmed that traditional fixed offshore platform has been replaced with state-of-the-art deep-water production facilities. Examples of these include compliant towers, Tension leg platforms, Spars, Subsea systems, Floating production systems, and Floating production, storage and offloading (FPSO) systems are now being used in water depths exceeding 500 m. All of these systems are proven technology, and are in use in offshore production worldwide. In another development, Chakrabarti (2005) stated that compliant structures are structures that extend to the ocean beds and are directly anchored to the seafloor by piles and or guidelines. These structures are typically designed to have the lowest modal frequency which is below the wave energy, as opposed to the fixed structures which have a first modal frequency greater than the frequency of wave energy.

University of Malaya

2.2.2.1 Articulated platforms

In Chakrabarti (2005), articulated tower has been defined as an upright tower which has its base pinned with a cardan joint, this is left free to rotate about its axis as a result of wave environment. The tower is normally being used as a single-point mooring system to moor storage and production tankers permanently. Its application is limited to few hundred metres and a typical articulated platform is shown in Figure 2.4. the base below the universal joint can be gravity or pile in nature.

Figure 2.4: Articulated tower platform

2.2.2.2 Compliant tower

Nallayarasu (2008) explained that the compliant tower consists of slender, elastic and a pile foundation, (Figure 2.5). The tower is primarily being used to support

University of Malaya

conventional deck when hydrocarbons are being drilled and stored. It has advantage to resist huge environmental forces by sustaining significant deflections. It has been found applicable in the range of water depth between 300 m and 600 m. The tower uses less steel than a conventional platform for the same water depth. Furthermore, a compliant tower is designed to flex with the forces of waves, wind and current as described in Chakrabarti (2005)

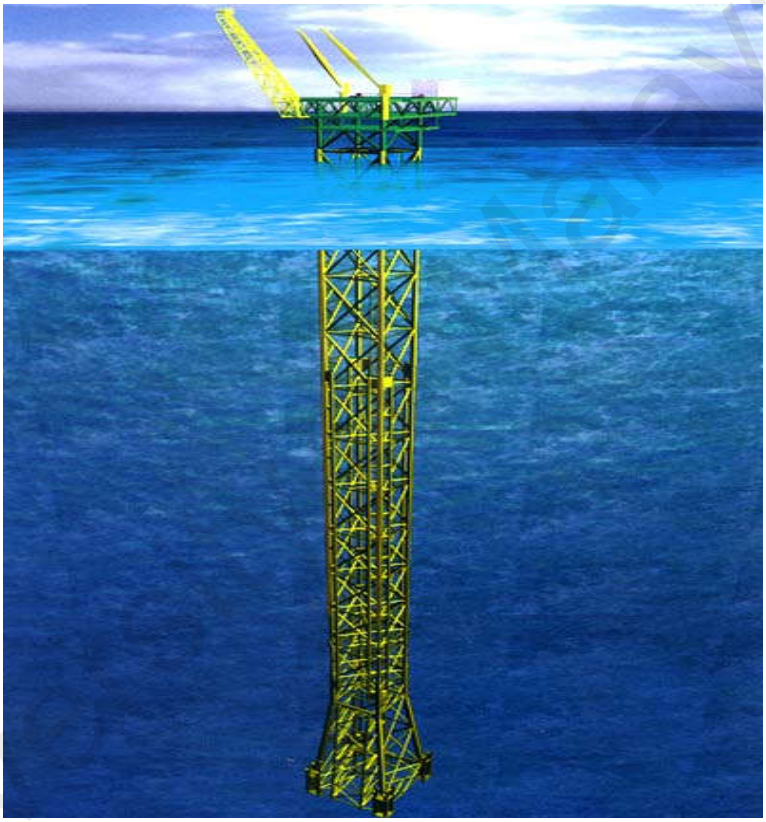

Figure 2.5: Compliant tower

2.2.2.3 Guyed tower

In Chakrabarti (2005), a guyed tower is defined as a slender structure made up of truss members which rest on the ocean floor and is held in place by a symmetric array of catenary guy lines as shown in Figure 2.6. A guyed tower may be applicable in deep hostile waters where the loads on the gravity base or jacket type structures from the environment

are prohibitively high. Nallayarasu (2008), attested that guyed tower has been identified as the development on compliant tower due to the anchor lines that are used to tie the tower to the seabed. The displacement of the platform is controlled by the tension in the guy ropes.

Figure 2.6: Guyed tower platform

2.2.3 Floating structures

Floating structures can either be neutrally or positively buoyant structures. Examples of neutrally buoyant structure include Spars, Semi-submersible, Floating Production System (FPS), Floating Production, Storage and Offloading System (FPSO), whereas the buoyant tower and the TLP are examples of a positively buoyant structure. The buoyancy force plays an important role in carrying the deck load. Figure 2.7 shows various types of floating structures found on the subsea. It should be noted that the response of floating structures to wave, current and wind is dynamic and complicated in nature.

University of Malaya

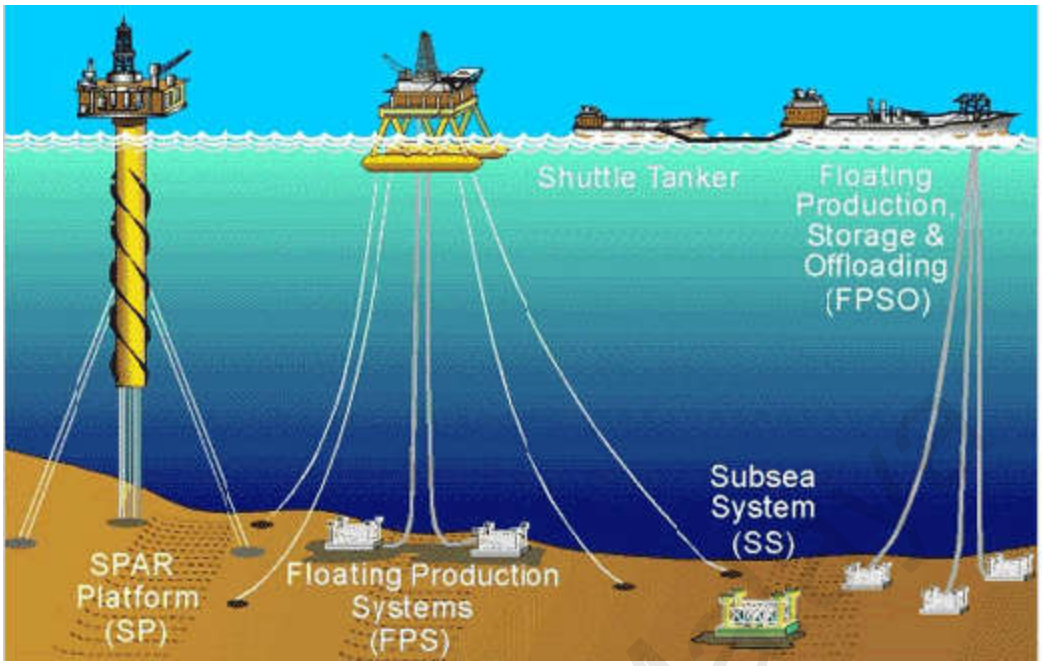

Figure 2.7: Floating structures

2.2.3.1 Floating Production System

Nallayarasu (2008) described floating production system (FPS) to be suitable for a deep-water depth ranging between 600 m and 2500 m. The FPS has drilling and production gadgets embedded inside the semi-submersible unit. The wire rope and chain are anchoring elements that keep the system in place. This can also be achieved dynamically by using rotating thrusters.

2.2.3.2 Floating Production, Storage and offloading System

In Nallayarasu (2008), Floating Production, Storage and Offloading System, FPSO is made up of large tanker type vessel. By design, FPSO has capacity to process and store production from not distant subsea wells to a smaller shuttle tanker. This is then conveyed by the tanker to the onshore for further processing.

University of Ma

2.2.3.3 Tension Leg Platform (TLP)

Veritas (2012) defined tension leg platform as the floating structure that is connected to the seabed through the tendon legs system. The manuscript reported that tendons are pre-tensioned, stiff in axial direction to constrain vertical TLP responses to very small amplitude. In another attempt,Veritas (2008) described the TLP as a positive buoyant unit connected to a fixed foundation or piles by pre-tensioned tendons. The TLP hull is made up of buoyant structural columns; pontoons and intermediate structural bracings. According to Veritas (2012), the TLP can be classified into various groupings as highlighted in the following section.

2.2.3.3 (a) Conventional TLP

This is a traditional design that follows the principle of column-stabilized units with four columns, four pontoons and a top tension connector either on the tension porches or inside the column. Examples of this type of TLP include Conoco Hutton, Auger and Mars TLPs. D'Souza, Aggarwal, and Basu (2013) reported that production risers are normally arranged at the middle of the platform deck. Figure 2.8 shows a typical hull configuration of the conventional TLP and this type of TLP is considered for the analysis in this thesis.

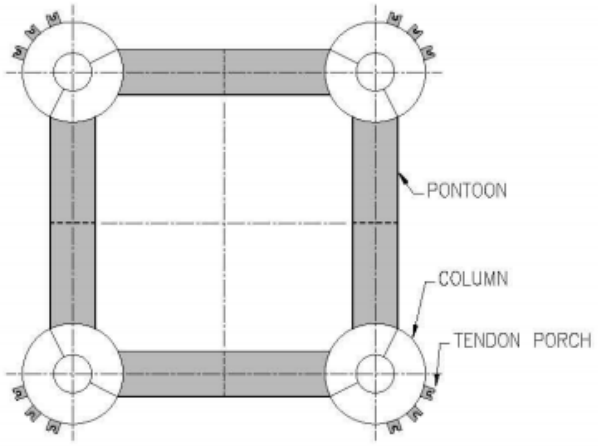

Figure 2.8: Hull configuration of Conventional TLP

University of Malaya

2.2.3.3. (b) Extended TLP

This type of TLP design is known to have smaller columns located in its inboard and extended pontoons. Here, the tendons are connected to the extreme part of the pontoon. Typical examples include KIZOMBA A, KIZOMBA B, and MAGNOLIA TLPs designed by ABB Lummus Global. It is reported in D'Souza et al. (2013) that topsides can be integrated quayside or in a drydock by heavy lift cranes. An extended tension leg platform is shown in Figure 2.9.

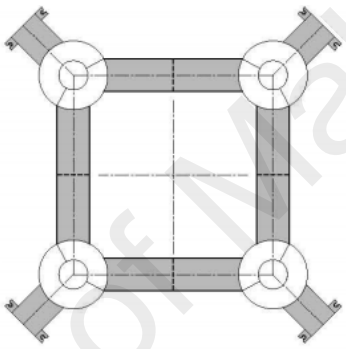

Figure 2.9: Hull configuration of Extended TLP

2.2.3.3 (c) SeaStar TLP

This is one of the newer concepts of TLP with only one central column and at least three cantilevered pontoons projecting from the column base to the tendon porches for easy connection of tendons. Examples of this type are the MATTERHORN and ALLEGHENY TLPs designed by Atlanta sea-star. Figure 2.10 shows the hull configuration of SeaStar TLP

University of Malaya

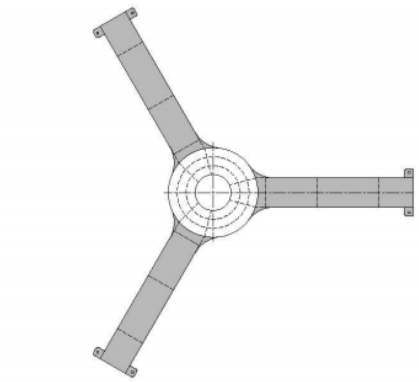

Figure 2.10: Hull configuration of SeaStar TLP

2.2.3.3 (d) Mini-TLP

This is a floating mini-tension leg platform that is developed for smaller deep-water reserves, where adopting conventional TLP is not cost-effective. The first Mini-TLP is the MORPETH TLP and was installed in the Gulf of Mexico in 1998. The elevation of different classification of TLP is demonstrated in Figure 2.11.

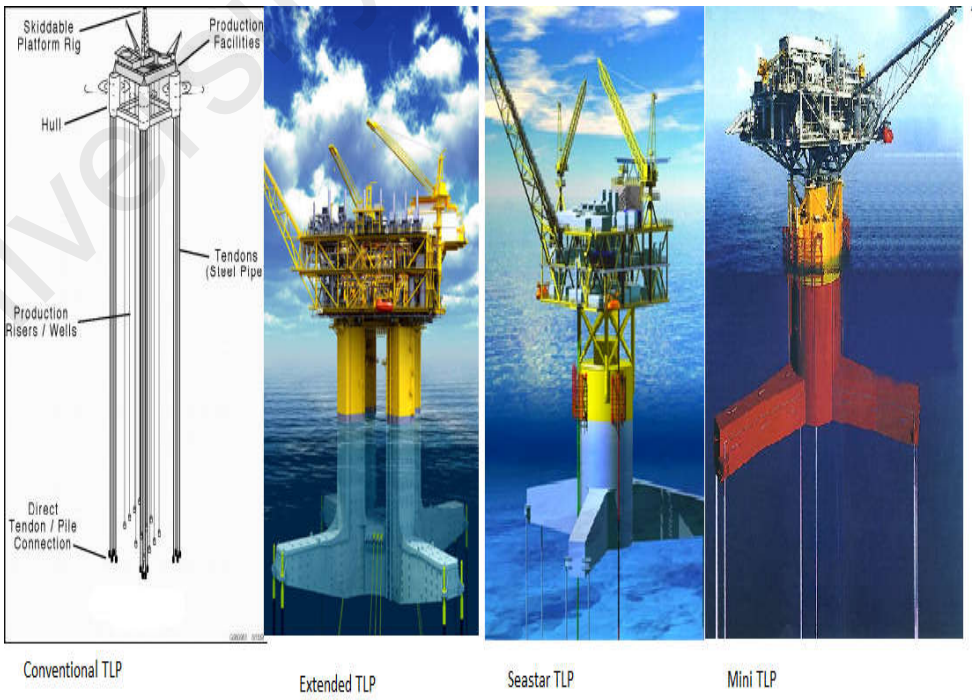

Figure 2.11: Various types of TLP

University of Malaya

Since the first TLP installation up till now, TLP has been tremendously use across the oil producing fields including the Gulf of Mexico, North Sea, West Africa and Asia countries. As of today, there are about twenty-eight installed TLP in various ocean fields across the globe and in different water depths with varied construction materials and operating in different environmental loadings. The progression of the existing TLPs and their current status is given in Table 2.1.

In Table 2.2, technology of the each TLP with the numbers, sizes of their respective tendons, tendon connection type and foundations are stated. Two of out of these platforms, Hutton and Typhoon TLPs have been de-commissioned. The world's largest TLP is the HEIDRUN TLP located in Norway with the hull made up of concrete while the world's deepest TLP is Big boot TLP in GOM, *Offshore Magazine* (2010) and D'Souza et al. (2013). The Riser-less Malaysian TLP started production in late 2016. The application of TLP according to Veritas (2008) includes the exploration, production and storage of hydrocarbons. In D'Souza et al. (2013), TLP is found suitable in production with full drilling capability and dry trees, production with light intervention capability and trees, production with dry trees, well head with tender or full drilling and dry trees.

University of Malaya

Table 2.1: List of existing TLPs with their characteristics D'Souza et al. (2013)

No	Field	Operator	Year installed	Location	Water Depth (m)	Displacement (Tons)	Hull type	Topsides function
1	Hutton	Conoco	1984	North Sea	148	69,788	6-col hull	DDP(8)
2	Jolliet	Conoco	1989	GOM	536	18,302	4-col hull	DWOW(9)
3	Snorre	Saga	1992	North Sea	320	117,416	4-col hull	DDP
4	Auger	Shell	1994	GOM	872	72,986	4-col hull	DDP
5	Heidrun	Conoco	1995	North Sea	346	320,056	Concrete hull	DDP
6	Mars	Shell	1996	GOM	896	54,133	CTLP(3)	DDP
7	Ram/Powell	Shell	1997	GOM	980	54,133	CTLP	DDP
8	Morpeth	British Borneo	1998	GOM	509	11,687	SeaStar(4)	WP(10)
9	Marlin	BP	1999	GOM	988	26,460	CTLP	DWOW
10	Allegheny	British Borneo	1999	GOM	1004	11,687	SeaStar	WP
11	Ursa	Shell	1999	GOM	1204	98,497	CTLP	DDP
12	Typhoon	Chevron	2001	GOM	639	13,395	SeaStar	WP
13	Brutus	Shell	2001	GOM	910	54,684	CTLP	DDP
14	Prince	El Paso	2001	GOM	442	14,443	MOSES(5)	DWOP(11)
15	Matterhorn	Total	2003	GOM	869	26,405	SeaStar	DWOP
16	West Seno A	Unocal	2003	Indonesia	975	25,468	CTLP	DTADW(12)
17	Marco Polo	Anadarko	2004	GOM	1311	27,563	MOSES	DWOP
18	Kizomba A	Exxon-Mobil	2004	Angola	1200	35,280	ETLP(6)	DDW(13)
19	Magnolia	Conoco	2004	GOM	1425	34,398	ETLP	DWOP
20	Kizomba B	Exxon-Mobil	2005	Angola	1015	33,075	ETLP	DDW
21	Okume	Hess	2006	Equ. Guinea	500	11,025	SSIP(7)	DTADW
22	Oveng	Hess	2006	Equ. Guinea	280	11,025	SSIP	DTADW
23	Neptune	BHP	2007	GOM	1295	27,011	SeaStar	WP
24	Shenzi	BHP	2009	GOM	1333	43,439	MOSES	WP
25	Papa Terra	PetroBras	2013	Brazil	1180	44,817	ETLP	DTADW
26	Big Foot	Chevron	2014	GOM	1585	120,614	ETLP	DDP
27	Olympus	Shell	2015	GOM	919	54,023	CTLP	DDP
28	Malikai	Shell	2016	Malaysia	500	26,000		

Notes

(1) Operator during construction phase
(2) Peak production during operation
(3) CTLP = Conventional four column TLP
(4) SeaStar = Mono Column TLP by SBM/Atlanta Production
(5) MOSES =Multi Column TLP by MODEC
(6) ETLP =Extended TLP by Floatec
(7) SSIP = Self stable Integrated Platform by MODEC
(8) DDP = Dry Tree, Drilling, Production
(9) DWOW = Dry Tree, Workover, Wellhead
(10) WP = Wet Tree, Production
(11) DWOP = Dry Tree, Workover, Drilling, Wellhead
(12) DTADW = Dry Tree, Tender Assist,
(13) DDW = Dry Tree, Drilling, Wellhead

University of Malaya

Table 2.2: Progression and evolution of TLP technology, D'Souza et al. (2013)

No	Field	Year Installed	Tendon Technology	Water depth (m)	Nos of tendons	Tendon dia X WT (Inch)	Tendon connection type	Foundation type and size
1	Hutton	1984	First TLP with machined forging elements with threaded ends (this design is also classed as solid with central hollow core for inspection) Tendons transported within the hull columns Tendons connected at bottom of hull columns Collet type connector at bottom end	148	16	10.23 (machined forging) & 16.5 at connectors w/ 3" bored hole	Threaded connection	Pile foundation templates (4 no.); 8 piles/template; Spacer frame for positioning
2	Jolliet	1989	Single piece thin walled tubular, welded One piece towed tendons Installed after the TLP hull arrived at side Tendons connected to the porches outside of hull by pull in clamps; tendon in-situ inspection system	536	12	24 x 0.812	Welded & towed tendon design	Single template (200' x 200'); 16 main piles (60" x 300'); 4 leveling piles (60" x 275')
3	Snorre	1992	Steel tubulars with threaded connections, transported within hull columns Installed with bayonet connection with flex element for bottom end	320	16	32 x 1.5	Threaded connection	Concrete foundation templates (4 no., 5,700 st each) w/skirts & solid ballast
4	Auger	1994	Stabbed connection (box and pin Hunting connectors) for tubular pipe sections done in SSCV Additional lateral mooring for positioning the TLP for drilling operations	872	12	26 x 1.3	Stabbed box and pin Hunting connection	Pile foundation templates (4 no.); 16 driven pipe piles (72" x 427' long)
5	Heidrun	1995	Single piece installation of towed tendons Tendons pre-installed with temporary buoyancy at top	346	16	44 x 1.5	Welded & towed tendons	Concrete foundation templates w/skirts (4 no., 22,500 st each)
6	Mars	1996	Tendons pre-assembled and hung-off at the installation vessel TLP hull moored to the stern of installation vessel and tendons passed over to hung-off the TLP hull	896	12	28 x 1.2	Merlin	1 driven pipe pile/tendon 12 piles (84" x 375')
7	Ram Powell	1997	-	980	12	28 x 1.2	Merlin	84" x 349'
8	Morpeth	1998	First SeaStar TLP design Pre-installed tendons w/temporary buoyancy	509	6	26 x 0.881	Merlin	84" x 318'
9	Marlin	1999	-	988	8	28 x 1.15	Merlin	84"
10	Allegheny	1999	-	1,004	6	28 x 0.949/1.02	Merlin	84"
11	Ursa	1999	Maximum water depth (4,000 ft) for TLP tendons and foundation with available installation equipment in 1999	1,204	16	32 x 1.5	Merlin	96" x 440'

University of Malaya

Table 2.2, Continued

No	Field	Year Installed	Tendon Technology	Water depth (m)	Nos of tendons	Tendon dia X WT (Inch)	Tendon connection type	Foundation type and size
12	Typhoon	2001	-	639	6	26 x 0.881	Merlin	84"
13	Brutus	2001	-	910	12	32 x 1.25	Merlin	82" x 340'
14	Prince	2001	First Moses TLP design TLP designed for relocation in 6,000 ft water depth	442	8	24 x 0.812	Merlin	64" x 320'
15	Matterhorn	2003	First SeaStar TLP design with TTRs Fairings on upper 1,100 ft of tendon length to reduce VIV response in currents	869	6	32 x 1.143	Merlin	96" x 411'
16	West Seno A	2003	First TLP tendons fabricated outside USA and in Asia Installation by a small vessel	975	8	26 x 1.06	Merlin	72" x 251'
17	Marco Polo	2004	TLP design in deepest water depth in 2003	1,311	8	28 x 1.1/1.2	Merlin	76" x 390'
18	Kizomba A	2004	First ETLP design & offshore Angola	1,200	8	32 x 1.4	Merlin	84"
19	Magnolia	2004	First stepped tendon design extending TLP WD limit to 4,700 ft and beyond Menck to procure additional umbilicals to enable do pile driving beyond 4,000 ft Evaluated alternative composite tendon design	1,425	8	32 x 1.42/1.5 & 40 x 1.19/1.32	Merlin	96" x 313' Evaluated alternative foundation designs
20	Kizomba B	2005	Design 1 Build 2 TLP case	1,015	8	32 x 1.4	Merlin	84"
21	Okume	2006	First SSIP hull design, offshore Equatorial Guinea	500	8	24 x 0.812	Merlin	64" x 198'
22	Oveng	2006	-	280	8	24 x 0.812	Merlin	64" x 173'
23	Neptune	2007	-	1,295	6	36 x 1.36 to 1.5	Merlin	96" x 414'
24	Shenzi	2009	Maximum design tension for a tendon and its connectors Stepped tendon design	1,333	8	36 x 1.55 & 44 x 1.33/1.44	Merlin	NA
25	Papa Terra	2013	First TLP offshore Brazil	1,180	NA	NA	Merlin	NA
26	Big Foot	2014	Deepest water depth with large dia stepped tendons Heavy payload TLP	1585	16	36 / 44	Merlin	NA
27	Olympus	2015	Largest tendons ever built for a TLP	919	16	38 x 1.44	Merlin	NA
28	Malikai	2016	First TLP in Malaysia and third deep water project after Kikeh and Gumusut Kakap project	500				

University of Malaya

2.3 Advantages of tension leg platform

Tension leg platform is advantageous in deep water, and over other fixed and floating platform due to the following reasons:

- The amount of materials required is lesser compared to other floating structures since it is the only the hull that uses most of the material and this makes it cost-effective
- TLP is a compliant structure capable of avoiding exciting wave frequency due to its configuration
- It requires lesser manufacturing and installation time in deep water
- It accommodates both dry and wet trees and easy monitoring of risers and tendons
- It is suitable for deep water and harsh environments

2.4 Environmental forces on tension leg platform

This can be defined as the loads resulting from the actions of environment. They include waves, wind, current, ice and snow, earthquake, tidal effects, marine growth, scouring and other seabed instabilities.

2.4.1 Wave forces

According to American Petroleum Institute (2001), wind-driven waves are the major sources of environmental forces on tension leg platform. Such waves can be modelled as either regular or irregular in shape. The ocean waves can vary in height, length, and period, and may approach the TLP from one or more directions simultaneously. The effect of modelling waves as regular and irregular waves is considered in this work.

University of Malaya

2.4.2 Wind forces

Wind loading is important for accurate prediction of the global motion response of floaters. Accurate modelling of the wind effects on the TLP is therefore essential. This largely depends on the location and exposed area of the TLP. Wind load can be a dominating excitation depending on location. The global wind loads acting on a floating structure consists of two components, a static part resulting in a mean offset and mean tilt, and a fluctuating component due to wind gusts which mainly excite the low frequency motions in surge, sway and yaw. For some floater concepts, roll and pitch motions are also influenced, Veritas (2012). The mean and fluctuating wind components are modelled for the TLP in this study.

2.4.3 Current forces

Current is a constant motion of water that can emanate from wind-drag, tidal, and background circulation components. In deep-water, it has been noted that current force might produce large system loads. Current data is expected to be established for the site and included in the design criteria. Near boundary currents (e.g., the Gulf stream, meanders, and eddies) should also be considered. The current profile throughout the water column and current scatter diagram should be determined, American Petroleum Institute (2001). The current force co-exists with hydrodynamic force from wave motion in an ocean environment. Generally, variations of tidal current force is normally governed by power law and wind-drift current is usually modelled with linear profile, Dawson (1983). The wind-drift current force is simulated in this study by adding the horizontal current velocity to the horizontal water velocity caused by wave in the Morison equation.

University of Malaya

2.4.4 Earthquakes

Earthquakes give rise to dynamic loads that have a high potential for disastrous consequences for structures, as well as humans. There are different ways in which structures are affected by earthquakes, the vibration of the ground being the most common, but not the only one. Other earthquake effects are ground failures such as liquefaction (loss of strength in silt or sand layers due to build-up of pore water pressure), landslides and mudflows (usually triggered by liquefaction); further effects include sea waves (tsunamis) and lake waves, Kappos (2002)

2.5 Wave theory

The wave theory is essential for the design of offshore structures. Although, the assumption for formulation of wave theory is regular, the theory has been extended to realistic random waves. This implies that a regular wave has the same form for the cycles. With the wave height, wave period and depth of water known, it is possible to determine the wave profile, water wave velocities and accelerations. The following section describes some of the available wave theories.

2.5.1 Linear wave theory

In the work of Chakrabarti (2005), wind action on the ocean create a motion and this is normally brought back to the calmness by the action of gravity and the outcome of this disturbance is regarded as wind generated gravity waves. Linear wave theory is formulated with the assumption that velocity potential depends on the position and time. The wave height is assumed small compared to the wavelength and water depth. The velocity potential is made to satisfy Laplace equation, linearized form of Bernoulli's dynamic equation and boundary conditions at the free and bottom surfaces. The solution of

University of Malaya

the velocity potential give rise to fluid kinematics that are employed for the calculation of wave-induced forces on the platform, Wilson (2003)

2.5.2 Stokes wave theory

This theory is formulated by modelling velocity potential and wave elevation with perturbation parameters. These parameters can be extended to any order so as to obtain wave theory. The assumptions used in the theory is that fluid is inviscid and incompressible. The fluid particle velocities and accelerations can then be calculated from velocity potential. The advantage of stoke wave theory is that the fluid kinematics are calculated up to the instantaneous fluid level for all values of time.

2.5.3 Stream function theory

Unlike linear wave theory, Chakrabarti (2005) defined stream function theory as a nonlinear wave theory which can either be regular or irregular stream function theory. The regular stream function theory is formulated using wave parameters of wave height, wave period and water depth. The irregular stream function theory is not limited by the wave form of horizontal or vertical symmetry as it is the case for regular type. This theory is normally being applied where free surface wave elevation or wave basin data are available.

2.5.4 Numerical theory

Numerical wave theory gained popularity as a result of introduction of sophisticated computers with high speed. The theory is based on deterministic solutions of the governing equations of the flow field. The assumption for the fluid in this theory include non-viscous, irrotational and incompressibility properties of the fluid. The governing equation is solved in terms of stream function. The theory has been applicable for deep-water waves, shallow waters where linear wave theory is not suitable as well as nonsymmetrical waves.

University of Malaya

2.6 Dynamic analysis of tension leg platform

Veritas (2008) revealed that the time domain approach is beneficial for global motion response analyses because it is possible to include all environmental load effects and typical nonlinear effects such as hull drag forces (including relative velocities), finite wave amplitude effects and non-linear restoring functions from tendon and risers. The frequency domain motion analysis has been identified by as the basis for generating transfer functions for frequency dependent first and second order excitation forces, added mass and damping (potential & viscous). It might also be possible to work with motion response amplitude operators, but this is considered more cumbersome when transferring into the time domain. The frequency domain analysis is capable of solving the equations of motions for each of the incoming regular wave components for a wave frequency analysis, and for each of the sum or difference- frequency combinations for a second-order analysis (high- or low frequency response). The output from a traditional radiation/diffraction frequency domain analysis is typically the excitation forces/moments, added mass/moments and potential damping and motion RAOs.

2.6.1 Time and Frequency domain analyses

In Garrett (2005), procedures for the time and frequency domain analyses were given for floating production system. The vessel was idealized as rigid body while mooring lines and risers were modelled as slender elastic rods; these are all coupled together with connecting link. The frequency solution was formulated for nonlinear static and harmonic loads while nonlinear dynamic problem was fully coupled for floating production system in the time domain. Correa, Jacob, and Mansur (2010) presented a hybrid time-frequency approach for the solution of dynamic problems in order to overcome long time simulation

University of Malaya

and also preserve nonlinearities in the system. Low (2009) carried out statistical linearization for the tendon restoring forces in six degree of freedoms in order to overcome high computational cost. The formulation in the frequency domain was said to include nonlinear couplings. The reported results of the frequency and the time domain show some level of agreement subject to certain conditions.

Lei et al. (2014) carried out lateral response analysis of floating production, drilling, storage and offloading unit riser in the frequency domain. This was achieved by linearizing the drag wave force. Low and Langley (2006) developed procedure for fully coupled floating production system in the time and frequency domain. The two methods were reported to have good comparison. Zou (2003) argued that dynamic interaction among the TLP platform, tendons and risers cannot be fully captured using de-coupled analysis. The study also reinstated that physical model tests are limited in terms of facilities and scaling the model might lose the true representation of the platform. The study estimated the hydrodynamic forces in the frequency domain and solved the problem in the time domain. Masciola and Nahon (2008) employed the Newton and Euler equations of motion to model the platform as rigid body in the six degree of freedoms and tendons are assumed as cables. The first and second order wave forces were analytically developed in MATLAB and solved by the Runge-Kutta method of numerical integration. Chitrapu and Ertekin (1995) carried out numerical analysis of the TLP in the time domain. The equations of motion were developed using the Newton- Euler approach; both the Morison and Potential theory method were used for the computation of hydrodynamic forces. Ormberg, Baarholm, and Stansberg (2003) argued that de-coupled analysis has the tendency to evaluating inertia properties of the dynamical TLP model inconsistently due to the absence of real effective mass that come from slender structures. The study employed WAMIT software for the calculation of low, high and wave frequency excitation forces. RIFLEX-C and SIMO

University of Malaya

software were used for coupled and de-coupled analysis in the time domain. The present study formulated the problem in time-domain so as to include nonlinear effects from the system and hydrodynamic force. The Newmark numerical method is employed for the solution of the formulation.

2.7. Analysis of coupled and uncoupled of TLP models

This review opens with Morgan (1983) who developed a computer program that calculate dynamic response for second order differential equation of motion for tension leg platform. The equation of motion was formulated from nonlinear stiffness coefficients and Morison's equation and this was solved numerically using the Newmark beta-method. Yoshida, Ozaki, and Oka (1984) studied the applicability of the linear response analysis method for the tension leg platform. The study compared the proposed linear response with small scale models and the results of structural response were validated. Jefferys and Patel (1982) study reported that ignoring lateral tether dynamics can fairly estimate platform motion but seriously impaired tether displacement. There is a wide range difference between the natural frequencies of the platform and wave excitation frequencies from the past study. However, the results of the TLP models show that in deep water, tether can possess lateral resonant frequencies with the exciting wave frequency and this correspondingly cause instability. This submission was verified to be true in this study. Bar-Avi (1999) carried out nonlinear dynamic analysis of tension leg platform. The study modelled the platform as rigid and tethers as flexible cables using beam continuous systems. The response result from equation of motion was presented. Lyons and Patel (1984) in an earlier study showed comparison of wave induced motion results of theoretical and experimental tensioned buoyant platforms. Similarly, a close and good agreement was

University of Malaya

reported for surge motions with magnitude discrepancies for tether tension at some wave frequencies in Spanos and Agarwal (1984)

The state of art for the analysis of the TLP had always been undertaken either in uncoupled or semi-coupled form. The procedures for uncoupled analysis as stipulated in American Petroleum Institute (1996), Sen (2002), Chakrabarti (2008) involve analysis of hydrodynamic floating structure for its motion while tendons were taken as external nonlinear stiffness. This is followed by component analysis of mooring line and riser individually. The floating structure motion can then be applied at the connection top points together with the disturbed wave and current loads on the components solved by lumped mass approach or finite element method. The mass and damping forces of the tendons are always neglected in uncoupled analysis. Yang et al. (2014) identified the need for coupled dynamic analysis of integrated platform and mooring lines. Both quasi-static and coupled dynamic for truss Spar and mooring lines were developed in the time domain for irregular waves. The coupling between the platform and mooring was achieved through appropriate displacement and force boundary conditions. The hydrodynamic forces were calculated in the time domain unlike in the method of using specialized software and doing transfer back to the time domain as usually undertaken by previous researches. The effect of coupled dynamic analysis of floater motions on the mooring and riser system response of a floating production storage offloading was emphasized in Caire and Schiller (2012) to lower the conservatism adopted in the current practice of fatigue assessment. Similarly, Ormberg and Larsen (1998) illustrated that motions of platform in de-coupled analysis were modelled and calculated by simplifying forces from the mooring and riser lines. This has traditionally been followed with simulation of the platform motion as top end excitation in the calculation of dynamic loads of the mooring lines and risers. The analysis in the time domain was carried out with SIMO software and RIFLEX software was used for coupling

University of Malaya

and modelling of floater and mooring lines together. Coupling effect between the floater and mooring lines have been reported by Astrup, Nestegård, Ronæss, and Sødahl (2001) as the influence on floater mean position and dynamic response due to slender restoring, damping and inertia forces. The current practice by industry as reported by Caire and Schiller (2012) was the de-coupled analysis. This is always achieved by excluding mooring lines and tendons from the floater motion. Consequently, this is then imposed as the external force during the dynamic analysis of the mooring line. Most hydrodynamic software such as WAMIT, AQWA, HOBEM employ this methodology. Without fully integrating the coupling between the floater and lines, the accuracy of the platform motion may be undermined. Both coupled and uncoupled TLP models are modelled so as to assess their behaviour in Abaqus/Aqua software.

Bhattacharyya et al. (2003), Chatterjee et al. (1996), Natvig and Johnsen (2000) suggested that motion characteristics and structural response of compliant structures can be better idealized as a coupled model using the finite element method. In another attempt, Giron, Correa, and Jacob (2014) developed a hybrid semi-coupled model that combines the features of coupled and de-coupled analysis for the floating production system. Le, Ding, and Zhang (2014) discussed coupled motion characteristics of the floating mooring platforms under regular and in a coupled model against the de-coupled analysis. The agreement and differences between the de-coupled and coupled analysis results were presented.

The need for coupled formulation was identified by Correa et al. (2002), which simply implies that hydrodynamic model of the floating structure is coupled to the finite element model of mooring and riser lines with mass and damping included. The equations of motion must then be solved simultaneously. Adrezin et al. (1996) reported that tendons were mostly modelled as massless springs in most studies but in advanced models, tendons

University of Malaya

can be represented as beams, cables or springs with increased complexity. Due to the extreme tension experienced by tendons in deep water with fluid flowing around them there is a need to consider higher order effects in loading and structure.

Adrezin and Benaroya (1999a) employed extended Hamilton's approach to derive sets of nonlinear equations for single tendon TLP. The Lagrangian approach was used to develop energies on the tendons. The hull was represented as a rigid body and the system simulated for random waves and current load. The Morison equation and the Pierson Moskowitz spectrum were used for simulation of random sea. Results for the quarter ISSC TLP was reported and for wave only, the TLP vibrates about vertical position and about offset position when current force was added. Application of forces on tendons increases amplitude and offset position as compared to when the forces were absent.

In another paper, Adrezin and Benaroya (1999b) derived sets of equation of motion for the calculation of surge and pitch responses for the hull as well as the surge response along the tendon. Ahmad, Islam, and Ali (1997) investigated the response of the TLP when excited by wind forces in the time domain. The Simiu's spectrum was adopted for this problem and major nonlinearities as considered earlier in Ahmad (1996) were also incorporated. The effects of mean wind and fluctuating wind over random wave simulation in coupled and uncoupled motion were examined. The response of the TLP to wind-induced load found that surge and yaw responses were greatly affected by the intensity of the wind force, however, the magnitude of pitch and roll were not pronounced due to vertical restraints.

2.8 Finite element modelling of TLP

Jayalekshmi et al. (2010) studied the behaviour of TLP in random waves. Pierson–Moskowitz, (PM) spectrum was used to simulate time history of random waves of TLP

University of Malaya

with and without risers under the action of random waves and current. The response spectral densities were reported to be significantly reduced and this was attributed to the riser hydrodynamic damping related to the riser drag. There was an increase in the offset and set-down values due to the nonlinearities that arise from steady current drag on the risers and wave drift force. Joseph, Mangal, and George (2009) used finite element numerical for the analysis of a 3- column mini TLP and compared their result with a 4-column mini TLP. It was reported that dynamic responses were close to a 4-column mini TLP with relatively high surge and tendon variation. Zou (2003) carried out coupled dynamic analysis of the hull, tendon and riser and reported that up-wave and down-wave tendon tensions do exist even though static offset and set-down of coupled and uncoupled agreed.

Bachynski and Moan (2012) employed the concept of TLP for wind turbine in accessing offshore wind resources under different wave –wind conditions. The JONSWAP and Kaimal spectra were used for the simulation of random waves and fluctuating wind. Parametric studies were carried out on a single column tension leg platform wind turbine. This was followed by the evaluation of platform motions and structural loads on the turbine components and tendons. Commercial aero- and- hydrodynamic software were used for the analysis and design. It was reported that the presence of wind turbine on the TLP platform showed no large effect on the turbine blade but rather causes an increase in variation of the bending moment at the base when compared with land based turbine. Bhattacharyya et al. (2003) conducted nonlinear dynamic analysis of the Sea-Star mini TLP using the finite element method coded in FORTRAN. Based on the comparison between the experimental and numerical, it was recommended that the result of the finite element procedure can be relied upon. The same principle of general finite element method is used for model discretization in Abaqus/Aqua in this study.

University of Malaya

2.9 Different analysis method and load combinations

Liu (2014) carried out a parametric study of the TLP under varying incident wave angles, wave heights and wave periods. It was reported that these parameters had little effect on the tension variation. However, the increase in the wave period increases the surge position, and decreases the heave, roll and pitch. Also, the wave height effect was minimal on heave but more on other degrees of freedom. In another similar work, the radiation/diffraction theory with the boundary element method was employed by Gao et al. (2013) to compute motion responses and wave forces on floating TLP wind turbine. Their findings show that the maximum response of sway and the minimum response of surge have the same direction. It was the same with the maximum response of pitch and the minimum response of roll. Again, motion responses of heave and yaw did not acutely change as the other four directions did. Kareem and Li (1993) presented a frequency domain analysis procedure in the evaluation of wind excited surge response of a TLP in the presence of wave and currents. Vickery (1995) and Ahmad et al. (1997) examined the combined effect of wind and wave loads on the response of the TLP. An agreement between the theoretical results and experimental findings was established. Chandrasekaran and Gaurav (2008) analysed non-linear dynamic equations of motion for a triangular tension leg platform at different water depths operating under the high sea waves and earthquake motion. Similarly, Chandrasekaran et al. (2004) studied the influence of hydrodynamic drag coefficient and hydrodynamic inertia coefficient on the non-linear response behaviour of two different tension leg platform models operating under regular waves. It was reported that constant coefficient throughout the water depth yielded higher motion response compared to the results from varying the coefficients. Muhittin and Oguz

University of Malaya

(2003) analysed motion of platform by both single-wave prediction and spectral method and found the latter produced more favourable results.

Chandrasekaran, Jain, Gupta, and Srivastava (2007) reported results for two triangular TLP operated under the combined action of regular wave and impact loadings. It was concluded that the platform was affected when the impact was on the corner column and that the impact on the pontoon seems not to affect the platform. Chandrasekaran and Jain (2002b) also, reported that heave and surge responses of square TLP was higher than that of triangular TLP but the pitch degree of freedom attracted more forces due to the pontoons arrangement to the unidirectional wave. A similar work by Tabeshpour, Golafshani, and Seif (2006) made use of simple stable numerical integration known as the Modified Euler Method (MEM) for the analysis of the dynamic response of structures in the time domain. In their study, the stability of the method for solving differential equation of motion of a nonlinear TLP offshore system in random wave excitation was presented. The key point of suitability of the MEM for solving the TLP system was that the maximum frequency of the system is about 0.5Hz. The stability criterion and the convergence of the numerical solution for critical time steps were numerically discussed.

Ahmad (1996) carried out an analysis of stochastic response of TLP in the time domain under long crested random sea. The stiffness coefficients for square tension leg platform were developed for coupled motion in six degrees of freedom. The result of stochastic response was summarized in statistical forms. The study concluded that geometry characteristics, angle of incidence, variable submergence, current velocity and tether tension affect the dynamic response of the TLP to the random wave and currents. Siddiqui and Ahmad (2003) studied the response behaviour of tension leg platforms under impulsive forces. Siddiqui and Ahmad (2000) carried out a reliability analysis of an intact and one tether missing tension leg platform in various sea conditions. The focus of their

University of Malaya

paper was on annual and life time probability of other tethers when one tether is missing or broken under regular wave, regular wave and wind and long crested seas due to maximum and minimum tension in the cable. Amanullah, Siddiqui, Umar, and Abbas (2002) studied the reliability of tension leg platforms against various limit states of failure. Khan, Siddiqui, Naqvi, and Ahmad (2006) examined the reliability behaviour of tether to derived limit state maximum tension under action of wave and impulsive load. The sensitivity of the random variables on reliability was also undertaken. Ardakani and Ketabdari (2007) presented the results of experimental work performed on a scaled model for the Sea-star TLP in a wave flume.

Hydrodynamic responses analysis of tension leg platform was investigated by Chen et al. (2013). The modelling of their platform was performed using the DNV/SESAM software. The study carried out the optimization of wave direction and period that gave worst motion responses in both frequency and in the time domain. Lee and Wang (2000) investigated the surge response of tension-leg twins platform. The equations were derived and the effects of reflection coefficient and dimensions of the platform on the response were also studied. Chandak and Chandrasekaran (2010) investigated response the behaviour of TLP with triangular geometry using the dynamic Morison equation. Nonlinearities associated with vortex shedding effects were considered along with standard Morison equation. Rudman and Cleary (2013) used smoothed particle hydrodynamics to simulate large waves on tension leg platform. The platform motions and tensions in the cable were investigated to the effects of wave impact angle and mooring line pretension. Tabeshpour and Shoghi (2014) carried out solution for surge motion of TLP with the homotropy perturbation method. Karlinsky and Kuteynikov (2008) proposed formulas and presented result for ice resistant TLP. It was concluded that the stability requirement of the ice-resistant TLP has to be different from the normal floating TLP. Similarly, Chernetsov

University of Malaya

and Karlinsky (2006) analyzed four platform floating substructures. Two of the platforms were Spar-type, whereas the other two was of TLP-type structure in ice middle sea depth. Rijken and Leverette (2007) reported that the dynamic tension levels resulting from earthquake near the tension leg platform in the Gulf of Mexico are minor and are far less than the extreme tensions under storm and hurricane conditions.

Kim et al. (2007) conducted a dynamic response analysis of tension leg platforms including hydrodynamic interaction in regular waves. The study assumed the whole structure as flexible and used a numerical method based on a combination of three-dimensional source distribution and dynamic structural analysis method for the analysis. Chandrasekaran and Jain (2002b) investigated the dynamic response of a triangular configuration Tension Leg Platform (TLP) under random sea wave loads. The random wave was generated synthetically using the Monte-Carlo simulation with the Pierson–Moskowitz (P–M) spectrum. The effect of the coupling of various structural degrees-of-freedom on the dynamic response of the TLP under random wave loads was also studied. The paper concluded that in the presence of current, the response behaviour of the TLP was altered significantly introducing a nonzero mean response in all degrees-of-freedom. Kurian et al. (2008) developed a MATLAB computer program for determining the dynamic responses of square TLPs subjected to regular and random waves. The structure was treated as a rigid body and all the six motions as well as the tether tensions were determined. The linear Airy wave theory and the Morison equation were used for wave force calculations. The equation of motion was organised in MATLAB and the Newmark Beta numerical integration method was used for the time domain analysis. The response amplitude operators for the motions of a typical TLP were compared with the available theoretical and experimental results. Besides, parametric studies of different parameters such as water

University of Malaya

depth, pretension, wave angle and position of center of gravity (CG) were also undertaken. The work reported results of platform responses caused by varying these parameters.

Li and Kareem (1990) researched on the dynamic behaviour of tension leg platforms (TLPs) under the simultaneous action of random wind and wave fields. Computationally efficient time and the frequency domain analysis procedures were developed to analyze the wind-wave- current-structure interaction problems. The aerodynamic load effects were described by the space-time description of the random wind field. The hydrodynamic loads were expressed in terms of a combination of viscous and potential effects. A stochastic decomposition technique was developed which significantly enhanced the efficiency of the frequency domain analysis of complex systems. A numerical scheme involving iterative and perturbation techniques was utilized to evaluate the second order response statistics. The response of a typical TLP in six degrees of freedom showed excellent agreement between the time and frequency domain analyses. Chandrasekaran, Jain, and Chandak (2006) analysed the nonlinearities due to the change in tether tension and nonlinear hydrodynamic drag forces. The coupled response of TLP under moderate regular sea waves due to the change in initial pretension in the tethers caused by seismic forces was then investigated. Seismic forces were imposed at the bottom of each tether as axial forces. The tether tension becomes unbalanced when the hull was under offset position. The change in initial pretension due to the vertical component of the earthquake influenced the response of the triangular TLP in degrees-of-freedom experiencing such forces. The tether tension varied nonlinearly when the platform was subjected to seismic forces caused by the El-Centro earthquake and artificially generated earthquake using the Kanai–Tajimi's power spectrum. The response due to earthquakes varied with the intensity of the input ground motion. Naess, Gaidai, and Teigen (2007) carried out an analysis for TLP in first order, second order wave frequency and slow-drift

University of Malaya

motions. The analysis predicted results for extreme response statistics of the horizontal surge motions. Masciola and Nahon (2008) presented a non-linear six degree-of-freedom dynamics model results for a tension leg platform type structure. The dynamics model and simulation presented was different from other previous models in the derivation approach. Existing models were usually based on deriving stiffness coefficients from an analysis of single-degree-of-freedom perturbations of the platform. Their study analysed the generalized platform motion based on fundamental kinematic principles and calculate the forces and moments resulting from this motion. Yongjun, Jiemin, and Qingyong (2008) carried out a diffraction analysis of short-crested wave with uniform current. The study reported that wave frequency was influenced by incident angle and strength of the current velocity.

2.10 TLP-Tendon-Riser system

Mekha, Johson, and Roesset (1996) investigated the implications of tendon modelling on TLP response by using constant lateral tendon stiffness, time varying axial tendon stiffness and coupled analysis of hull and tendons. Also, Chandrasekaran, Chandak, and Anupam (2006) reported that tension variation in the TLP tendon played a significant role in its stability. Gadagi and Benaroya (2006) loaded a tether at the free end and subject it to various end tensions. The parametric effect of harmonically varying the end tendon brought an increase in the constant end tension. Results of the effect of different significant wave heights on the axial and transverse motion were also presented. Aguiar, Almeida, and Paulino (2014) formulated and implemented finite element modelling for Timoshenko beams on multi-layered pipe beam element. Also, axial, bending and torsional degrees of freedoms were included in the derivation. Jayalekshmi, Sundaravadivelu, and Idichandy (2009) studied the effects of the dynamics of riser on TLP behaviour in nonlinear finite

University of Malaya

element program for regular waves. It was reported that the riser effect reduced the dynamic surge due to hydrodynamic damping from the riser and increase the mean drift surge and set-down due to additional hydrodynamic forces and current forces. Islam, Jameel, Ahmad, Jumaat, and Kurian (2013) carried out an analysis of coupled Spar-mooring system using finite elements in Abaqus software. The environment was simulated for severe sea states and the Morison equation was used for force computation. It was reported that time histories of surge, heave, pitch and maximum mooring tension decreased and remained steady after the transient state. Yang, Teng, Ning, and Shi (2012) analysed the coupled dynamic response of truss Spar and its mooring line/riser in the time domain. The analysis program for the equation of motion was developed and simultaneously solved for truss Spar and mooring systems using the Newmark-β and Newton-Raphson iterations. Bahtui, Alfano, Bahai, and Hosseini-Kordkheili (2010) adopted the finite element formulation for a nonlinear analysis of flexible riser. The approach was based on the incrementally updated Lagrangian together with the modified linearization scheme for the analysis of annular section of 3-D beam element. The influence of buoyancy force and current force were considered on the riser pipeline. Adamiec-Wojcik, Brzozowska, and Drag (2015) derived set of formulas for the dynamic analysis of risers during vessel motion using the modified rigid finite element that included bending and longitudinal deformations of the planar slender links. Drag forces, uplift forces, sea currents and added mass influences through the Morison equation were applied on the slender structures.

Jameel, Ahmad, Islam, and Jumaat (2014) analysed the motion response of the Spar platform under wave and wind loading using the coupled model. It was reported that wind induced forces affect mooring and motion response significantly. In another development, Han and Benaroya (2002) formulated coupled nonlinear equation for axial and transverse motion of a tower. The nonlinear free and forced responses were later compared with the

University of Malaya

linear model. Khan et al. (2006) examined the reliability behaviour of tether to derive limit state maximum tension under action of wave and impulsive load. The sensitivity of the random variables on reliability was also undertaken. Chatterjee et al. (1996) studied the hydrodynamic behaviour of the long floating structure and reported that as the mean wave direction increases, the response ratio decreases. The increase in the spreading parameter made the response of short-crested idealization closer to the long-crested sea state. More recently, Ng, Kurian, and Liew (2014) examined the responses of the classic Spar in short and long crested wave generation experimentally. Their study reported that the responses from long-crested simulation were found to be thirty-five percent higher than those from short-crested sea. Zaheer and Islam (2012) examined the response of an Articulated Leg Platform (ALP) to wave alone, wind alone, and to correlated wind and waves. The fluctuating component of the wind was modelled with different wind spectra while the sea state was characterized by the Pierson–Moskowitz (P–M) spectrum. Their work demonstrated that the Davenport wind spectrum response was lower as compared to other spectra used. Bisht and Jain (1997) studied the response of guyed tower platform to random wave and wind and came to the submission that wind forces increased the mean values of the platform responses. The effects of the magnitudes and the directions of wave, wind, current at different wave heights were simulated in the work Yilmaz and Incecik (1996b) on moored floating platforms. The study concluded that the direction of wave incidence and reduction in the number of mooring legs affect the motion of the system. Han and Benaroya (2002) formulated a coupled nonlinear equation for the axial and transverse motion of a tower. The nonlinear free and forced responses were later compared with the linear model. Benfratello, Di Paola, and Spanos (1998) analysed the stochastic response of multi degree of freedom of wind-excited structures by means of the Volterra series approach and stated that computational effort of this method was lesser as compared to

University of Malaya

earlier methods used for the computation of multiple integrals. Islam, Jameel, Jumaat, Shirazi, and Salman (2012), Jameel et al. (2013), Mohd Zaki, Abu Hussain, and Najafian (2014) studied the behaviour of the integrated Spar-mooring system under the actions of wave, wind and current forces. Shehata and Raheem (2013) employed a finite element analysis in determining the displacements and stresses in the steel jacket structure and the results of the nonlinear analysis were presented for a safe platform operation. Barranco-Cicilia, Lima, and Sagrilo (2008) presented the methodology to perform a Load and Resistance Factor Design (LRFD) criterion for the design of Tension Leg Platform (TLP) tendons in their intact condition.

2.11 Summary of previous works

From the foregoing, the bulk of the research in this area had traditionally been on de-coupled analysis with limited works on semi-coupled in trying to bridge the gap between the uncoupled and coupled analysis of the TLP due to the high computational cost and analysis time involvement. In view of this, this study will consider both uncoupled and coupled TLP models in regular and irregular seas. A mathematical numerical code was formulated in FORTRAN for uncoupled model and the Abaqus finite element software with Abaqus/Aqua module techniques were used for the discretization and application of loads for coupled models. These are discussed in greater detail in the next chapter.

University of Malaya

CHAPTER 3: METHODOLOGY

3.0 Introduction

As discussed in the previous chapter, the time domain numerical model is developed for uncoupled and coupled TLP. The mass, stiffness and damping forces of the TLP are calculated and balanced with the external exciting forces. The environmental forces considered for this analysis include regular and random waves; current and wind forces. The regular wave was simulated with the linear wave theory while random waves were calculated through the Pierson-Moskowitz spectrum, followed by the calculation of hydrodynamic forces with the Morison equation. Also, the current force was calculated by adopting the linear current profile type of Veritas (2007). For the superstructure, the effects of mean and fluctuating wind loads were calculated using Emil Simiu and API spectra respectively. The TLP was assumed to be a small structure since the ratio for diffraction parameter of characteristic dimension and wavelength is less than 0.2, hence wave diffraction and radiation was neglected.

The present problem was solved using two different approaches. For the first approach, equations of motion for the TLP were formulated from the first principle. Then the equations of motion were coded and numerically solved in FORTRAN software embedded with subroutines that calculate inertia, damping, restoring forces matrices as well as the external forces vector on the TLP. The second method employed the Abaqus finite element analysis software to model platform as rigid beams and tendons as finite elements with proper connector to impose boundary conditions. The Abaqus/Aqua product which was designed originally for application of hydrodynamic wave loading on offshore pipelines, was used to apply hydrodynamic forces on the platform model and tendon legs.

University of Malaya

Numerical model incorporates various degrees of nonlinearities on the TLP such as variable submergence, added mass, drag force, tension fluctuation, and large displacement. The equation of motion was formulated in an efficient manner and this was solved by using the Newmark-βeta integration scheme. A numerical model known as the Uncoupled Nonlinear Analysis Program (UNAP-TLP-2016) was developed and solved for uncoupled TLP in FORTRAN. The solution of the coupled TLP system was successfully accomplished by Abaqus finite element software and named as Coupled Nonlinear Program (CNAP-TLP-2016).

3.1 TLP structural idealization and assumptions

For both uncoupled and coupled TLP models, a double symmetric rectangular ISSC platform with four solid tendons at each corner was employed. The TLP structural configuration adopted for this study is the International Ship and Offshore Structures Congress (ISSC). Model geometry of this platform consists of four vertical cylindrical columns and four horizontal pontoons with a group of tendons at each corner end. ISSC sketch plan and elevation are shown in Figure 3.1 with other mechanical characteristics outlined in Section 4.3. The basic differences between the coupled and uncoupled as it affects the mathematical formulation is stated in Table 3.1

University of Malaya

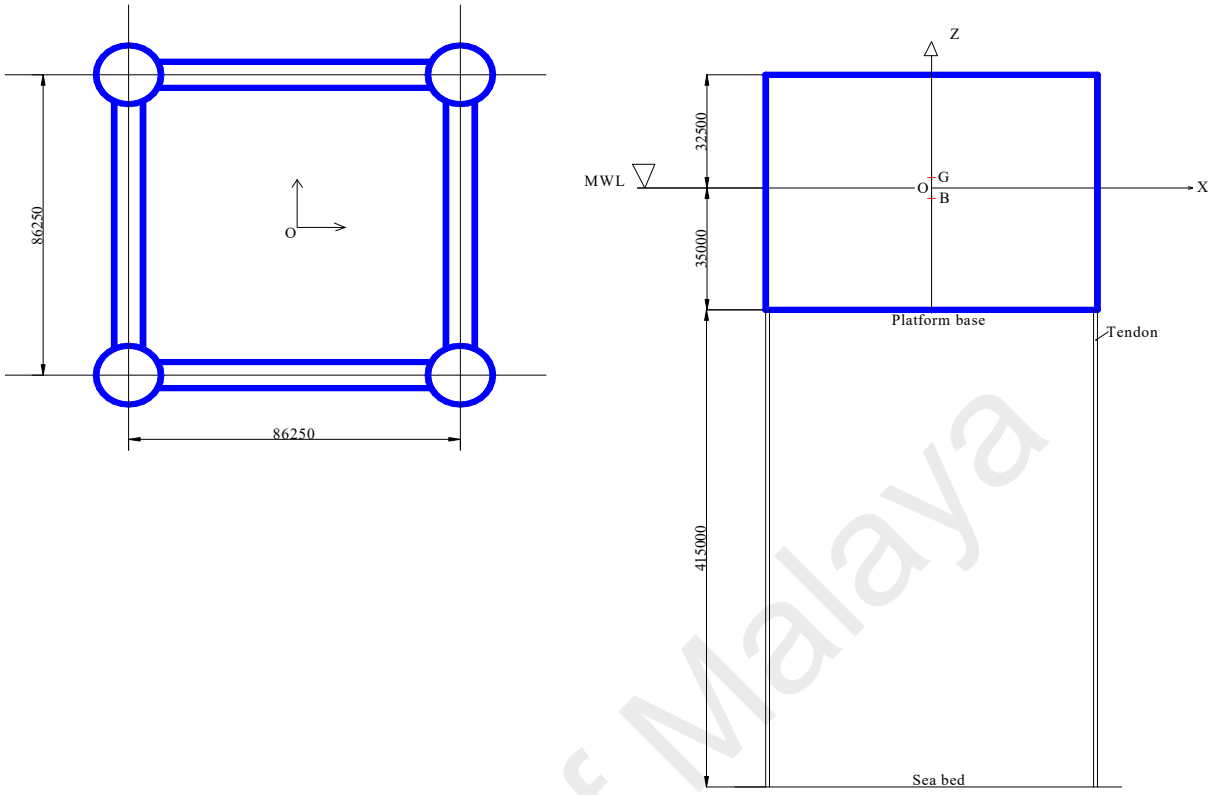

Figure 3.1: TLP model configuration (All dimensions are in millimeters)

Table 3.1: Basic differences between coupled and uncoupled TLP models

No	Uncoupled TLP model	Coupled TLP model
1	Tendons effect on the platform is modelled as LINEARIZED SPRING STIFFNESS and considered WEIGHTLESS (AXIAL). The total stiffness element is a summation of axial, geometric and hydrostatic stiffness.	Effect of tendons is modelled as NONLINEAR FINITE BEAM ELEMENTS with tendon mass included. (AXIAL, GEOMETRIC STIFFNESS). The total stiffness element is a summation of axial tendon, tendon geometric and platform hydrostatic stiffness.
2	The restoring forces are derived finding equilibrium of reaction forces one after the other due to finite displacements. Nonlinear interactions among DOFs not fully captured.	The restoring forces are derived using virtual work approach and applying displacements in all DOFs simultaneously. Nonlinear interactions among DOFs was fully captured.
3	Platform 6-DOFs motion was calculated in a Separate model and results were used as forced displacement in the stress analysis of the tendons.	Platform 6-DOFs and tension variation in the tendons were solved simultaneously.
4	Tendon dynamics are neglected.	Tendon dynamics are included.
5	The problem is solved from the first principle by writing a FORTRAN Program.	The problem is solved using adapted finite element modelling and Abaqus/Aqua module by writing script and solving in Command line.

University of Malaya

The following assumptions were adopted in the derivation of the mathematical model in this research while some of the previous simplifications were avoided:

(1) The TLP was idealized as a rigid body, symmetrical about the x- and y- axes with the centre of gravity taken as the origin.

(2) The motions of the platform were governed by three translational and three rotational degrees of freedom at the platform centre of gravity as shown in Figure 3.2.

(3) Surge, sway, heave, roll, pitch and yaw motions were coupled together.

(4) The structural mass of the TLP and moment of inertia were lumped at the centre of gravity.

(5) The tendons that anchor the TLP to the seabed were idealized as linear springs for uncoupled TLP and hybrid beam elements for coupled TLP.

(6) Hydrodynamic loads on the platform were due to the gravity waves and current forces while aerodynamic force was applied on the superstructure.

(7) The Morison empirical formula was adopted for wave induced forces with the verification that sectional dimension was far less than wavelength hence diffraction effect is ignored.

(8) The linear wave theory was employed for calculation of water particle velocity and acceleration.

(9) The water was assumed inviscid, incompressible and the motion was irrotational.

(10) Gravity, inertia, hydrostatic and hydrodynamic forces were applied on the tendons and connecting elements for the coupled model.

(11) Variable submergence and instantaneous buoyancy were active and significantly influence the heave response of the TLP.

University of Malaya

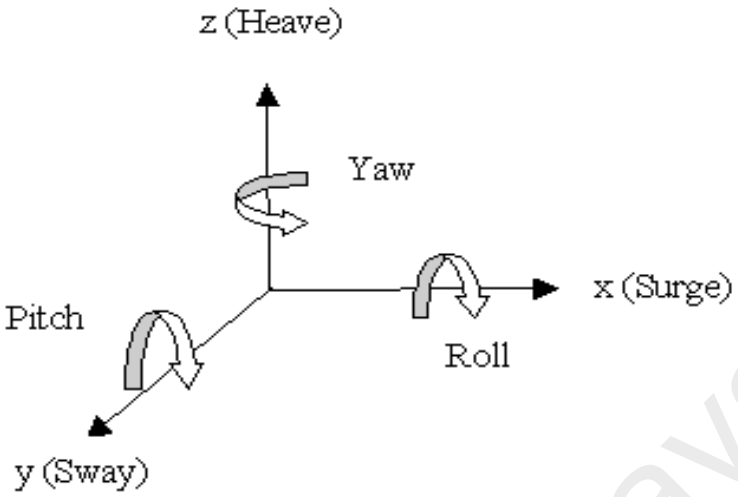

Figure 3.2 TLP coordinates system

3.2 Derivation of equations of motion for TLP platform

The Cartesian coordinate system is shown in the Figure 3.1 with the origin at the intersection of centre of gravity and mean water surface. The x-y plane is on the mean surface with the z-axis vertically pointing up through the centre of mass of the TLP. The motion of the TLP is a Multi-Degree of Freedom (MDOF), however, six independent degrees of freedom, (N = 6) are adopted. The dynamic equation of motion in the time domain for the TLP is of second order ordinary differential equation and can be written as

$$[\mathbf{M}]\{\ddot{\mathrm{U}}\} + [\mathbf{C}]\{\dot{\mathrm{U}}\} + [\mathbf{K}]\{\mathrm{U}\} = \left\{\mathbf{F}\left(\mathrm{t}, \mathrm{U}, \dot{\mathrm{U}}\right)\right\} \quad (3.1)$$

The {U} is a column vector that represents the structural motion of the rigid body. Therefore, the elements of this vector composed of translational and angular displacements that describe the motion at the rigid body centre of gravity and idealized as

$$\{\mathrm{U}\} = [\mathrm{Surge}, \mathrm{Sway}, \mathrm{Heave}, \mathrm{Roll}, \mathrm{Pitch}, \mathrm{Yaw}]^{T} \quad (3.2)$$

The single and double over-dots on {U} represent the velocity and acceleration of the coordinate respectively. The mass, [**M**], damping, [**C**], and stiffness [**K**] matrices are of the

University of Malaya

order (N x N) and $\{\mathbf{F}\}$ is a (1x N) time-dependent column vector, these are discussed and formulated in the following sections.

3.2.1 Mass matrix

With the assumption of the rigid body for the platform coupled and generalized coordinates that defines the motion at the centre of gravity, lumped mass matrix approach was adopted to calculate and allocate the mass along the degrees of freedom. The total platform mass was lumped in surge, sway and heave directions. In respect to vertical centerline, the structural mass was assumed to be symmetric and diagonal. The rest of the three diagonal terms represent the mass moment of inertia due to the structural and added mass with respect to roll, pitch and yaw degrees of freedom.

The total mass matrix is a summation of structural mass above the mean sea level and fluid added mass as a result of accelerated motion of water around the TLP structural members. The formulation for the constant added mass matrix was calculated as the product of volume of the hull, water density and length of the hull. Thus, varying added mass was considered as the product of body acceleration and mass quantity. Therefore, elements of diagonal mass matrix were [$M_{11} = M_{22} = M_{33} = M + M_a$] along the surge, sway and heave directions. [$\mathbf{M}$] and 'M_a' are the total mass in the air and added mass respectively. Similarly, the last three terms in the matrix were $M_{44} = Mr_x^2 + M_a$; $M_{55} = Mr_y^2 + M_a$, and $M_{66} = Mr_z^2 + M_a$ representing mass moment of inertia about the x, y and z directions respectively. The $'r_x'$ $'r_y'$ and $'r_z'$ were the radius of gyration about the x, y and z directions. The fluctuating component of added mass due to variable submergence was also included in the force vector of Equation 3.81.

University of Malaya

$$[\mathbf{M}] = \begin{bmatrix} M_{11} & & & & & \\ & M_{22} & & & & \\ & & M_{33} & & & \\ & & & M_{44} & & \\ & & & & M_{55} & \\ & & & & & M_{66} \end{bmatrix} \quad (3.3)$$

The unsteady motion flow around the TLP members created a force known as added mass. This effect was considered in all forces associated with acceleration rather than along the surge, sway and yaw only and they were lumped alongside with structural mass as shown in Equation 3.81.

3.2.2 Damping matrix

Damping is the capability of a body to dissipate energy. Sources of damping include structural, material and fluid for the type of floating body problems. The major source of damping that was considered for this analysis was of the viscous effect type of fluid damping due to the movement of fluid relative to the vibrating TLP. The structural damping occurs as a result of friction among various parts of the body. Thus, structural damping matrix, [**C**] in Equation 3.4 was defined to be a symmetric matrix of order (N x N), degrees of freedom and proportional to mass and stiffness matrices

$$[C] = \alpha[M] + \beta[K] \quad (3.4)$$

Where

α = alpha and β = Beta are Rayleigh constants calculated from modal damping ratio and fixed for the dynamic system respectively. The nodal damping forces and nodal velocities are related through a constant known as damping influence coefficient.

University of Malaya

Following the orthogonal transformation in Clough and Penzien (1993)Equation 3.1 was transformed to

$$\{\phi\}^T[M]\{\phi\}\{\ddot{\xi}\} + \{\phi\}^T[C]\{\phi\}\{\dot{\xi}\} + \{\phi\}^T[K]\{\phi\}\{\xi\} = \{\phi\}^T\{F(t)\} \quad (3.5)$$

Subsequently, for the uncoupled equation of motion, Equation 3.5 was further reduced to

$$\{\ddot{\xi}_j\} + 2\zeta_j\omega_j\{\dot{\xi}_j\} + \omega_j^2\{\xi_j\} = \{F_j(t)\} \quad (3.6)$$

Where

$\{\xi_j\}$ is the displacement of the structure in the transformed coordinate; ζ is the damping ratio in the uncoupled mode; ω is the natural frequency of the structure; $\{F(t)\}$ is the modified force vector in transformed coordinate and $\{\phi\}$ is the normalized Eigen-vector for the structure. For the validity of this orthogonal transformation, $[\mathbf{C}]$ matrix must be proportional to mass and stiffness matrices and Equation 3.4 is now represented as:

$$\{\phi\}^T[C]\{\phi\} = \begin{bmatrix} \alpha + \beta\omega_1^2 & 0 & 0 & 0 & 0 & 0 \\ 0 & \alpha + \beta\omega_2^2 & 0 & 0 & 0 & 0 \\ 0 & 0 & \alpha + \beta\omega_3^2 & 0 & 0 & 0 \\ 0 & 0 & 0 & \alpha + \beta\omega_4^2 & 0 & 0 \\ 0 & 0 & 0 & 0 & \alpha + \beta\omega_5^2 & 0 \\ 0 & 0 & 0 & 0 & 0 & \alpha + \beta\omega_6^2 \end{bmatrix} \quad (3.7)$$

From the Equations 3.6 and 3.7 respectively and using symmetry property, it was deduced that:

$$2\zeta_1\omega_1 = \alpha + \beta\omega_1^2$$

$$2\zeta_2\omega_2 = \alpha + \beta\omega_2^2$$

$$2\zeta_i\omega_i = \alpha + \beta\omega_i^2 \quad (3.8)$$

Equation 3.8 was further simplified to become

$$\zeta_i = \frac{\alpha}{2\omega_i} + \frac{\beta\omega_i}{2} \quad (3.9)$$

University of Malaya

It is clearly seen from Equation 3.9 that the damping ratio is proportional to natural frequencies of the structure. For the uncoupled TLP model, this equation was solved interactively.

The procedures adopted for determining the alpha and beta Rayleigh constants were as follows:

(i) Damping ratio (2- 5%) was selected for the first mode and k^{th} significant mode of the structure

(ii) A linear interpolation method was adopted for the determination of damping ratios of intermediate modes in form of

$$\zeta_i = \frac{\zeta_k - \zeta_1}{\omega_k - \omega_1}(\omega_i - \omega_1) + \zeta_1 \quad (3.10)$$

(iii) The value of β was calculated from

$$\beta = \frac{2\zeta_1\omega_1 - 2\zeta_k\omega_k}{{\omega_1}^2 - {\omega_k}^2} \quad (3.11)$$

(iv) Value of β was back-substituted into $2\zeta_1\omega_1 = \alpha + \beta{\omega_1}^2$ and obtain the value for α

(v) The above steps were repeated for the subsequent natural frequencies and their respective alpha and beta were calculated.

The average of all these values were calculated and used as rayleigh constants for the dynamic analysis.

3.2.3 Stiffness matrix

The restoring stiffness matrix consists of axial, geometric and hydrostatic stiffness. The nonlinear coefficients of stiffness matrix [K_{ij}] were derived from the first principles by large displacement approach. Before employing the proposed formulation, Low (2009) and

University of Malaya

Senjanovic, Tomic, and Rudan (2013) had argued against Morgan (1983) approach of stiffness derivation and proposed new formulation for restoring stiffness. Morgan's approach was based on equilibrium of forces which has been widely adopted (Ahmad (1996), Jain (1997), Chandrasekaran and Jain (2002a), Abou-Rayan, Seleemah, and El-Gamal (2012) and Tabeshpour and Shoghi (2014)). In spite of this, the same approach, due to its simplicity and because of time limitation, was modified by including hydrostatic stiffness with restoring coefficients from tendon effect for the uncoupled model and virtual work method was employed for coupled TLP model.

This was achieved by giving an arbitrary displacement in the degree of freedom 'j' and the corresponding force in the degree of freedom 'i' was computed while all other degrees of freedom were restrained from movement. The restoring stiffness matrix was formulated as a joint contribution from the hydrostatic restoring force and restoring force from the tendons. In the following derivation of the stiffness matrix, restoring forces in the horizontal degree of freedoms are as a result of the horizontal component of pretension in the tendons while the vertical degrees of freedom derived their restoring forces from the elastic properties of the tendon. In addition, the hydrostatic restoring force was also accounted for, but the magnitude is relatively small.

3.2.3.1 Surge motion

The first column in the stiffness matrix of Equation (3.46) was formulated by giving arbitrary displacement, 'x_1' along the surge direction as seen in Figure 3.3 while other degrees of freedom were kept fixed. This action caused an increase in initial pretension of the tendons as written in Equation 3.13. By taking the equilibrium of forces for the platform, this resulted in K_{11}, K_{31} and K_{51} terms in Equations 3.16, 3.18 and 3.22 respectively, while the remaining terms on this column were zero.

University of Malaya

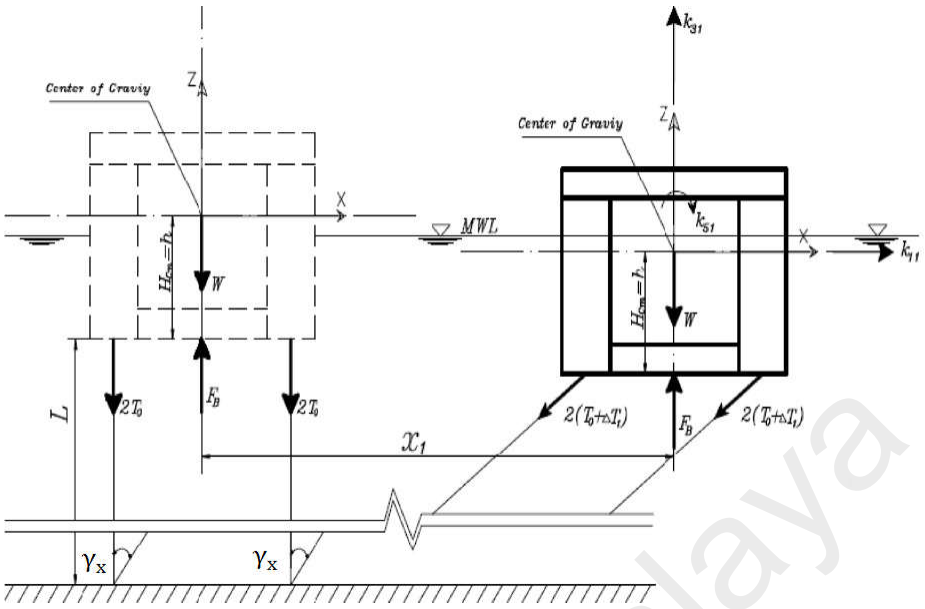

Figure 3.3: Surge displacement
Abou-Rayan et al. (2012)

In Figure 3.3, the equilibrium equation of forces in the surge direction was calculated to be

$$K_{11}x_1 = 4(T_0 + \Delta T_1)\sin\gamma_x \tag{3.12}$$

Also, the change in initial pretension in each tendon leg was given as

$$\Delta T_1 = \frac{E*A*\Delta L}{L} \tag{3.13}$$

By Pythagoras theorem,

$$\Delta L = \sqrt{L^2 + {x_1}^2} - L \tag{3.14}$$

$$\sin\gamma_x = \frac{x_1}{\sqrt{L^2+{x_1}^2}} \tag{3.15}$$

Re-arranging Equation 3.12 yields

$$K_{11} = \frac{4(T_0+\Delta T_1)}{\sqrt{L^2+{x_1}^2}} \tag{3.16}$$

In addition, by taking the summation of vertical forces in Figure 3.3 in the displaced position, this yielded:

$$K_{31}x_1 + F_B = 4(T_0 + \Delta T_1)\cos\gamma_x + W \tag{3.17}$$

University of Malaya

Again, re-writing Equation 3.17 resulted in

$$K_{31} = \frac{4T_0}{x_1}(\cos\gamma_x - 1) + \frac{4\Delta T_1}{x_1}\cos\gamma_x \quad (3.18)$$

$$\cos\gamma_x = \frac{L}{\sqrt{L^2 + {x_1}^2}} \quad (3.19)$$

Furthermore, the summation of moments about y-axis in Figure 3.3 yielded

$$K_{51}x_1 + 4(T_0 + \Delta T_1)\sin\gamma_x * h = 0 \quad (3.20)$$

$$K_{51} = -\frac{4(T_0 + \Delta T_1)\sin\gamma_x * h}{x_1} \quad (3.21)$$

By combining Equations 3.16 and (3.2) then

$$K_{51} = -hK_{11} \quad (3.22)$$

From Figure 3.3, 'h' is the distance measured from the TLP centre of gravity and the bottom of the platform. The negative sign came up due to the counterclockwise moment. There was no restoring force in K_{21} and no roll moment K_{41} because arbitrary displacement along the surge had no influence along the sway and roll direction. Similarly, there no rotation in K_{61} due to symmetry.

3.2.3.2 Sway motion

Similar to the surge restoring stiffness formulation, an arbitrary displacement was given along the sway direction (y-direction) as in Figure 3.4. The coefficients of the second column of Equation 3.46 yielded K_{22}, K_{32} and K_{42} in a manner similar to the surge motion.

University of Malaya

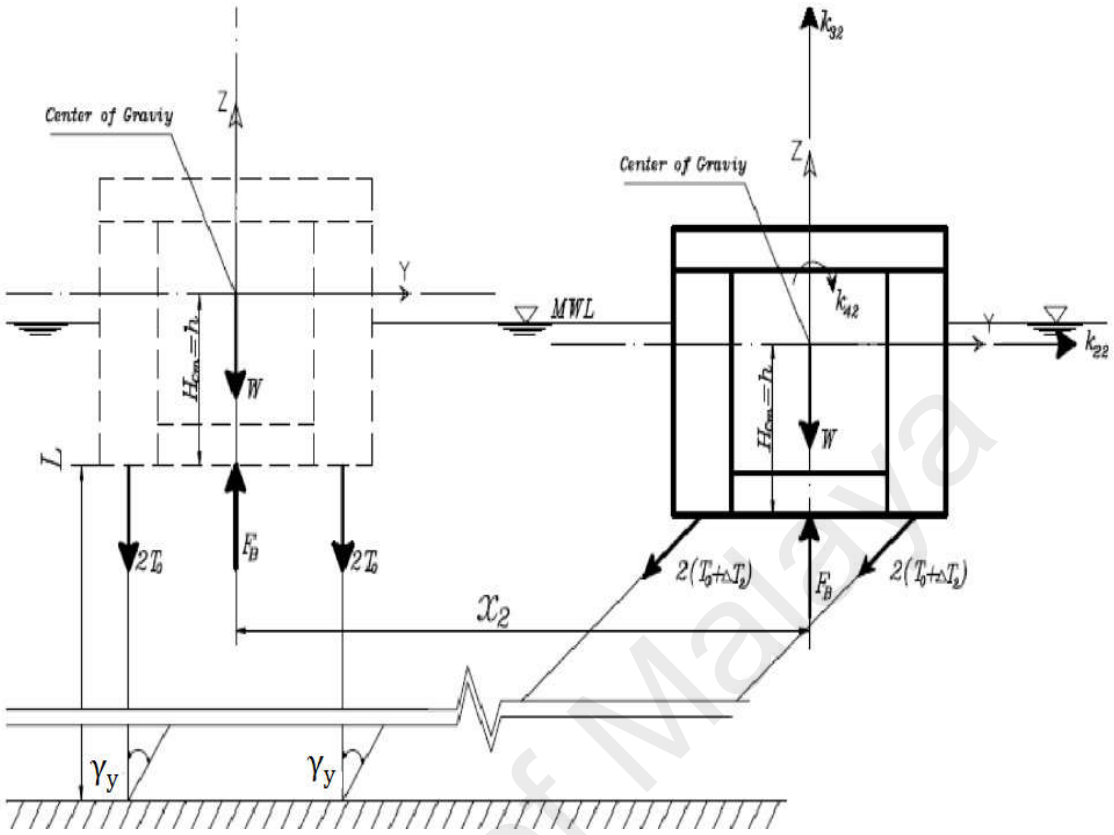

Figure 3.4: Sway displacement
Abou-Rayan et al. (2012)

By writing the equilibrium equation in the sway direction for the Figure 3.4, the result was

$$K_{22}x_2 = 4(T_0 + \Delta T_2)\sin\gamma_x \tag{3.23}$$

$$K_{22} = \frac{4(T_0+\Delta T_2)}{\sqrt{L^2+{x_2}^2}} \tag{3.24}$$

Again, the summation of vertical forces resulted in

$$K_{32} = \frac{4T_0(\cos\gamma_y - 1)}{x_2} + \frac{\Delta T_2}{x_2}\cos\gamma_y \tag{3.25}$$

$$\cos\gamma_y = \frac{L}{\sqrt{L^2+{x_2}^2}} \tag{3.26}$$

From Equation 3.24 and Equation 3.26, Equation 3.25 can be written in a compact form as

University of Malaya

$$K_{32} = \frac{\left\{4T_0\left(\frac{L}{\sqrt{L^2+x_2{}^2}}-1\right)\right\}+4\Delta T_2\frac{L}{\sqrt{L^2+x_2{}^2}}}{x_2} \quad (3.27)$$

Next, the summation of moments about the x-axis in Figure 3.4 yielded

$$K_{42}x_2 + 4(T_0 + \Delta T_2)\ \sin\gamma_y * h = 0 \quad (3.28)$$

$$\sin\gamma_y = \frac{x_2}{\sqrt{L^2+x_2{}^2}} \quad (3.29)$$

$$K_{42} = -\frac{4(T_0+\Delta T_2)\ \sin\gamma_y * h}{x_2} \quad (3.30)$$

By combining Equation 3.24 and Equation 3.29, the result was in the form of Equation 3.31

$$K_{42} = -h * K_{22} \quad (3.31)$$

The increase in tension in the sway direction was given as

$$\Delta T_2 = \frac{E*A*\Delta L}{L} \quad (3.32)$$

3.2.3.3 Heave motion

Apart from arbitrary displacements along x and y degree of freedoms, arbitrary displacement, x_3 along z-direction yielded coefficient in the third column of Equation 3.46. The vertical summation of forces was calculated as follows:

$$K_{33}x_3 + (F_B - \Delta F_B) - 4(T_0 + \Delta T_3) - W = 0 \quad (3.33)$$

The change in buoyancy force, ΔF_B and change in tension in heave direction, ΔT_3,were calculated as

$$\Delta F_B = \left(\frac{\pi}{4}D^2\rho_w g x_3\right) * 4 \quad (3.34)$$

$$\Delta T_3 = \frac{E*A}{L}x_3 \quad (3.35)$$

The equilibrium of forces yielded

University of Malaya

$$K_{33} = \frac{4EA}{L} + \pi D^2 \rho_w g x_3 \quad (3.36)$$

3.2.3.4 Roll motion

In order to derive coefficients in the fourth column of the stiffness matrix, an arbitrary rotation was given about the x-axis in Figure 3.5. The summation of forces in the z-direction led to

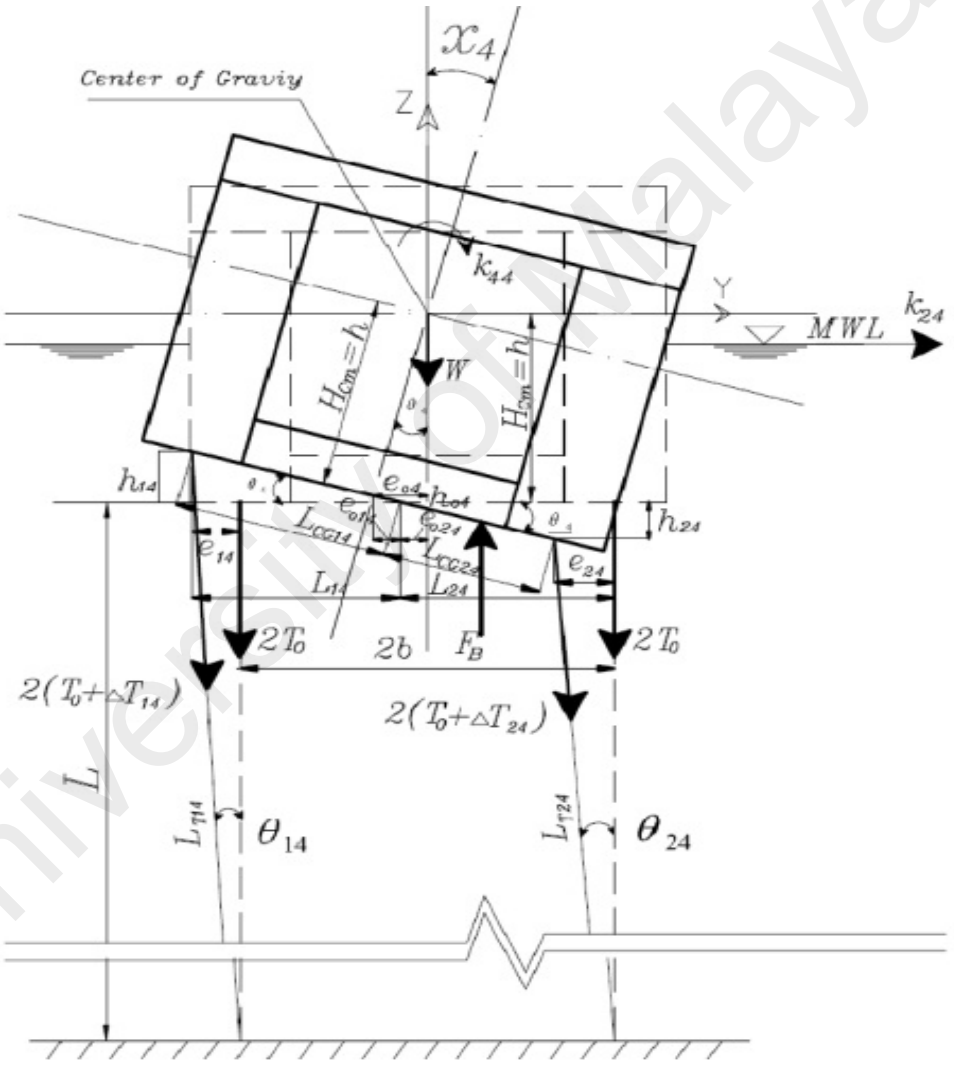

Figure 3.5: Roll displacement
Abou-Rayan et al. (2012)

$$K_{34}x_4 + F_B = [2(T_0 + \Delta T_{14})\cos\theta_{14} + 2(T_0 - \Delta T_{24})\cos\theta_{14} + W] \quad (3.37)$$

University of Malaya

Due to the symmetry, change in tension in the near and rear tendon legs were equal and expressed as

$$\Delta T_{14} = \Delta T_{24} = \frac{AE}{L} x_4 \tag{3.38}$$

$$K_{34} = \frac{2}{x_4} (\Delta T_{14} + \Delta T_{24}) \tag{3.39}$$

However, $K_{34} = 0$ for the TLP tendons that is symmetrically placed to each other as observed in the case at hand.

Again, the moment of resultant forces about the x-axis in Figure 3.5 was formulated as:

$$K_{44} = F_B * e_{04} + \langle 2(T_0 + \Delta T_{14}) \cos\theta_{14} * (b + e_{14}) - 2(T_0 + \Delta T_{24}) \cos\theta_{14} * (b - e_{14}) \rangle * {}^{1}/_{x_4} \tag{3.40}$$

3.2.3.5 Pitch motion

The coefficients of the fifth column for the stiffness matrix as a result of pitching were derived by giving an arbitrary moment about the y-axis in Figure 3.6.

University of Malaya

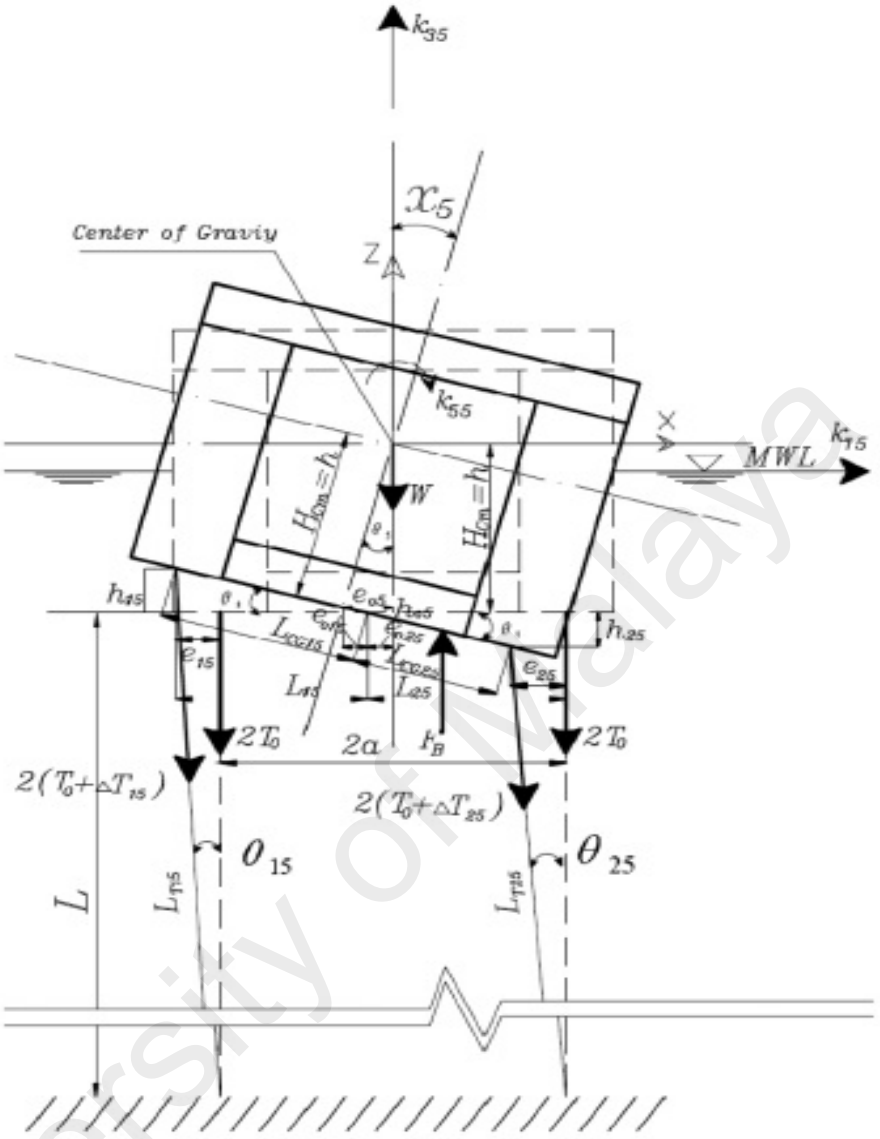

Figure 3.6: Pitch displacement
Abou-Rayan et al. (2012)

The equilibrium of forces in the heave direction yielded

$$K_{35} = \langle 2(T_0 + \Delta T_{15}) + 2(T_0 + \Delta T_{25}) - 4T_0 \rangle * {}^{1}/_{x_5} \quad (3.41)$$

Due to symmetry, $K_{35} = 0$

Again, by taking the moment of resultant forces about the x-axis in Figure 3.6,

$$K_{55} = F_B * e_{05} + \langle 2(T_0 + \Delta T_{15}) \cos\theta_{15} * (a + e_{25}) - 2(T_0 + \Delta T_{25}) \cos\theta_{25} * (a - e_{25}) \rangle * {}^{1}/_{x_5} \quad (3.42)$$

University of Malaya

3.2.3.6 Yaw motion

Finally, elements of the sixth column of the master stiffness matrix occurs when the TLP was rotated about the z-axis as in Figure 3.7, the stiffness coefficients were obtained by taking the summation of moment about the z-axis to be

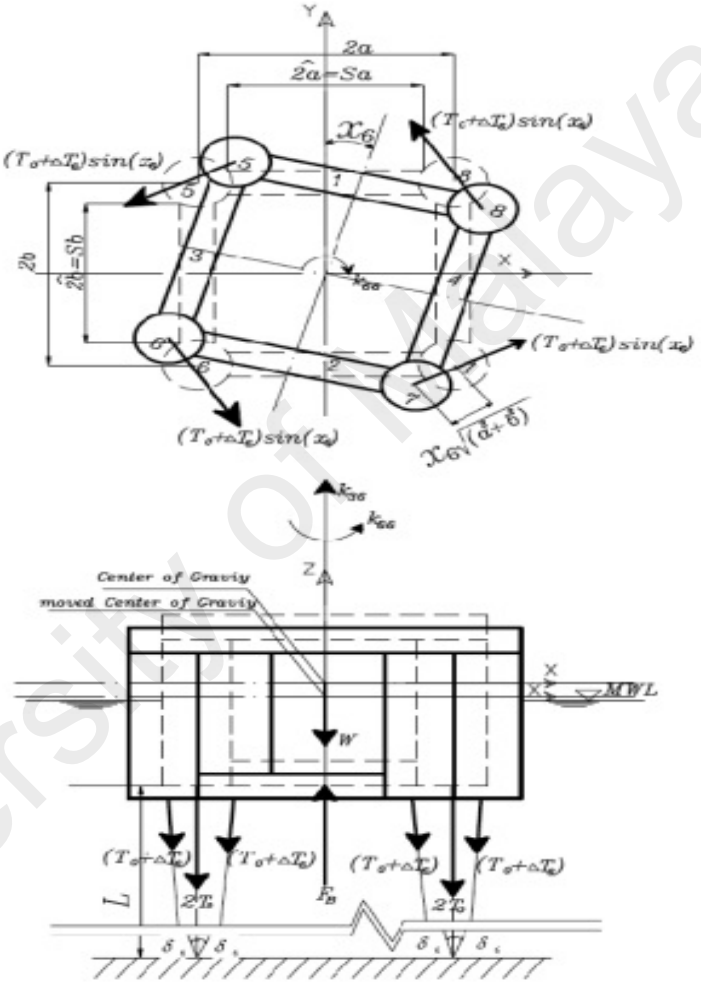

Figure 3.7: Yaw displacement
Abou-Rayan et al. (2012)

$$K_{66} = 4(T_0 + \Delta T_6) * (a^2 + b^2)/[L^2 + {x_6}^2 (a^2 + b^2)]^{05} \quad (3.43)$$

ΔT_6 is the change in tendon tension force as a result of yaw rotation and this was given as:

$$\Delta T_6 = \frac{AE}{L}([L^2 + {x_6}^2 (a^2 + b^2)]^{05} - L) \quad (3.44)$$

University of Malaya

Similarly, the equilibrium of vertical forces in the z-direction resulted in

$$K_{36} = \left[\frac{4T_0}{x_6}\left(\frac{L}{[L^2 + {x_6}^2\,(a^2 + b^2)]^{05}} - 1\right) + \frac{4\Delta T_6}{x_6}\left(\frac{L}{[L^2 + {x_6}^2\,(a^2 + b^2)]^{05}}\right)\right] \tag{3.45}$$

From the foregoing, the elements of the resulting coupled stiffness matrix are assembled in Equation 3.46 as

$$[\mathrm{K}] = \begin{bmatrix} K_{11} & 0 & 0 & 0 & K_{15} & 0 \\ 0 & K_{22} & 0 & K_{24} & 0 & 0 \\ K_{31} & K_{32} & K_{33} & K_{34} & K_{35} & K_{36} \\ 0 & K_{42} & 0 & K_{44} & 0 & 0 \\ K_{51} & 0 & 0 & 0 & K_{55} & 0 \\ 0 & 0 & 0 & 0 & 0 & K_{66} \end{bmatrix} \tag{3.46}$$

Where, T_0 = Initial pretension in the tendons; L = Length of tendon; E = Modulus of elasticity; A = total cross-sectional area of tendons in one leg; x_1, x_2, x_3 = displacements in positive surge, sway and heave directions respectively; x_4= arbitrary rotation about x-axis; x_5= arbitrary rotation about y-axis; x_6= arbitrary rotation about z-axis; h = distance between Centre of Gravity (COG.) and the bottom of the platform; F_B = total upward buoyant force; e_{04} = perpendicular distance of new centre of buoyancy from x-axis through COG.; e_{05} = perpendicular distance of new centre of buoyancy from y-axis through COG.; $(b + e_{14})$, $(b - e_{14})$ = horizontal tendon distances from the centre of gravity along x-axis; $(a + e_{14})$, $(a - e_{14})$= horizontal tendon distances from the centre of gravity along y-axis; ΔT= Change in tendon tension; ΔL= Change in tendon length; γ = Angle of tendon with the vertical axis; ρ_w = mass density of water; [K] = stiffness matrix; 2a, 2b = length and breadth of TLP; D = Diameter of cylinder; K_{ij} = stiffness coefficients.

University of Malaya

3.3 Simulation of sea waves and water particle kinematics

Sea waves were generated as a result of wind drag on the surface of the water. The waves can be regarded as the moving succession of irregular humps and hollows on the ocean surface, Dawson (1983). For the simulation at hand and in order to calculate wave velocity, acceleration and pressure under the water surface, both regular and random sea waves were simulated following the linear Airy wave theory. The assumption of the theory is that wave height is small in comparison to the wavelength and water depth as shown in Figure 3.8.

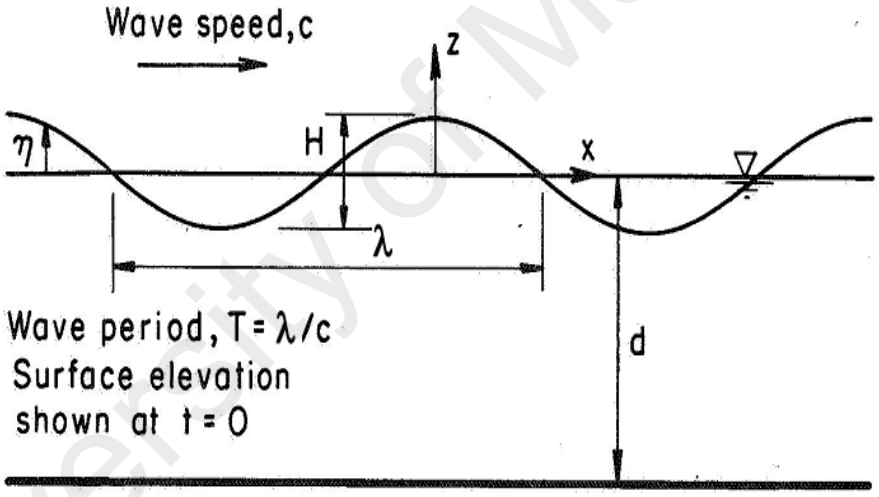

Figure 3.8: Representation of wave profile

3.3.1 Regular sea waves

The wave profile for the regular wave was determined using the parameters given in Figure 3.8. The water particle kinematics and pressure were calculated for the submerged length of TLP column and pontoon, up to the instantaneous water surface. The definitions of the parameters are: d = water depth; H = wave height; λ = wave length; T = wave period; η = wave profile. The wave travelling along the x-z direction was computed by considering

University of Malaya

the governing equation for velocity potential with their respective boundary conditions as found in standard texts such as Dawson (1983) and Chakrabarti (2005).

The wave profile equation was given in Equation 3.47 as:

$$\eta(x, z, t) = \frac{H}{2} \cos \Theta \tag{3.47}$$

Where

$$\Theta = k\,(x \cos\beta + z \sin\beta) - \omega t \tag{3.48}$$

Θ is the wave phase; and β is the direction of propagation measured from the positive x-axis.

$$k = \frac{2\pi}{L} \quad \text{is the wave number} \tag{3.49}$$

$$\omega = \frac{2\pi}{T} \text{ is the wave circular frequency} \tag{3.50}$$

The relationship between wave period and wavelength was given by the dispersion equation as

$$\omega^2 = gk \tanh kd \tag{3.51}$$

By differentiating the wave profile equation with respect to 'x' and 'z' coordinates, the accompanying horizontal and vertical velocities from the motion were calculated and stated in Equations 3.52 and 3.53 as

$$u = \frac{\omega H}{2} \frac{\cosh kz}{\sinh kd} \cos\,(kx - \omega t) \tag{3.52}$$

$$v = \frac{\omega H}{2} \frac{\sinh kz}{\sinh kd} \sin\,(kx - \omega t) \tag{3.53}$$

The water particle accelerations were calculated by differentiating velocities with respect to time and written in Equations 3.54 and 3.55 as:

$$a_x = \frac{\omega^2 H}{2} \frac{\cosh kz}{\sinh kd} \sin\,(kx - \omega t) \tag{3.54}$$

$$a_y = -\frac{\omega^2 H}{2} \frac{\sinh kz}{\sinh kd} \cos\,(kx - \omega t) \tag{3.55}$$

University of Malaya

The dynamic pressure for the linear wave theory was given as

$$P = \rho g \frac{H}{2} \frac{\cosh kz}{\cosh kd} \cos(kx - \omega t) + \rho g (d - z) \quad (3.56)$$

3.3.2 Random sea waves

A more realistic ocean environment was modelled by summing the individual wave components of different directions, frequencies, phases and amplitudes altogether. Here, ocean surface was assumed to be a random field that is stationary in time, homogeneous in space and ergodic in nature. Since wave generates free surface motion, superposition of the regular waves with Gaussian random variable was used to create random waves. The random waves were simulated as unidirectional and directional sea waves.

3.3.2.1 Unidirectional and directional sea waves

The wave profile for unidirectional and directional sea waves were stated in Equations 3.57 and 3.59 to be

$$\eta(x,t) = \sum_{i=1}^{N} A_i \cos(k_i x - w_i t + \emptyset_i) \quad (3.57)$$

$$A_i = \sqrt{2\, S_{\eta\eta}(w_i) \Delta w_i} \quad (3.58)$$

$$\eta(x,y,t) = \sum_{i=1}^{k} A_i \cos[k_i (x \cos\theta_i + y \sin\theta_i) - w_i t + \emptyset_i] \quad (3.59)$$

$$A_i = \sqrt{2 S_{\eta\eta}(w_i) D(W, \theta) \Delta w_i \Delta\theta_i} \quad (3.60)$$

Where N is the number of wave components; A_i is the amplitude of the ith wave component; k_i is wave number of the ith wave component; x is the x-coordinate of the point along the wave direction. The $\emptyset_i$ represent the phase angle for the individual wave, which are random variables in nature and uniformly distributed between (0, 2π). Furthermore, Equation 3.57 was differentiated with respect to x and z and this led to the estimation of the horizontal and vertical water velocities in Equations 3.61 and 3.62 respectively. Further

University of Malaya

differentiation with time yielded water particle accelerations are expressed in Equations 3.63 and 3.64

$$\dot{u}\,(x,t) = \sum_{i=1}^{k} A_i w_i \cos(k_i x - w_i t + \phi_i)\,\frac{\cosh k_i z}{\sinh(k_i(d+\eta))} \tag{3.61}$$

$$\dot{v}\,(x,t) = \sum_{i=1}^{K} A_i\, w_i \sin(k_i x - w_i t + \phi_i)\,\frac{\sinh k_i z}{\sinh(k_i(d+\eta))} \tag{3.62}$$

$$\ddot{u}(x,t) = \sum_{i=1}^{K} A_i\, {w_i}^2 \sin(k_i x - w_i t + \phi_i)\frac{\cosh k_i z}{\sinh(k_i(d+\eta))} \tag{3.63}$$

$$\ddot{v}(x,t) = -\sum_{i=1}^{K} A_i\, {w_i}^2 \cos(k_i x - w_i t + \phi_i)\frac{\sinh k_i z}{\sinh(k_i(d+\eta))} \tag{3.64}$$

The linear airy wave theory is limited to water particle kinematics calculation up to the mean water level only. In order to include the wave profile, several extrapolations were proposed such as hyperbolic extrapolation by Hogben and Standing (1974), linear extrapolation was adopted by Nwogu and Irani (1990), Wheeler stretching approximation was suggested by Wheeler (1969) and Chakrabarti approximation as proposed by Chakrabarti (1971). The Chakrabarti approach was adopted and the water particle kinematics modification up to the wave free surface was included in Equations 3.61 to 3.64. By looking at the water particle kinematics equations as stated above, the equations comprised of three distinct components. These are wave amplitude, which is independent of water depth, variation of water depth as attenuation in the form of hyperbolic function and parameter that depends on time and position. For deep-water formulation, the attenuation part was modified according to the recommendation from Dawson (1983) as follows:

$$\sinh kd = \frac{e^{kd} - e^{-kd}}{2} \approx \frac{1}{2} e^{kd} \tag{3.65}$$

$$\cosh kd = \frac{e^{kd} + e^{-kd}}{2} \approx \frac{1}{2} e^{kd} \tag{3.66}$$

$$\tanh kd = \frac{e^{kd} - e^{-kd}}{e^{kd} + e^{-kd}} \approx 1 \tag{3.67}$$

University of Malaya

The dispersion relation for the deep-water case was simplified and given as

$$w^2 = gk \tag{3.68}$$

This can also be formulated in terms of wavelength and wave period as follows

$$L = \frac{g}{2\pi} T^2 \tag{3.69}$$

As earlier reported, random wave was simulated as the summation of different regular wave components. The contribution of each component was accounted for via the wave spectrum. Quite a number of empirical wave spectra that were simulated from the collected data over time and for a particular place are available. Some of the wave spectra include the Pierson Moskowitz (PM) spectrum, the Joint North Sea Wave Project (JONSWAP), the TMA spectrum, the Bretschneider spectrum, the Torsethaugen spectrum and the Ochi-Hubble spectrum among many others. A modified Pierson-Moskowitz (PM) spectrum which was formulated based on significant wave height and angular peak frequency was adopted from Veritas (2007) and represented in Equation 3.70 as

$$\mathrm{S_{PM}(w)} = \frac{5}{16} \mathrm{H_s^2 w_p^4 w^{-5}} exp\left\{-\frac{5}{4}\left(\frac{\mathrm{w}}{\mathrm{w_p}}\right)^{-4}\right\} \tag{3.70}$$

Where

$\mathrm{S_{PM}(w)}$ is the Pierson Moskowitz (PM) spectrum; $\mathrm{H_s}$ is the significant wave height; $\mathrm{w_p}$ is the angular peak frequency. With the known wave spectrum, the linear wave theory and the wave height, synthetic sea state was simulated using random phase method, Chakrabarti (1987). The algorithm for Monte Carlo simulation of individual wave frequencies and their bandwidths were simulated from the Borgman (1967) and Goda (1970). A similar approach was adopted by Ahmad (1996) and, Chandrasekaran and Jain (2002b) respectively. The individual component frequencies $w_1, w_2, w_3, \ldots w_N$ are required to be non-correlating so

University of Malaya

that they will not constitute harmonics. The selection of frequency was achieved in FORTRAN by dividing the range of frequency from the lowest, w_{min} to the highest, w_{max} into (N-1) sub-ranges with the dividing frequencies constituting a power series of

$$w_{1'} = w_{min} + \frac{w_{max} - w_{min}}{N-1} \tag{3.71}$$

$$w_{2'} = w_1{}' \times C_N \ldots, \tag{3.72}$$

$$w_{i'} = w_{i-1'} \times C_N \tag{3.73}$$

$$w_{N-1'} = w_{1'} \times C_N{}^{N-2} \tag{3.74}$$

Where

$$C_N = \left[\frac{w_{max}}{w_{1'}}\right]^{1/(K-2)} \tag{3.75}$$

This was followed with the secondary dividing frequencies w''_1, w''_2, w''_3, ... w'_{N-1} that were chosen at random from the respective sub-ranges. The initial frequency w''_0 was set equal to w_{min} and the last was as $w_{N''} = w_{max}$. The selection was done with the aid of random number generation. The component frequency, w_i and its band width Δw_i were calculated for i = 1, 2, 3….. N as

$$w_i = \frac{1}{2}(w''_{i-1} + w''_i) \tag{3.76}$$

$$\Delta w_i = w''_i - w'_{i-1} \tag{3.77}$$

The random process for the wave component frequency described above was repeated for each run of the wave spectrum. The phase angle for each wave was achieved with the help of the in-built random number in the FORTRAN software in the range of (0, 2π) so that the wave profile function would follow the Gaussian distribution. The number of component waves, length of time step and duration of wave record were controlled so as to realize an ocean environment that has characteristics of the real sea state. The length of time step for the simulation of the wave profile equation and the numerical Newmark-Beta

University of Malaya

equation was controlled so that the time interval satisfied the condition of $\Delta t \leq {}^{1}/_{5f_{max}}$. The value of 0.2 seconds, which was smaller than the required was used as time step for the simulation. The duration of the simulated wave record was 5000 seconds and 25000 data points were generated in one run for the random waves.

From the uni-directional wave spectrum, cosine power-type energy spreading function of directional short-crested wave spectra was expressed according to Veritas (2007) as

$$S(w,\theta) = S(w)\, D(\theta, w) = S(w)\, D(\theta) \qquad (3.78)$$

Where $D(\theta, w)$, and $D(\theta)$ are directionality functions, θ is the angle between the direction of elementary wave trains and the main wave direction of the short-crested wave system. The directional function, $D(W, \theta)$ for wind sea in Equation 3.78 was simulated with the frequency-dependence neglected and the approximation of $D(W, \theta) = D(\theta)$. The directional function used in this study was also employed in Sannasiraj et al. (1995) as given below

$$D(\theta) = \frac{\Gamma(1+{}^{n}/_{2})}{\sqrt{\pi}\Gamma(1/2+n/2)} \cos^{n}(\theta - \theta_p) \qquad (3.79)$$

Γ is the Gamma function and $\left|\theta - \theta_p \leq \frac{\pi}{2}\right|$ (3.80)

$D(\theta)$ is the directional function; θ_p as the main wave direction, and 'n' is a constant ranging between n = 2 to n = 4 for wind sea. Veritas (2007)

3.4 Modified Morison wave force

A modified Morison equation that was based on strip method was employed to calculate the wave force on the submerged portion of the TLP. Figure 3.9 shows the regions where the Morison formula is applicable and the ISSC TLP lies in region III of the small drag and large inertia. From the calculation of diffraction parameter and, the ratio of

University of Malaya

characteristic dimension to wavelength, it was established that the diameter of the member is small and did not distort the wave propagation.

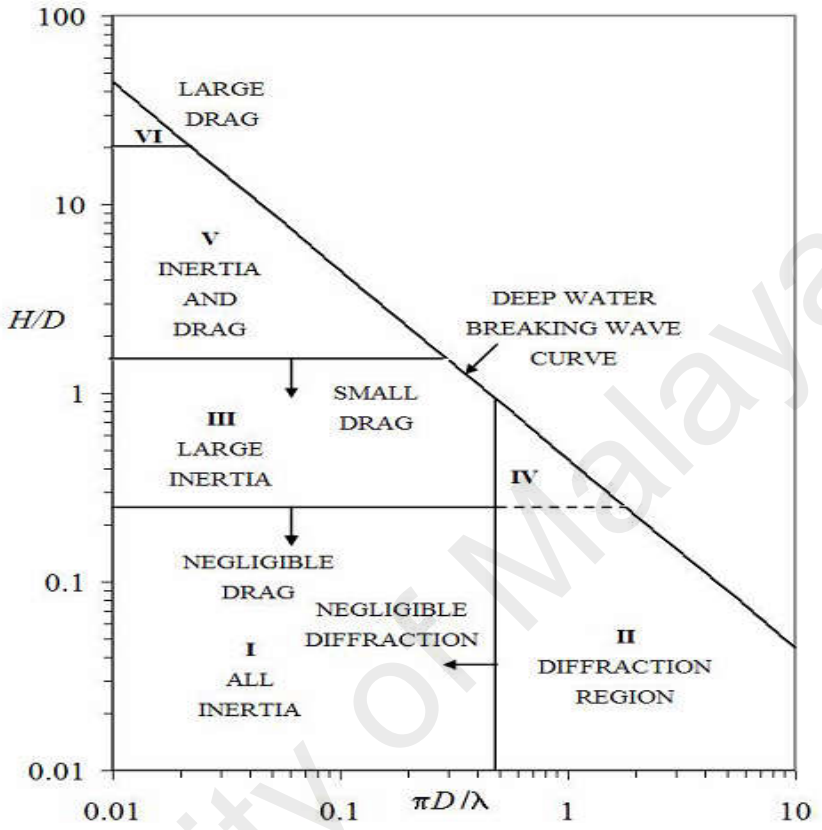

Figure 3.9 Limit of application of Morison formula for small versus large structure Chakrabarti (2005)

At each point (x, z, t) along the submerged length of the TLP, the Morison formula was used to compute the drag force that is proportional to the square of the water velocity, inertia force that is proportional to the acceleration, and added mass effects were also considered as the third term in Equation 3.81

$$f(x,z,t) = 0.5\rho_w C_D D\left|u - \dot{x} + \dot{U}_c\right|\left(u - \dot{x} + \dot{U}_c\right) + 0.25\pi D^2 \rho_w C_M \ddot{u} \pm 0.25\pi D^2 [C_M - 1]\rho_W \ddot{x} \quad (3.81)$$

3.4.1 Simulation of wave force on column and pontoon

The ISSC TLP has four cylindrical columns and four cylindrical pontoons with the numbering as shown in Figure 3.10. To determine the water kinematics properties and the

University of Malaya

hydrodynamic forces on these members, a 6 points coefficient Gauss-Legendre of numerical integration was programmed in FORTRAN and employed as

$$z = 05 * \quad (b1 + a1) + 05 * \quad (b1 - a1) * z \tag{3.82}$$

Where 'a1' and 'b1' are the lower and upper limit of integration as shown in Figure 3.10. Equation 3.82 is in accordance with Chapra and Canale (2012) for determining integral.

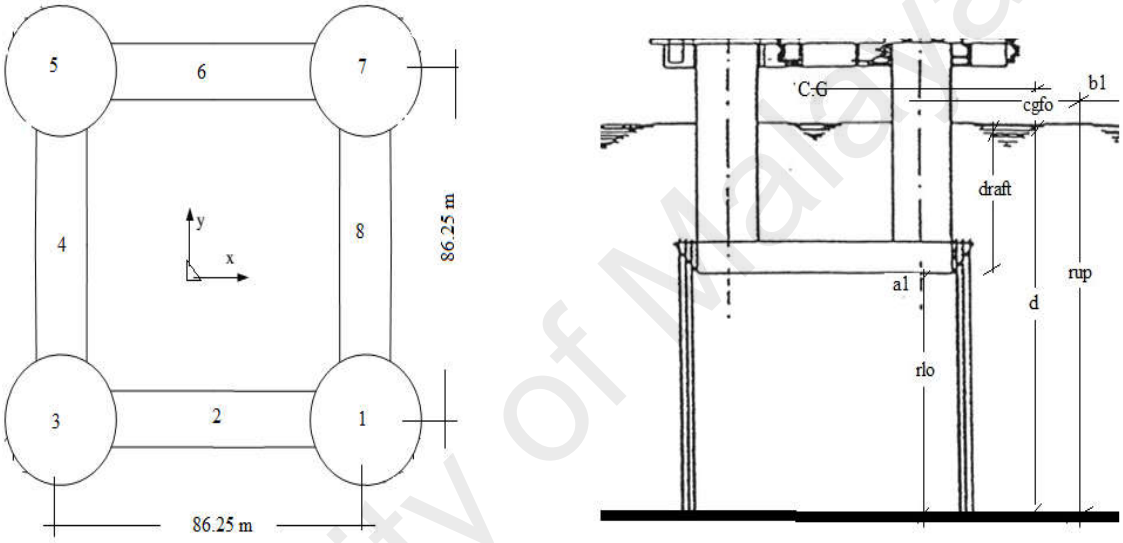

Figure 3.10: Sketch of TLP plan and elevation

For arbitrarily oriented cylinder, the angle of orientation needs to be specified. The orientation of the vertical column members is defined by 'phi' and 'theta' in the FORTRAN program to be zero. For horizontal members 2 and 6, phi is 90^0 and theta is 0^0 while members 4 and 8 have phi as 90^0 and theta as -90^0 respectively.

The water motion produces horizontal and vertical velocities; and accelerations along the x- and y-direction. The magnitude of the water velocity which is normal to the cylinder axis is given in Equation 3.83 in accordance with Dawson (1983)

$$\mathcal{V} = \left[u^2 + v^2 - \left(c_x u + c_y v\right)^2\right]^{1/2} \tag{3.83}$$

The velocity components along the x, y and z directions are

University of Malaya

$$u_n = u - c_x(c_x u + c_y v)$$

$$v_n = v - c_y(c_x u + c_y v)$$

$$w_n = -c_z(c_x u + c_y v) \tag{3.84}$$

Where

$$c_x = \sin phie \cos theta \ ;$$

$$c_y = \cos phie;$$

$$c_z = \sin phie \sin theta \tag{3.85}$$

The values of water acceleration in the x, y and z directions are as given below

$$a_{nx} = a_x - c_x(c_x a_x + c_y a_y)$$

$$a_{ny} = a_y - c_y(c_x a_x + c_y a_y)$$

$$a_{nz} = -c_z(c_x a_x + c_y a_y) \tag{3.86}$$

From the water kinematics calculated above, the force per unit of cylinder length in the x, y and z directions are given by general Morison equation as

$$f_x = \frac{1}{2}\rho C_D D v u_n + \rho C_I \frac{\pi D^2}{4} a_{nx}$$

$$f_y = \frac{1}{2}\rho C_D D v v_n + \rho C_I \frac{\pi D^2}{4} a_{ny}$$

$$f_z = \frac{1}{2}\rho C_D D v w_n + \rho C_I \frac{\pi D^2}{4} a_{nz} \tag{3.87}$$

The total force along the x, y and z directions were calculated by numerical integration with the limits covering the entire area where the hydrodynamic force acts as

$$F_x = \int_{a1}^{b1} f_x \, dz; \quad F_y = \int_{a1}^{b1} f_y \, dz;$$

$$F_z = \int_{a1}^{b1} f_z \, dz \ ; \ M_x = \int_{a1}^{b1} z * f_x \, dz;$$

$$M_y = \int_{a1}^{b1} z * f_y \, dz; \ M_z = \int_{a1}^{b1} z * f_z \, dz \tag{3.88}$$

University of Malaya

Due to the limited experimental data, drag and inertia coefficient constants were chosen from the range of (0.6 to 1.0) for drag and (1.5 to 2.0) for inertia as recommended by the American Petroleum Institute.

3.4.2 Total wave and current induced forces

Finally, the total force and moment on each column and pontoon along the six degrees of freedom were added together. The wave force was further simplified into surge, sway and heave components as stated in Equations 3.89 – 3.94.

$$\text{Surge Force} = F_x = \left[\sum_{k=1}^{n}\{F_{D_X}(k) + F_{I_X}(k)\}\right]_{\text{Column}} \cos\alpha + \left[F_{d_x} + F_{i_x}\right]_{\text{pontoon}} \quad (3.89)$$

$$\text{Sway Force} = F_Y = \left[\sum_{k=1}^{n}\{F_{D_Y}(k) + F_{I_Y}(k)\}\right]_{\text{Column}} \sin\alpha + \left[F_{d_Y} + F_{i_Y}\right]_{\text{pontoon}} \quad (3.90)$$

$$\text{Heave Force} = F_Z = [F_V]_{\text{Column}} + \left[F_{d_Z} + F_{i_Z}\right]_{\text{pontoon}} \quad (3.91)$$

The total force in the x, y and z directions are F_X, F_Y, and F_Z respectively. The parameter $\sum_{k=1}^{n}$ is the summation over the vertical column; k is the number of columns; α is the angle of wave incidence; F_D (k) and F_I (k) are total drag and inertia forces on k^{th} column; F_d and F_i are the total drag and inertia force on the pontoon; F_v is the total vertical hydrodynamic pressure force on the column bottom; and subscripts x, y and z represent the directions respectively.

Drag and inertia loadings on pontoon and vertical column members also caused moment about the x, y and z-axes which were known as roll, pitch and yaw moments respectively. These moments about the x, y and z- axes were obtained by multiplying the above-mentioned forces with their respective lever arms and with respect to their axes of rotations as follows:

University of Malaya

$$M_x = [\sum_{k=1}^{n}\{M_D(k) + M_I(k)\}]_{Column} \sin\alpha + [M_{v_x} + M_{h_x}]_{hull} + [M_{p_x}]_{Column} \quad (3.92)$$

$$M_y = [\sum_{k=1}^{n}\{M_D(k) + M_I(k)\}]_{Column} \cos\alpha + [M_{v_y} + M_{h_y}]_{hull} + [M_{p_y}]_{Column} \quad (3.93)$$

$$M_z = \sum_{k=1}^{n}[F_D(k) + F_I(k)]\, y_k \quad (3.94)$$

3.4.3 Current force

The parameter $\dot{U}_c$ in the first component of Equation 3.81 is the wind-drift current velocity. This was modelled with linear profile in the form of Equation 3.95 and taken to be steady, horizontal and linearly varying with the water depth as

$$\dot{U}_{c,tide} = \dot{U}_{c,tide}(0)\left(\frac{z}{d}\right) \quad (3.95)$$

Where

$\dot{U}_c$ is the current velocity at the level z, $z \leq 0$; z is the distance from the Still Water Level (SWL) and positive upwards; $\dot{U}_{c,tide}(0)$ is the tidal current velocity at the SWL; d is the water depth to the SWL.

3.4.4 Wind forces

The superstructure of the tension leg platform, which lies above the still water line, is open to the wind forces, also known as aerodynamic forces. The wind forces on the TLP are primarily governed by the local wind speed for the TLP location. This is calculated by using simplified approach where the force is made proportional to the square of the relative velocity through the use of the slope coefficients. However, for the computation of wind force per unit area acting above the still water line part of the TLP, wind speed profile, the Simiu and Leigh wind spectrum and American Petroleum Institute (API) spectrum were

University of Malaya

used in FORTRAN coding and Abaqus/Aqua module respectively. The overall wind load on the platform is given in Equation 3.96 as

$$F_u(t) = 0.5\rho_a C_a A_a [\bar{u}(z) + U_{eq}'(t) - \dot{x}(t)]^2 \quad (3.96)$$

Where,

ρ_a = Mass density of the air, C_a is the wind drag coefficient, A_a is the projected area along the wind direction, $\bar{u}(z)$ is the mean wind speed, $U_{eq}'(t)$ is the fluctuating wind component, $\dot{x}$ is the structural velocity.

In Equation 3.96, it was assumed that the directions of the mean wind and wave force on the platform surge motion coincide with each other.

The wind speed u (y, z, t) may be expressed as the summation of mean and fluctuating part of the wind as written in Equation 3.97:

$$u(y,z,t) = \bar{u}(z) + u'(y,z,t) \quad (3.97)$$

Where

$\bar{u}(z)$ is the mean wind speed; and $u'(y,z,t)$ is the fluctuating wind velocity. These two components were evaluated in the manner discussed below.

3.4.4.1 Mean wind speed

The wind speed above the sea surface varies with time and height. In order to estimate the value of wind speed at the height 'z', the mean wind speed at the reference height together with the logarithmic wind speed profile from Veritas (2007), and Simiu and Leigh (1984) was used in Equation 3.98 as

University of Malaya

$$\bar{u}(z) = \bar{u}(z_{ref}) \frac{\ln\left[z / z_0 \right]}{\ln\left[z_{ref} / z_0 \right]} \tag{3.98}$$

Where,

z_{ref} = reference elevation which is considered as 10 m.

z_o = Terrain roughness parameter over the sea surface. This is estimated following Simiu and Leigh (1984) approach as:

$$z_0 = \frac{10}{\exp\left(\frac{K}{\sqrt{C_{D_{sea}}}} \right)} \tag{3.99}$$

Where K is the Von Karman's constant and C_{Dsea} is the drag coefficient. The roughness length from the sea drag coefficient $C_{d\ sea}$ expression is calculated as 0.002 and K = 0.4 respectively.

$$C_{Dsea} = \left[\frac{K}{\ln\left(\frac{10}{z_0} \right)} \right]^2 \tag{3.100}$$

3.4.4.2 Fluctuating wind velocity

The empirical formula of the Simiu and Leigh wind spectrum $S_u(z, n_i)$ which is suitable for the estimation of low-frequency energy in the ocean is programmed in the FORTRAN. The detail of the spectrum as stated in the Equation 3.101 was extracted from Simiu and Leigh (1984), and Ahmad et al. (1997).

$$\frac{nS_u(z,n_i)}{U^2} = \begin{cases} a_1 f + b_1 f^2 + d_1 f^3 & for 0 < f \leq f_m \\ c_2 + a_2 f + b_2 f^2 & for f_m < f < f_s \\ 0.2\ 6 f^{-2/3} & for f \geq f_s \end{cases} \tag{3.101}$$

University of Malaya

This spectrum was then divided into a finite number of strips so as to estimate the fluctuating wind velocity component using the Monte-Carlo technique as written in Equation 3.102.

$$u'_{eqi} = \sqrt{\left(2S_u\left(z, n_i\right)\Delta n_i\right)} \tag{3.102}$$

For this purpose, each strip of the division was of 'Δn_i' width and $S_u\left(z, n_i\right)$ represents the spectrum with longitudinal velocity of $\left(u'_{eqi}\right)$. The summation of velocities of 'k' such-strips represents approximately the instantaneous velocity. The fluctuating component of velocity having the frequencies n_i, i = 1 …k, with random phases was expressed as follows:

$$u' = \sum_{i=1}^{k} u'_{eqi} \cos\left(2\pi n_i t + \phi_i\right) \tag{3.103}$$

The phase angle was represented by $\emptyset_i$ in the Equation (3.103) for each frequency component of the velocity. This was generated with in-built random numbers and was randomly sampled for each frequency component from a uniform distribution in the interval of $0 < \phi_i < 2\pi$. The simulation of time history for velocity fluctuations was achieved with this equation.

3.5 Assembly and solution of equation of motion for UNAP-TLP-2016

The mathematical model for the mass, stiffness and damping matrices and for force vector in Equation 3.1 was assembled and reformulated in the time domain step. The model consists of nonlinearity from hydrodynamic force, structural configuration and structural response. This equation included the effect of acceleration-dependent inertia forces and velocity-dependent damping force. The Newmark method also known as the constant average acceleration method which is unconditionally stable due to the acceleration

University of Malaya

assumptions and iteration in each time step, is adopted for the solution of the problem. The dynamic equation for the next time step is shown in Equation 3.104.

$$M\ddot{U}^{t+\Delta t} + C\dot{U}^{t+\Delta t} + KU^{t+\Delta t} = \left\{\mathbf{F}\left(t, U, \dot{U}\right)\right\}^{t+\Delta t} \quad (3.104)$$

The method was founded on the assumptions that acceleration varies in each time step as:

$$\dot{U}^{t+\Delta t} = \dot{U}^{t} + \left[(1-\delta)\ddot{U}^{t} + \delta\ddot{U}^{t+\Delta t}\right]\Delta t \quad (3.105)$$

$$U^{t+\Delta t} = U^{t} + \dot{U}^{t}\Delta t + \left[\left(\frac{1}{2} - \alpha\right)\ddot{U}^{t} + \alpha\ddot{U}^{t+\Delta t}\right]\Delta t^{2} \quad (3.106)$$

To determine the displacement at the next time step, $U^{t+\Delta t}$, $\ddot{U}^{t+\Delta t}$ is solved in terms of $U^{t+\Delta t}$ and substituted into Equation 3.105. This yields expression for $\ddot{U}^{t+\Delta t}$ and $\dot{U}^{t+\Delta t}$ in terms of $U^{t+\Delta t}$. These terms were then substituted into Equation 3.104 for the computation of $U^{t+\Delta t}$. The value was substituted into Equation 3.105 and 3.106 to calculate $\ddot{U}^{t+\Delta t}$ and $\dot{U}^{t+\Delta t}$. The second ordinary differential equation of Equation 3.104 is nonlinear, changes at every time step and also the variation in tendon tension makes the TLP response-dependent in nature.

In order to cater for these changes, a stable and accurate numerical method is essential. The Newmark-beta integration method was adopted due to the inherent parameters (α and δ) in the method that control the accuracy and stability. The algorithm for the numerical method from Bathe (1982) was programmed in the following sequence inside the FORTRAN as follows:

1. Formulation of stiffness matrix 'K', mass matrix 'M' and damping matrix 'C'
2. Initialize values for U, $\dot{U}$, $\ddot{U}$
3. Assign values to time step Δt and to parameters α and δ. This was followed with computation of the following integration constants:

$$\delta \geq 0.5\ \alpha \geq 0.25\ (\delta + 0.5)^2;$$

University of Malaya

$$a_0 = \frac{1}{\alpha(\Delta t)^2}\ ;\ \ a_1 = \frac{\delta}{\alpha\,\Delta t}\ ;\ a_2 = \frac{1}{\alpha\,\Delta t}\ ;\ \ a_3 = \frac{1}{2\,\alpha} - 1;\ \ a_4 = \frac{\delta}{\alpha} - 1;\ \ a_5 = \frac{\Delta t}{2}\left(\frac{\delta}{\alpha} - 2\right);$$

$$a_6 = \Delta t(1-\delta);\ a_7 = \delta\Delta t \qquad (3.107)$$

4. Formulation of effective stiffness matrix, $\widehat{K}$

$$\widehat{K} = K + \alpha_0 M + \alpha_1 C \qquad (3.108)$$

5. Triangularization of the matrix

$$\widehat{K} = LDL^T K \qquad (3.109)$$

At each time step

6. Computation of the effective load vector

$$\hat{F}_{t+\Delta t} = F_{t+\Delta t} + M\left(\alpha_0 U_t + \alpha_2 \dot{U}_t + \alpha_3 \ddot{U}_t\right) + C\left(\alpha_1 U_t + \alpha_4 \dot{U}_t + \alpha_5 \ddot{U}_t\right) \qquad (3.110)$$

7. Solution for displacement at time '$t + \Delta t$'

$$(LDL^T)_{t+\Delta t} x = \hat{F}_{t+\Delta t} \qquad (3.111)$$

8. Computation of accelerations and velocities at time '$t + \Delta t$'

$$\ddot{U}_{t+\Delta t} = \alpha_0 (U_{t+\Delta t} - U_t) - \alpha_2 \dot{U}_t - \alpha_3 \ddot{U}_t \qquad (3.112)$$

$$\dot{U}_{t+\Delta t} = \dot{U}_t + \alpha_6 \ddot{U}_t + \alpha_7 \ddot{U}_{t+\Delta t} \qquad (3.113)$$

The α and δ terms control variation of acceleration over the time step as well as the acucuracy and stability of the method. The results of the dynamic analysis are displacement, velocity and acceleration at the end of each time step. The program flowchart for the analysis of uncoupled TLP is presented in Figure 3.11.

University of Malaya

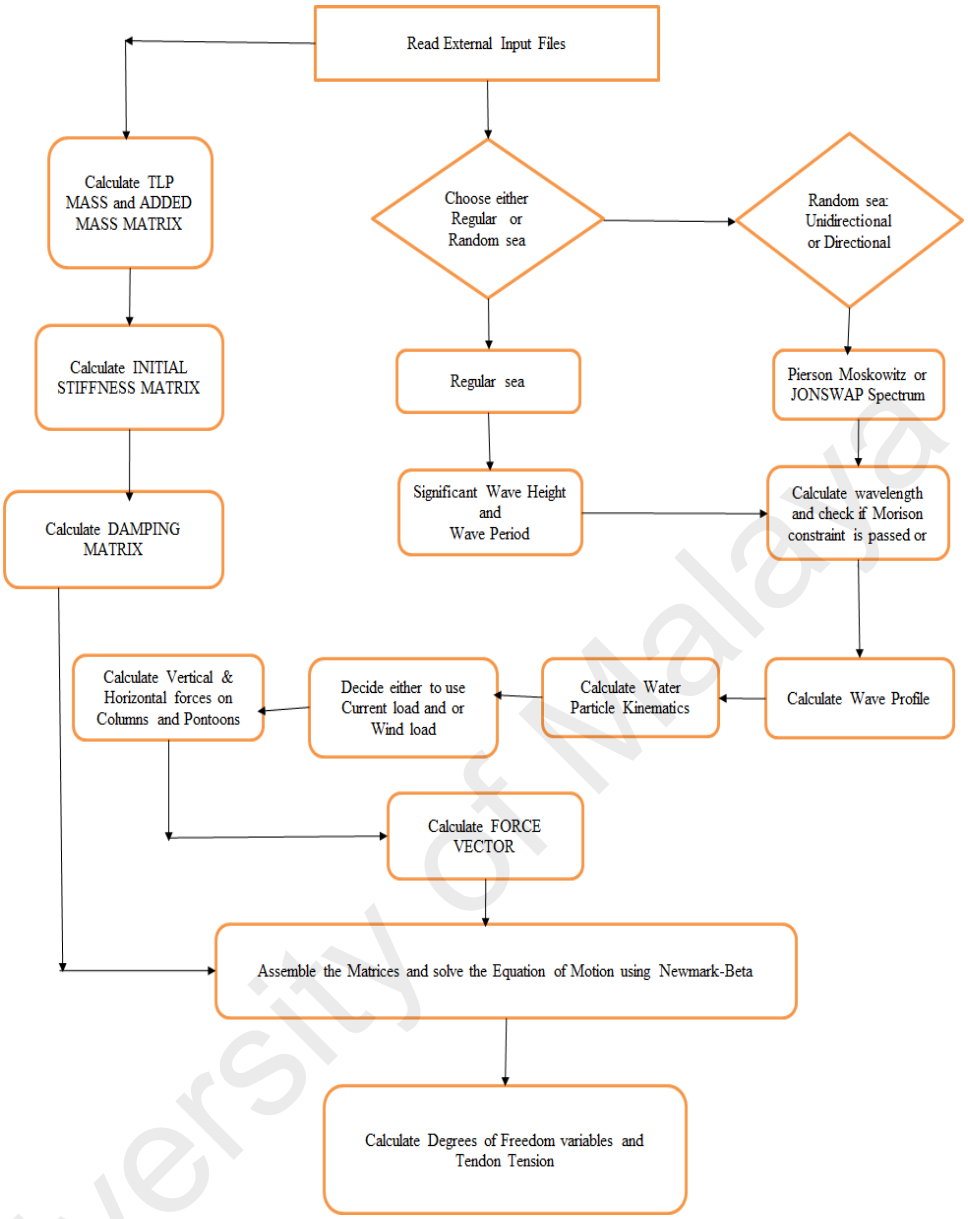

Figure 3.11: Flowchart for Uncoupled Nonlinear Analysis Program (UNAP-TLP-2016)

3.6 Simulation of CNAP-TLP-2016 in Abaqus Software

Unlike the stiffness approach in an uncoupled model, Abaqus finite element tool modelled the platform and tendons together with proper couplings among the various modes of degree of freedoms. With this approach, derivation of stiffness coefficients was achieved without resulting in reaction of forces as previously adopted by other authors and for uncoupled model in this present study. The general-purpose finite element tool was

University of Malaya

used to discretize the platform as shown in Figure 3.12. The model geometry of Figure 4.12 consists of 84 nodes and 80 elements for all the tendons, while platform column and pontoon is made up of 86 nodes and 87 elements in 450 metres water depth for ISSC TLP.

The fluid flow environment is modelled using the empirical formulas of the linear wave theory and the Morison formula while the platform and mooring lines are represented with the aid of finite element formulation in the Abaqus environment. The Abaqus/Aqua analysis module of the Abaqus software is specifically designed to apply current, wave and wind loading to submerged structures such as marine risers and offshore pipelines installation, Dassault (2009). The module is not an alternative option for hydrodynamic software for offshore problems but rather, this thesis used general purpose finite element software for the solution of nonlinear dynamic analysis of the TLP.

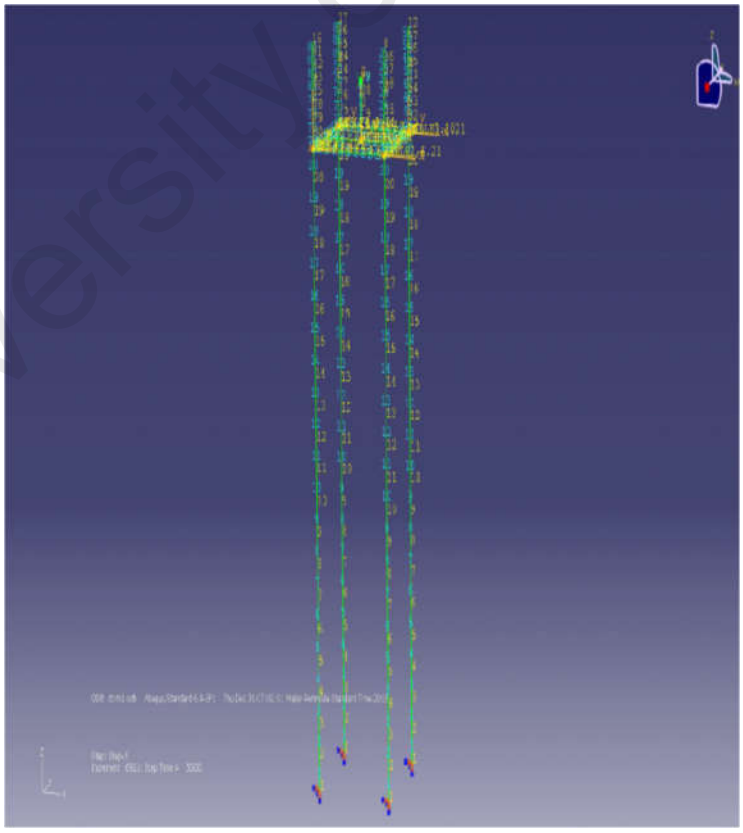

Figure 3.12: Finite element discretization of model geometry

University of Malaya

3.6.1 TLP hull

The platform columns and pontoons are simulated using rigid beam element of the finite element tool due to its high stiffness. Thus, Mass and rotary inertia elements of the Abaqus software that are associated with translational and rotational degrees of freedom for a rigid body are used to represent mass properties at the reference node (COG), Figure 3.12. The hull is connected to the tendon top for a coupled analysis with the help of the connector element (CONN3D2) that makes the two ends act at the same point. The vertical and horizontal movements of these joints are restrained but rotation is allowed so as to prevent rigid body motion. The principle and formulas adopted here are similar to the ones used for FORTRAN coding. In Abaqus (2011), it is assumed that mass and rotary inertia are introduced at the centre of mass; this is represented as body reference node, COG in Figure 3.1 but simply referred to point 'C' in this subsection.

Taking the local principal axes of inertia of the body to be a_ς, $\varsigma = 1,2,3$; also, let **r** be the vector between **C** and some points in the rigid body with current coordinates **x**,

$$r = x - x_C = x_\varsigma a_\varsigma \tag{3.114}$$

$\boldsymbol{x_\varsigma}$ are local coordinates in the rigid body. The mass of the rigid body is the integral of the mass density $\rho(\boldsymbol{x_\varsigma})$ over the body,

$$m = \int_V \rho \, dV \tag{3.115}$$

Hence, $\int_V \rho \, x_\varsigma \, dV = 0$, since C is taken to be at the centre of mass of the body.

Again, since a_ς are the principal axes of the body,

$$\int_V \rho \, x_\varsigma x_\iota dV = 0 \text{ for } \varsigma \neq \iota \tag{3.116}$$

The second moments of inertia of the body about their principal axes $a_1, a_2 \; and \; a_3$ are $\mathrm{I}_{11}, \mathrm{I}_{22}$ and I_{33}

University of Malaya

$$I_{11} = \int_V \rho\,((x_2)^2 + (x_3)^2)dV \tag{3.117}$$

$$I_{22} = \int_V \rho\,((x_3)^2 + (x_1)^2)dV \tag{3.118}$$

$$I_{33} = \int_V \rho\,((x_1)^2 + (x_2)^2)dV \tag{3.119}$$

The rotary inertia tensor is computed and written using this notation

$$I = \sum_{\varsigma=1}^{3} I_{\varsigma\varsigma}\, a_\varsigma a_\varsigma \tag{3.120}$$

The velocity of any point of the rigid body is stated as

$$\dot{u} = \dot{u}_C + \omega \times r \tag{3121}$$

Where $\omega = \phi$ is the angular velocity of the body. The acceleration of the body is determined from the time derivate of Equation 3.121 as

$$\ddot{u} = \ddot{u}_C + \dot{\omega} \times r + \omega \times (\omega \times r) \tag{3.122}$$

The equilibrium equations in a strong form represent the balance of linear momentum and balance of angular momentum and these are given as follows:

$$m\,\ddot{\bar{u}}_C = \bar{f} \tag{3.123}$$

$$I\dot{\omega} + \omega \times I\omega = \bar{m} \tag{3.124}$$

In the weak form, the equilibrium equation is

$$\delta W_A + \delta W_{ext} = 0 \tag{3.125}$$

The internal or d'Alembert force contribution is

$$\delta W_A = -\int_V \rho\,\delta u \ddot{u} d\,V$$

$$= -m\,\ddot{u}_C \delta u_C - (I\dot{\omega} + \omega \times I\omega)\delta\,\theta \tag{3.126}$$

Where $\delta u = \delta u_C + \delta\theta \times r$ is the variation of the position of a point in the body, $\delta \boldsymbol{u}_C$ is the variation of the position of the rigid body reference mode and $\delta\boldsymbol{\theta}$ is the variation of the rotation of the rigid body reference node.

The external loading condition contribution is

University of Malaya

$$\delta W_{ext} = \bar{f}\delta u_{C} + \overline{m}\,\delta\,\theta \quad (3.127)$$

3.6.2 TLP tendons

Tendons are modelled with the help of finite beam elements. Although a beam element is a line element, it has stiffness connected with the deformation line. The hybrid beam element of the Timoshenko beam type is used for tendon modelling because of its advantage over the usual finite element displacement method. Basically, for geometrically nonlinear problems in which beams undergo large displacement and rigid in axial, hybrid beam elements employ general formulation that considers axial, bending and transverse shear forces in the elements, as well as nodal displacements and rotations. Timoshenko beam is suitable for slender structures and also allows for transverse shear deformation. The mass matrix formulation is based on consistent mass method. The orientation of the beam cross-section is correctly chosen so as to define correct bending plane. The axis system is local right-handed t, n1, n2, where 't' is the tangent to the axis of the element, positive from the first node to the second node of the element, n1 and n2 are local directions of the cross-sections. Each node of the beam has six degrees of freedom active. Hybrid beam elements of Abaqus which are suitable for slender situations and for which the axial stiffness is very large compared to the bending stiffness are adopted. A solid cross-section Timoshenko beam is adopted. The ISSC TLP case study that is considered does not expressly provide the cross-section except the area. Nevertheless, the cross-section and the dimensions are determined from the mass moment of inertia and existing TLPs. The axial and bending behaviour of the beam according to Abaqus (2011)

can be expressed in the following manner:

The internal virtual work of the beam is stated as

$$\delta W_1^{\,I} = \int_L (N\,\delta\epsilon + M_1\delta K_1 + M_2\delta K_2 + M_3\delta e_1)\,dL \quad (3.128)$$

University of Malaya

This can be written in another form by introducing axial force variable, $\bar{N}$ as

$$\delta W_2{}^{I} = \int_L \left(\bar{N}\delta\varepsilon + M_1\delta K_1 + M_2\delta K_2 + M_3\delta e_1 + \delta\lambda(N - \bar{N})\right) dL \quad (3.129)$$

Here, $\delta\lambda$ is a Lagrange multiplier introduced to impose the constraint $N = \bar{N}$. A linear combination of these expressions is

$$\delta W_C{}^{I} = \rho\delta W_1{}^{I} + (1 - \rho)\delta W_2{}^{I} \quad (3.130)$$

$$\delta W_C{}^{I} = \int_L [(\rho N + (1 - \rho)\bar{N})\delta\varepsilon + M_1\delta K_1 + M_2\delta K_2 + M_3\delta e_1 + (1 - \rho)\delta\lambda(N - \bar{N})]\, dL \quad (3.131)$$

The contribution of this term to the Newton scheme is then stated as

$$\int_L \begin{bmatrix} (\rho dN + (1 - \rho)\delta\bar{N})\delta\varepsilon + dM_1\delta K_1 + dM_2\delta K_2 + dM_3\delta e_1 + \\ (1 - \rho)\delta\lambda(dN - d\bar{N}) + \\ \bar{N}d\delta\varepsilon + M_1 d\delta K_1 + M_2 d\delta K_2 + M_3 d\delta e_1 \end{bmatrix} dL \quad (3.132)$$

Where

$$\bar{N} = \rho N + (1 - \rho)\bar{N} \quad (3.133)$$

The tangent stiffness of the section behaviour yielded

$$\begin{Bmatrix} d\bar{N} \\ dM_1 \\ dM_2 \\ dM_3 \end{Bmatrix} = \begin{bmatrix} A_{00} & A_{01} & A_{02} & A_{03} \\ & A_{11} & A_{12} & A_{13} \\ \text{sym} & & A_{22} & A_{23} \\ & & & A_{33} \end{bmatrix} \begin{Bmatrix} d\varepsilon \\ dK_1 \\ dK_2 \\ de_1 \end{Bmatrix} \quad (3.134)$$

ε is axial strain, K_1 $K_2$are beam curvature, e_1 is the torsional strain, N= axial force, M_1 = bending moment, M_2 = warping moment and M_3 is the twisting moment.

if $L^2 A_{00} < A_{11}, A_{22}$ (where L is the element length), then the beam is flexible axially and the mixed formulation is unnecessary. Otherwise, the assumption is that an inverse of the first equation above defines $d\varepsilon$ from $d\bar{N}$:

$$d\varepsilon = \frac{1}{A_{00}}(d\bar{N} - A_{01}dK_1 - A_{02}dK_2 - A_{03}de_1) \quad (3.135)$$

University of Malaya

Also

$$dM_1 = \left(A_{11} - \frac{A_{01}^{\,2}}{A_{00}}\right) dK_1 + \left(A_{12} - \frac{A_{01}A_{02}}{A_{00}}\right) dK_2 + \left(A_{13} - \frac{A_{01}A_{03}}{A_{00}}\right) de_1 + \frac{A_{01}}{A_{00}} d\bar{N} \quad (3.136)$$

$$dM_2 = \left(A_{12} - \frac{A_{01}A_{02}}{A_{00}}\right) dK_1 + \left(A_{22} - \frac{A_{02}^{\,2}}{A_{00}}\right) dK_2 + \left(A_{23} - \frac{A_{02}A_{03}}{A_{00}}\right) de_1 + \frac{A_{02}}{A_{00}} d\bar{N} \quad (3.137)$$

$$dM_3 = \left(A_{13} - \frac{A_{01}A_{03}}{A_{00}}\right) dK_1 + \left(A_{23} - \frac{A_{02}A_{03}}{A_{00}}\right) dK_2 + \left(A_{33} - \frac{A_{03}^{\,2}}{A_{00}}\right) de_1 + \frac{A_{03}}{A_{00}} d\bar{N} \quad (3.138)$$

By multiplying first tangent section stiffness by ρ and the second is multiplied by $(1 - \rho)$, the Newton contribution of the element becomes

$$\int_L [\delta\varepsilon \delta K_1 \delta K_2 \delta e_1 A_{00} \delta\lambda] [\bar{A}] \begin{Bmatrix} d\varepsilon \\ dK_1 \\ dK_2 \\ de_1 \\ d\bar{N} \end{Bmatrix} + \int_L (\bar{N} d\delta\varepsilon + M_1 d\delta K_1 + M_2 d\delta K_2 + M_3 d\delta e_1)\, dL \quad (3.139)$$

$$= -\int_L \begin{bmatrix} \bar{N}\delta\varepsilon + M_1\delta K_1 + M_2\delta K_2 + M_3\delta e_1 \\ + A_{00}\delta\lambda(1-\rho)\left(\frac{N-\bar{N}}{A_{00}}\right) \end{bmatrix} dL \quad (3.140)$$

Where $[\bar{A}]$ is

$$\begin{bmatrix} \rho A_{00} & \rho A_{01} & \rho A_{02} & \rho A_{03} & 1-\rho \\ & A_{11} - (1-\rho)\frac{A_{01}^{\,2}}{A_{00}} & A_{12} - (1-\rho)\frac{A_{01}A_{02}}{A_{00}} & A_{13} - (1-\rho)\frac{A_{01}A_{03}}{A_{00}} & (1-\rho)\frac{A_{01}}{A_{00}} \\ & & A_{22} - (1-\rho)\frac{A_{02}^{\,2}}{A_{00}} & A_{23} - (1-\rho)\frac{A_{02}A_{03}}{A_{00}} & (1-\rho)\frac{A_{02}}{A_{00}} \\ & symm & & A_{33} - (1-\rho)\frac{A_{03}^{\,2}}{A_{00}} & (1-\rho)\frac{A_{03}}{A_{00}} \\ & & & & -(1-\rho)\frac{1}{A_{00}} \end{bmatrix} \quad (3.141)$$

University of Malaya

The variable $\bar{N}$ is taken as an independent value at each integration point in the element. ρ as $\bar{\rho}/A_{00}$ is chosen where $\bar{\rho}$ is a small value. With this choice and by ensuring the variables $\bar{N}$ are eliminated after the displacement variables of each element, the Gaussian elimination has no difficulty in solving the equations.

3.6.3 Connector elements

In order to have an integrated TLP unit, the connector element is used to link platform hull and tendons together. The advantage of using the connector element is due to the fact that they do not eliminate degrees of freedom at the connection node but rather imposed kinematic constraints with Lagrange multipliers. The CONN3D2 connector element for 3-dimensional space and JOIN type of translational basic connection are used in fixing the connecting nodes together. Therefore, kinematic constraints are u1 = u2 = u3 = 0. The rotational degrees of freedom are not fixed but free to rotate to prevent rigid mode.

3.6.4 Numerical solution for CNAP-TLP-2016

The problem at hand is all about finding a solution to the developed finite element model and this can only be made possible by writing force and moment equilibrium equations at all times for the entire body. The equation of motion was written internally by Abaqus software using the virtual work principle and the finite element approximation of the equilibrium equation in accordance with

$$M^{NM}\ddot{u}^{M} + I^{N} - P^{N} = 0 \qquad (3.142)$$

Where, $M^{NM} = \int_{v_0} \rho_0 N^N N^M dV_0$ is the consistent mass matrix; $I^N = \int_{V_0} \beta^N : \sigma \, d V_0$ is the internal force vector and $P^N = \int_S N^N t \, d s + \int_V N^N F \, d v$ as the external force vector. The matrix and vector refer to matrices and vectors in the space of nodal variables u^N.

University of Malaya

The implicit integration method which is a generalization of the Newmark operator is employed due to its control on numerical damping. This solves the dynamic problem at time (t + Δt) based not only at the value 't' but also on the same quantity at 't + Δt'. The in-built automatic time step control based on half-increment residual is employed.

Equation 3.142 is replaced with a balance of D'Alembert forces at the end of the time step and a weighted average of the static forces at the beginning and end of the time step as follows:

$$M^{NM}\ddot{u}^{M}\Big|_{t+\Delta t} + (1+\alpha)\left(I^{N}\Big|_{t+\Delta t} - P^{N}\Big|_{t+\Delta t}\right) - \alpha\left(I^{N}\Big|_{t} - P^{N}\Big|_{t}\right) + L^{N}\Big|_{t+\Delta t} = 0 \quad (3.143)$$

Where $L^{N}\big|_{t+\Delta t}$ is the sum of Lagrange multiplier forces associated with the degree of freedom N. Equation 3.143 is then solved using the Newmark formula for displacement and velocity integration

$$u\Big|_{t+\Delta t} = u\Big|_{t} + \Delta t\dot{u}\Big|_{t} + \Delta t^{2}\left(\left(\frac{1}{2}-\beta\right)\ddot{u}\Big|_{t} + \beta\ddot{u}\Big|_{t+\Delta t}\right) \quad (3.144)$$

$$\dot{u}\Big|_{t+\Delta t} = \dot{u}\Big|_{t} + \Delta t\left((1-\gamma)\ddot{u}\Big|_{t} + \gamma\ddot{u}\Big|_{t+\Delta t}\right) \quad (3.145)$$

Where

$$\beta = \frac{1}{4}(1-\alpha)^{2}\,;\ \gamma = \frac{1}{2}-\alpha\,;\ -\frac{1}{3} \le \alpha \le 0 \quad (3.146)$$

The whole procedure is achieved by writing an input text-file to capture every detail of the platform following the flowchart in Figure 3.13 and a typical text file is included as Appendix B in this report.

University of Malaya

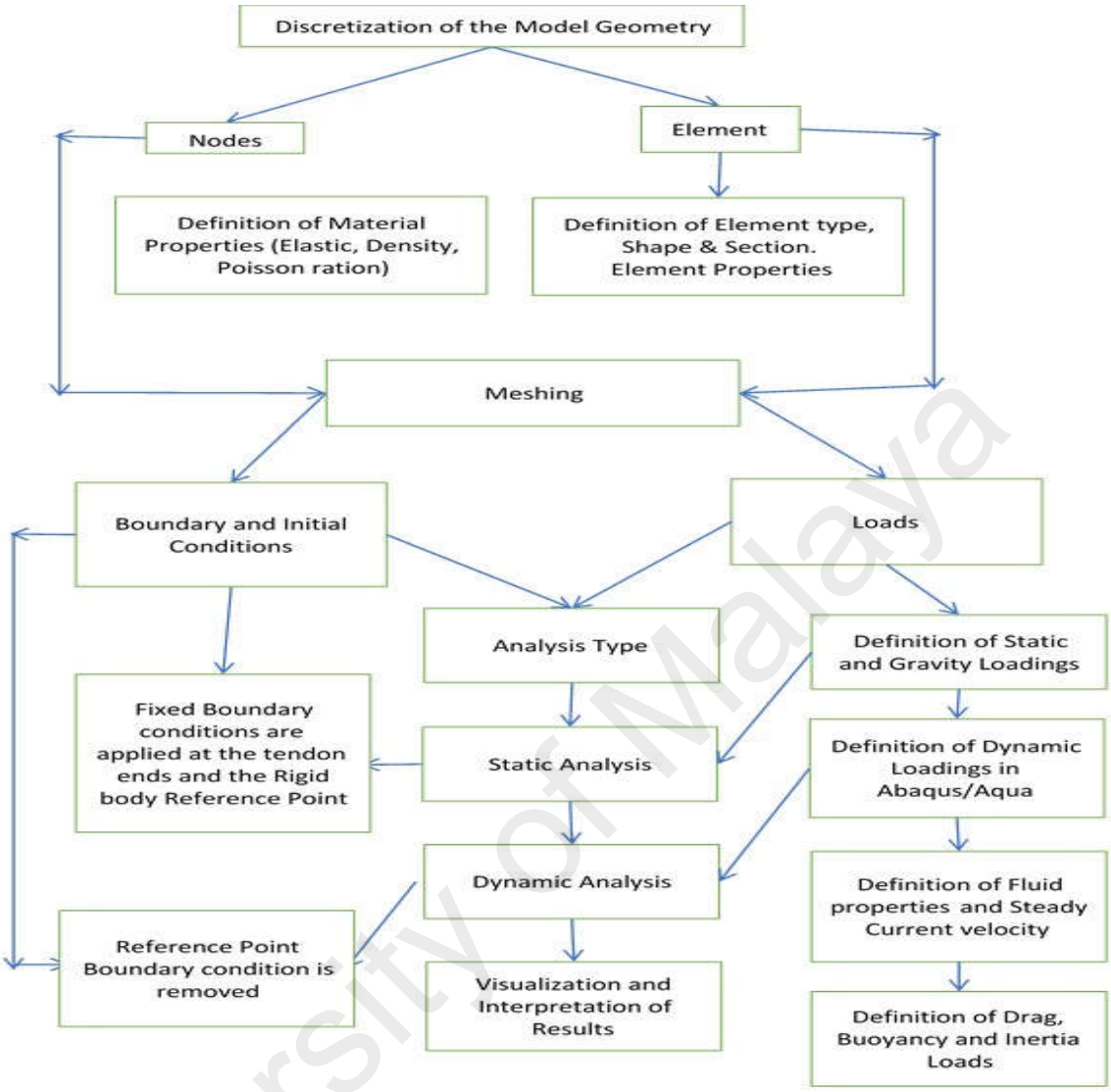

Figure 3.13. Flowchart of the numerical analysis of CNAP-TLP-2016

3.7 Summary

The method adopted for the idealization of the TLP and the simulation of forces has been described in this chapter. The integration method in the time domain was employed to solve the stochastic response of nonlinear dynamic problem of TLP for both uncoupled and coupled models. Thus, the efficiency of the proposed method is established by carrying out a numerical study in the next chapter where results of the analysis are also validated and outcomes of the TLP responses are discussed.

University of Malaya

CHAPTER 4: RESULTS AND DISCUSSION

4.1 Introduction

This chapter deals with the validation of the numerical model of Uncoupled Nonlinear Analysis Program (UNAP-TLP-2016) simulated in FORTRAN program with the published results so as to establish reliability of the proposed program. The proposed program was then used to simulate various environmental conditions on an uncoupled TLP model. The influence of current, wind and wave loads on the motion response in regular, random and directional seas were also studied. The characterization of sea-wave fundamentally governs the loads and responses of the TLP. This was proven by idealizing the ocean surface as regular wave, random wave and directional random wave seas. The real sea is probably not regular and representing it as one might not only be erroneous but also undermine accurate assessment of forces and motions of the TLP. The nonlinear analysis of the behaviour of the coupled TLP model was carried out in Abaqus software. This was followed with validation of the obtained results with results of time-domain from published works. The chapter concludes with various parametric studies on the effect of different load combinations, TLP tendon dynamics, varying wave height and wave period and vice-versa. The results and discussions are thus presented.

4.2 Validation of UNAP-TLP-2016 with published result

The outcomes of static and dynamic analysis obtained from the UNAP-TLP-2016 need to be validated either with an experimental or similar time-domain program. Due to the absence of an offshore experimental facility in our laboratory, the developed program was validated with the previous work by Chitrapu and Ertekin (1992), Chitrapu and Ertekin (1993), Chitrapu and Ertekin (1995); and Chitrapu, Ertekin, and Paulling (1993). The

University of Malaya

platform characteristics and principal dimensions that was used for the comparison are shown in Table 4.1 and Table 4.2 respectively. It should be noted that the platform geometry and fundamental characteristics were the same in both models.

Table 4.1: Geometrical and mechanical characteristics of TLP
Chitrapu and Ertekin (1992)

Number of Columns	4
Number of Pontoons	4
Tether diameter	0.40 m
Length of TLP hull	44.1 m
Diameter of Column	14.2 m
Water depth	500.0 m
Draft	26.6 m
COG above SWL	9.25 m
Displacement volume	33,400 m^3

Table 4.2: Mechanical features of TLP, Ahmad (1996)

Total Tether Pretension	1.245×10^8 N
Center to center spacing	58.3 m
Buoyancy force	3.34×10^8 N
Mass of Platform	2.095×10^7 kg
Axial Stiffness	5806 t/m
Weight of tether	5257 tons
Radii of Gyration (R_x, R_y, R_z)	29.15, 29.15 & 32.15 m

At the original equilibrium position of the TLP, the summation of vertical forces ensured static equilibrium going by Equation 4.1

$$W + 4T - F_b = 0 \quad (4.1)$$

Where, W= total weight of the platform in the air; T= Initial Pretension in each tendon and F_b= total buoyancy force. The natural time periods of the TLP as reported by Ahmad (1996) is given in Table 4.3 while Equation 4.2 was adopted to calculate the natural time periods of the TLP for the present study, and this was found corresponding with the

University of Malaya

published result. The peaks in Power Spectral Density (PSD) of the motion responses in Figures 4.3 and 4.6, further verified that the first prominent peak was at the same frequency with the surge (sway) direction. The results of the present study matched considerably with published results.

$$T_k = \sqrt[2\pi]{\frac{(M_{kk} + a_{kk})}{C_{kk}}} \tag{4.2}$$

Where, k stands for Surge, Sway, Heave, Roll, Pitch and Yaw degrees of freedom; M is the platform mass; a_{kk} is the calculated added mass for each degree of freedom; c_{kk} is the calculated restoring force coefficient for each degree of freedom.

Table 4.3: Natural time period of TLP, Ahmad (1996)

	Published		Present Study	
Degree of Freedom	Time (s)	Frequency (rad/sec)	Time (s)	Frequency (rad/sec)
Surge (Sway)	92.20	0.07	92.65	0.07
Heave	2.00	3.14	1.96	3.20
Roll (Pitch)	2.20	2.86	2.25	2.79
Yaw	70.50	0.09	70.02	0.09

4.2.1 Comparison of UNAP-TLP-2016 model result for regular wave

For the regular wave simulation, the wave height (WH) and wave period (WP) for the comparison were 5 m and 7 s respectively with a steady current velocity of 0.91 m/s. The result of the surge time history of the present study, Figure 4.1 was compared with published result of Chitrapu and Ertekin (1993), Figure 4.2. A considerable level of agreement was recorded in the pattern and values of the surge time history. It was clearly seen from Figure 4.3 that the vibration of the platform occurred at the surge natural frequency (first peak) and at the forcing frequency of the regular wave (second peak).

University of Malaya

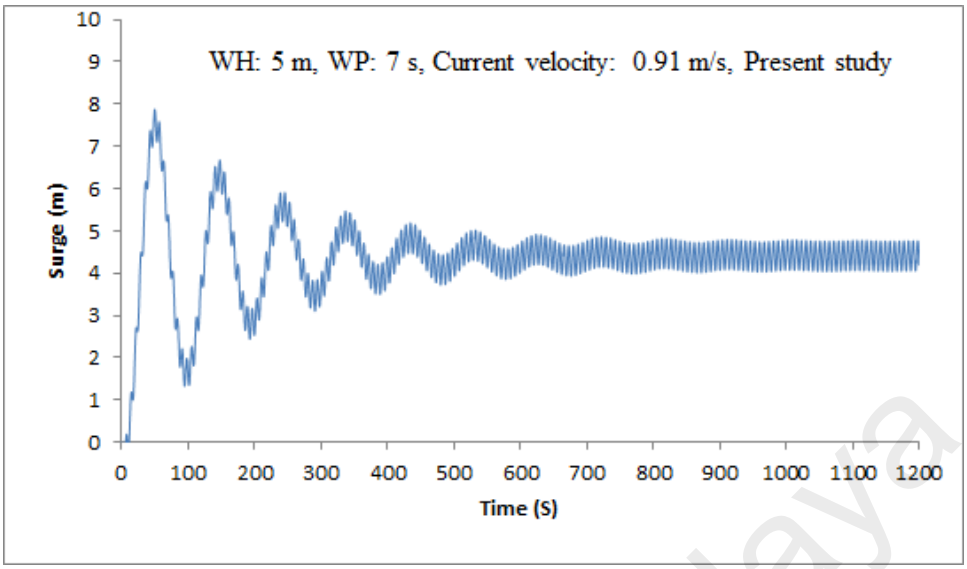

Figure 4.1: Time history of surge response

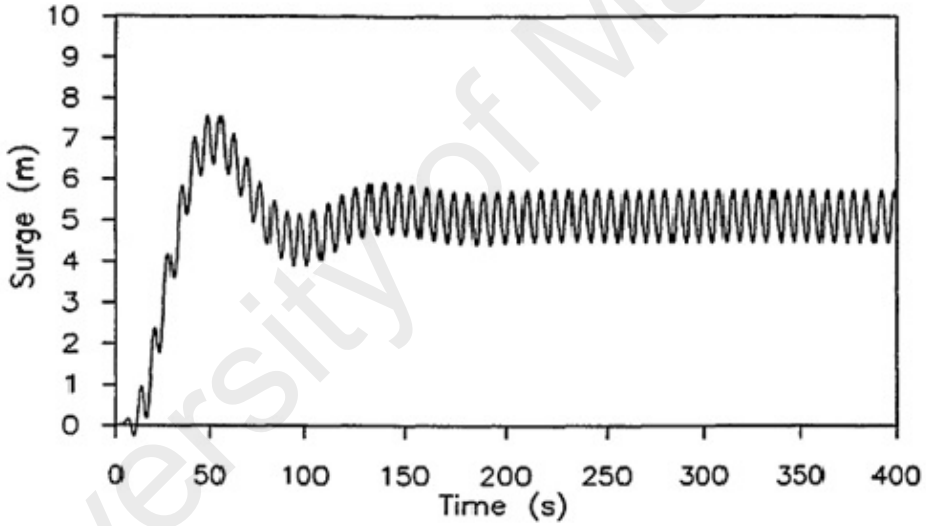

Figure 4.2: Reprint of time history of surge response
WH = 5 m, WP: 7 s, Current velocity: 0.91 m/s Chitrapu and Ertekin (1993)

University of Malaya

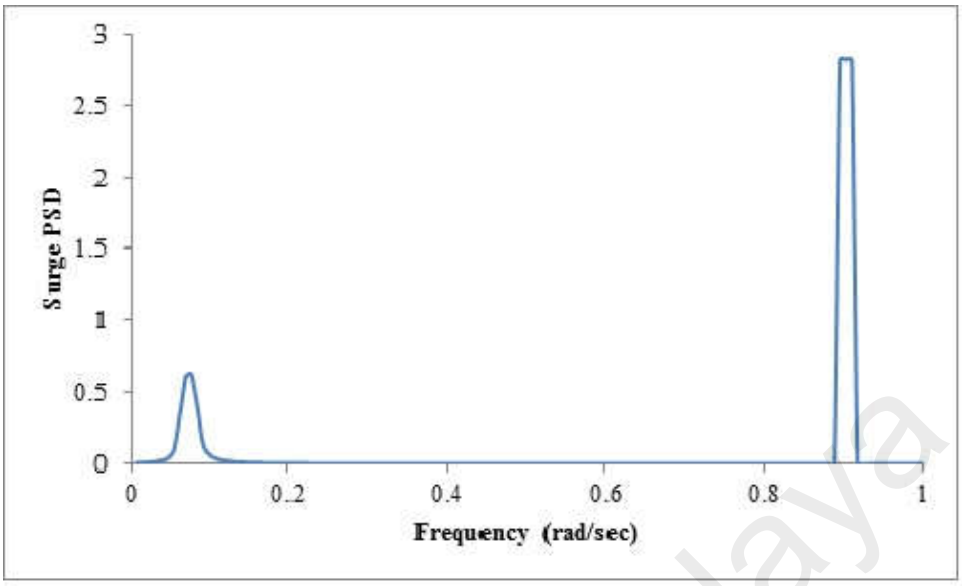

Figure 4.3: PSD of surge response (Present study)

Further levels of similarities were observed for heave time histories in Figures 4.4 and 4.5 respectively with the close matching in the trend and values. Figure 4.6 presents the heave PSD with the first prominent peak at surge natural period. By contrast, the second peak was due to forcing frequency of the wave. The steady state was reached earlier in the published result compared to the present study, this can be due to differences in numerical algorithm assumptions. At the final run, both models had similar steady state forms in the degrees of freedom. There is a widely-held view that the coupling due occur among the degrees of freedom.

University of Malaya

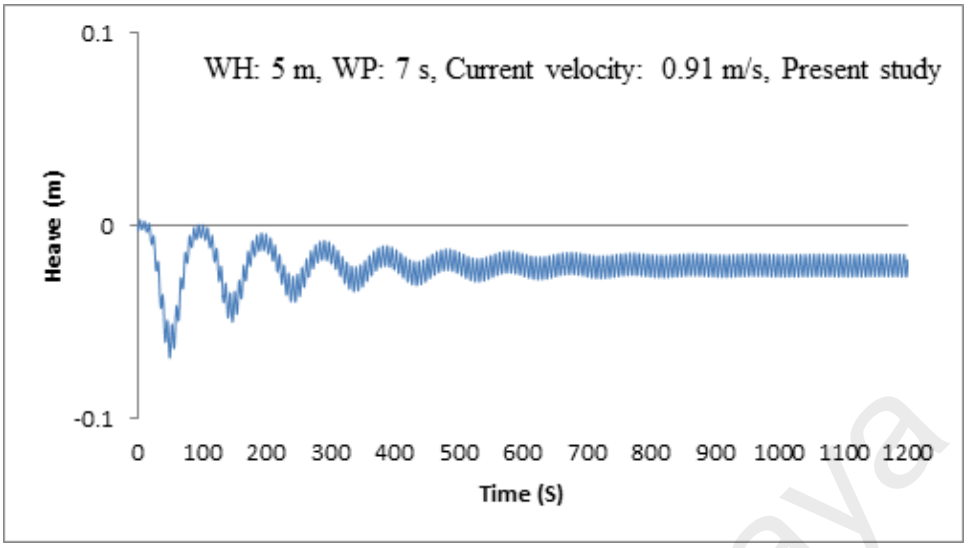

Figure 4.4: Time history of heave response

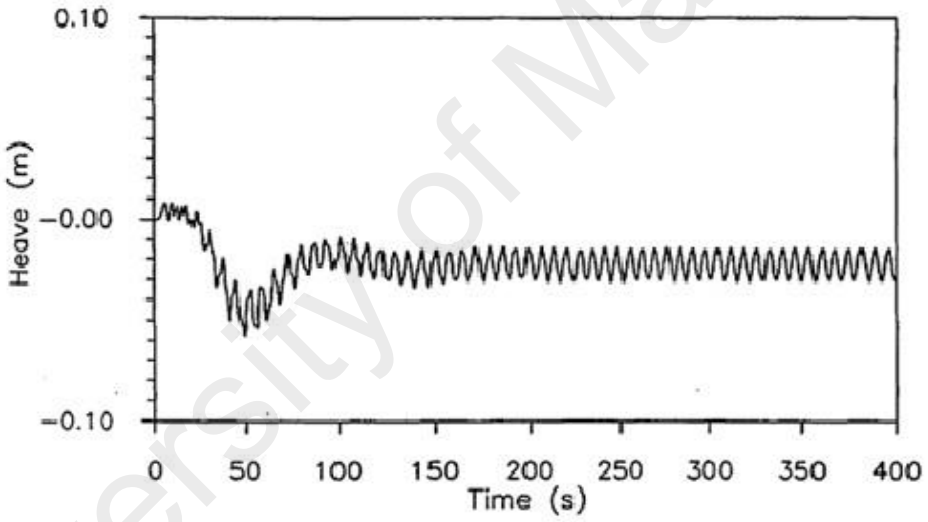

Figure 4.5: Reprint of time history of heave response

WH = 5 m, WP: 7 s, Current velocity: 0.91 m/s Chitrapu and Ertekin (1993)

University of Malaya

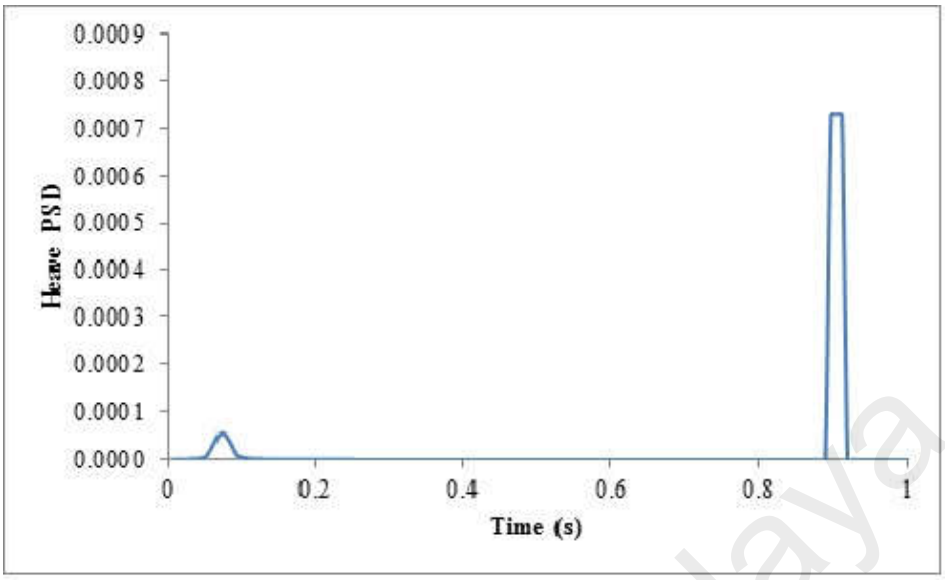

Figure 4.6: PSD of heave response (Present study)

There is a moderate discrepancy in Pitch time history of the present study in Figure 4.7 with the published result depicted in Figure 4.8, which in turn affects the tension variation in the tendons. In both cases, the maximum value of pitch response was less than 0.1 degree which can be regarded as trivial. The high-frequency fluctuation was observed in the time histories of tendon tension in Figures 4.9 and 4.10 respectively. However, the present study is with higher value and this was due to the increased value in Pitch motion, because both current force and vertical motion influence tension fluctuation in the tendons. The marked differences in the time history of tension variation can be due to the different formulation approaches and other inherent assumptions which were not clearly stated.

University of Malaya

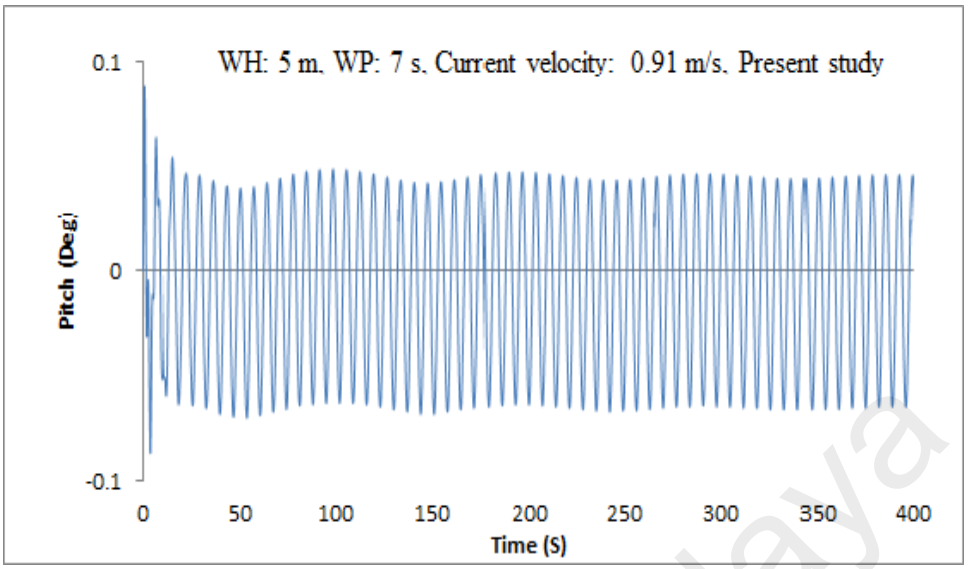

Figure 4.7 Time history of pitch response

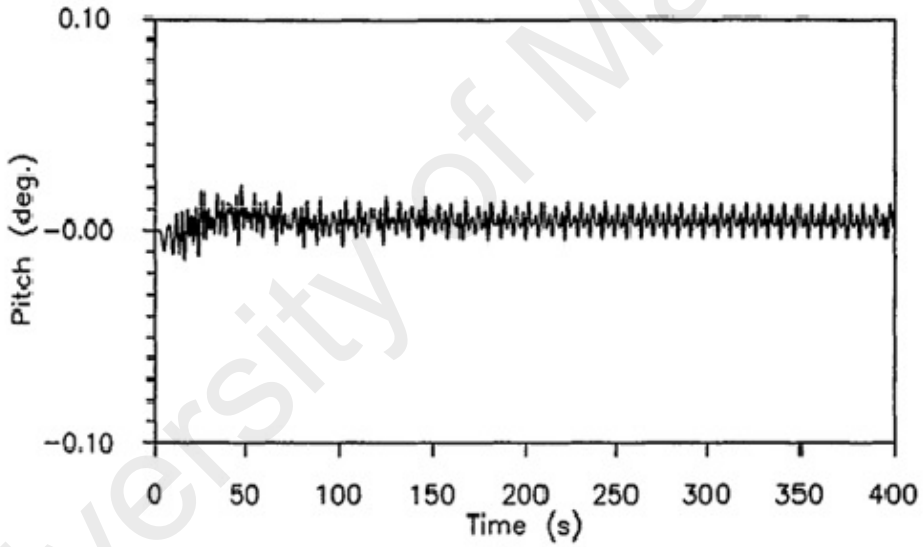

Figure 4.8 Reprint of time history of pitch response
WH = 5 m, WP: 7 s, Current velocity: 0.91 m/s Chitrapu and Ertekin (1993)

University of Malaya

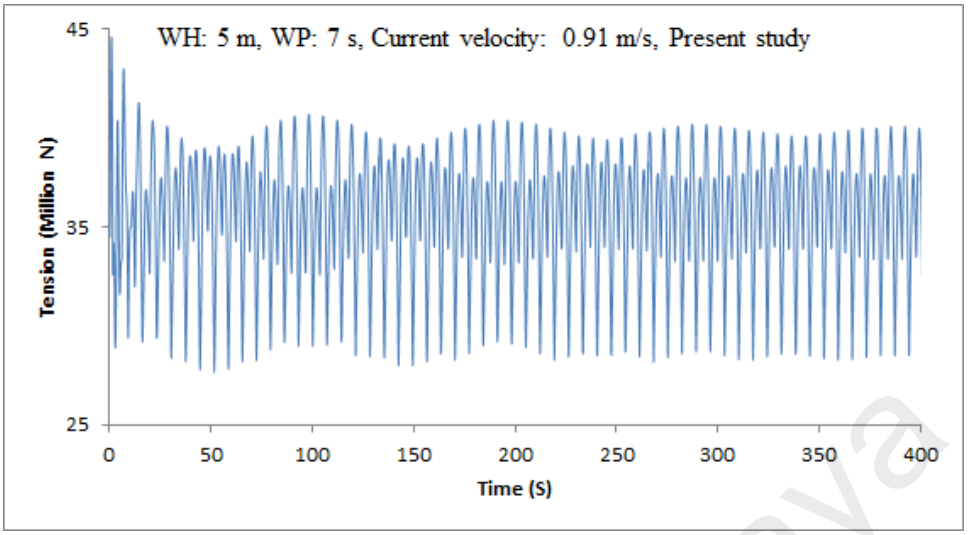

Figure 4.9 Time history of tension response

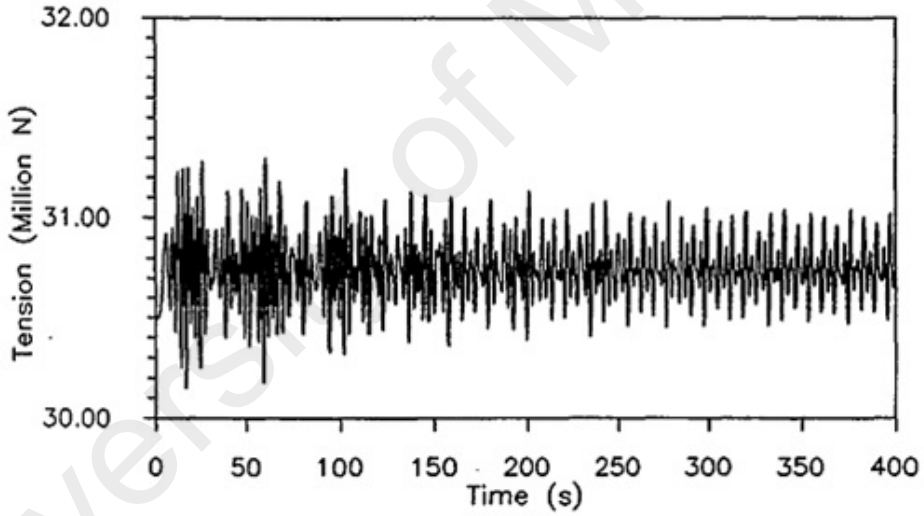

Figure 4.10 Reprint of time history of tension response
WH: 5 m, WP: 7 s, Current velocity: 0.91 m/s Chitrapu and Ertekin (1993)

University of Malaya

4.2.2 Validation of UNAP-TLP-2016 model result for random waves

The developed UNAP-TLP-2016 model program can handle regular waves and random waves in both long and short crested seas. Since the model was later used to simulate long and short crested seas, validation of the model was carried out for the

simulated random waves for the same platform characteristics. In Chitrapu and Ertekin (1993), the half- amplitude Bretschineder spectrum was used for the simulation of random waves while the present study employed the Pierson-Moskowitz spectrum. Guarga, Castells, Bosch, and Casals (2014) reported that the both half-amplitude Bretschineder and the Pierson-Moskowitz are for fully developed sea states in an open sea and have the same shape. As a result of the different spectrum methods, slight discrepancies may occur between the results from the two models but comparison can still be made since the platform geometry and ocean environment parameters are the same.

The wave parameters that were used for significant wave height are 11.4 metres and wave period of 15 seconds respectively. These are just statistical values and the wave time history are not expected to be exactly the same because the different wave spectrum and different sets of random numbers introduce differences into the results.

In Figures 4.11 and 4.12, time histories of wave surface elevation for the present study and for the published results showed good agreement. By comparing Figures 4.13 and 4.14 of the surge time histories, it could be said that there is a substantial level of similarity and uniformity in pattern and values.

University of Malaya

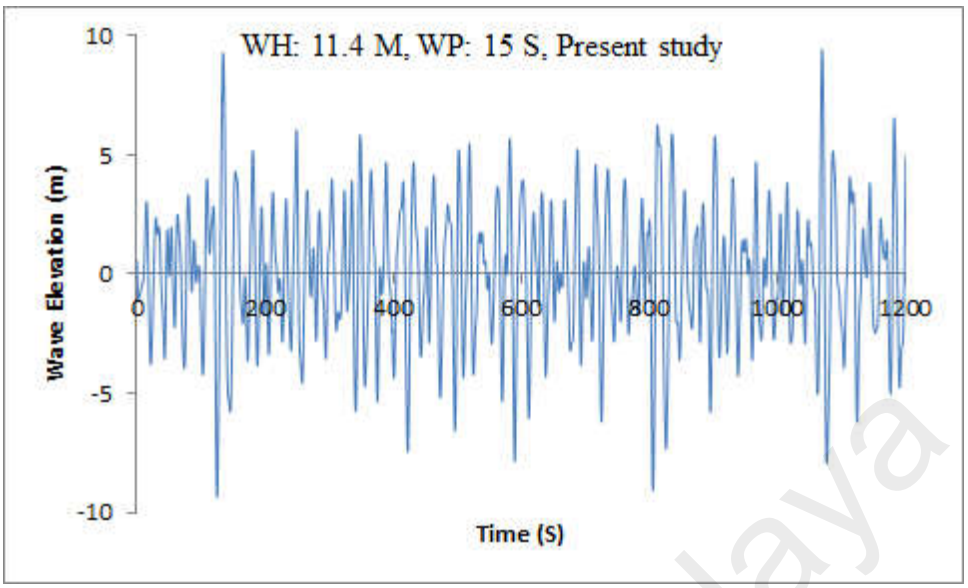

Figure 4.11: Time history of wave surface elevation

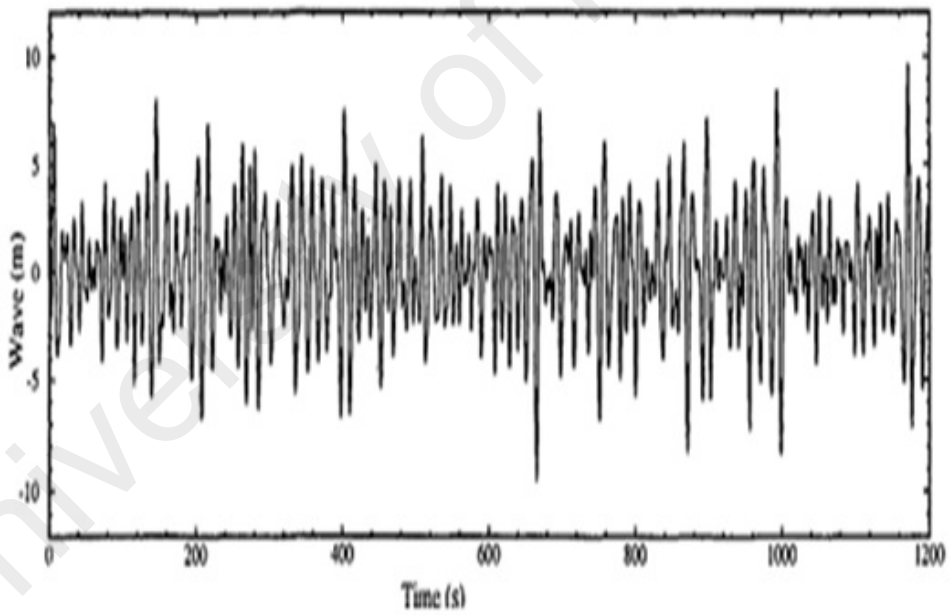

Figure 4.12: Reprint of time history of wave surface elevation
WH = 11.4 m, WP: 15 s, Current velocity: 0.91 m/s Chitrapu and Ertekin (1995)

University of Malaya

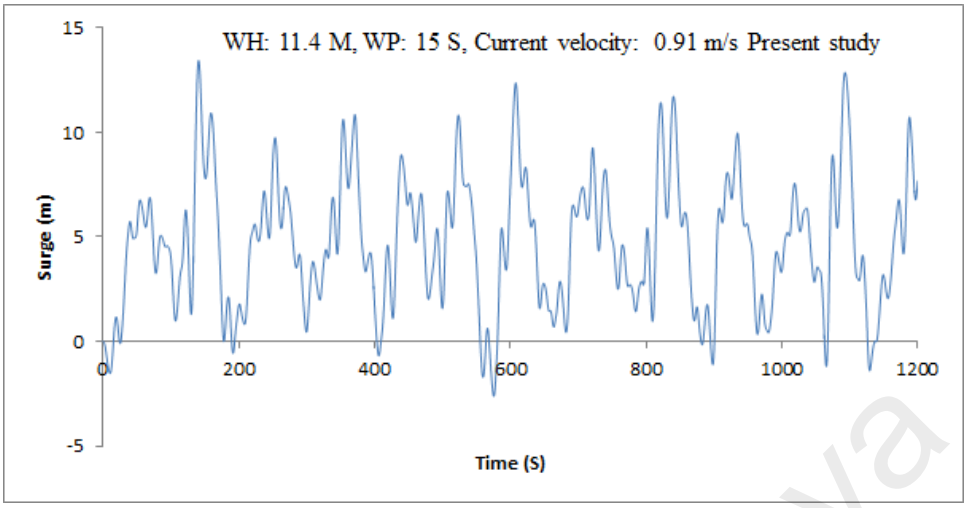

Figure 4.13: Time history of surge response (Random waves and current force)

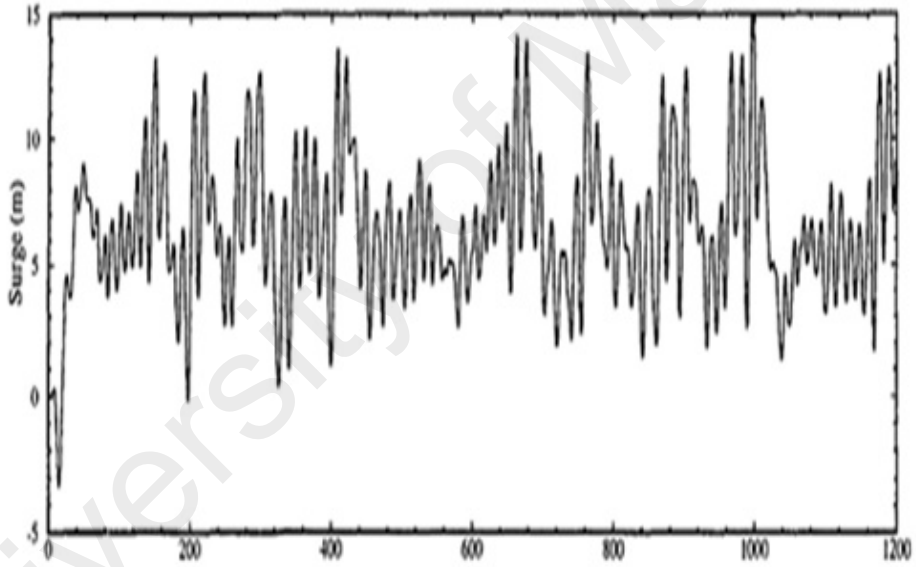

Figure 4.14: Reprint of time history of surge response
WH = 11.4 m, WP: 15 s, Current velocity: 0.91 m/s Chitrapu and Ertekin (1995)

In addition, Figures 4.15 and 4.16 show the time histories of heave and pitch motions for the present study and comparing with published results in Figures 4.17 and 4.18, the same pattern was observed. However, published results have a slight higher value. This may be attributed to differences in the wave elevation and spectrum that was used for the calculation of hydrodynamic forces which in turn determine the magnitudes of TLP

University of Malaya

degrees of freedom. As seen in Figures 4.19 and 4.20, there is a good similarity in trend with a considerable difference in the value of tension variation for time histories of tendon tension just as it was observed in regular wave simulation. Going by the power spectral densities for surge, heave, pitch and tension variation in Figures 4.21, 4.22, 4.23 and 4.24 respectively, there are evidences to suggest that platform oscillation is governed predominantly by surge natural frequency and wave forcing frequency. This fact was established from the first prominent peak and cluster of peaks that coincides with the surge and wave frequencies.

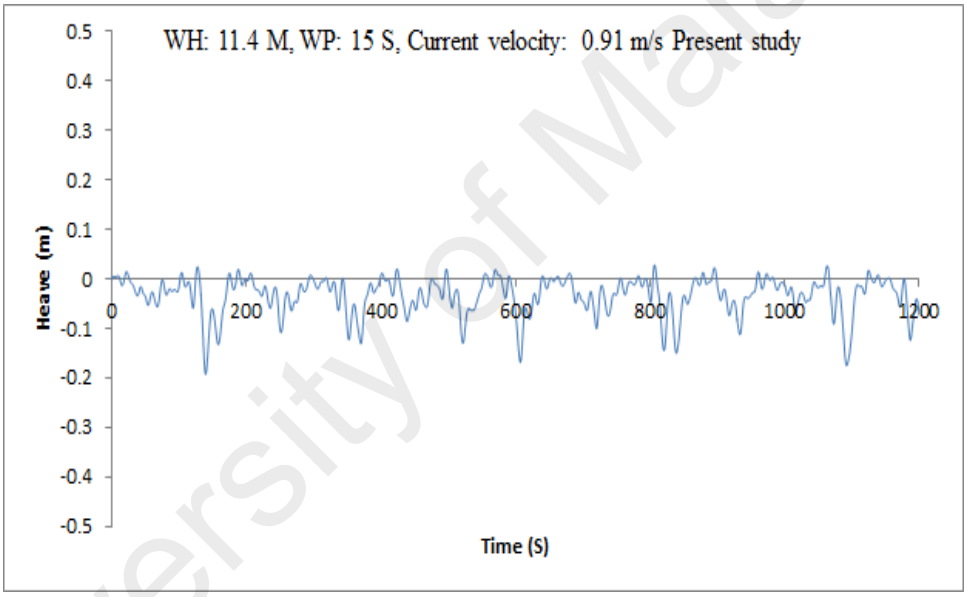

Figure 4.15: Time history of heave response (Random waves and Current force)

University of Malaya

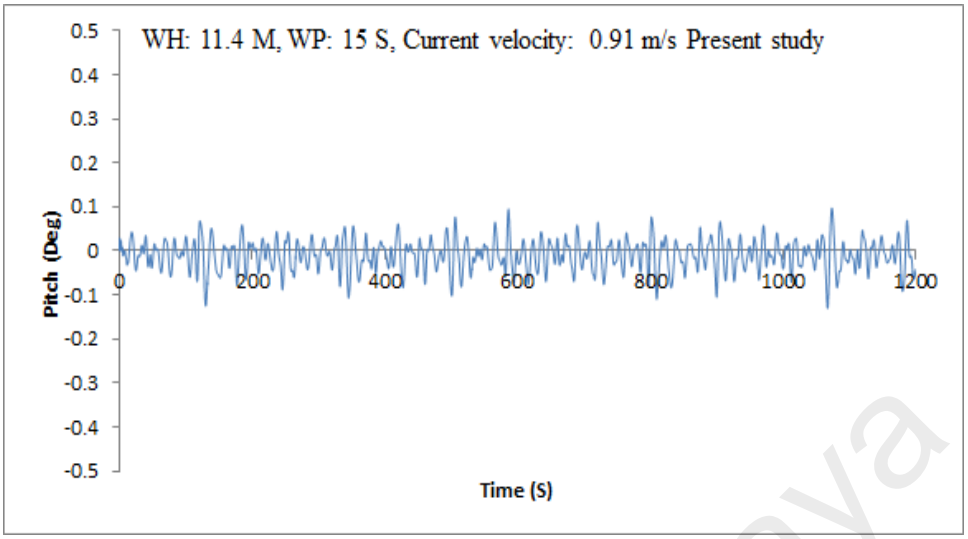

Figure 4.16: Time history of pitch response (Random waves and Current force)

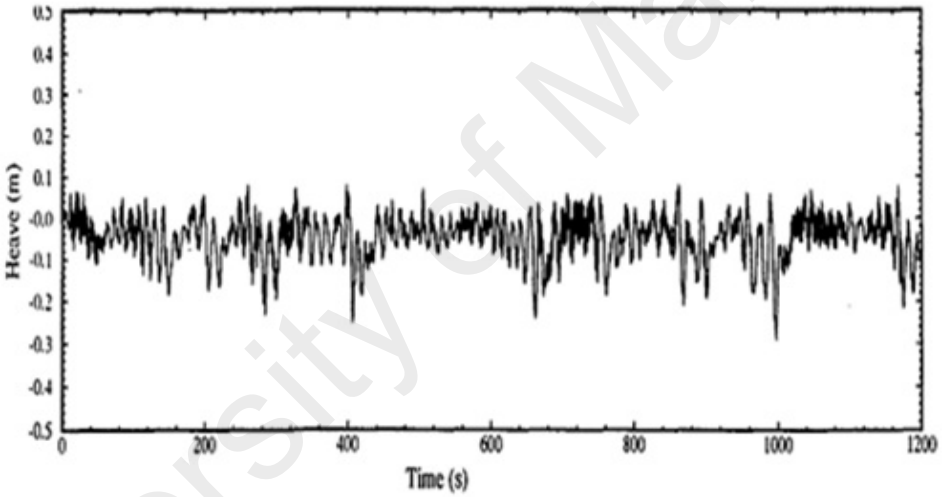

Figure 4.17: Reprint of time history of heave response
WH = 11.4 m, WP: 15 s, Current velocity: 0.91 m/s Chitrapu and Ertekin (1995)

University of Malaya

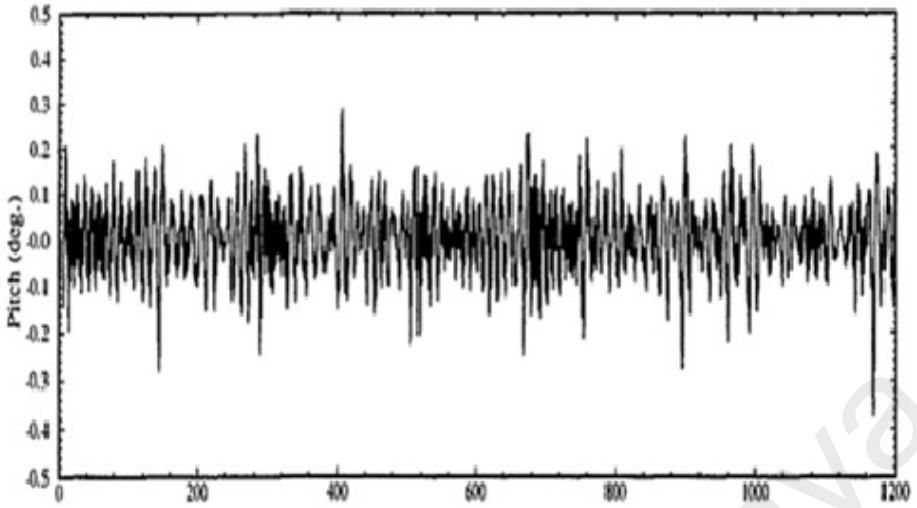

Figure 4.18: Reprint of time history of pitch response
WH = 11.4 m, WP: 15 s, Current velocity: 0.91 m/s Chitrapu and Ertekin (1995)

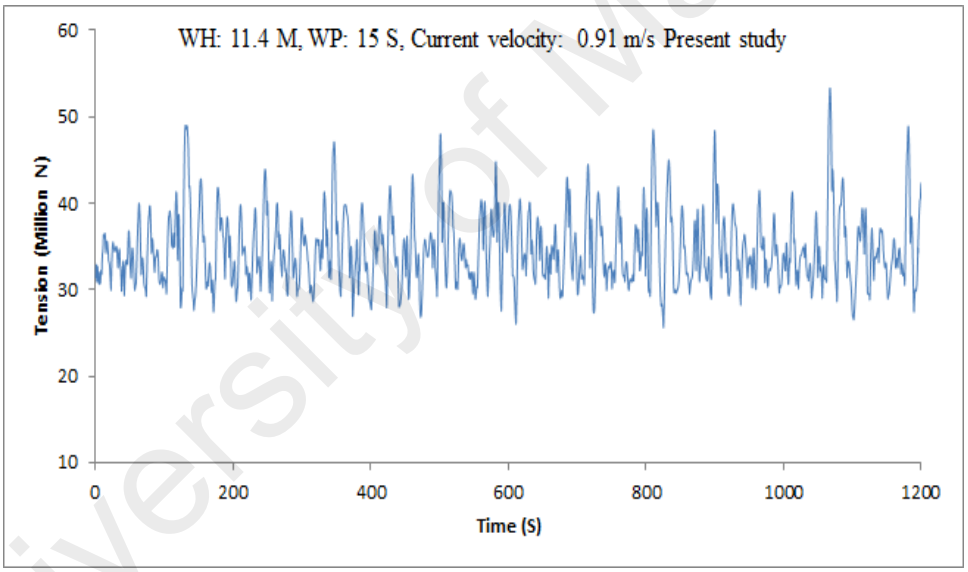

Figure 4.19: Time history of tension response

University of Malaya

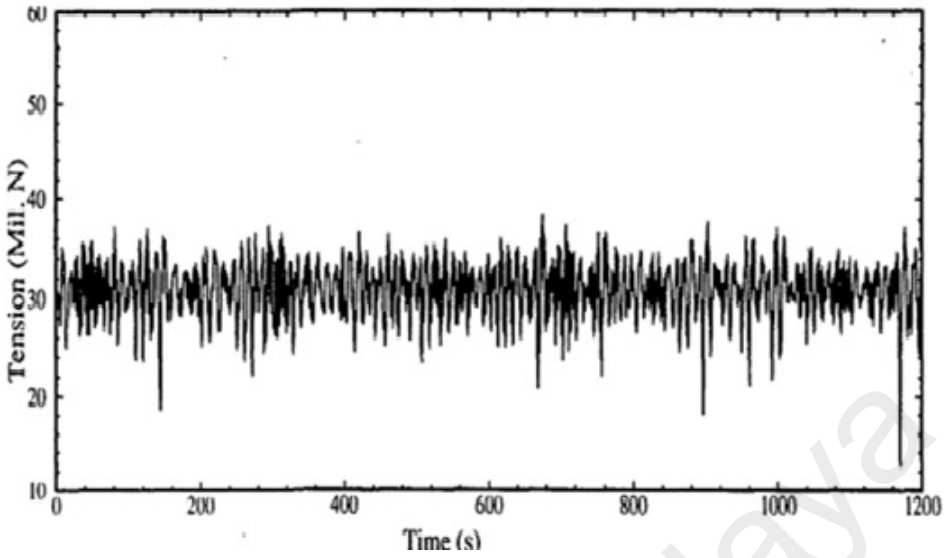

Figure 4.20: Reprint of time history of tension response
WH = 11.4 m, WP: 15 s, Current velocity: 0.91 m/s Chitrapu and Ertekin (1995)

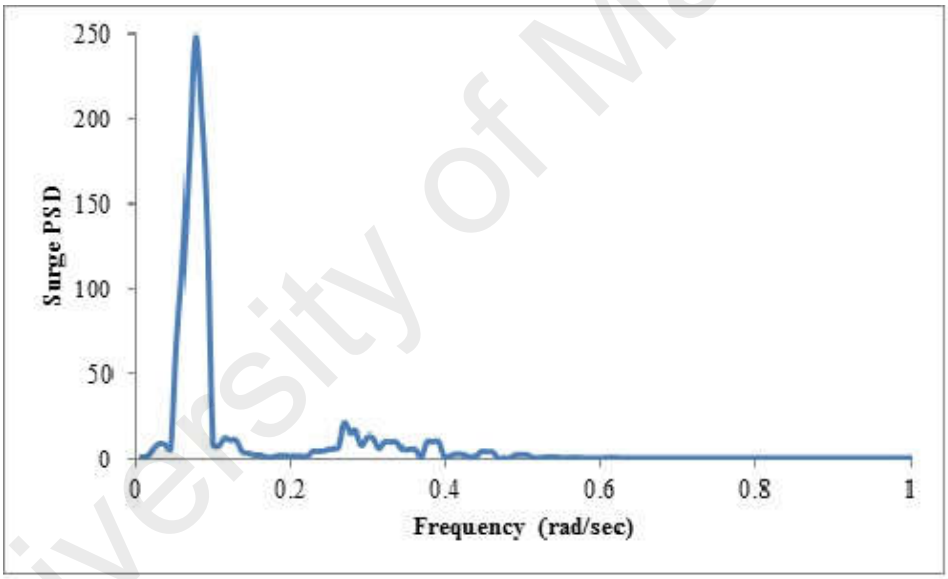

Figure 4.21: PSD of surge response (Present study)

University of Malaya

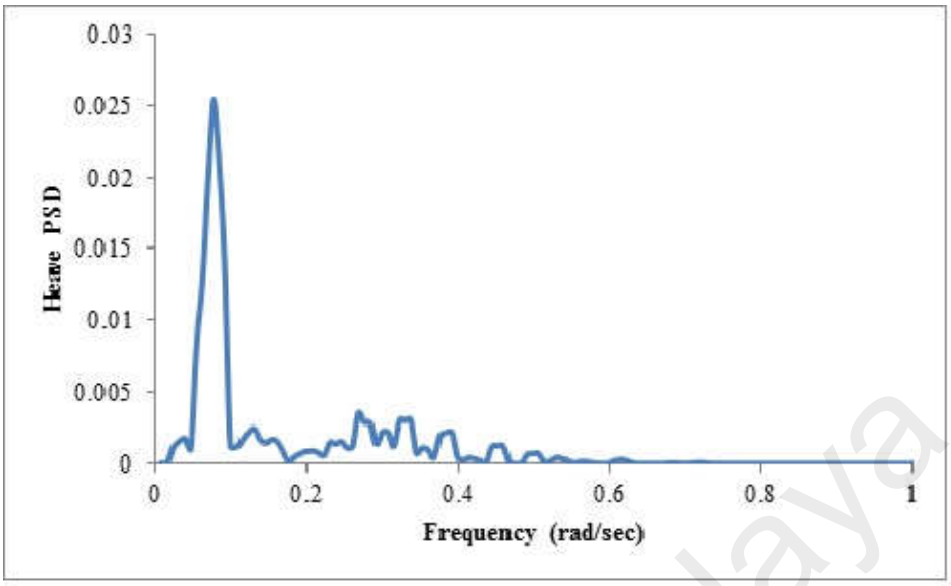

Figure 4.22: PSD of heave response (Present study)

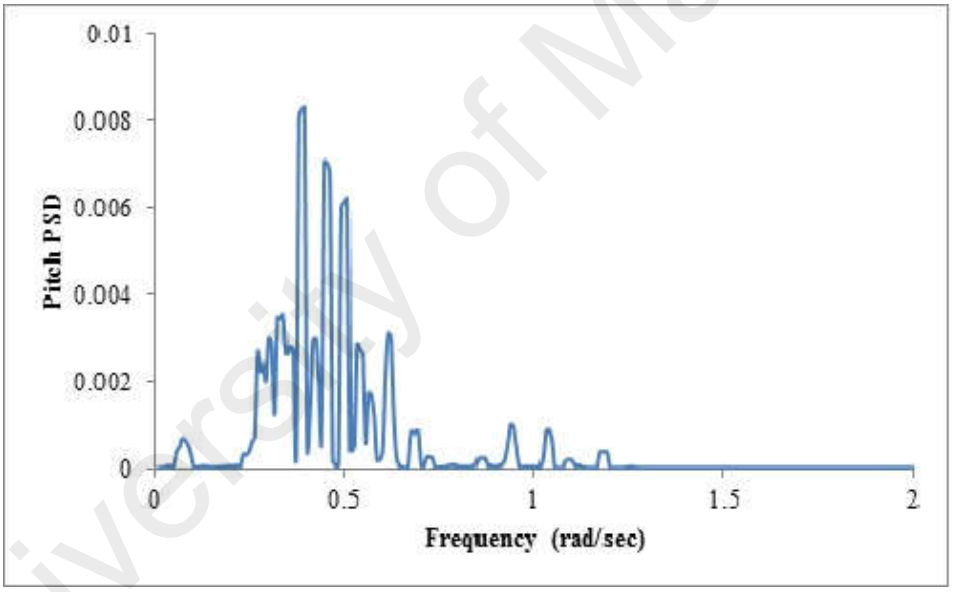

Figure 4.23: PSD of pitch response (Present study)

University of Malaya

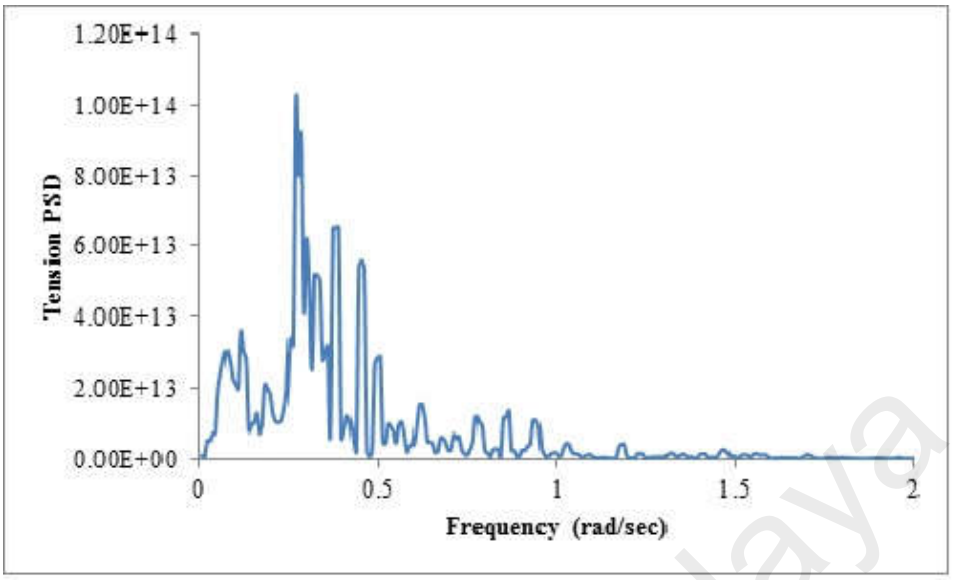

Figure 4.24: PSD of tension response (Present study)

4.3 Numerical study

The International Ship and Offshore Structures Congress (ISSC) TLP was employed for numerical simulation. The choice of the ISSC TLP is based on the fact that the TLP does not represent any existing TLP in operation but rather a case study that has been widely researched and reported on. In Taylor and Jefferys (1986), seventeen organisations participated in providing data for loads and responses of the TLP. The method adopted by the majority was boundary element formulation. In addition, the ISSC TLP has been widely used for research by different organisations and individuals such as Chatterjee et al. (1996), Senjanovic, Tomic, and Rudan (2013); Zeng, Liu, Liu, and Wu (2007), Low (2009), and Senjanovic, Tomic, and Rudan (2013).

The present research employed the Morison equation method and the linear airy wave theory for the calculation of wave kinematics with their corresponding forces and motion on the platform in the time domain. This approach was employed so as to incorporate viscous forces, nonlinearities in the time domain and to establish that the

University of Malaya

developed codes can be employed for the solution of hydrodynamic problems. The platform principal parameters are summarized in Table 4.4 while hydrodynamic and aerodynamic properties are also stated in Table 4.5

Table 4.4: Main particulars of ISSC TLP Senjanovic, Tomic, and Hadzic (2013)

Parameters	Value
Column spacing between centres	86.25 m
Column diameter	16.88m
Pontoon width	7.50 m
Pontoon height	10.50 m
Draft	35.00 m
Displacement	5.346×10^5 kN
Weight	3.973×10^5 kN
Total tether pretension	1.373×10^5 kN
Longitudinal metacentric height	6.0 m
Transverse metacentric height	6.0 m
Platform mass	40.5×10^6 kg
Roll mass moment of Inertia	82.37×10^9 kg m^2
Pitch mass moment of Inertia	82.37×10^9 kg m^2
Yaw mass moment of Inertia	98.07×10^9 kg m^2
Vertical position of COG above Keel	38.0 m
Length of Mooring tethers, L	415.0 m
Vertical stiffness of combined tethers, EA/L	0.813×10^6 kN/m
Roll and Pitch effective stiffness, EI_x/L, EI_y/L	1.501×10^9 kNm/rad

Table 4.5: Hydrodynamic and Aerodynamic Data

Parameter	Value
Sea Drag Coefficient, C_D	1.0
Sea Inertia Coefficient, C_M	2.0
Coefficient of Wind Drag, Ca	2.0
Surface current velocity (m/s)	1.05
Mean Wind Velocity (m/s)	50.10
Mass Density of Water	1025 kg/m^3
Mass Density of Air, $\boldsymbol{\rho}_a$	1.25 kg/m^3
Sea State parameters	H_s = 12m, T_p = 14s

4.3.1 Comparison of natural periods of oscillation of the ISSC TLP

The first set of results aimed at ensuring that the motion response was as a result of external forces and not from platform instability. This was achieved by summing vertical forces in accordance with Equation 4.1 for static equilibrium at the undisturbed position.

University of Malaya

The expected natural time period was reported in Gie and de Boom (1981) for the uncoupled TLP and reproduced in Table 4.6 along with the analytical calculation for the present study using Equation 4.2. From Table 4.6, we can see that results were in close agreement with each other. This authenticate that the platform simulated is the same with the one in the published result.

Table 4.6: Expected natural periods of motion

	Published		Present Study	
Degree of Freedom	Time (s)	Frequency (rad/sec)	Time (s)	Frequency (rad/sec)
Surge (Sway)	106.00	0.06	106.57	0.06
Heave	2.000	3.14	1.98	3.17
Roll (Pitch)	2.100	2.99	2.20	2.86
Yaw	86.00	0.07	85.50	0.07

4.3.2 Response of an uncoupled TLP in regular and random waves

The ISSC TLP was analysed for the Gulf of Mexico (GOM) sea conditions with significant wave height of 12 m and spectral peak period of 14 s respectively. In order to assess regular wave elevation, mathematical representation of regular wave in Section 3.3.1 was made use of. Random waves were characterized by summing individual regular wave energy which resulted in what is known as wave spectrum. The random waves were simulated based on the approach discussed in Section 3.3.2 of Chapter Three. Furthermore, the spectrum used in long-crested sea failed to incorporate wave directionality, which underestimate the true behaviour of the actual sea. The directional spectrum as calculated in Section 3.3.2.1 was formulated from unidirectional spectrum with frequency independent cosine power type energy spreading function. The simulation of wave profile was carried out for a length of 5000 seconds with the time interval of 0.2 seconds. The results of the wave profile shown in Figure 4.25 revealed regular wave idealisation have the same form in time and space which is thought to be in contrast with the random wave characterization which resembles what the ocean surface should look like because the shape, height and

University of Malaya

length differ from wave to wave and practically impossible to distinguish each wave from one another. Wave elevation profile for the directional random sea simulation comes with a reduced magnitude. In addition, Figure 4.26 is the equivalent energy spectrum based on the Pierson–Moskowitz model, (P.M) and the area under the curve gives the total energy for the considered ocean environment.

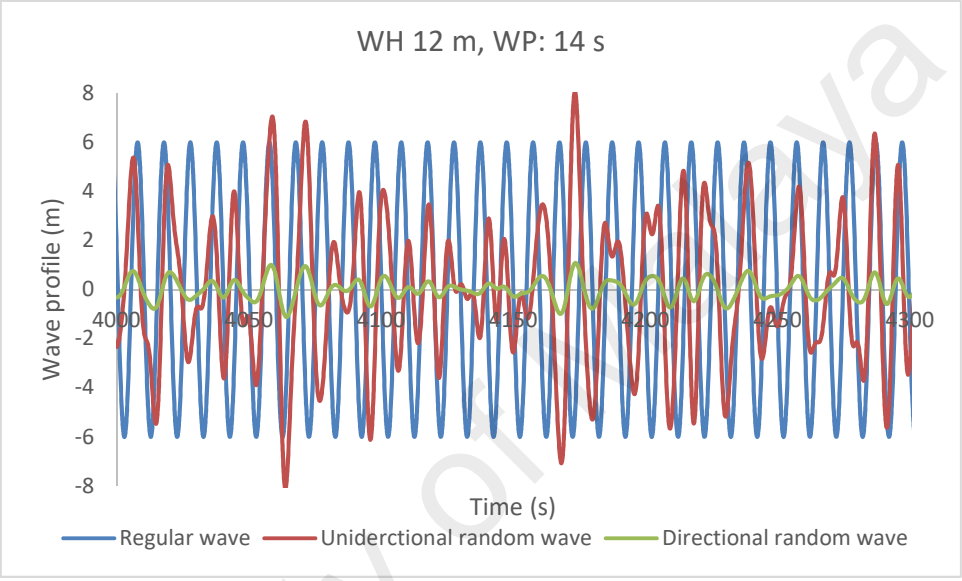

Figure 4.25: Time history of wave surface profiles

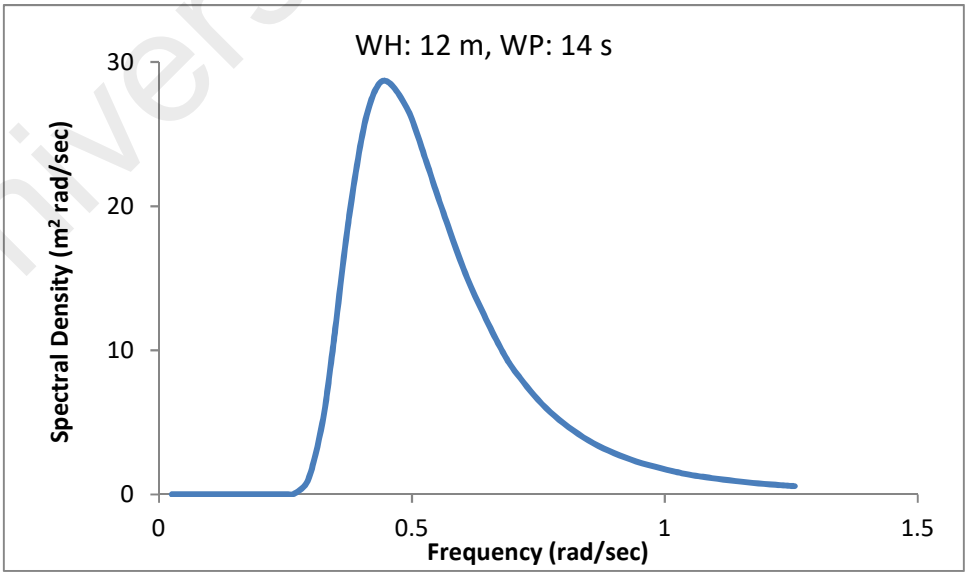

Figure 4.26: Pierson–Moskowitz spectrum

University of Malaya

In regular wave modelling, horizontal velocity was in phase with wave profile whereas vertical velocity differs with horizontal velocity and it was 90^0 out of phase. At deeper water depths, the values of vertical and horizontal velocities approached each other, (Figures 4.27 and 4.28) and this behaviour was also reported in Chakrabarti (2005). The same phenomenon was recorded for particle accelerations in Figures 4.29 and 4.30. However, inertia and drag forces in the horizontal component was in phase with each other as depicted in (Figures 4.27 and 4.29), and out of phase in vertical component as depicted in (Figures 4.28 and 4.30). These expressions are used for calculating the Morison forces in Equations 3.72 to 3.77. The total force in each direction, which was a summation of inertia and drag forces with the additional value of added mass, are represented in Figures 4.31 to 4.32. For unidirectional random waves, the horizontal velocity is out of phase with the vertical velocity whereas the horizontal acceleration is in phase with the vertical acceleration. Thus, the drag force from the horizontal velocity is out of phase with the inertia force from the corresponding horizontal acceleration while the vertical velocity is in phase with the vertical acceleration which also applies to their respective forces. When water kinematics of the unidirectional random wave were compared with regular wave, it was discovered that trend in the regular wave was repetitive with constant magnitudes, while the patterns in unidirectional random wave were not repetitive and the magnitudes were lower in values compare to the regular wave water kinematics. The values of water wave kinematics as well as the resulting hydrodynamic forces for the directional random waves were lower compared to the regular and unidirectional random waves.

University of Malaya

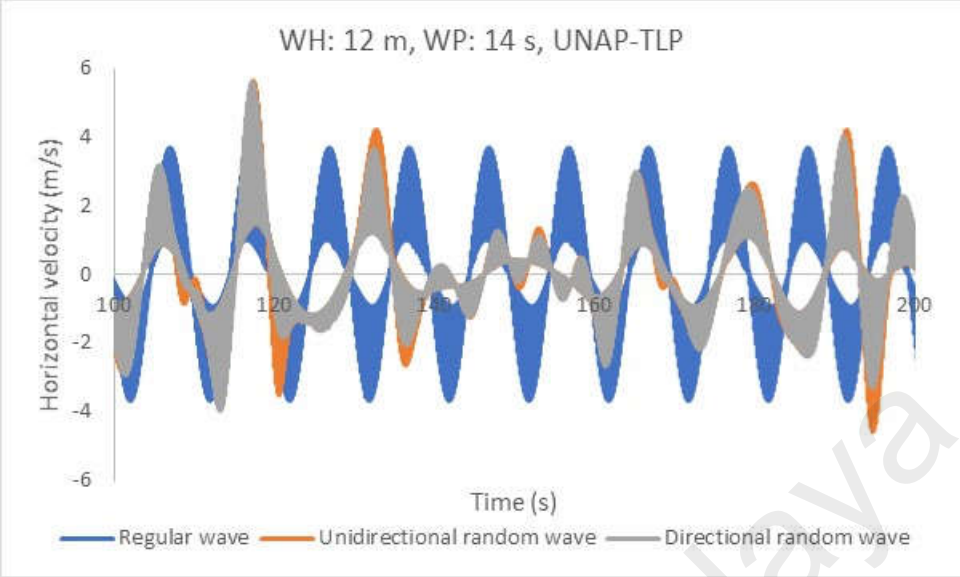

Figure 4.27: Horizontal velocity on vertical column one

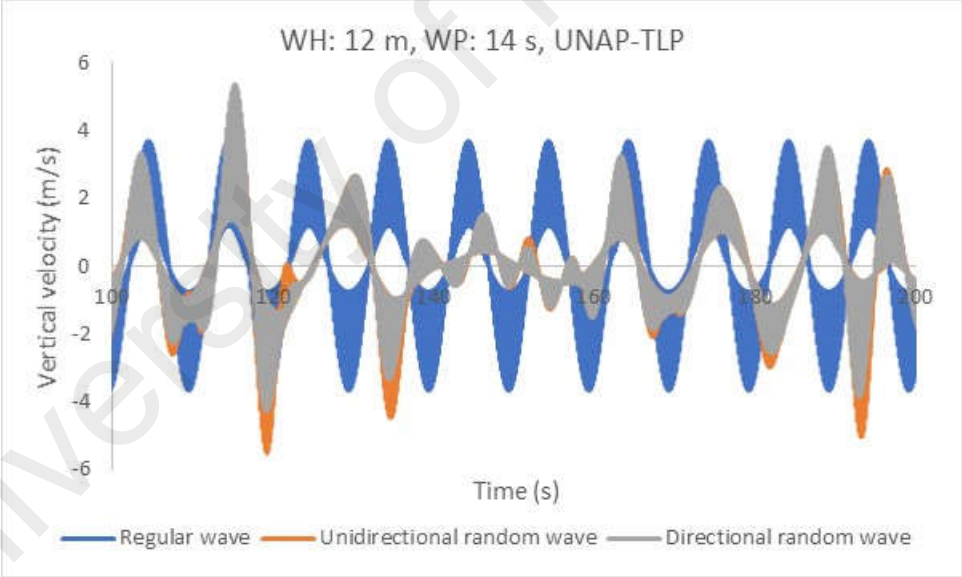

Figure 4.28: Vertical velocity on vertical column one

University of Malaya

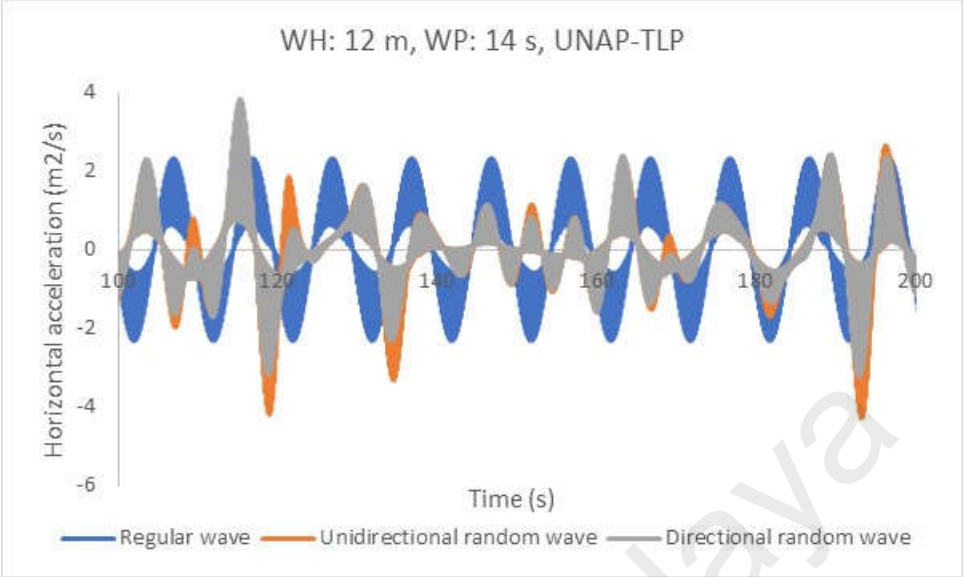

Figure 4.29: Horizontal acceleration on vertical column one

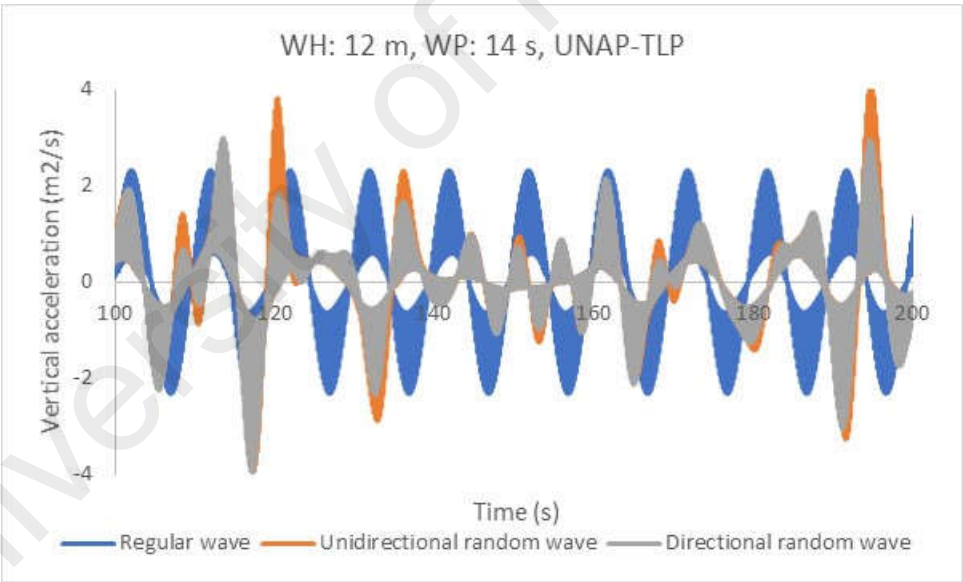

Figure 4.30: Vertical acceleration on vertical column one

University of Malaya

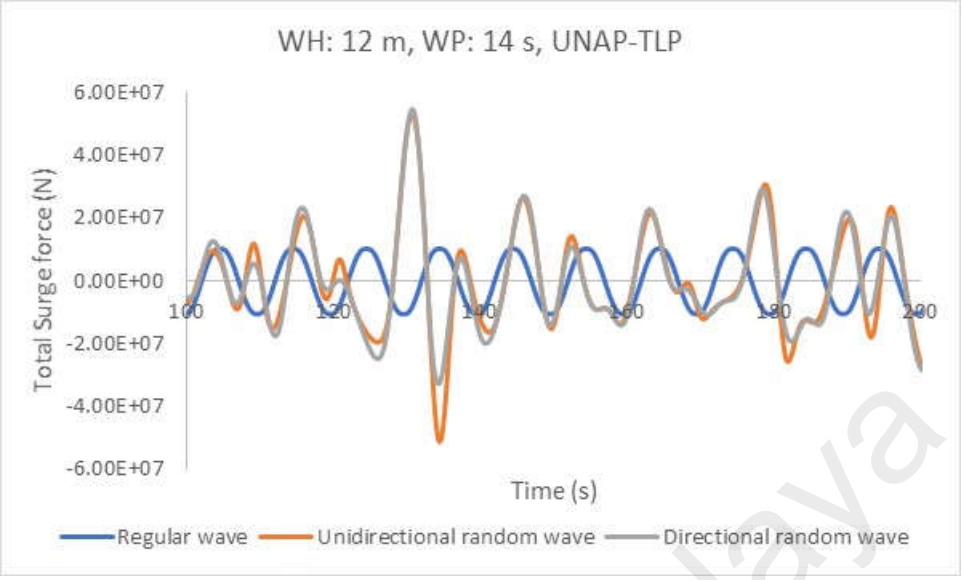

Figure 4.31: Time history of total Surge force

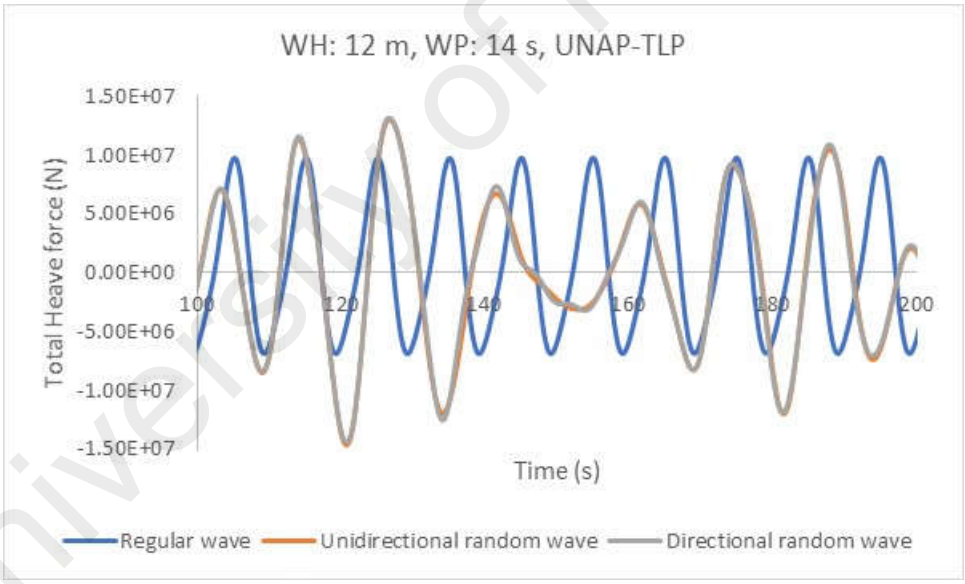

Figure 4.32: Time history of total Heave force

University of Malaya

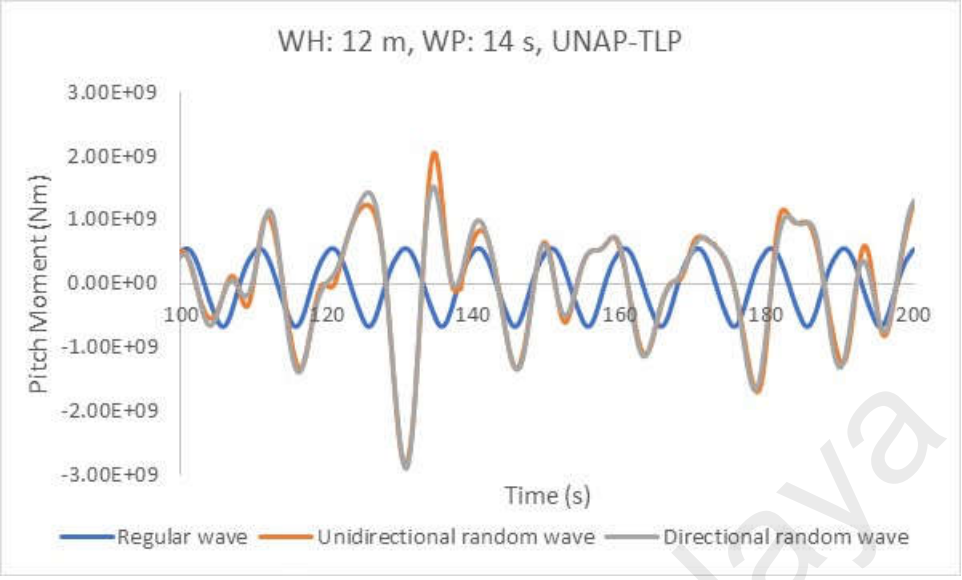

Figure 4.33: Time history of total Pitch force

The time history of the oscillation for the platform response in all degrees of freedom in Figure 4.34 showed regular patterns for regular wave and stochastic for unidirectional and directional random waves with platform being about the mean position and their values were found to be small in relation to the wave elevation. One key difference is that the surge magnitude in directional random wave is smaller compared to the outcome in unidirectional random seas. The time histories of high frequency response of heave and pitch motions are shown in Figures 4.35 and 4.36 with very high fluctuations. However, their numerical values are very small compared to surge, due to the huge tension in the tendons that restrain the vertical motions drastically. The time history of tendon tension variation shown in Figure 4.37 come with a rapid fluctuation which was due to the high-frequency motions and variable submergence associated with the vertical motions.

University of Malaya

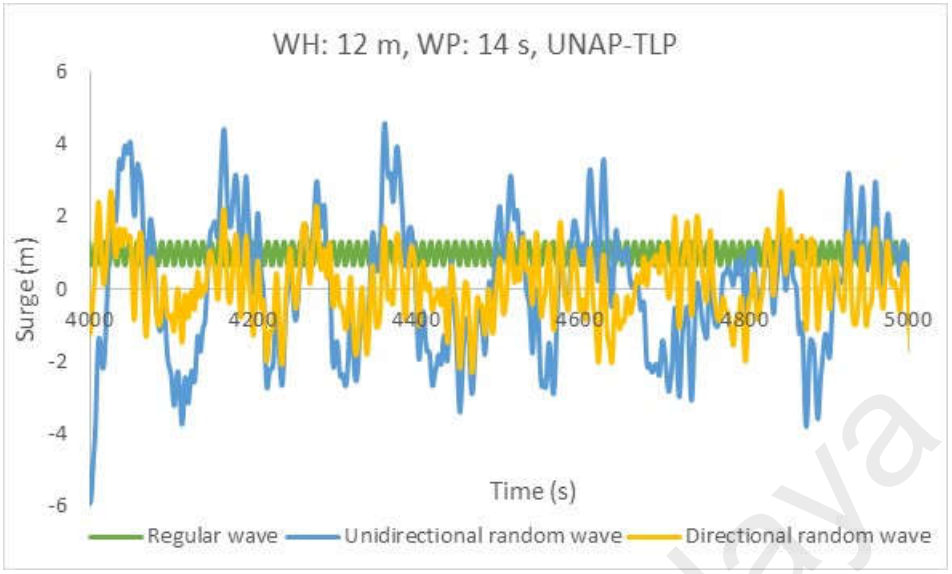

Figure 4.34: Time history of Surge response

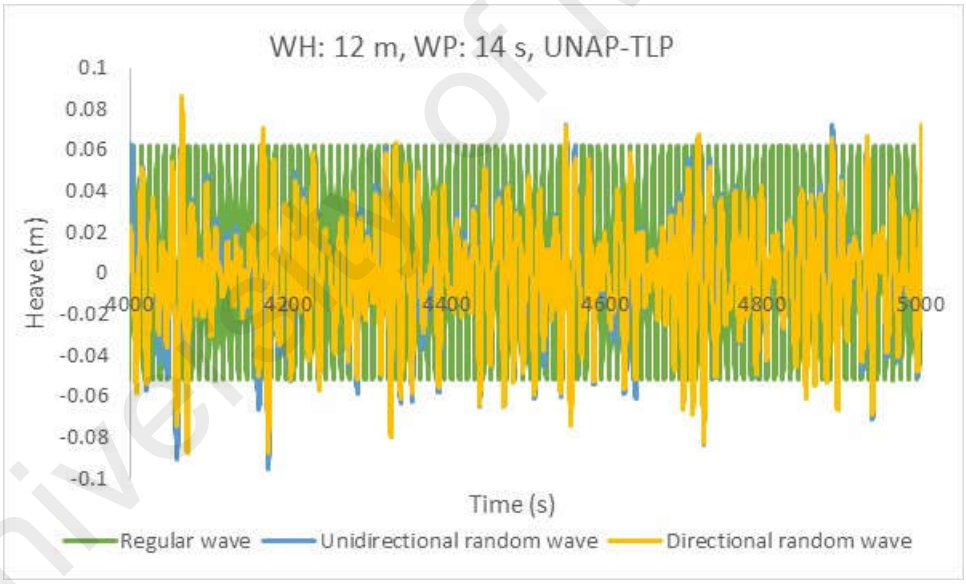

Figure 4.35: Time history of Heave response

University of Malaya

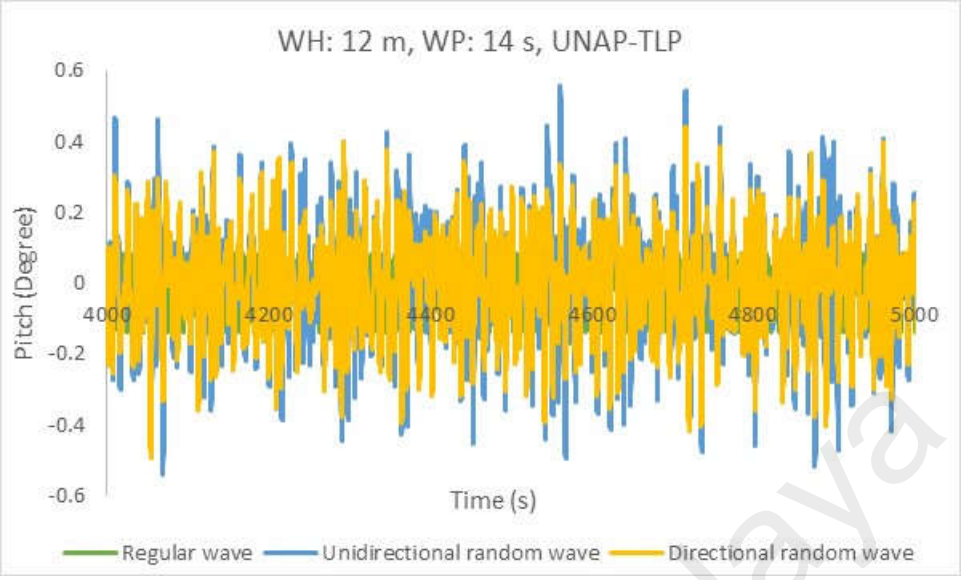

Figure 4.36: Time history of Pitch response

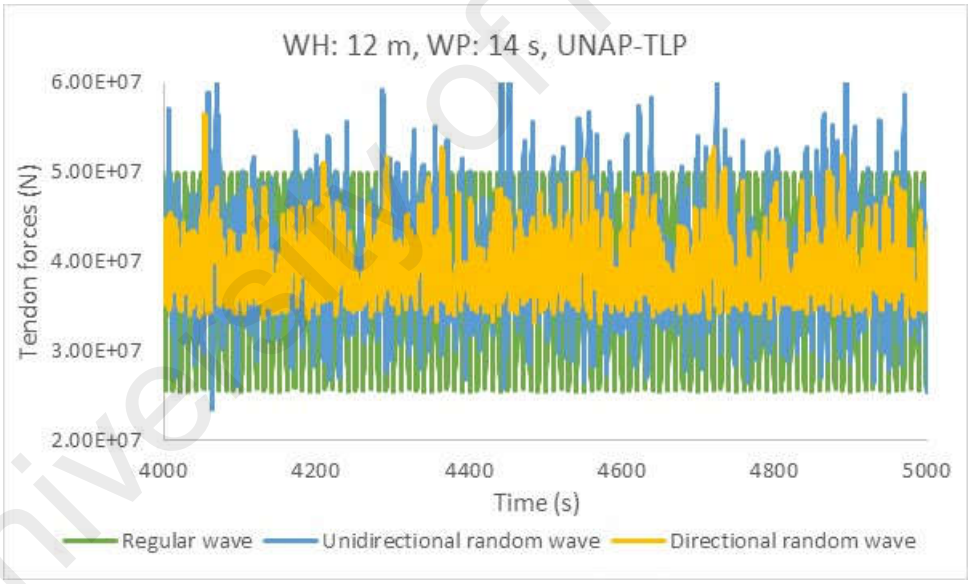

Figure 4.37: Time history of Tendon forces response

The only peak in the surge PSD for regular wave modelling in Figure 4.38 occurred at the frequency of 0.64 rad/sec which is equivalent to time period of 9.76 secs. This time period is the same with the zero up-crossing wave period for the wave frequency, and there is no appearance of peak at surge natural time period as noticed in unidirectional and directional random wave simulation. The heave PSD of the regular wave modelling in Figure 4.39

University of Malaya

shows two peaks. The first peak which is the most prominent peak occurred at the frequency of 0.64 rad/sec which happens to be the wave frequency while the second peak at the frequency of 1.27 rad/sec did not fall at any natural period of oscillation of the TLP. This can be regarded to have happened as a result of nonlinearity in the platform. The area under the PSD curve is smaller compared to the surge PSD. For motion response in unidirectional and directional random wave modelling, their first prominent peak was around the surge natural frequency, which was absolutely absent in the case of regular wave only and other cluster of peaks were noticed at the forcing frequency. The occurrence of other peaks in Figure 4.40 apart from the peaks at surge and wave forcing frequencies reveals the presence of nonlinearities and a very strong need for dynamic analysis.

In Figure 4.41, PSD of the tendon forces in regular wave modelling shows that the first prominent peak is at wave frequency and the second peak is most likely due to the nonlinearity. The PSD of the tendon tension variation of unidirectional and directional random waves also revealed that surge natural frequency attracted much energy as this affects other degrees of freedom as well as tendon tension. The lower peaks in the tendon tension PSD confirm evidence of nonlinearities and tension variation in the tendons.

The implication of wave characterization is that vibration of the platform occurred around the wave forcing frequency for regular wave and around surge natural frequency and forcing frequency for random waves. The same trend of regular behaviour of the platform in regular wave has been previously reported in Jameel, Oyejobi, Siddiqui, and Ramli Sulong (2016) and Jain (1997). The time average and other statistical parameters for each sea modelling were reported in Table 4.7. It is observed that the ratio of directional RMS values of surge, heave, pitch and tension to unidirectional random seas values are (1:2.08; 1:1.04; 1:1.12 and 1:1.03) which translate to 108%, 3.75%, 12.44% and 2.82%. The unidirectional random sea produced higher motion responses to the tune of calculated

University of Malaya

percentage due to the lack of wave directionality. Since the directional random waves incorporated waves of different heights, frequencies, phase angle and directions, the wave characterization and the platform response is recommended as an ideal result.

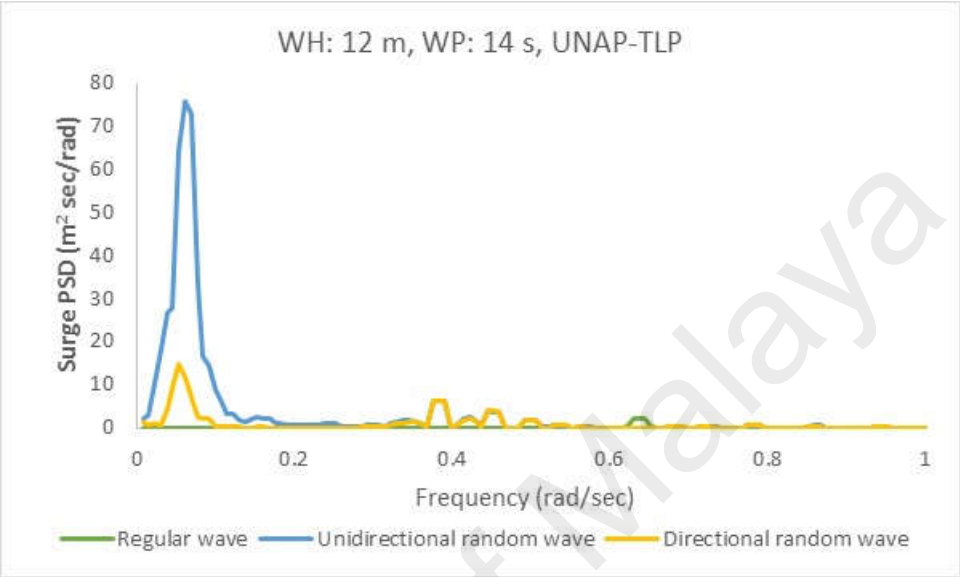

Figure 4.38: Power spectral density of Surge response

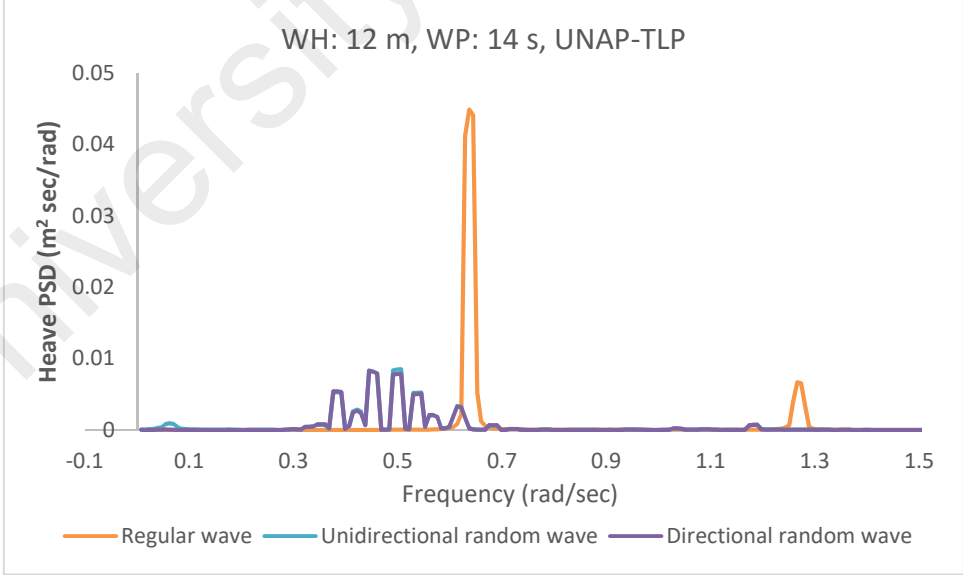

Figure 4.39: Power spectral density of Heave response

University of Malaya

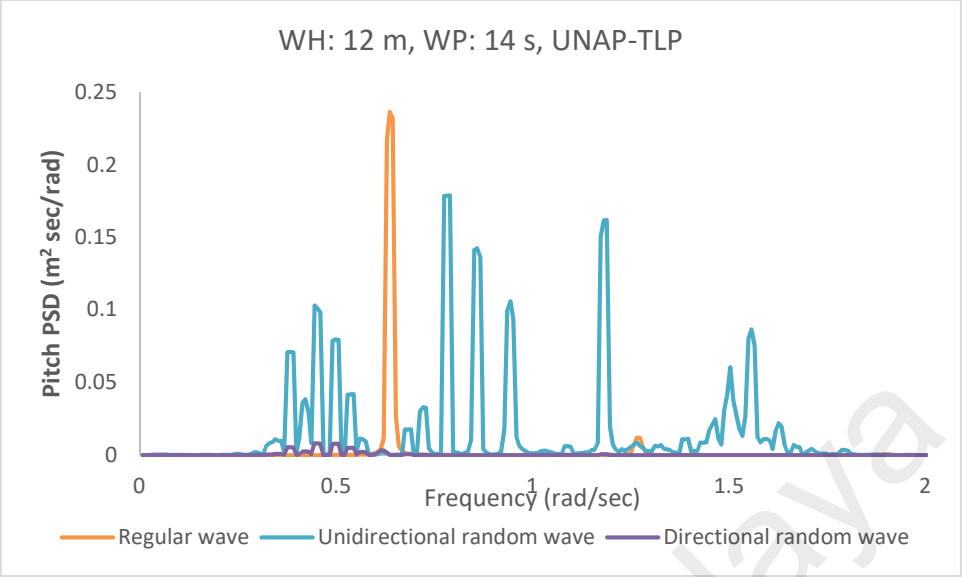

Figure 4.40: Power spectral density of Pitch response

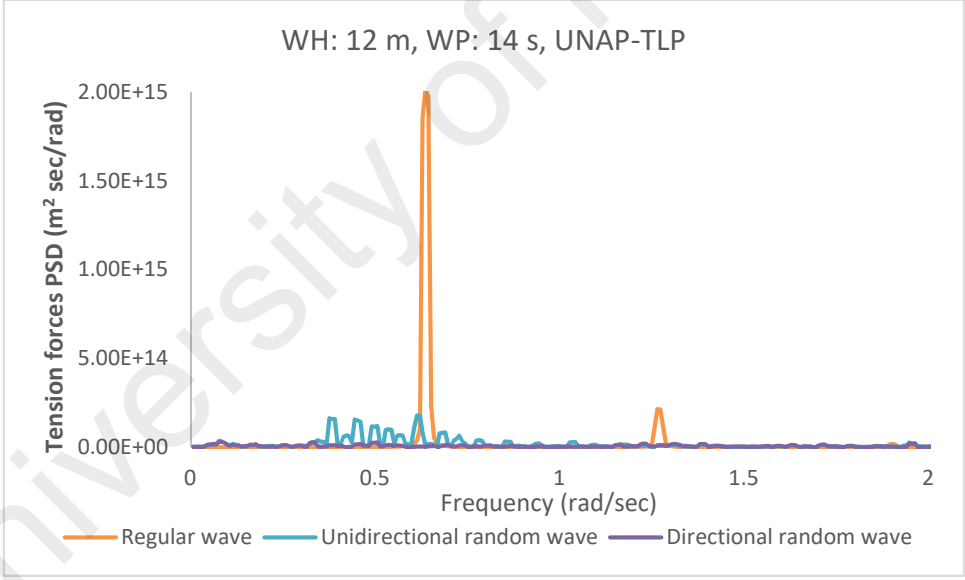

Figure 4.41: Power spectral density of Tendon forces response

University of Malaya

Table 4.7: Comparison of platform response in various wave characterization

Regular Wave					
Parameters	Minimum	Maximum	Mean	STD	RMS
Surge (m)	0.66	1.32	0.99	0.23	1.01
Heave (m)	-0.05	0.06	0.00	0.04	0.04
Pitch (Deg)	-0.14	0.08	-0.01	0.08	0.08
Tension (N)	2.56E+07	4.99E+07	3.88E+07	7.46E+06	3.95E+07
Unidirectional Random Wave					
Parameters	Minimum	Maximum	Mean	STD	RMS
Surge (m)	-6.47	5.60	-0.02	1.95	1.95
Heave (m)	-0.11	0.11	0.00	0.03	0.03
Pitch (Deg)	-0.66	0.84	-0.01	0.18	0.18
Tension (N)	2.21E+07	7.31E+07	4.09E+07	6.86E+06	4.15E+07
Directional Random Wave					
Parameters	Minimum	Maximum	Mean	STD	RMS
Surge (m)	-2.96	3.03	-0.01	0.94	0.94
Heave (m)	-0.11	0.11	0.00	0.03	0.03
Pitch (Deg)	-0.58	0.61	-0.01	0.16	0.16
Tension (N)	3.30E+07	5.90E+07	4.01E+07	3.78E+06	4.03E+07

4.3.3 Effect of current force on an uncoupled TLP in regular and random waves

The ocean waves take place in the presence of current force, which could act along or opposite the wave direction. The TLP used as case study is inertia-dominated as calculated in Section 3.4 and the surface current velocity of 1.05 m/s was assumed for the present study at the surface level and 0 m/s at the sea-bed along the wave direction. This was incorporated with the water wave velocity in Equation 3.81 and varied along the length of each platform member. The contributing effect of current velocity on platform response in regular and irregular waves is presented in form of time histories in Figure 4.42. This comes with an offset displacement from the original mean position compared to the regular and irregular wave actions only, (Figure 4.34). The increase in the surge response was as a result of current additional force added to the hydrodynamic force which reduced the restoring force. There was a decrease in positive heave magnitude and a downward increase in heave response in Figure 4.43. This can be attributed to the action of current drag force

University of Malaya

that increased surge response in horizontal direction, increased buoyancy force and also increased pretension force. The time history of pitch response in Figure 4.44 was not adversely affected by the presence of current when compared with Figure 4.36 without current force. Furthermore, the result of time history of variation of tension in the tendon is represented in the Figure 4.45 with regular and stochastic pattern behaviours in the oscillation for regular and irregular wave idealization. The current force caused a slight reduction in the minimum tension and slight increase in the maximum value. However, the mean and RMS values remained almost the same in both scenarios. This can be as a result of counter-action between surge that increased surge motion and the negative increase in heave motion.

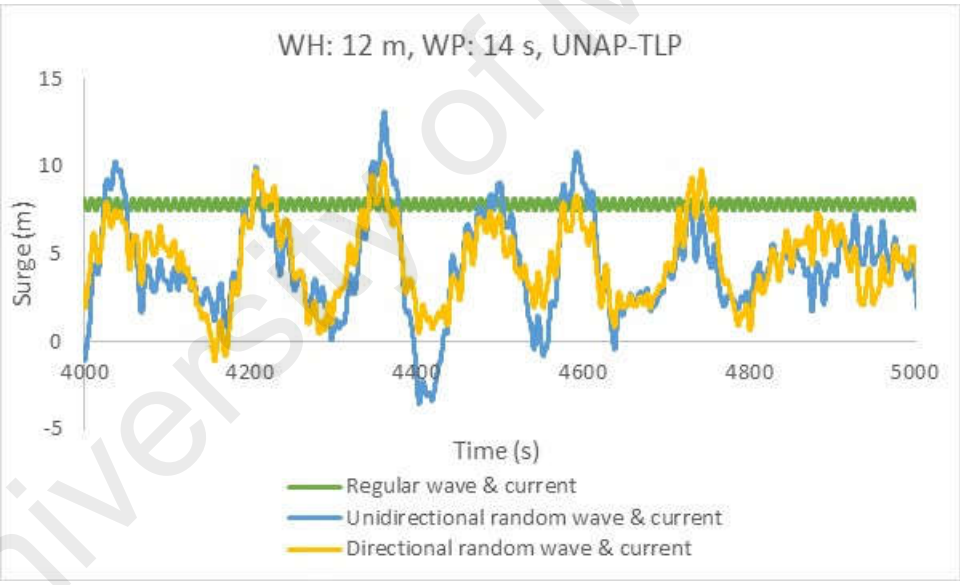

Figure 4.42: Time history of Surge response (Wave and current forces)

University of Malaya

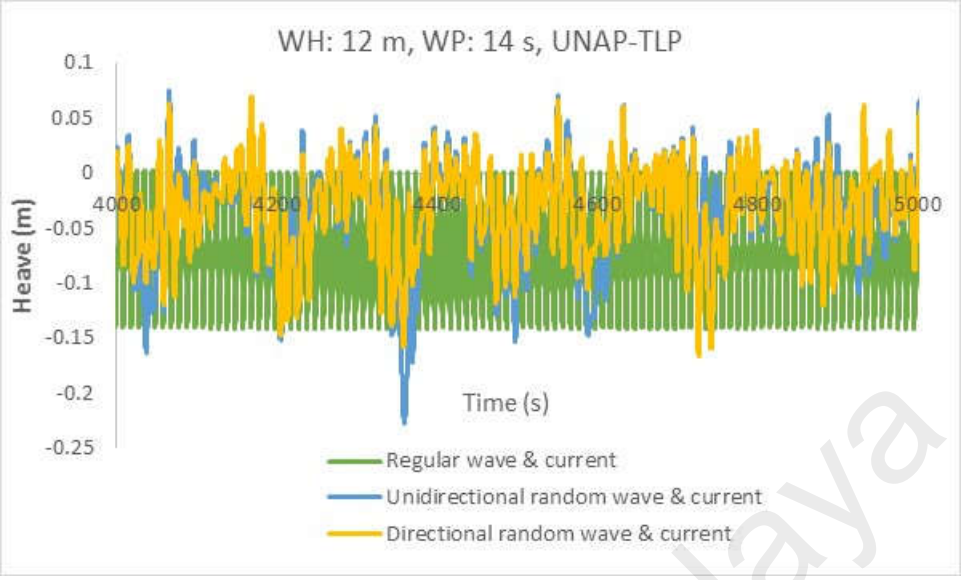

Figure 4.43: Time history of Heave response (Wave and current forces)

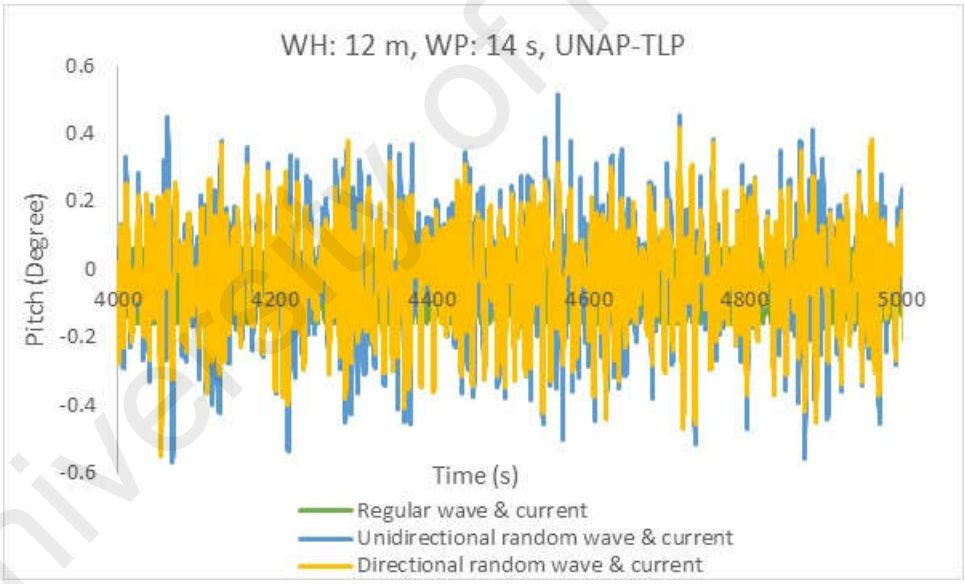

Figure 4.44: Time history of Pitch response (Wave and current forces)

University of Malaya

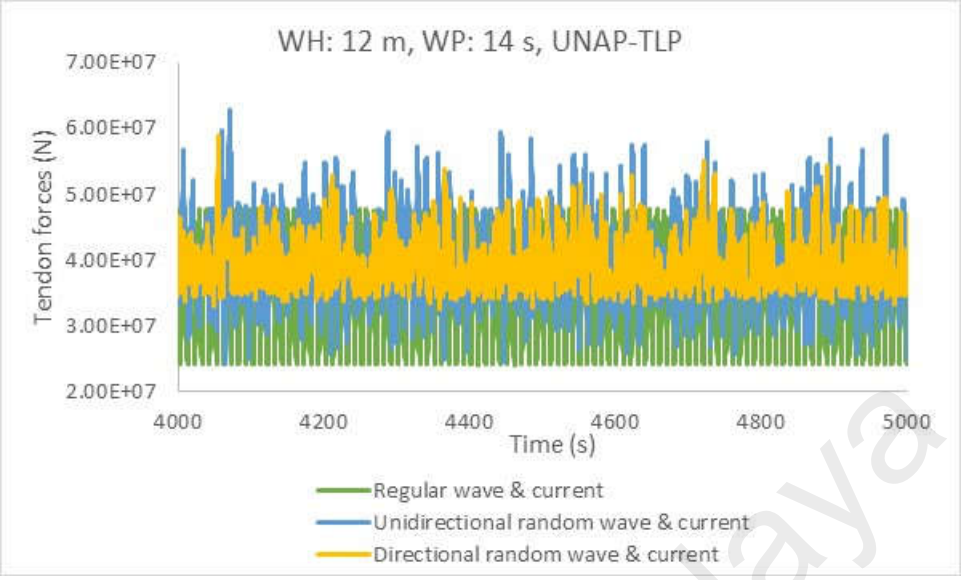

Figure 4.45: Time history of Tendon forces response (Wave and current forces)

The power spectral density in Figure 4.46 has the same trend with Figure 4.38 but there is an upward shift in the area of the PSD curve which was as a result of current force. The frequency of vibration occurred at 0.64 rad/sec which is at the wave frequency for regular wave and platform oscillates at surge and wave forcing frequency. The PSD for the heave response as reported in Figure 4.47 has the same pattern but slight increase in the energy density above the PSD heave response in Figure 4.39. The PSD of pitch response in Figure 4.48 has insignificant difference by the presence of current when compared with Figure 4.40. The tendon forces PSD in Figure 4.49 is slightly increased due to the presence of current force when compared with Figure 4.41. The different peaks in the pitch and tendon forces PSDs show the high fluctuation in the tendon tension variation and confirm presence of nonlinearities. The effect of wave directionality reduced the magnitude and energy densities in directional wave simulation compared to unidirectional random waves. By comparing Table 4.8 with Table 4.7, the effect of current velocity force reduced the

University of Malaya

restoring force on the platform and this action increased the platform motion and causes changes in the maximum and minimum tendon forces.

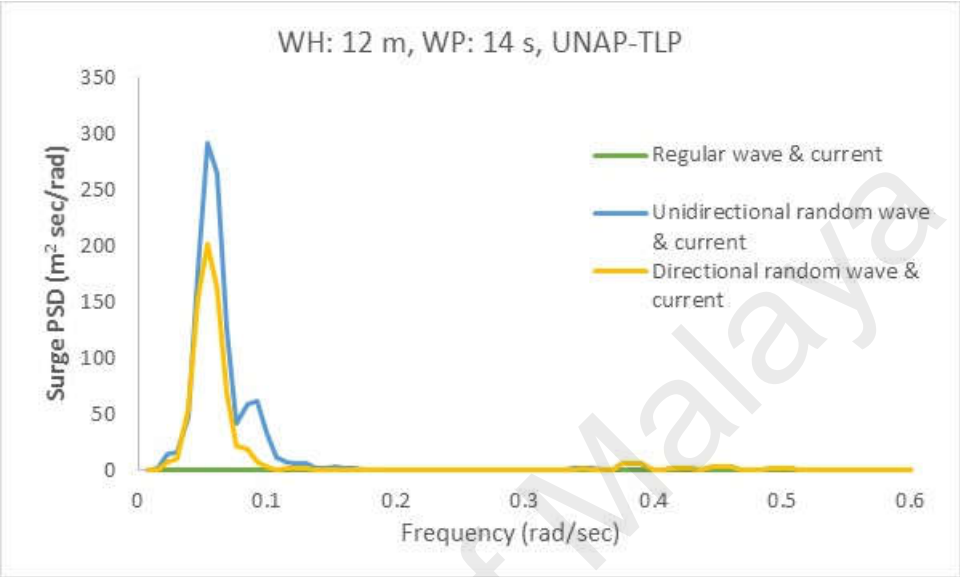

Figure 4.46: Power spectral density of Surge response (Wave and current forces)

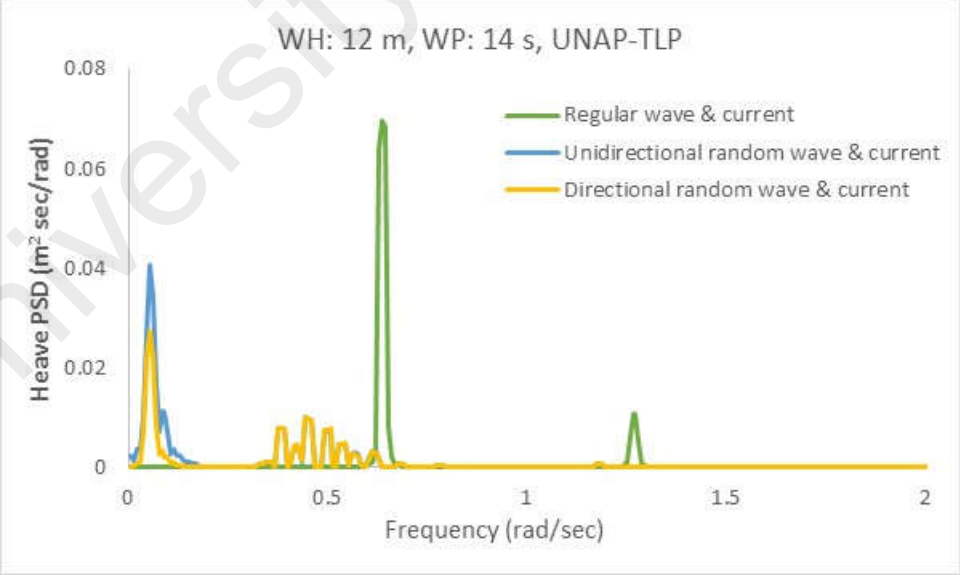

Figure 4.47: Power spectral density of Heave response (Wave and current forces)

University of Malaya

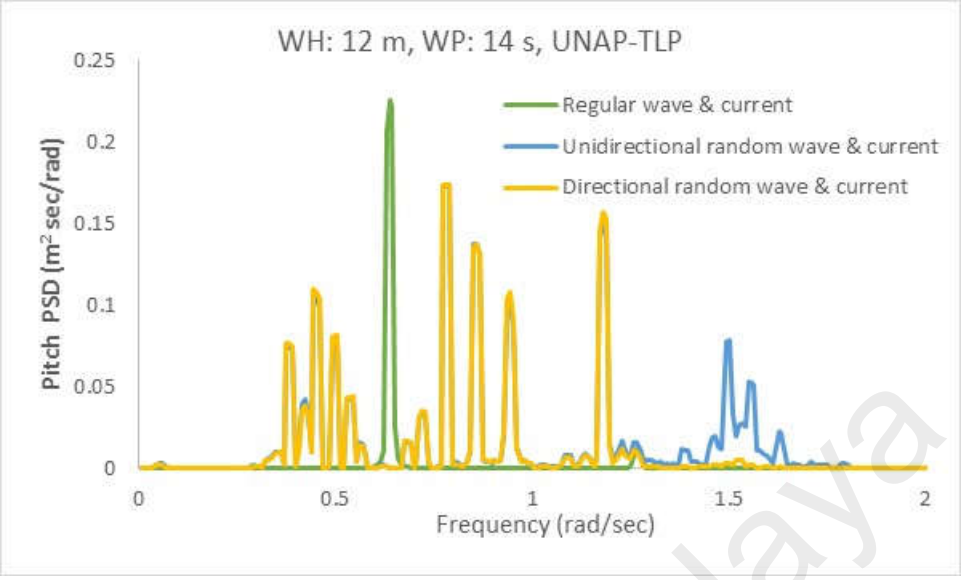

Figure 4.48: Power spectral density of Pitch response (Wave and current forces)

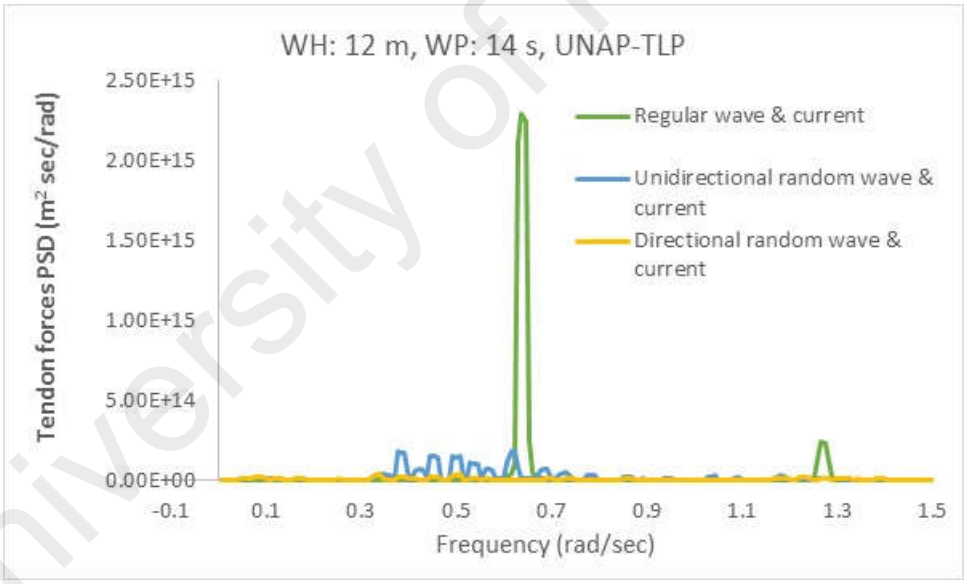

Figure 4.49: Power spectral density of Tendon response (Wave and current forces)

University of Malaya

Table 4.8: Comparison of platform response in different wave and current forces

Regular Wave and Current force					
Parameters	Minimum	Maximum	Mean	STD	RMS
Surge (m)	7.50	8.19	7.84	0.24	7.84
Heave (m)	-0.14	0.00	-0.07	0.04	0.09
Pitch (Deg)	-0.16	0.06	-0.04	0.08	0.09
Tension (N)	2.41E+07	4.77E+07	3.86E+07	7.91E+06	3.94E+07
Unidirectional random Wave and Current force					
Parameters	Minimum	Maximum	Mean	STD	RMS
Surge (m)	-7.15	14.06	4.22	3.38	5.40
Heave (m)	-0.31	0.09	-0.04	0.05	0.06
Pitch (Deg)	-0.71	0.76	-0.02	0.18	0.18
Tension (N)	1.99E+07	7.49E+07	4.07E+07	6.90E+06	4.13E+07
Directional random Wave and Current force					
Parameters	Minimum	Maximum	Mean	STD	RMS
Surge (m)	-4.34	11.67	4.40	2.64	5.13
Heave (m)	-0.22	0.09	-0.03	0.04	0.05
Pitch (Deg)	-0.58	0.50	-0.02	0.16	0.16
Tension (N)	3.28E+07	5.91E+07	4.01E+07	3.96E+06	4.03E+07

4.3.4 Effect of wind force on an uncoupled TLP in regular and random waves

The behaviour of TLP in wave - current - wind environment is discussed in this section. The mean and fluctuating component winds have been detailed out in Section 3.4.4 and the results of their simulation are represented using time history, PSD and statistical properties. With the magnitude of mean wind speed of 50.1 m/s for the GOM case study, the platform was substantially influenced by this amount, resulting in a maximum departure from the negative minimum surge value to the positive maximum value as shown for surge time history. The behaviour of surge response in combined effect of regular wave, current and wind force in Figure 4.50 is observed to be totally different from regular pattern as witnessed for regular wave only, this can be accentuated to be the effect of fluctuating wind component. The surge statistical values are all positive and stochastic in its behaviour for unidirectional and directional waves. The positive response is as a result of drag forces from current and wind forces.

University of Malaya

The time history of the heave response is shown in Figure 4.51 with increase in negative displacement direction due to the wind force. The higher increased values were as a result of current and wind forces on the platform. In addition, the time history of pitch response in regular and random waves along with current and wind forces is reported in Figure 4.52. The pitch response did not significantly increase in value as much as surge and heave responses increased. This suggests that undue discomfort due to rotational moment was not envisaged on the platform. The time history of force variation in the tendon shown in Figure 4.53 for the combined actions of regular wave, current and wind forces portrayed regular shape but not completely sinusoidal in its form. It can be concluded that platform under the influence of wave, current and wind forces experienced large excursion with an increase in heave displacement but the variation of tension in the tendon is not as high as the motion response.

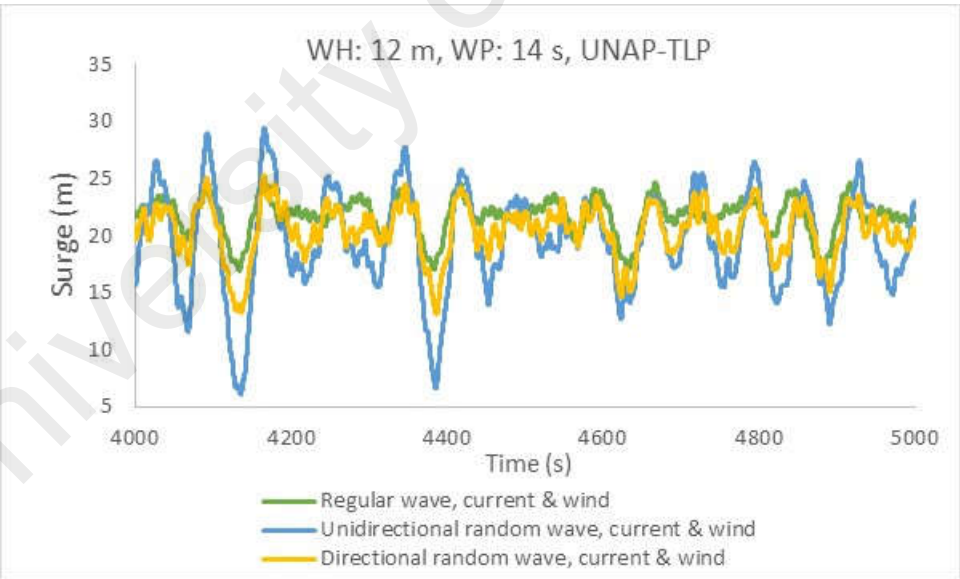

Figure 4.50: Time history of Surge response (Wave, current and wind forces)

University of Malaya

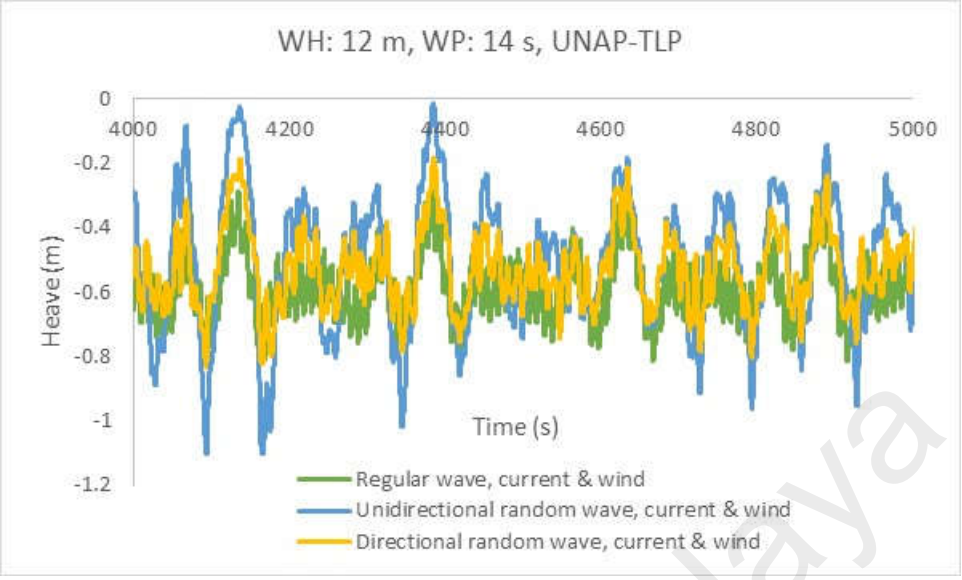

Figure 4.51: Time history of Heave response (Wave, current and wind forces)

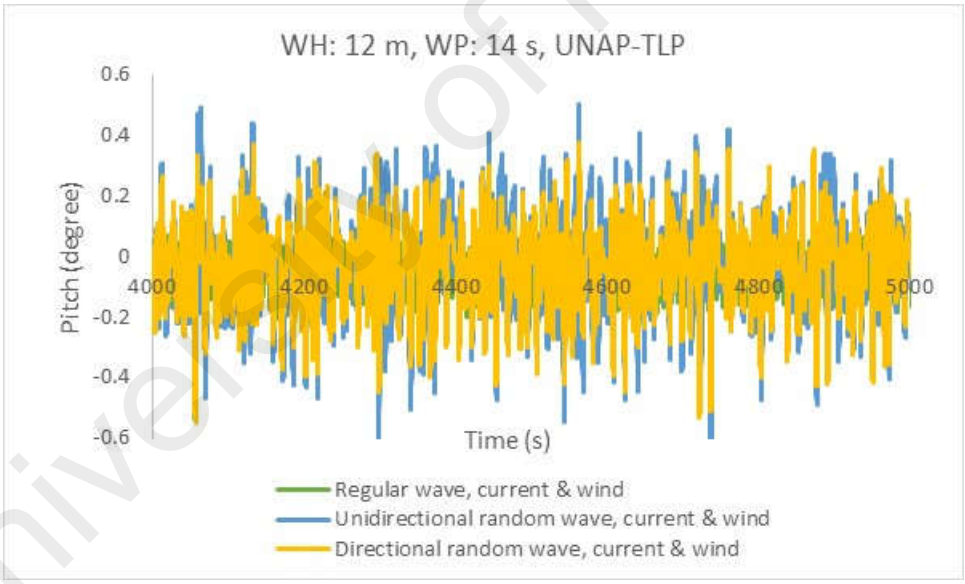

Figure 4.52: Time history of Pitch response (Wave, current and wind forces)

University of Malaya

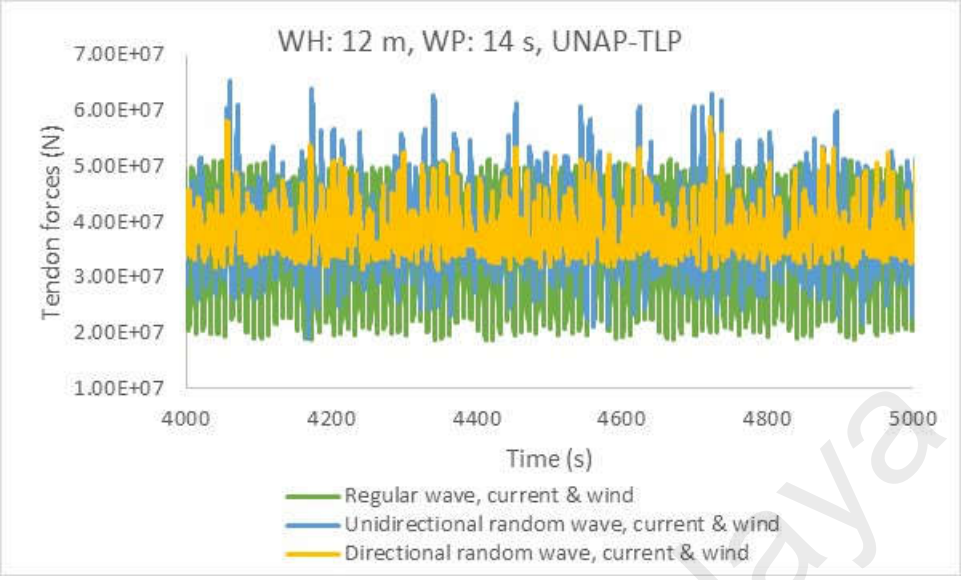

Figure 4.53: Time history of Tendon response (Wave, current and wind forces)

The surge PSD is represented in Figure 4.54 and there is a cluster of peaks in the spectrum which was absent in the previous PSD. This suggest that wind load is a low-frequency and cause the platform to amplify at these frequencies. The area under the cluster of the peaks of low frequencies is larger than the area under the amplification at the wave frequency. Figure 4.55 shows the PSD for the heave response and there are three sets of peaks. The first cluster of peaks was at lower frequencies and these are absent in heave response for previous discussion. This can be concluded to be as a result of wind force, the second peak occurred at the wave frequency and the last peak with reduced mean square can be assumed to be the effect of nonlinearity. The pitch PSD in Figure 4.56 shows about three different peaks but the only prominent peak occurred at the wave frequency and this can be implied that effect of wind loading as seen in surge and heave PSD is not pronounced in pitch degree of freedom. The existence of additional peaks at 0.03068 rad/sec in the PSD for regular wave suggest that the wind load is a low frequency force. Figure 4.57 shows the PSD for the tendon tension with only two peaks at wave frequency and the other as a result

University of Malaya

of variation in the tension for regular wave. The area under the PSD curve in this combined loading is larger than the area under the PSD curve of regular wave and this indicates the contribution of other forces. In unidirectional random wave, current and wind forces case, the energy content in the surge PSD curve in Figure 4.54 had also increased when compared with the surge PSD in Figures 4.38 and 4.46 for random wave only and random wave and current force respectively. The PSD in Figures 4.54, 4.55, 4.56 and 4.57 respectively shows cluster of peaks at some very low frequencies of 0.02301, 0.03835, 0.05369 rad/sec, which is as a result of wind load with the first prominent peak at 0.08437 rad/sec. Subsequently, the platform is governed mainly at these frequencies which are absent in the previous simulations. Thus, it is confirmed that TLP is sensitive to low-frequency load. Furthermore, there were also prominent peaks in pitch and tendon tension PSD, Figures 4.56 and 4.57 which can be attributed to outcomes of nonlinearities, variable tendon tension and wind random load on the platform. While tension variation remains almost unchanged, the motion responses behave differently in magnitude. It could be concluded from Table 4.9 that maximum, minimum, mean and RMS motions greatly increased when random wave, current and wind forces acted together except for tension RMS variation that diminished due to what can be likened to countering effect between surge and heave motion. Again, the wave directionality has reduced the energy content of PSDs for surge, heave, pitch motions and tendon tension variation in Figures 4.54, 4.55, 4.56 and 4.57 when compared with their counterparts for unidirectional random wave in the same Figures. The first set of the peaks in the PSDs of directional random waves are not pronounced and their frequencies are very low which can be termed to be as a result of wind forces on the platform. The first prominent peak and other cluster of peaks occurred at the surge natural frequency and wave forcing frequencies respectively. Other peaks prove the presence of nonlinearities and effect of tension variation in the tendons.

University of Malaya

Low frequency structural response has been identified to be of great importance in the dynamic behaviour of the TLP, Ahmad et al. (1997).

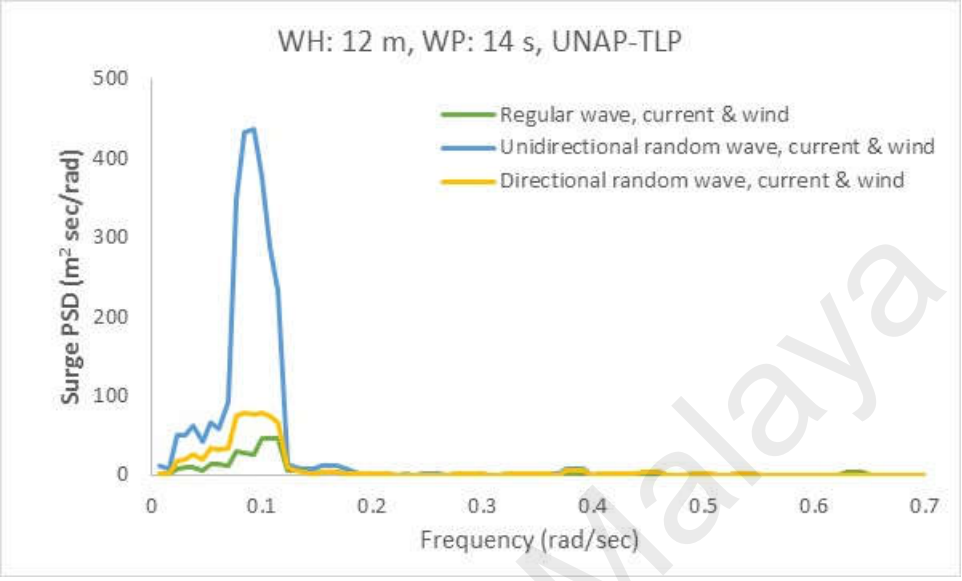

Figure 4.54: Power spectral density of Surge response (Wave, current and wind forces)

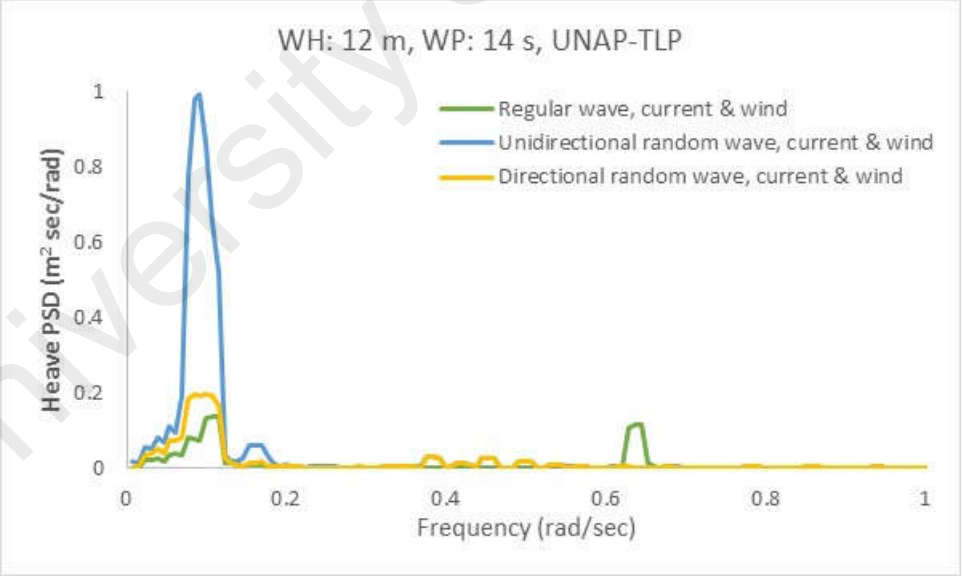

Figure 4.55: Power spectral density of Heave response (Wave, current and wind forces)

University of Malaya

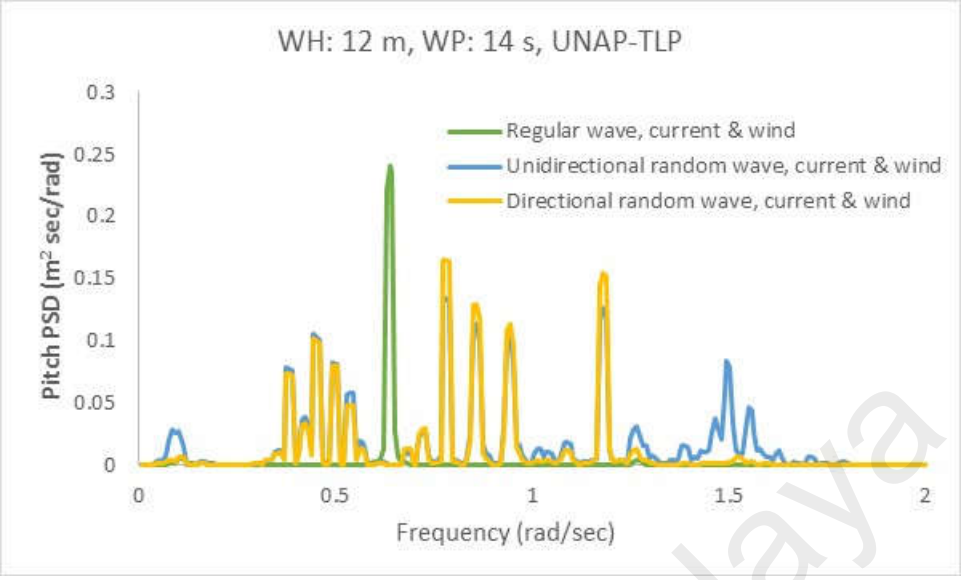

Figure 4.56: Power spectral density of Pitch response (Wave, current and wind forces)

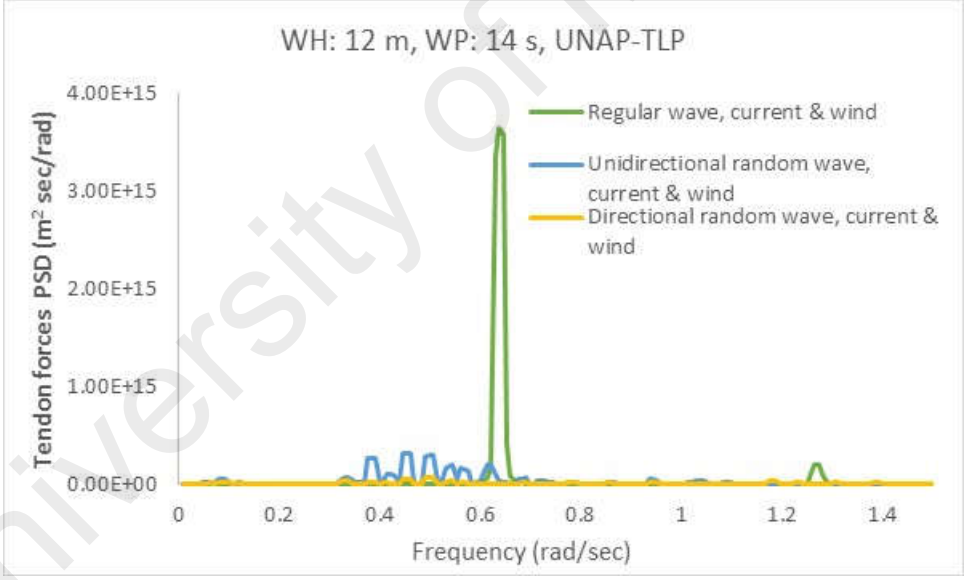

Figure 4.57: Power spectral density of Tendon response (Wave, current and wind forces)

With a small current velocity of 1.05 m/s and wind velocity of 50.1 m/s, noticeable differences were observed both in time history and power spectral densities of motion and tension responses. The tension RMS variation remained almost the same in all the load combinations. The maximum and minimum values give an indication of the extreme

University of Malaya

response values for the platform while the Root Mean Square (RMS) is recommended for the analysis of this type of problem since the simulation was carried out for a long period of time and is of stochastic in nature. The principle of 68 - 95 - 99.7 rule in statistics field was adopted to determine the percentage of values that lie around the mean value. Probability of RMS values of the responses proved that 99.7 percent of the values were included and these values are recommended for analysis purpose.

Table 4.9: Comparison of platform response in different wave, current and wind forces

Regular Wave, Current and Wind forces					
Parameters	Minimum	Maximum	Mean	STD	RMS
Surge (m)	16.96	24.73	21.70	1.65	21.76
Heave (m)	-0.81	-0.29	-0.59	0.10	0.60
Pitch (Deg)	-0.21	0.10	-0.04	0.08	0.09
Tension (N)	1.87E+07	5.15E+07	3.77E+07	9.78E+06	3.90E+07
Random Wave, Current and Wind forces					
Parameters	Minimum	Maximum	Mean	STD	RMS
Surge (m)	4.60	29.44	19.58	4.15	20.01
Heave (m)	-1.12	0.02	-0.50	0.20	0.54
Pitch (Deg)	-0.72	0.66	-0.03	0.18	0.18
Tension (N)	1.60E+07	7.25E+07	3.96E+07	7.51E+06	4.03E+07
Directional Wave, Current and Wind forces					
Parameters	Minimum	Maximum	Mean	STD	RMS
Surge (m)	11.07	26.11	20.40	2.44	20.55
Heave (m)	-0.90	-0.14	-0.53	0.13	0.55
Pitch (Deg)	-0.57	0.53	-0.03	0.16	0.16
Tension (N)	3.04E+07	5.99E+07	3.91E+07	4.37E+06	3.93E+07

4.4 Effect of the sea states on TLP motions

Table 4.10 shows eight different sea states from Siddiqui and Ahmad (2001) with sea state parameters in descending order. Results of the effect of each state were simulated with the Pierson-Moskowitz, (PM) spectrum. It was observed, as illustrated in Table 4.11, that a decrease in each sea state (from severe to less severe sea state) leads to a decrease in TLP motions. This trend is justified due to the fact that the PM spectrum is a function of wave height and wave period. The difference between the RMS motion response in sea

University of Malaya

state 1 and sea state 8 is quite large. Also, the higher sea state leads to increase in tension value in the tendons as seen in Table 4.16. A comparison of RMS tendon tension between sea state S1 and S8 showed that the difference in tendon tension for a least occurring sea state and the most occurring sea state was small, about 13%. However, for the surge and heave response, the differences are quite large, 296.98% and 257.14% respectively. This can be interpreted that although surge and heave responses are the major cause of tension variation in tendon, their combined influence over the tendon tension is considerably less.

The maximum and minimum tension values were determined from the combined actions of initial pretension and environmental forces on the TLP. Very interestingly, the maximum tension values largely determine the RMS tension values. Throughout the sea states in Table 4.16, the higher the sea state parameters, the higher the maximum tension value. Also, the lower the minimum tension value, the higher the RMS. The obtained results are in order because the maximum tension is normally used to evaluate strength criteria for tendons and their components while the minimum tendon tension in all the tendons are expected to be positive and this was confirmed to be so.

Table 4.10: Simulated sea states (Siddiqui and Ahmad 2001)

Sea State	WH (m)	WP (sec)	Wind velocity (m/s)	Probability of occurrence
S1	17.15	13.26	24.38	0.00000037
S2	15.65	12.66	23.29	0.00000238
S3	14.15	12.04	22.15	0.00001437
S4	12.65	11.39	20.94	0.00007980
S5	11.15	10.69	19.66	0.00040572
S6	9.65	9.94	18.29	0.00187129
S7	8.15	9.14	16.81	0.00773824
S8	6.65	8.26	15.18	0.02822122

University of Malaya

Table 4.11: Effect of different wave heights and wave time periods on TLP motion

	TLP Motions											
	Surge (m)				Heave (m)				Pitch (Deg)			
Sea States	Max	Min	STD	RMS	Max	Min	STD	RMS	Max	Min	STD	RMS
S1	9.98	-7.20	2.98	3.02	0.13	-0.20	0.05	0.05	0.98	-0.69	0.21	0.21
S2	8.76	-6.70	2.63	2.66	0.12	-0.18	0.04	0.04	0.93	-0.65	0.20	0.20
S3	7.95	-6.31	2.29	2.30	0.12	-0.16	0.04	0.04	0.86	-0.60	0.18	0.18
S4	6.46	-5.77	1.95	1.96	0.12	-0.14	0.03	0.03	0.78	-0.54	0.17	0.17
S5	4.99	-5.04	1.64	1.65	0.10	-0.11	0.03	0.03	0.71	-0.51	0.15	0.15
S6	3.46	-4.12	1.34	1.34	0.09	-0.09	0.02	0.02	0.62	-0.47	0.14	0.14
S7	2.77	-3.17	1.04	1.04	0.07	-0.07	0.02	0.02	0.54	-0.44	0.12	0.12
S8	2.24	-2.26	0.76	0.76	0.05	-0.04	0.01	0.01	0.45	-0.40	0.11	0.11

4.4.1 Effect of current velocity on the sea states

A linearly varying current velocity of 1.05 m/s at the sea surface and 0 m/s at the sea bed was assumed. With the same value of current velocity, as the sea state increased, the surge RMS values also increased, as presented in Table 4.12. The current velocity in conjunction with water particle along the same direction increased the drag force on the platform. For sea states 1 and 2, the maximum heave values increased when wave and current forces acted concurrently and started decreasing from sea state 3 to sea state 8. Additionally, there was an increase in negative direction for the minimum heave motion. The net RMS heave values were positive, increasing from the lowest sea state to the highest sea state. The current force caused a decrease in maximum pitch rotational motion and an increase in minimum pitch motion when compared with the action of random wave only. However, there was a slight increase in pitch RMS values in lower sea states while higher sea states decreased. This could be as a result of the decline in RMS tension values in higher sea states and this correspondingly lead to increased RMS heave motion and insignificant difference in pitch motion. Current force caused an increase in maximum tension force values and a decrease in minimum tension force when it is compared with

University of Malaya

simulation of random wave only. However, the RMS tension values decreased slightly from higher sea states to the lower sea states.

Table 4.12: Effect of current velocity and different sea states on TLP motion

	TLP Motions											
	Surge (m)				Heave (m)				Pitch (Deg)			
Sea States	Max	Min	STD	RMS	Max	Min	STD	RMS	Max	Min	STD	RMS
S1	20.79	-11.63	5.25	8.17	0.19	-0.56	0.11	0.13	0.78	-0.73	0.21	0.21
S2	18.20	-9.37	4.60	7.39	0.13	-0.43	0.09	0.11	0.73	-0.68	0.19	0.20
S3	15.77	-6.41	4.02	6.62	0.10	-0.34	0.07	0.09	0.69	-0.62	0.18	0.18
S4	13.31	-4.68	3.47	5.86	0.09	-0.29	0.06	0.07	0.65	-0.56	0.17	0.17
S5	12.61	-4.34	3.02	5.13	0.08	-0.25	0.05	0.06	0.61	-0.53	0.15	0.15
S6	11.56	-4.14	2.68	4.43	0.07	-0.21	0.04	0.04	0.56	-0.51	0.14	0.14
S7	10.02	-3.51	2.38	3.75	0.06	-0.16	0.03	0.03	0.50	-0.48	0.13	0.13
S8	8.25	-3.61	2.04	3.07	0.05	-0.11	0.02	0.02	0.43	-0.42	0.11	0.11

4.4.2 Effect of wind velocity on sea states

The effect of wind velocity presented in Table 4.10 on each sea state caused an increase in maximum surge, a decrease in minimum surge and a subsequent increase in RMS when comparison is made with the effect of random wave only. Maximum heave motion decreased whereas minimum heave motion and RMS heave value increase in their values. The wind force on the platform caused the maximum and RMS pitch values to decrease while minimum pitch value increased. This phenomenon can be credited to the fact that wind velocities caused a steady maximum positive offset along with the increase in minimum heave set-down on the tendons. The presence of wind velocity caused reduction in the pitch RMS value when compared with the random wave only. The effect of the wind velocity does not increase maximum tension force as current force does, but rather decreases maximum tension force, and minimum tension force, RMS tension force is eventually decreased. Table 4.13 shows that wind load increased the surge and heave

University of Malaya

responses substantially, but decreased the tendon tension slightly. Due to this counteracting action, the net tendon tension has been decreased.

Table 4.13: Effect of wind velocity and different sea states TLP motion

	TLP Motions											
	Surge (m)				Heave (m)				Pitch (Deg)			
Sea States	Max	Min	STD	RMS	Max	Min	STD	RMS	Max	Min	STD	RMS
S1	17.78	-4.26	3.41	7.97	0.10	-0.49	0.08	0.12	0.80	-0.70	0.20	0.20
S2	15.92	-2.10	2.94	7.20	0.10	-0.40	0.07	0.10	0.76	-0.65	0.19	0.19
S3	14.37	-1.37	2.54	6.45	0.09	-0.33	0.06	0.08	0.73	-0.59	0.18	0.18
S4	12.43	-0.75	2.19	5.70	0.08	-0.25	0.05	0.06	0.69	-0.55	0.16	0.16
S5	10.50	-0.60	1.89	4.97	0.07	-0.19	0.04	0.05	0.64	-0.52	0.15	0.15
S6	8.61	-0.76	1.64	4.26	0.06	-0.14	0.03	0.04	0.59	-0.51	0.14	0.14
S7	7.30	-0.87	1.42	3.58	0.05	-0.10	0.02	0.03	0.53	-0.48	0.12	0.12
S8	6.13	-0.84	1.23	2.94	0.04	-0.07	0.02	0.02	0.45	-0.43	0.11	0.11

4.4.3 Effect of current and wind velocities on sea states

The effect of simultaneous action of current and wind velocities was studied next and Table 4.14 shows there was an increase in the surge RMS value. This increase is almost five times the response in random wave simulation only. In the same way, the effect on the heave degree of freedom leads to a decrease in maximum heave motions, an increase in minimum heave motions and a subsequent increase in heave RMS value. Also, there was a decrease in maximum with an increase in minimum pitch values. These resulted into a decrease in pitch RMS values in S1 – S5 and an increase in pitch RMS values for lower sea states (S6 – S8). This trend is not out of order as current and wind forces cause steady offsets and set-down. The pitch response, however, is not affected by these forces. The values of maximum tension values in random wave, current and wind simulation depend on each sea state while there was a decrease in minimum tension values across the sea states. The steady forces reduced the RMS tension forces when compared with action of random

University of Malaya

wave only, which is in line with simulation of random wave and current, and random wave and wind forces respectively.

Table 4.14: Effect of current, wind velocities and different sea states on TLP motion

	TLP Motions											
	Surge (m)				Heave (m)				Pitch (Deg)			
Sea States	Max	Min	STD	RMS	Max	Min	STD	RMS	Max	Min	STD	RMS
S1	24.93	-7.97	5.21	12.25	0.12	-0.86	0.15	0.24	0.75	-0.72	0.20	0.21
S2	23.27	-6.51	4.67	11.37	0.10	-0.71	0.13	0.21	0.73	-0.67	0.19	0.19
S3	21.23	-4.18	4.08	10.45	0.10	-0.59	0.11	0.17	0.70	-0.61	0.18	0.18
S4	18.32	-2.91	3.51	9.48	0.08	-0.43	0.09	0.14	0.65	-0.55	0.17	0.17
S5	15.35	-1.50	2.97	8.45	0.07	-0.33	0.07	0.11	0.61	-0.53	0.15	0.15
S6	13.16	-0.56	2.53	7.39	0.05	-0.26	0.05	0.09	0.56	-0.52	0.14	0.14
S7	11.37	-0.61	2.19	6.31	0.04	-0.20	0.04	0.06	0.50	-0.48	0.12	0.13
S8	9.43	-1.18	1.96	5.21	0.03	-0.14	0.03	0.04	0.42	-0.44	0.11	0.11

4.4.4 Effect of one tendon missing in random waves and current forces

When one tendon was removed from a group of sixteen tendons at the corner one, (Figure 4.85) due to its closeness to environmental and accidental loadings, there was an increase of less than 1% in maximum and RMS surge values when compared with results of intact TLP in Table 4.12. The values of heave RMS motion are believed to have reduced as a result of the removal of one tendon to the values of 1.78 to 3.08% for sea state 1 to 5. For lower sea states of 6 to 8, the RMS heave values remain unchanged. The removal of one tendon in comparison to intact TLP in Table 4.12 caused an increase in maximum, minimum and RMS pitch values with a percentage increase of RMS values between 8.13% to 12.5% as presented in Table 4.15.

It can be said that the TLP becomes less stiff when a tendon was removed and this lead to increase in maximum, minimum and RMS tension values between the values of 0.9 to 1.3%. The lower sea states suffered further increase in the tension value and this limits the increase in motion response as shown in Table 4.16, compared to the higher sea states.

University of Malaya

This was due to the fact that as one tendon fails the relative stiffness of the tendon system and the horizontal restoring force decrease and thus surge response increased. With the limited percentage increase in the response motions, platform is expected to survive and perform its operation without any failure.

Table 4.15: Effect of One tendon missing on TLP motion

	TLP Motions											
	Surge (m)				Heave (m)				Pitch (Deg)			
Sea States	Max	Min	STD	RMS	Max	Min	STD	RMS	Max	Min	STD	RMS
S1	20.87	-11.54	5.26	8.22	0.18	-0.53	0.10	0.13	0.88	-0.76	0.22	0.23
S2	18.24	-9.19	4.61	7.43	0.12	-0.41	0.09	0.11	0.84	-0.71	0.21	0.21
S3	15.84	-6.06	4.04	6.65	0.11	-0.33	0.07	0.09	0.78	-0.69	0.20	0.20
S4	13.47	-4.68	3.49	5.89	0.10	-0.28	0.06	0.07	0.74	-0.65	0.18	0.18
S5	12.72	-4.44	3.04	5.15	0.08	-0.24	0.05	0.06	0.69	-0.60	0.17	0.17
S6	11.64	-4.22	2.70	4.45	0.07	-0.21	0.04	0.04	0.64	-0.55	0.15	0.15
S7	10.02	-3.51	2.38	3.75	0.06	-0.16	0.03	0.03	0.50	-0.48	0.13	0.13
S8	8.28	-3.60	2.05	3.08	0.05	-0.11	0.02	0.02	0.50	-0.44	0.12	0.13

Table 4.16: Effect of tension fluctuation on TLP motion

	TLP Tensions							
	Random Wave (N)				Random wave and Current Force (N)			
Sea States	Max	Min	STD	RMS	Max	Min	STD	RMS
S1	8.29E+07	1.48E+07	9.78E+06	4.34E+07	8.37E+07	1.35E+07	9.88E+06	4.30E+07
S2	7.79E+07	1.73E+07	8.86E+06	4.26E+07	7.89E+07	1.51E+07	8.90E+06	4.22E+07
S3	7.36E+07	1.85E+07	7.95E+06	4.19E+07	7.34E+07	1.59E+07	7.98E+06	4.16E+07
S4	6.90E+07	1.98E+07	7.06E+06	4.11E+07	6.90E+07	1.87E+07	7.10E+06	4.09E+07
S5	6.63E+07	2.19E+07	6.19E+06	4.04E+07	6.75E+07	2.01E+07	6.26E+06	4.03E+07
S6	6.38E+07	2.47E+07	5.38E+06	3.97E+07	6.53E+07	2.23E+07	5.46E+06	3.96E+07
S7	6.07E+07	2.68E+07	4.61E+06	3.90E+07	6.19E+07	2.48E+07	4.69E+06	3.90E+07
S8	5.65E+07	2.73E+07	3.89E+06	3.84E+07	5.73E+07	2.66E+07	3.95E+06	3.84E+07

University of Malaya

Table 4.16: Continued

TLP Tensions								
	Random wave and Wind Force (N)				Random wave, current and Wind Forces (N)			
Sea States	Max	Min	STD	RMS	Max	Min	STD	RMS
S1	8.22E+07	1.40E+07	9.61E+06	4.25E+07	8.44E+07	1.23E+07	1.00E+07	4.26E+07
S2	7.78E+07	1.44E+07	8.71E+06	4.19E+07	7.83E+07	1.48E+07	9.04E+06	4.19E+07
S3	7.26E+07	1.59E+07	7.83E+06	4.13E+07	7.24E+07	1.66E+07	8.09E+06	4.13E+07
S4	6.71E+07	1.85E+07	6.98E+06	4.07E+07	6.71E+07	1.78E+07	7.18E+06	4.07E+07
S5	6.55E+07	2.09E+07	6.16E+06	4.01E+07	6.57E+07	1.96E+07	6.31E+06	4.01E+07
S6	6.38E+07	2.30E+07	5.39E+06	3.95E+07	6.37E+07	2.18E+07	5.50E+06	3.95E+07
S7	6.10E+07	2.52E+07	4.64E+06	3.89E+07	6.09E+07	2.40E+07	4.72E+06	3.89E+07
S8	5.69E+07	2.71E+07	3.91E+06	3.84E+07	5.69E+07	2.53E+07	3.97E+06	3.84E+07

Table 4.16: Continued

One Tendon Missing				
	Random wave and Current Force (N)			
Sea States	Max	Min	STD	RMS
S1	8.40E+07	1.64E+07	9.93E+06	4.38E+07
S2	7.91E+07	1.61E+07	8.96E+06	4.30E+07
S3	7.38E+07	1.78E+07	8.05E+06	4.23E+07
S4	6.92E+07	1.94E+07	7.19E+06	4.16E+07
S5	6.76E+07	2.08E+07	6.38E+06	4.09E+07
S6	6.54E+07	2.28E+07	5.60E+06	4.02E+07
S7	6.19E+07	2.48E+07	4.69E+06	3.90E+07
S8	5.76E+07	2.63E+07	4.12E+06	3.89E+07

4.5 Verification of coupled TLP model

This section is concerned with the coupled model that has been simulated with the same platform mass, water depth and the value of AE/L as reported for uncoupled TLP. Based on past studies conducted by Taylor and Jefferys (1986), Chatterjee et al. (1996), Senjanovic, Tomic, and Rudan (2013), very little was known about the tendon cross-sectional area resulting in uncertainty regarding the cross-section type, (solid or hollow cross-section). After several iterations, the simulation that gave close cross-section and mass moment of inertia is the cross-sectional area of 0.4 metres square per corner and the tendon diameter of 0.71 metres. This is similar to the tendon diameter used in MARLIN and SNORRE A TLP respectively. The roll and pitch mass moment from the Abaqus finite

University of Malaya

element software is 82.64 x 10^9 kg m^2 against the reported roll and pitch mass moment of inertia of 82.37 x 10^9 kg m^2. This can be said to be fairly acceptable. However, there is a wide discrepancy in yaw mass moment of inertia. The value of yaw moment of inertia for the present study is 18.96 x 10^9 kg m^2 against 98.07 x 10^9 kg m^2 that was recorded in past literature. From this foregoing analysis, there may be differences in the natural periods due to the variances in the calculated mass moment of inertia.

4.5.1 Results of static and vibration analysis

The static equilibrium was verified by equating the right-hand side of Equation 3.104 to zero. The equilibrium under the vertical forces were checked and balanced with pretension and buoyancy forces. The results of the zero displacements of the COG degree of freedoms indicated that the platform is at equilibrium. This is shown in Figure 4.58 with the actual and deflected TLP superimposed together.

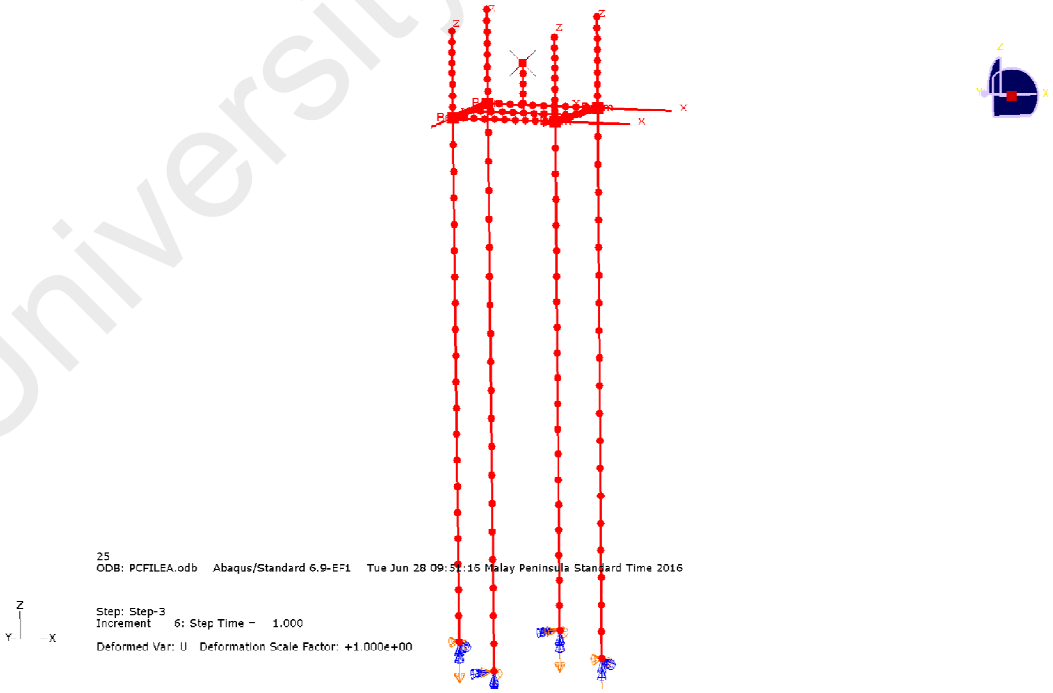

Figure 4.58: Static equilibrium of TLP model

University of Malaya

The undamped natural frequencies and mode shapes were calculated by the Lanczos eigenvalues extraction method inside the Abaqus finite element software. The result of the analytical calculation of the uncoupled natural period has been calculated and validated in Section 4.3.1. Referring to Table 4.17, results of natural frequencies and periods for the uncoupled TLP in the Abaqus software are stated. A comparison of Table 4.6 with Table 4.17 showed some level of agreement between the analytical and finite element method for the calculation of natural frequencies.

Table 4.17: Uncoupled Eigenvalue output

Mode No	Degree of Freedom	Time (s)
1	Surge	112.04
2	Sway	112.04
3	Yaw	93.31
31	Roll	2.09
34	Pitch	2.08
38	Heave	2.03

The results of mode shapes 1, 2 and 3 that correspond to surge, sway and heave degrees of freedom are presented in Figure 4.59 while Mode shapes 31, 34 and 38 correspond to roll, pitch and heave degrees of freedom as shown in Figure 4.60. It was observed that the surge, sway and yaw degrees of freedom are well above the dominant wave periods. Also, roll, pitch and heave are below the prominent wave frequency because the important wave natural periods have been identified to be between 3 to 25 seconds, Bhattacharyya et al. (2003) and Taylor and Jefferys (1986).

University of Malaya

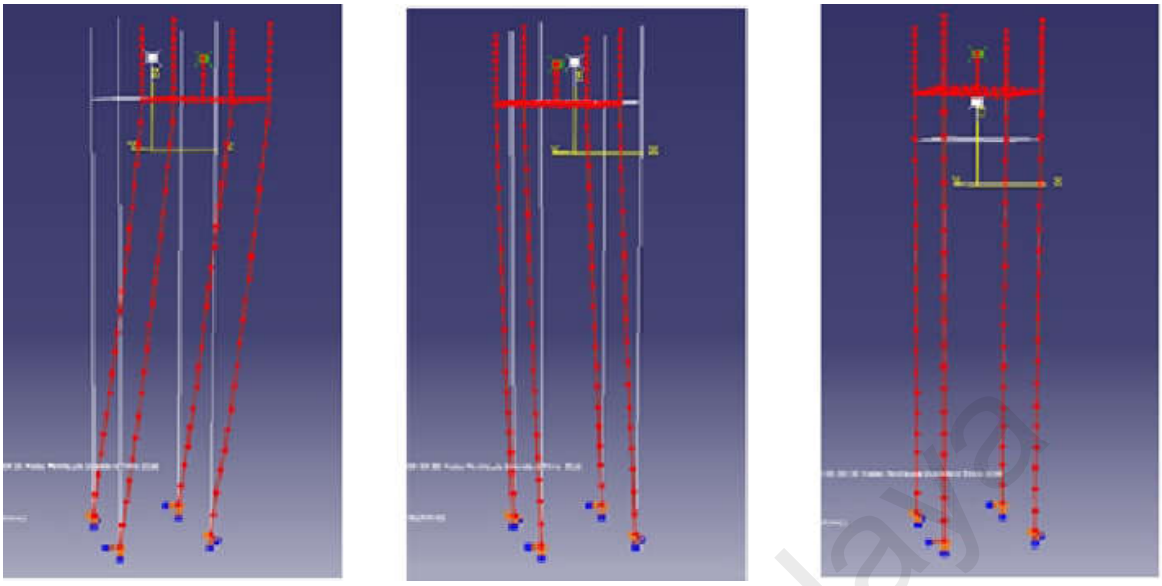

Figure 4.59: Mode shapes of uncoupled TLP (Surge, Sway and Heave)

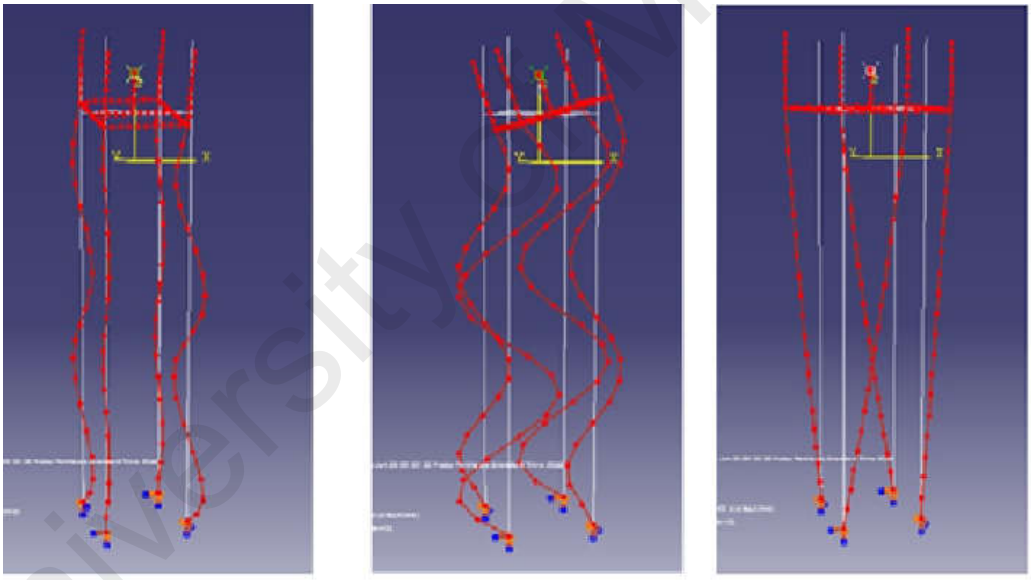

Figure 4.60: Mode shapes of uncoupled TLP (Roll, Pitch and Heave)

For the coupled TLP, the result of the eigenvalue output is presented in Table 4.18 with the omission of some mode numbers where it is believed that there is no strong coupling between the TLP and the tendons. Mode shapes 1, 2 and 3 correspond to sway, surge and yaw degrees of freedom and these are presented in Figure 4.61, while roll, pitch

University of Malaya

and heave degrees of freedom are shown in Figure 4.62. It could be concluded that there is no pure roll and pitch degrees of freedom but coupled with tendon modes.

Modes 4 to 11 following surge, sway and yaw degrees of freedom have their natural frequencies close to each other. One striking observation about these modes is that they have half-wave transverse vibration mode for the tendon. Figure 4.63 shows the representative modes for these tendons. It is apparent from Table 4.18 that as the mode number increases, the number of half wave transverse vibration mode also increased as can be seen in mode 12 - 19. In all, a total number of six half-waves were recorded for fifty mode shapes and Figure 4.64 shows the trend in the increase of half-wave transverse vibration. There is a strong indication from Table 4.18 and Figures 4.62 to 4.64 that a dynamic stochastic analysis is indispensable due to the coupling between the platform rigid body and tendon members. Another important finding is that some of the mode shapes as listed in Table 4.18 falls within the frequency of the ocean wave. For this reason, a dynamic analysis of the system is crucial to obtain the true behaviour of the system.

University of Malaya

Table 4.18: Coupled eigenvalue output

Mode No	Eigenvalue	Frequency (rad/sec)	Time (s)	Remarks (Mode)
1	0.002	0.049	129.386	Sway
2	0.002	0.049	129.385	Surge
3	0.003	0.058	107.501	Yaw
4	0.405	0.636	9.877	Tendon
5	0.407	0.638	9.845	Tendon
6	0.407	0.638	9.843	Tendon
7	0.409	0.639	9.829	Tendon + Small Surge
8	0.443	0.666	9.439	Tendon
9	0.446	0.668	9.405	Tendon
10	0.446	0.668	9.404	Tendon
11	0.448	0.670	9.384	Tendon + Small Surge
12	1.661	1.289	4.875	Tendon
13	1.664	1.290	4.871	Tendon + Small Surge
23	3.872	1.968	3.193	Tendon
35	7.774	2.788	2.254	Tendon
36	8.723	2.954	2.127	Tendon + Roll
37	8.723	2.954	2.127	Tendon + Pitch
38	9.164	3.027	2.076	Heave
39	11.784	3.433	1.830	Tendon + small heave
40	11.788	3.433	1.830	Tendon
41	11.807	3.436	1.829	Tendon
42	11.808	3.436	1.829	Tendon
43	12.717	3.566	1.762	Tendon + small heave
50	17.995	4.242	1.481	Tendon

University of Malaya

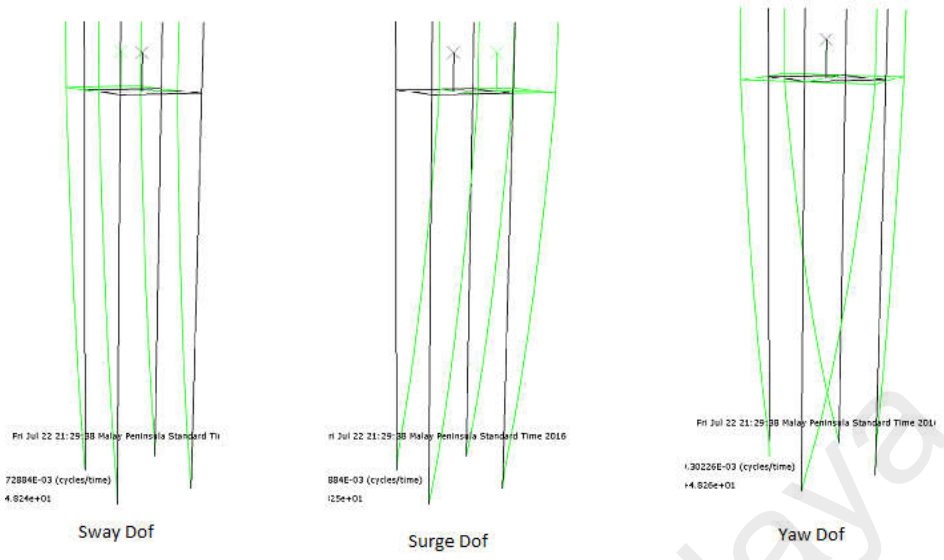

Figure 4.61: Mode shapes for Coupled TLP (Sway, Surge and Yaw)

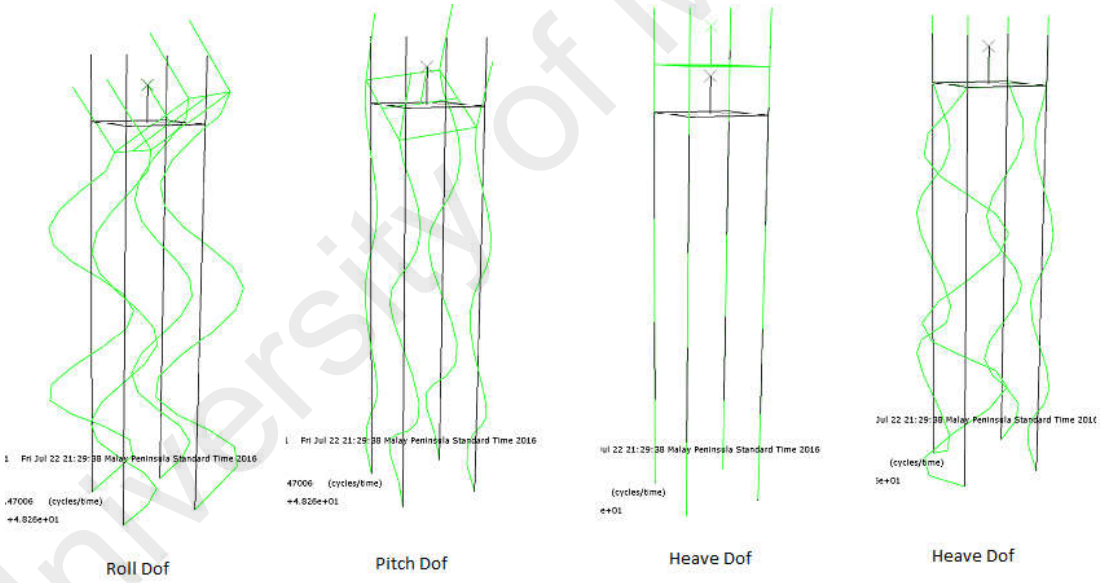

Figure 4.62: Mode shapes for Coupled TLP (Roll, Pitch and Heave)

University of Malaya

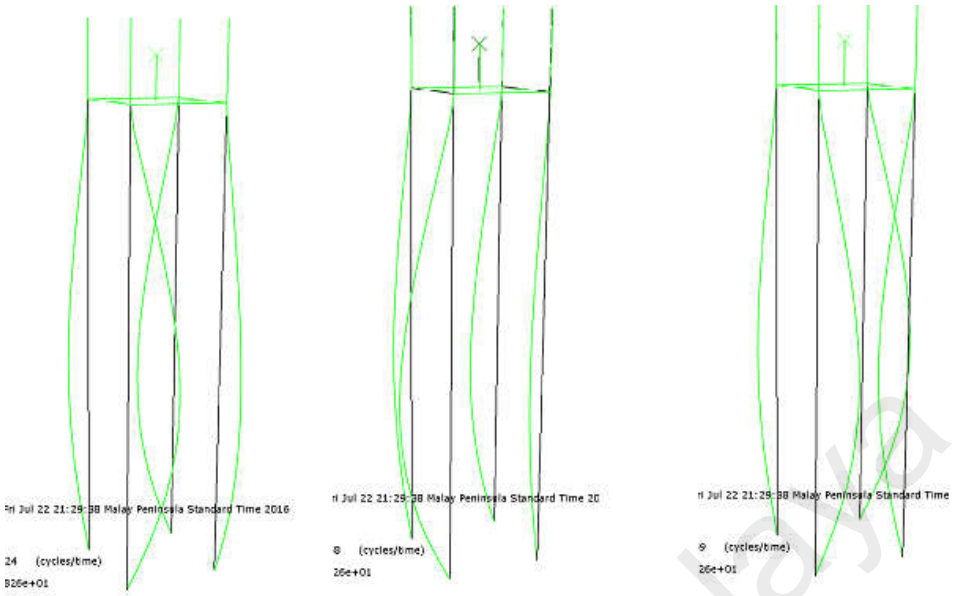

Figure 4.63: Mode shapes with Half-wave transverse vibration mode for the tendon

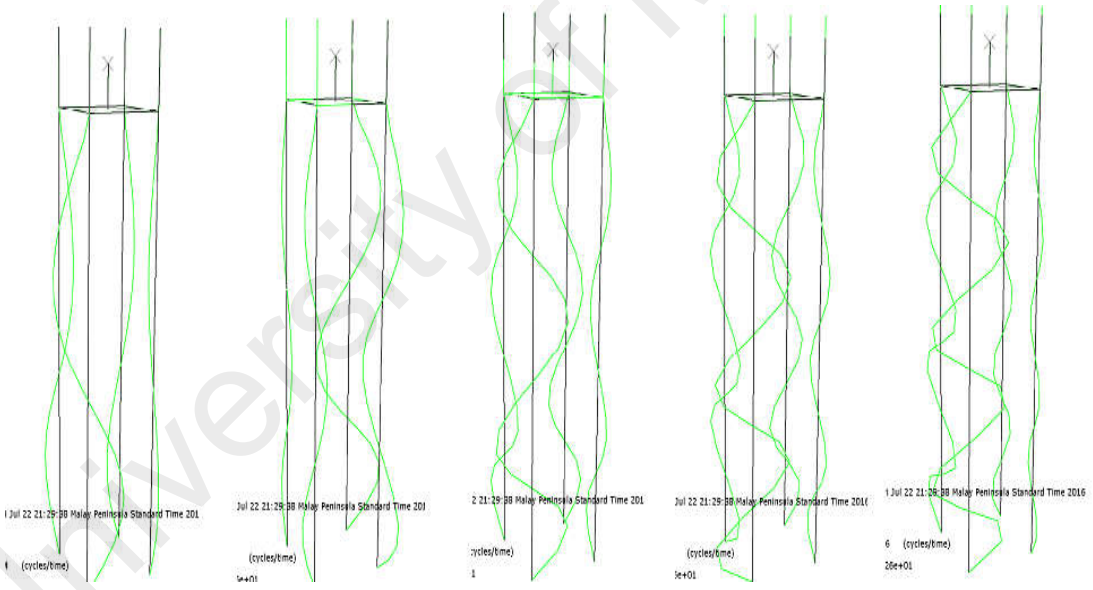

Figure 4.64: Mode shapes with increasing Half-wave transverse vibration modes

4.5.2 Verification of CNAP-TLP model motion with published results

Before employing the present methodology and approach for modelling the solution of coupled TLP, it is necessary to validate the process. Chatterjee et al. (1996) was used for the verification of the CNAP-TLP model. The study developed a tool known as the

University of Malaya

DCATLP computational program that employed 3-dimensional finite beam elements and these are programmed in the Sun FORTRAN software in their study. There may be slight differences between the two models due to the manners TLP are modelled and noticeable differences in the method of hydrodynamic force calculation.

Firstly, the platform hull and tendons are modelled as finite elements in the DCATLP and not as a rigid body. Also, the DCATLP was developed to handle regular waves and not random waves, so the validation will be for regular waves. Both models employed the same integration method for the numerical analysis but there a was slight difference in the force calculation. The ISSC TLP was used for the study comparison although the tendon cross-section and diameter employed in the DCATLP are not explicit.

By comparing surge responses of the present study with Chatterjee et al. (1996) in Figures 4.65, it was observed that the both magnitude and trend of the oscillation are the same in the steady state in which the slight difference in the figures occurred in the transient state. Figure 4.66 presents results of heave motion of the present study and Chatterjee et al. (1996); the same trend and frequency of oscillation is observed in the two figures. A likely explanation to the slight change in the magnitude can be attributed to uncertainty in the tendon cross-section of the DCATLP model and different finite element properties.

The results of pitch motion and tension variation in the tendons are not reported in Chatterjee et al. (1996). However, the time histories of pitch and tension variation for the present study are shown in Figures 4.67 and 4.68 respectively. Furthermore, the frequency of platform vibration was not explicitly expressed in Chatterjee et al. (1996). However, going by surge and heave time histories that were reported, one cycle of vibration is completed in twenty seconds, which turns out to be a frequency value of 0.3142 rad/sec.

University of Malaya

In the CNAP-TLP-2016 model, the frequency of platform vibration was calculated by writing a Fast Fourier Transform program that converts the time histories to response spectra as shown in Figures 4.69 and 4.70. Figures 4.69 and 4.70 show the peak frequency of 0.3771 rad/sec which is approximately at the wave forcing frequency. This is in the vicinity of visual calculation of frequency platform vibration for the DCATLP. It could be said that wave forcing frequency governs the platform vibration.

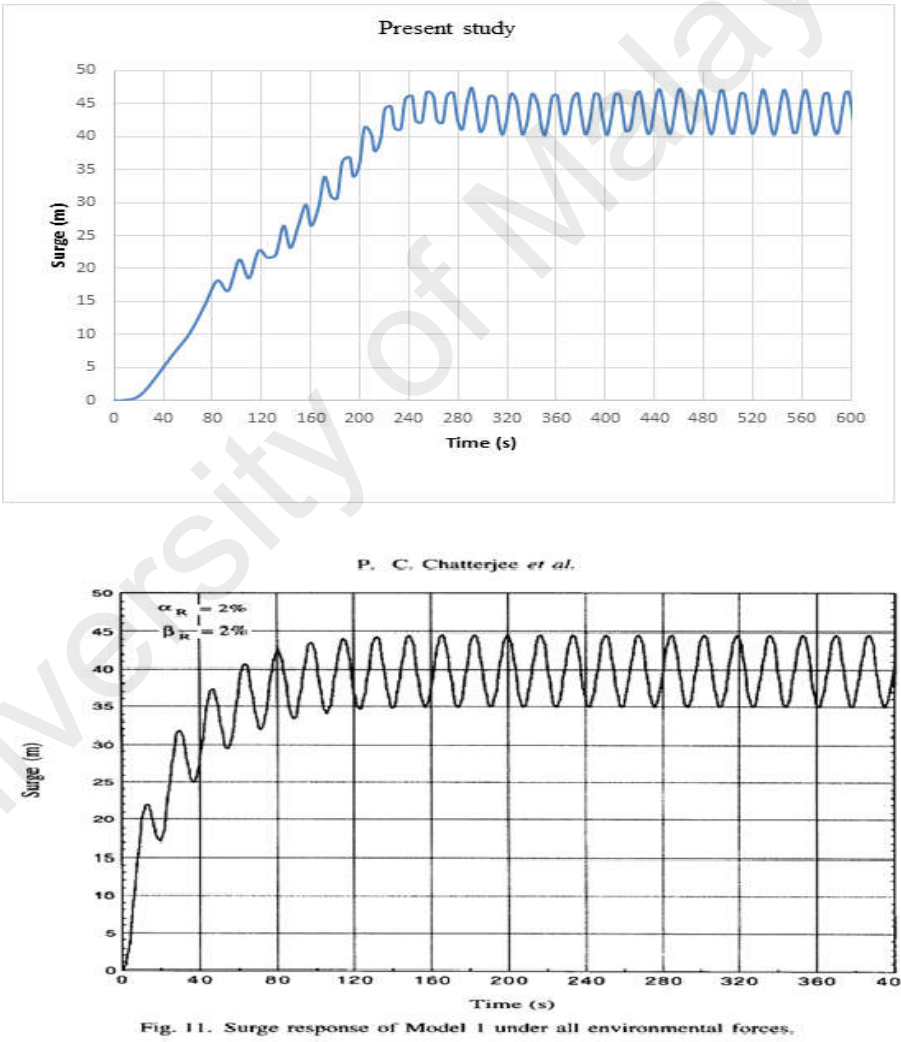

Figure 4.65: Comparison of surge response: WH: 18 metres, WP: 17 secs, Current: 2 m/s, Wind: 30 m/s (Present study and Chatterjee et al. (1996))

University of Malaya

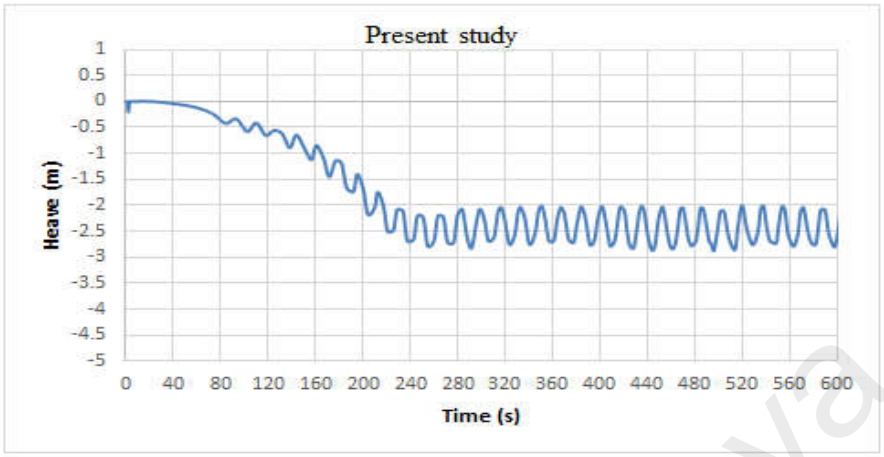

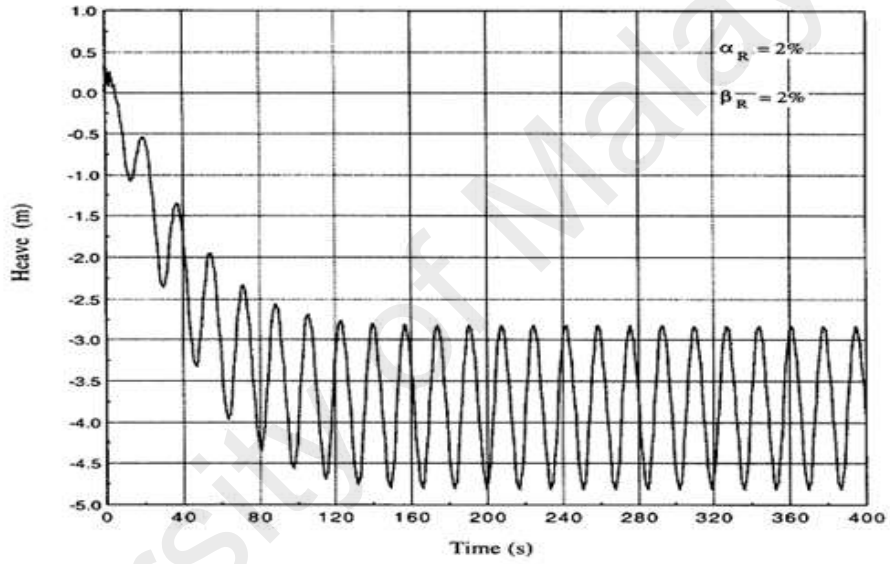

Fig. 12. Heave response of Model 1 under all environmental forces.

Figure 4.66: Comparison of heave response: WH: 18 metres, WP: 17 secs, Current: 2 m/s, Wind: 30 m/s (Present study and Chatterjee et al. (1996))

University of Malaya

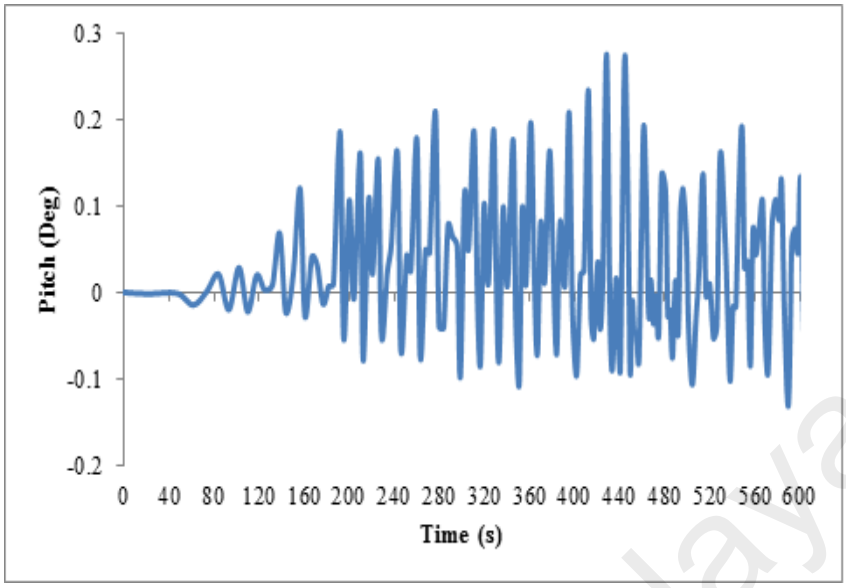

Figure 4.67: Pitch response of the Present study (WH: 18 metres, WP: 17 secs, Current: 2 m/s, Wind: 30 m/s)

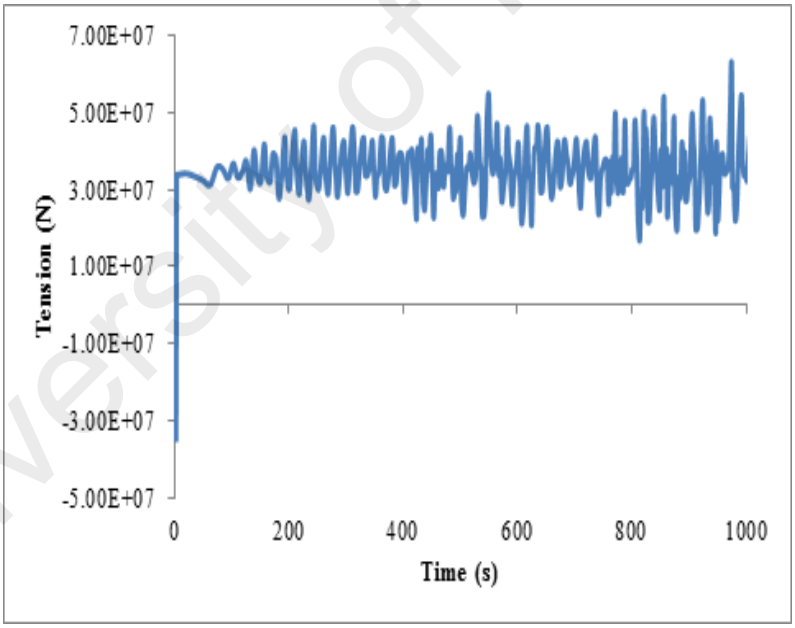

Figure 4.68: Tension response of TLP of the Present study (WH: 18 metres, WP: 17 secs, Current: 2 m/s, Wind: 30 m/s)

University of Malaya

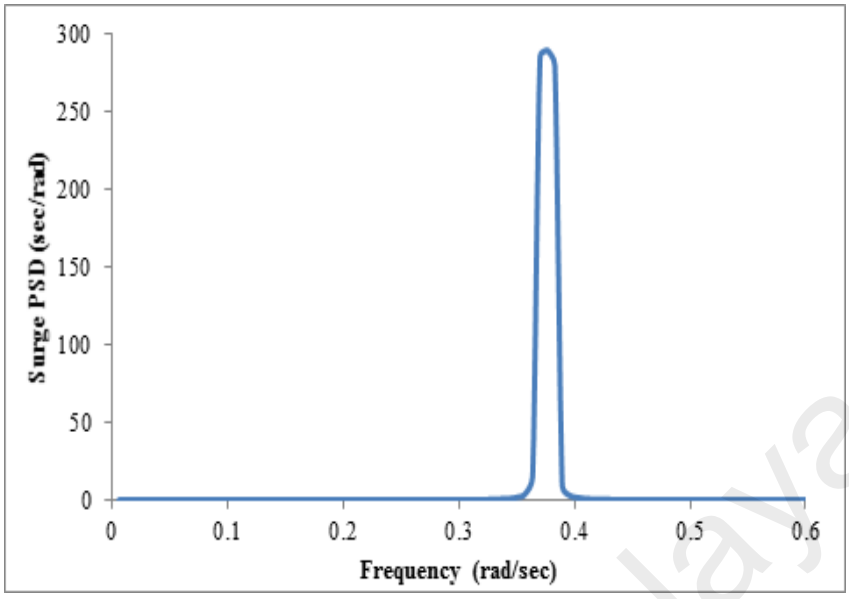

Figure 4.69: Surge PSD of TLP of the Present study

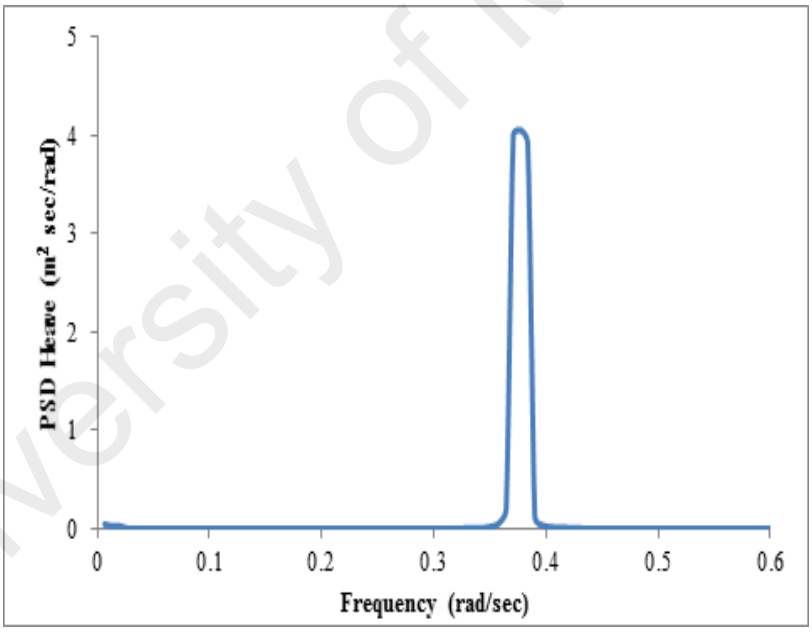

Figure 4.70: Heave PSD of TLP of the Present study

4.5.3 Validation of massless Abaqus-TLP model with UNAP-TLP model

This section presents the verification of massless Abaqus TLP model with the UNAP-TLP-2016 model program developed in Section 4.3.3 for random waves only. As

University of Malaya

can be seen in Figures 4.71 and 4.72, the surge time histories and response spectral densities compared well in magnitudes, trends, peaks and energy content.

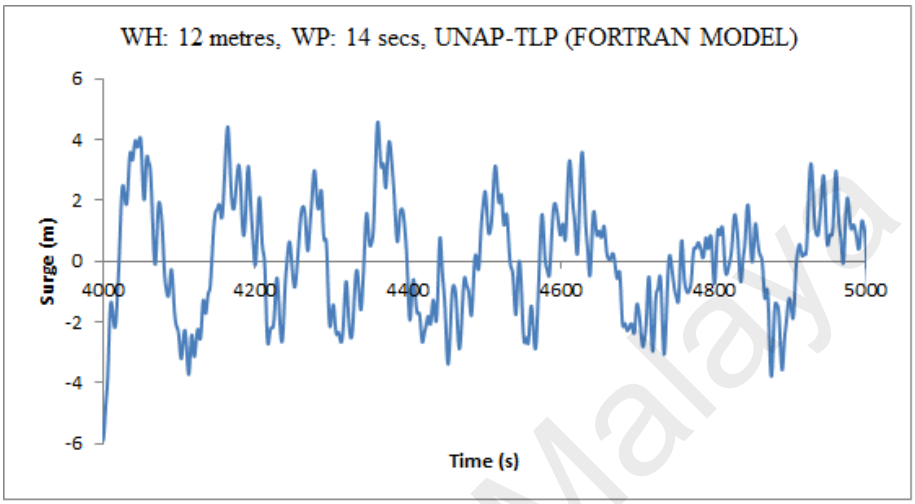

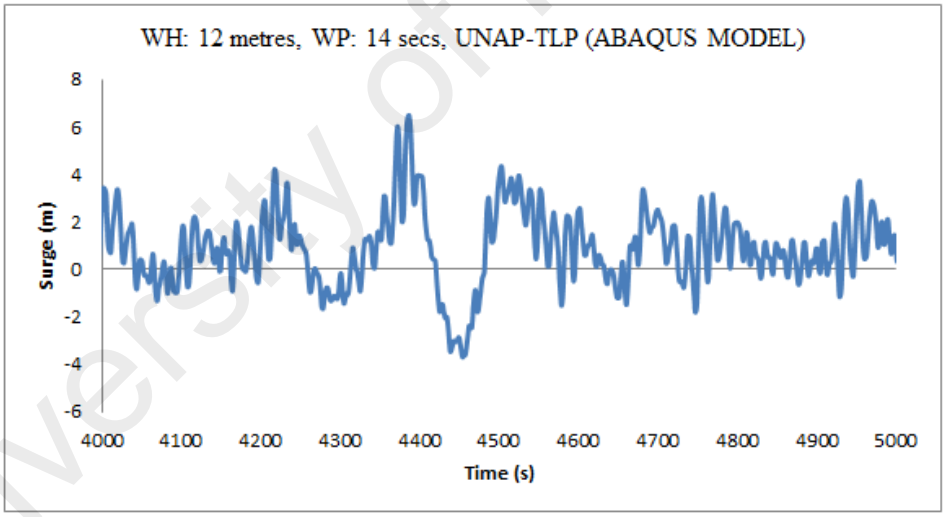

Figure 4.71: Comparison of surge response of the TLPs

University of Malaya

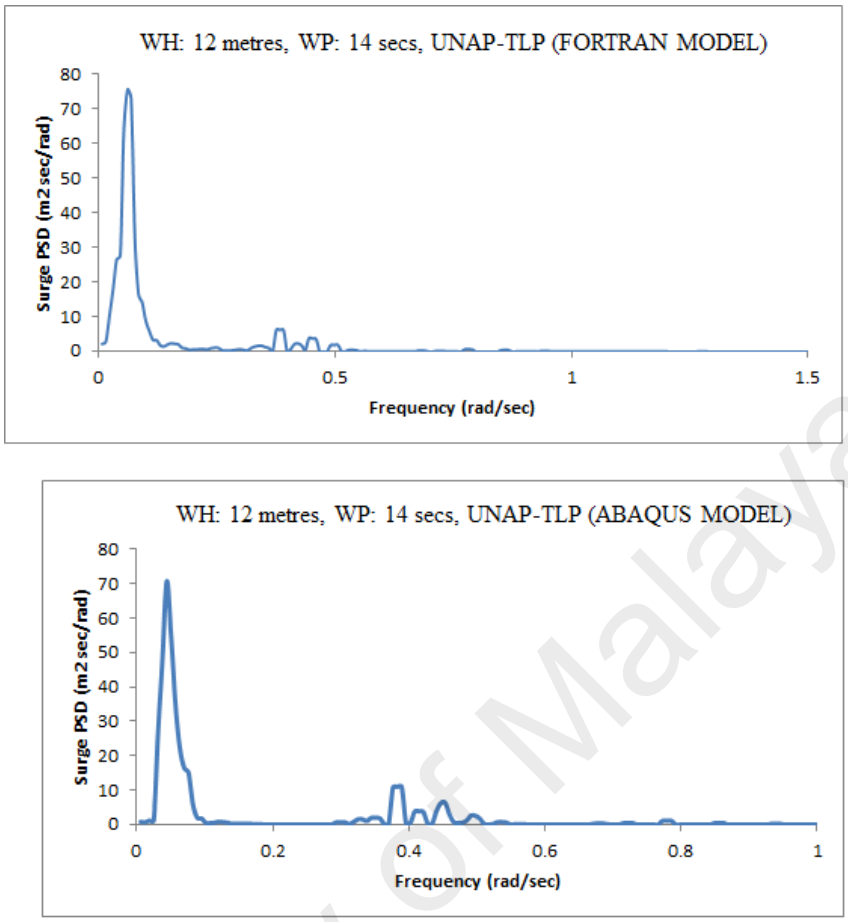

Figure 4.72: Comparison of surge PSD of the TLPs

The heave response in Figures 4.73 and 4.74 and the pitch response in Figures 4.75 and 4.76 show significant difference in behaviours. For the UNAP-TLP-2016 model program, the heave fluctuation was around the mean position while it is completely off the mean position and in negative direction for the massless Abaqus TLP model. The pitch response in both models showed vibration around the mean position with high level of nonlinearities noticed in the two models. The magnitudes are not completely deviated from each other and a likely explanation is that the disparity might have occurred due to the fact that the Abaqus finite elements for the tendons are standard elements that incorporates other factors which are absent in the UNAP-TLP-2016 model.

University of Malaya

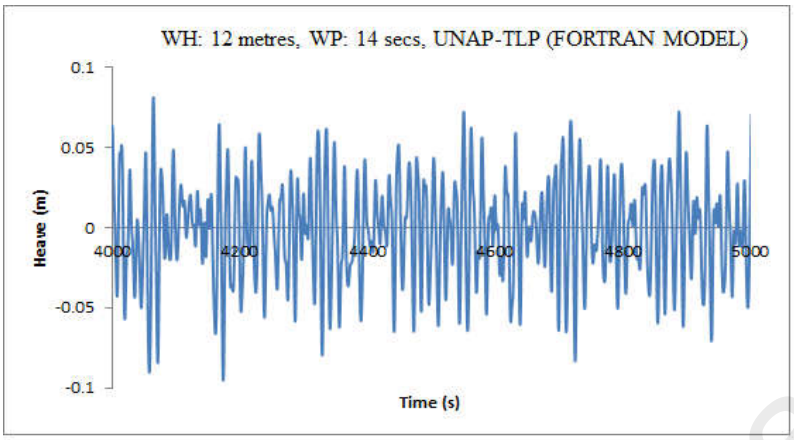

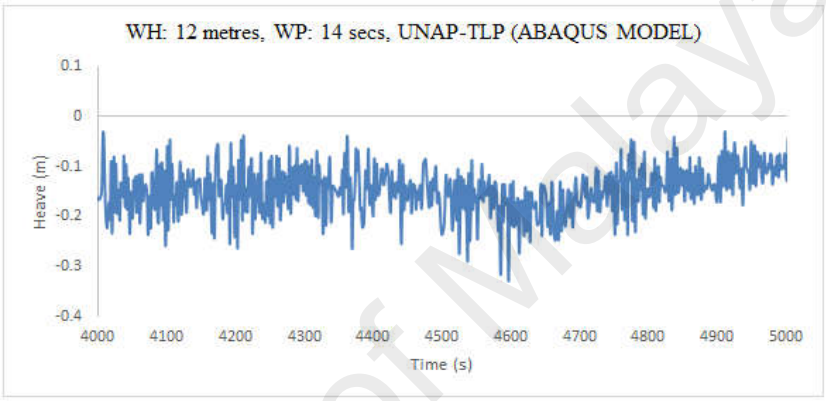

Figure 4.73: Comparison of heave response of the TLPs

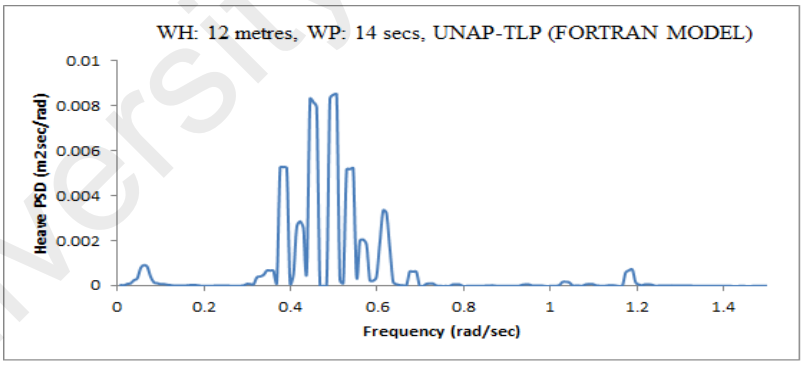

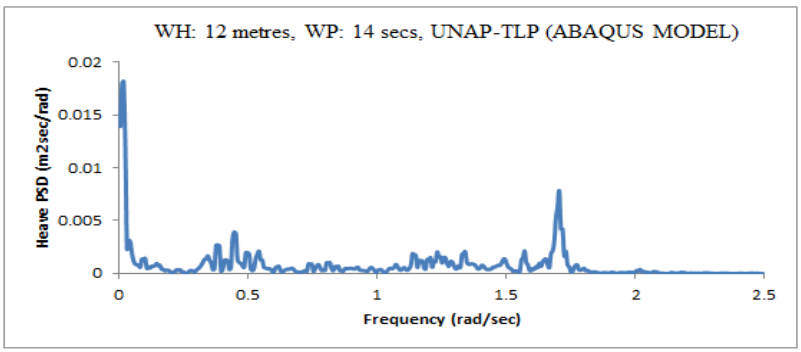

Figure 4.74: Comparison of heave PSD of the TLPs

University of Malaya

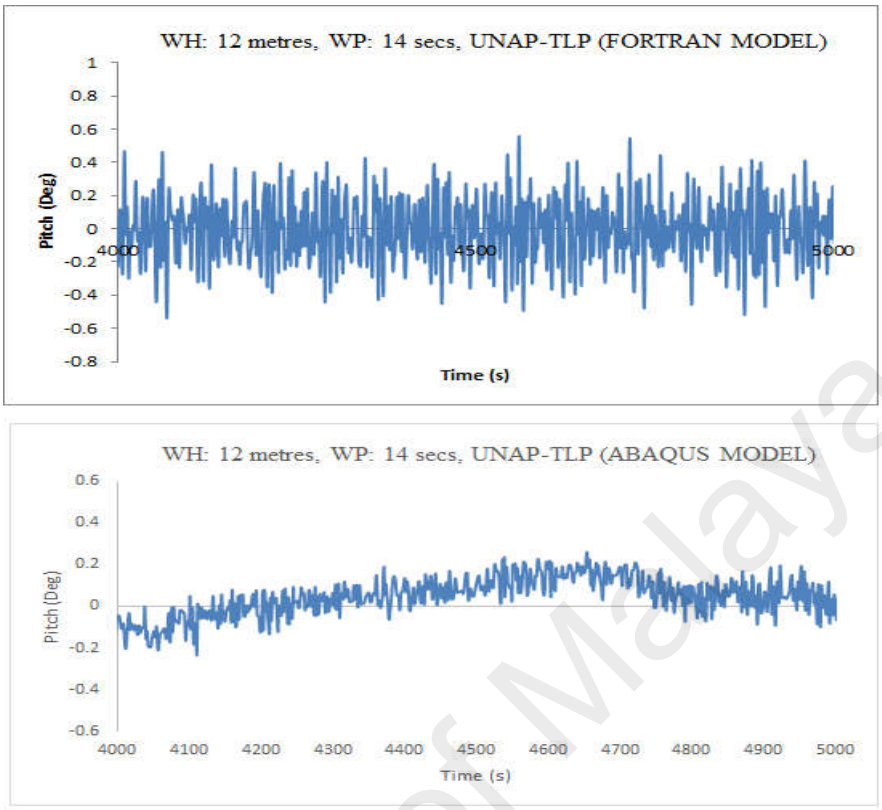

Figure 4.75: Comparison of pitch response of the TLPs

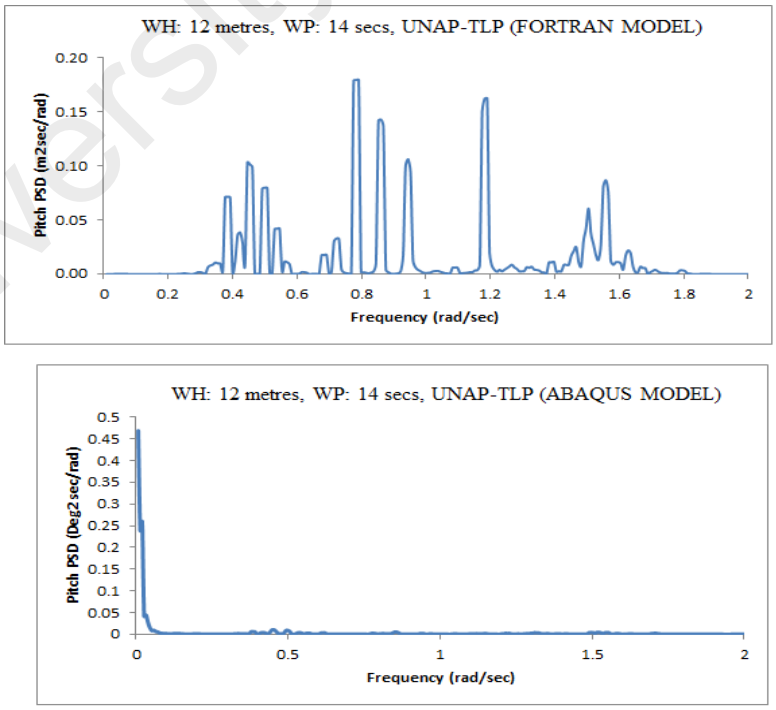

Figure 4.76: Comparison of pitch PSD of the TLPs

University of Malaya

The results of tendon tension response are shown in Figures 4.77 and 4.78. For the cross-section of time histories and power spectral densities, their response shows some degree of similarity in oscillation, magnitudes and in terms of peaks.

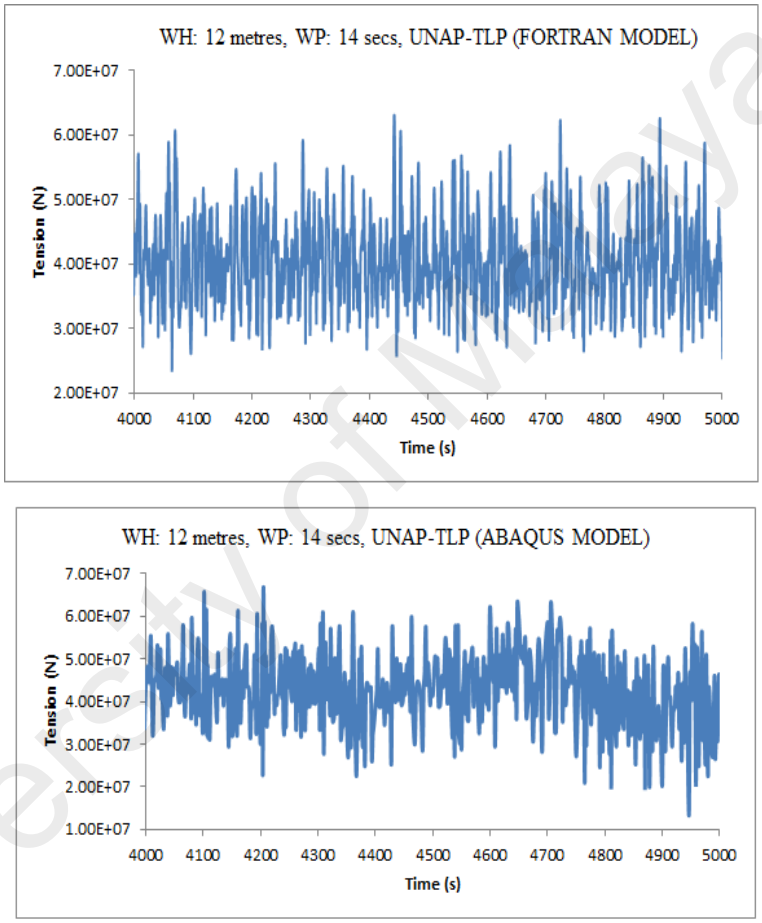

Figure 4.77: Comparison of tension response of the TLPs

University of Malaya

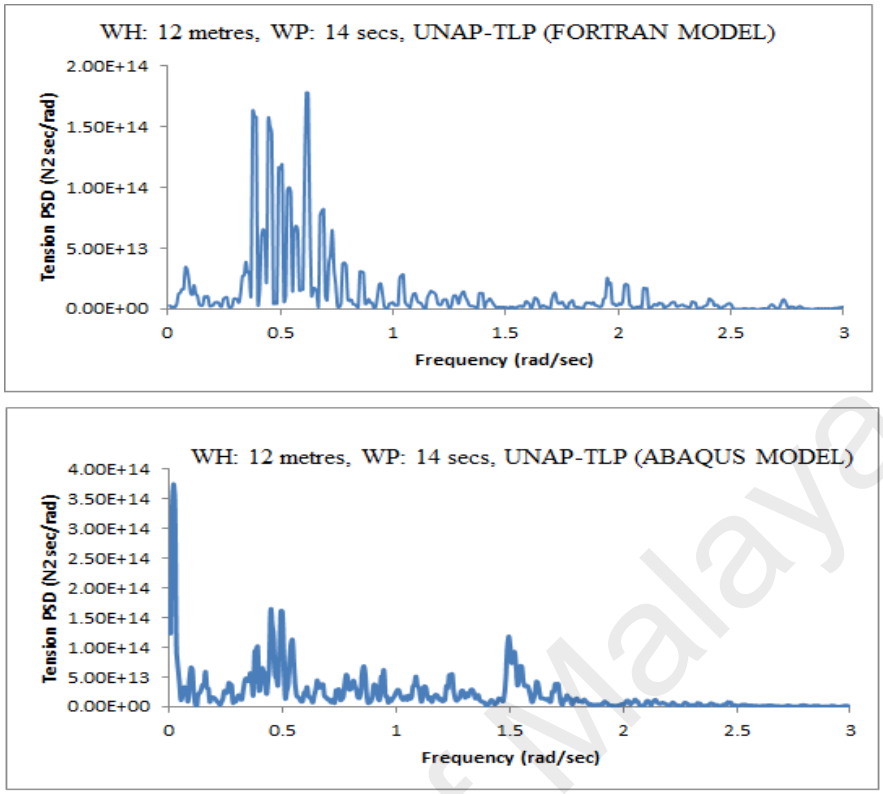

Figure 4.78: Comparison of tension PSD of the TLPs

4.6 Effect of wave, current and wind loads on the response of CNAP-TLP model

The behaviour of the coupled TLP model was analysed for different load combinations in 450 metres water depth. As a result of the zero-wave incident angle, the platform was only activated in three degrees of freedom, which were surge, heave and pitch motions.

4.6.1 Surge time history

What is interesting in the modelling of TLP for random wave excitation only is that the platform oscillates around the mean position. The random wave excitation simulated from significant wave height of 12 m and peak time period of 14 s causes a maximum displacement of 7.37 m and a minimum displacement of 3.84 m in the negative direction. As seen in Figure 4.79, the oscillation is stochastic in nature, which follows the wave elevation behaviour.

University of Malaya

On the other hand, it is thought that the presence of current and wind forces causes medium and large offsets to the platform. This can be verified in the surge time history shown in Figure 4.79. When current and wind forces acted along with random wave force, there is evidence of a steady offset from the mean position due to drag forces. The outcome of combined loadings of random wave, current and wind forces are more pronounced in magnitude and altitude when compared with the action of random waves only, random waves and current forces only, and random waves and wind forces only respectively.

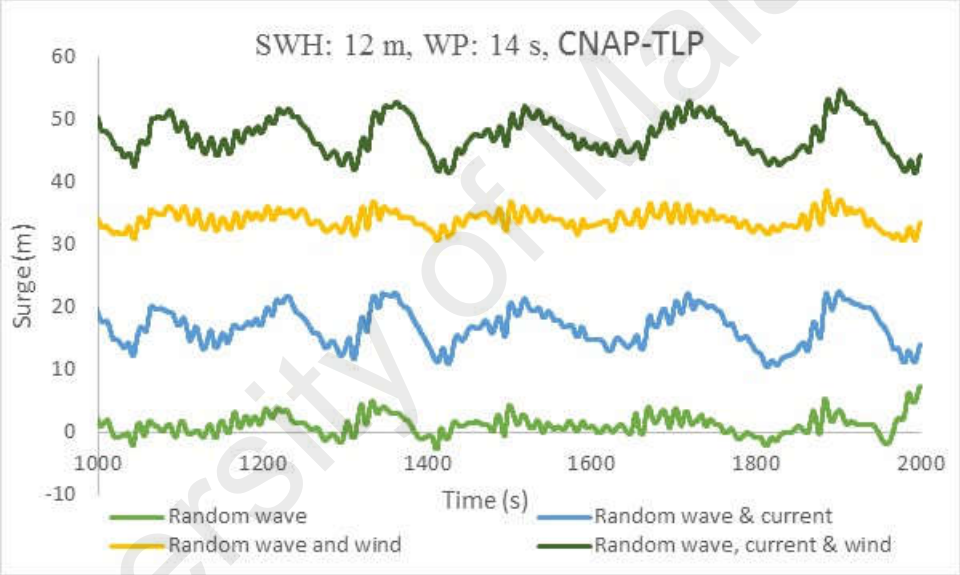

Figure 4.79: Comparative cross-section of surge time history

With a current velocity of 1.05 m/s magnitude on the hull and tendons of the TLP together with a wind velocity of 50.1 m/s, there was an increase in the statistics of motion responses, as reported in Table 4.19, after the transient path has been removed. Current velocity force causes almost nine times increase, wind force causes almost eighteen times increase, and almost twenty-five times increase when random wave, current and wind jointly acts on the platform over random wave only. Thus, it can be concluded that for a

University of Malaya

realistic motion analysis of any TLP, the predominant loadings on the platform and the site location must be considered during the analysis.

Table 4.19: Surge statistical characteristics of TLP response

Surge (m)	Random wave	Random wave and Current forces	Random wave and Wind forces	Random Wave, Current and Wind forces
Minimum	-3.84	10.05	30.45	41.19
Maximum	7.37	26.40	39.80	56.10
Mean	1.13	16.99	34.27	48.12
STD	1.58	3.02	1.54	2.94
RMS	1.94	17.25	34.31	48.21

In Figure 4.80, the response power spectral densities for different load combinations presented and the first prominent peaks in the Figure 4.80 is at 0.04474 rad/sec which translates to be 140.44 seconds. This is very close to the surge and sway natural time periods in Table 4.18. A probable explanation for this is that platform vibration is predominantly governed by the natural frequency of the TLP. There are other clusters of peaks around the peak period of wave frequency with the frequency of 0.4538 rad/sec, which is 13.85 seconds. This shows possibility of TLP vibration at the wave frequency. The difference between the two frequencies is wide, so resonance is not expected. Thus, the energy content of the wave frequency is low compared to the energy at surge natural frequency, this shows that natural degree of freedom may amplify the platform more than the wave frequency.

University of Malaya

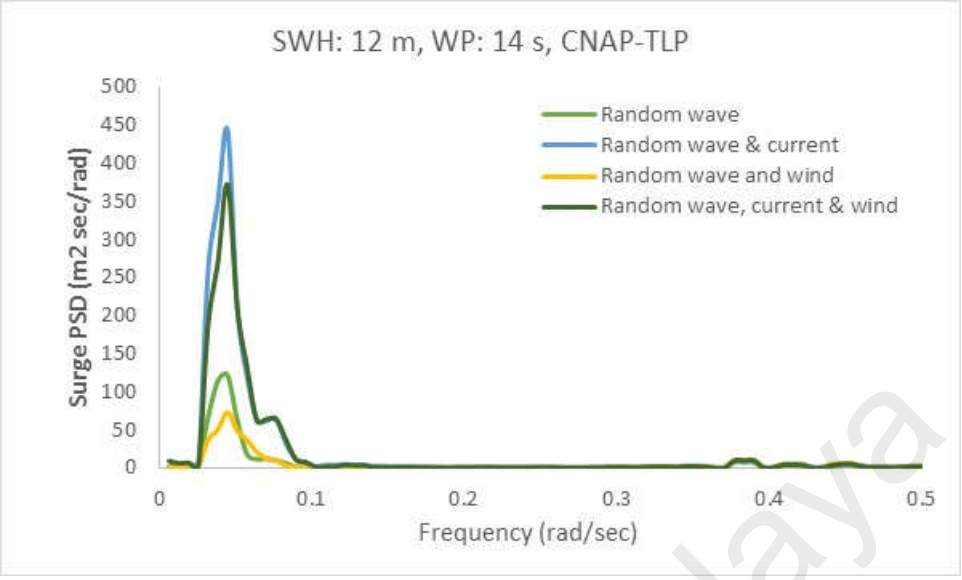

Figure 4.80: Comparative cross-section of surge power spectral density

4.6.2 Heave time history

Results of the vertical displacement of the TLP are presented in this section. From the analysis carried out, the minimum and maximum heave responses in random wave excitation are -0.19 m and - 0.01 m respectively. The values were not unexpected due to the heave restrained nature of the TLP. In contrast to the surge motion, the heave motion is greatly of low value due to the high elastic properties of the tendons that constrain and eliminate vertical motions. Figure 4.81 shows the cross-section of heave time history for different load combinations. It is thought that large displacement together with drag effects from current and wind load on the TLP cause the platform to undergo dramatic increase in the negative heave forces when compared with random wave only.

The platform maximum and minimum heave motion values are -0.17 m to -1.06 m for random wave and current forces only, and -1.24 m and -2.98 m under random wave and wind forces. The maximum and minimum heave responses in combined actions of random waves, current and wind forces are -2.24 m and -5.34 m respectively. The statistics are reported in Table 4.20 and as earlier explained the low response can be attributed to the

University of Malaya

high stiffness of the tendon together with the tendon damping that restrains the motion in vertical mode.

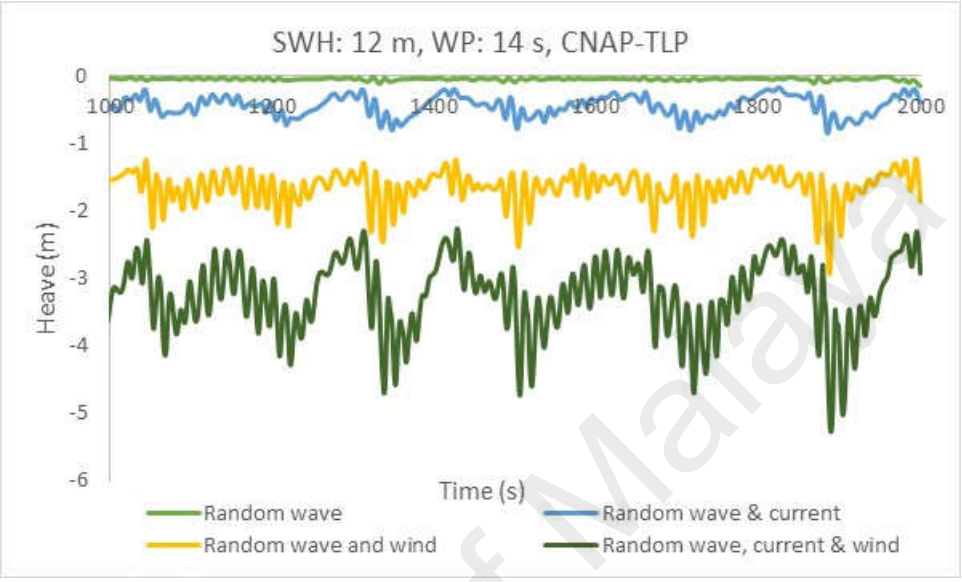

Figure 4.81: Comparative cross-section of heave time history

Table 4.20: Heave statistical characteristics of TLP Response

Heave (m)	Random wave	Random wave and Current forces	Random wave and Wind forces	Random Wave, Current and Wind forces
Minimum	-0.19	-1.06	-2.98	-5.34
Maximum	-0.01	-0.17	-1.24	-2.24
Mean	-0.04	-0.45	-1.71	-3.34
STD	0.02	0.16	0.27	0.54
RMS	0.05	0.48	1.73	3.38

From Figure 4.82, it is clear that there is a strong coupling between surge and heave degrees of freedom. This is because the first dominant peaks in all load combinations occurs at surge natural time period and other noticeable cluster of peaks occur around wave frequency. The strong coupling is due to the fact that wave direction is along the surge direction and also the surge offset causes set down along the heave direction.

University of Malaya

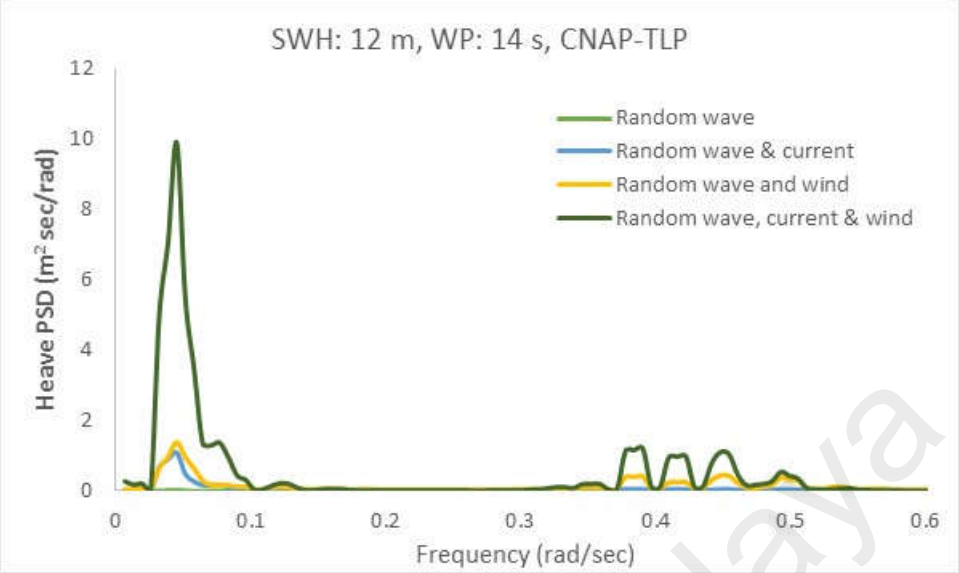

Figure 4.82: Comparative cross-section of heave power Spectral density

4.6.3 Pitch time history

The cross section of pitch time history as presented in Figure 4.83 and its statistics in Table 4.21 depict small magnitudes in all load combinations. This is as a result of axial stiffness of the tendon that constrains the motion and it is high enough to restrain rotational motion just as heave motion is restrained. These high-frequency degrees of freedom (heave and pitch), although small in values, greatly affect fluctuation of the tendon. The addition of wind forces greatly increases the maximum and minimum pitch responses. Although the RMS value is less than one degree under the actions of wave, current and wind forces, yet their cyclic behaviour demands proper attention for the fatigue analysis of the tendons.

University of Malaya

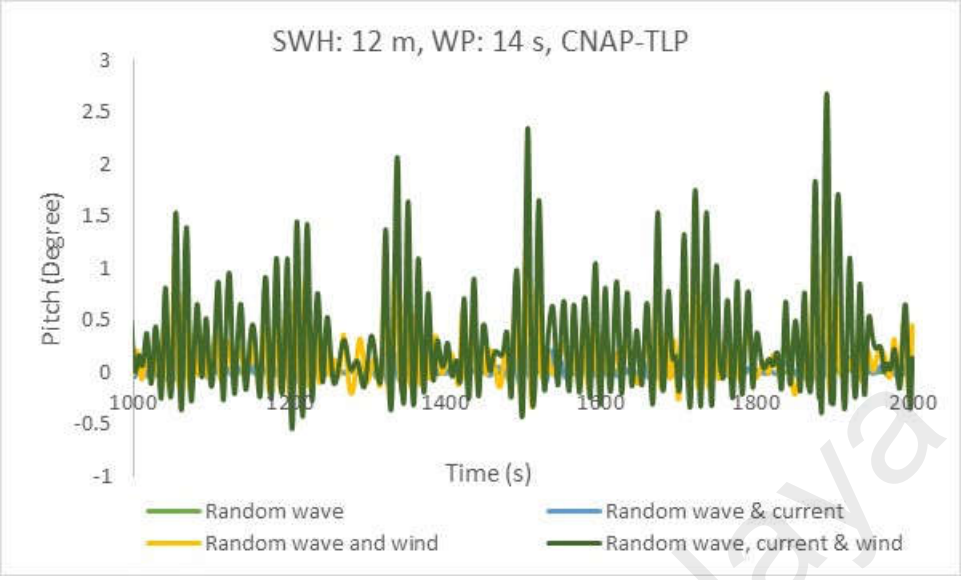

Figure 4.83: Comparative cross-section of pitch time history

Table 4.21: Pitch statistical characteristics of TLP response

Pitch (Deg)	Random wave	Random wave and Current forces	Random wave and Wind forces	Random Wave, Current and Wind forces
Minimum	-0.06	-0.12	-0.21	-0.39
Maximum	0.10	0.38	1.67	2.58
Mean	0.00	0.02	0.18	0.33
STD	0.02	0.07	0.29	0.50
RMS	0.02	0.07	0.34	0.60

The pitch power spectra shown in Figure 4.84 follow the same trend of noticeable peaks at surge natural frequency and at wave forcing frequency. This further strengthened the evidence for coupling and nonlinearities embedded in the TLP system.

University of Malaya

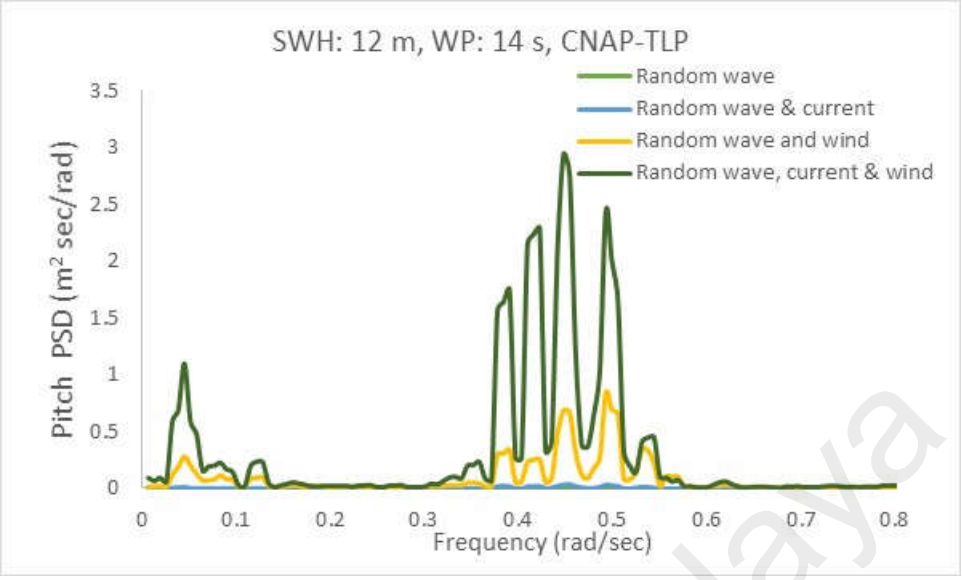

Figure 4.84: Comparative cross-section of pitch power spectral density

4.6.4 Tendon tension time history

Having discussed the TLP motion, the high-frequency tension fluctuation in the tendon is discussed next. This occurred due to variable submergence, large offset from environmental forces that changed the tension at every time instant in the tendon. Besides this, time varying forces in the tendon and unequal set-down that accompany the offset caused the tension to vary from tendon to tendon.

In this study, equivalent tendon representation was used and the top tension in the corner, C1 (Figure 4.85) in the random wave, random wave and current, random wave, current and wind forces simulation is recorded in Table 4.22.

University of Malaya

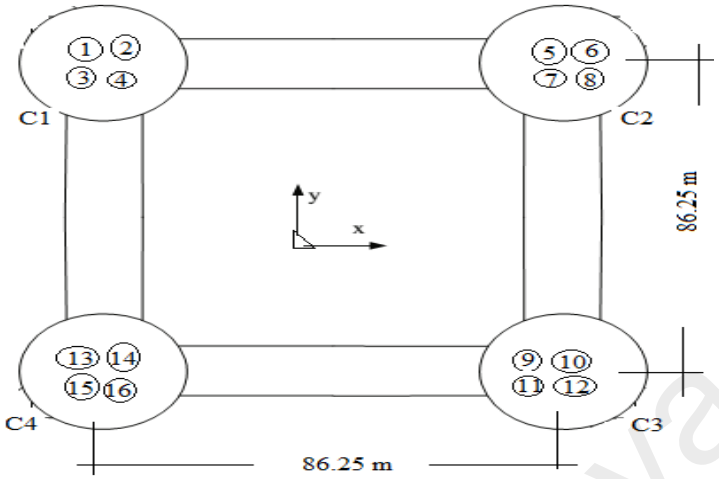

Figure 4.85: Arrangement of TLP tendon

Table 4.22: Tension statistical characteristics of TLP response

Tension (N)	Random wave	Random wave and Current forces	Random wave and Wind forces	Random Wave, Current and Wind forces
Minimum	2.37E+07	2.49E+07	1.99E+07	2.41E+07
Maximum	4.38E+07	4.58E+07	6.74E+07	6.32E+07
Mean	3.38E+07	3.47E+07	3.83E+07	3.85E+07
STD	3.19E+06	3.16E+06	6.17E+06	5.84E+06
RMS	3.40E+07	3.48E+07	3.88E+07	3.89E+07

The current drag force increases both minimum and maximum tension in the tendon while the wind drag force increased the maximum tension and decreased the minimum tension. The effects of load combination on the response of tendon are represented in time history (Figure 4.86). In all, the nonlinearity in the TLP was confirmed by the presence of fluctuation in the time history of tendon tension. Although, the motion behaviour greatly increased when current and wind forces were added to wave force as previously discussed, the difference in tension RMS was not so much as there is only 2.4%, 14.12%, and 14.41% increase in tension when random wave and current forces, random wave and wind forces, and joint occurrence of random wave, current and wind forces act together over random wave simulation only. it can be said that the initial tendon pretension and buoyancy forces

University of Malaya

were sufficient in carrying the imposed structural load and resisting the environmental forces on the TLP structure.

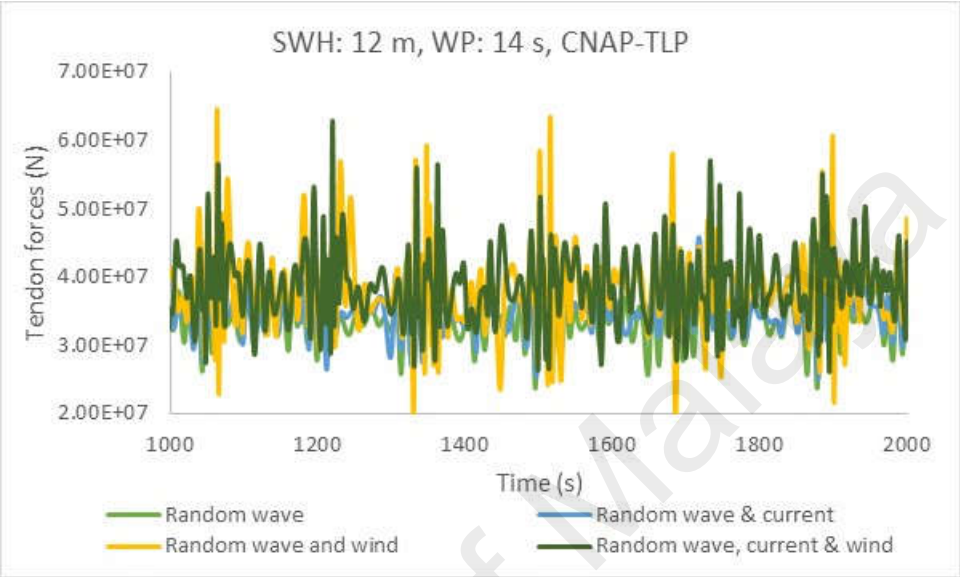

Figure 4.86: Comparative cross-section of tension time history

Apart from peaks at surge and wave frequencies, there were other peaks in the tendon power spectra model as depicted in Figure 4.87. These were the result of nonlinearities in the platform. The tension fluctuation in the tendon is directly influenced by the heaving on the platform. It can be seen in Figure 4.87 that the energy content under the actions of random wave, current and wind forces were considerably larger than the random wave simulation only due to the drag load effects and the rapid fluctuations caused by variable submergence and tension fluctuation.

University of Malaya

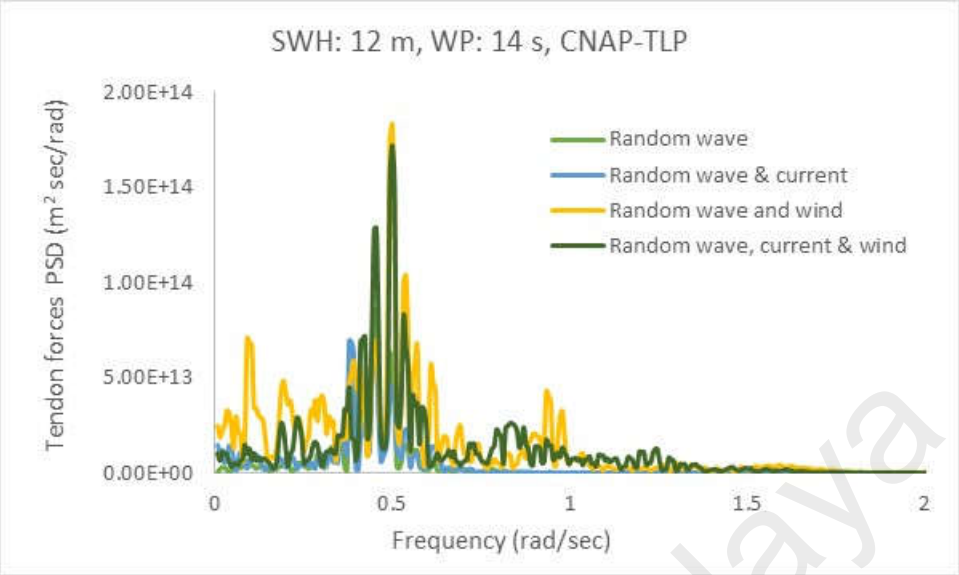

Figure 4.87: Comparative cross-section of tension power spectral density

The objective of this section is to show the contribution of likely loadings on the platform response for the purpose of design. As discussed earlier, Tables 4.19 to 4.22 present the statistical characteristics of the TLP with the maximum, minimum, mean, standard deviation and Root Mean Square (RMS) provided. Since the loadings on the platform are random in nature with the assumption of normal distribution, statistical measures are necessary so as to determine the range of values and their variability. The RMS values represent more than 90% of the observed values and it can be possibly concluded that for normal distribution, as we have assumed for random waves, the RMS represent an ideal data for design.

4.7 Effect of tendon dynamics on TLP response

The effect of modelling tendons as linear spring and beam element was studied here. The hydrodynamic loadings, damping force as well as the mass per unit length were applied on the beam element, which was in contrast with spring modelling.

University of Malaya

For the surge response, the values were in close range for both coupled and uncoupled models as reported in Table 4.23. The percentage difference in maximum, minimum and RMS absolute values between the coupled and uncoupled analysis of TLP was found to be 14.01%, 3.47% and 26.55%. Coupled TLP had additional loadings incorporated into the equation of motion and this made the surge motion to be higher compared to result of surge from uncoupled TLP. The response was also properly damped as a result of hydrodynamic damping forces from the tendons. The heave response is a high frequency response and due to the high axial stiffness of the tendon that restrains the vertical motion, the heave response is low when compared to the surge motion. The highest response values were recorded when the tendon was modelled as linear spring with stiffness only against the non-linear beam element that incorporate tendon dynamics. The percentage difference in the absolute maximum, minimum and RMS heave values are 200%, 100% and 256.52% respectively. A possible reason for the higher response in linear spring tendon might be due to the fact that hydrodynamic damping from the tendon is absent. In addition, the negative heave value was also due to the induced set-down from large offset of the platform.

The magnitudes of the statistical pitch response are low and the highest RMS value was also observed when tendons were modelled as linear spring against non-linear beam element. This is high-frequency response that influenced the maximum and minimum tensions in the tendon although, discomfort was not envisaged on the platform deck since pitch values were small. The percentage difference in the absolute maximum, minimum and RMS pitch values are 173%, 400% and 331.82% respectively. The results in this section indicated that the uncoupled model without tendon dynamics predicted surge response fairly but heave and pitch responses had huge discrepancies. This can be assumed to be a result of the linear spring modelling adopted for the tendon.

University of Malaya

Table 4.23: Comparison of statistical motion characteristics of TLP response

TLP Model	Uncoupled	Coupled	Uncoupled	Coupled	Uncoupled	Coupled
Parameters	Surge (m)		Heave (m)		Pitch (Degree)	
Minimum	-3.71	-3.84	-0.38	-0.19	-0.30	-0.06
Maximum	6.47	7.37	0.05	-0.01	0.26	0.10
Mean	0.70	1.13	-0.15	-0.04	-0.02	0.02
STD	1.36	1.58	0.06	0.02	0.09	0.02
RMS	1.53	1.94	0.16	0.05	0.10	0.02

Table 4.24: Comparison of statistical tension characteristics of TLP response

TLP Model	Uncoupled	Coupled	Uncoupled	Coupled	Uncoupled	Coupled	Uncoupled	Coupled
Parameters	Tendon 1		Tendon 2		Tendon 3		Tendon 4	
Minimum	-3.94E+06	2.37E+07	3.73E+06	2.06E+07	-1.00E+07	2.19E+07	-2.13E+06	2.39E+07
Maximum	7.22E+07	4.38E+07	7.13E+07	4.31E+07	7.29E+07	4.48E+07	7.01E+07	4.43E+07
Mean	3.30E+07	3.38E+07	3.51E+07	3.33E+07	3.30E+07	3.38E+07	3.51E+07	3.34E+07
STD	1.17E+07	3.19E+06	1.16E+07	3.80E+06	1.16E+07	3.79E+06	1.12E+07	3.24E+06
RMS	3.50E+07	3.40E+07	3.70E+07	3.35E+07	3.49E+07	3.40E+07	3.68E+07	3.35E+07

There was an unequal tension distribution in the tendons as presented in Table 4.24. This was said earlier to be as a result of unequal set-down. The maximum tension variation in the linear spring models without tendon dynamics were higher and the minimum tension variation was lower compared to the beam elements with tendon dynamics. The RMS tension values were approximately in the same the range as the initial tension values. The minimum and maximum tension values are important because they determine what the strength of the tendon materials should be. The linear spring model produced the highest maximum tension and negative minimum tension in some of the tendons. In the beam elements of tendon modelling, the maximum and minimum tension values are positive and of smaller magnitude when compared with linear spring elements.

4.8 TLP response in constant wave height and varying wave period

The parametric study on coupled ISSC TLP was carried out for random wave and current forces simulation. The geometric data is the same with Table 4.5 for constant wave height of 12 metres. The wave periods of 10, 12, 14 and 16 seconds that fall within the

University of Malaya

dominant wave periods are selected for the study. Also, 10 seconds wave period was close to the natural frequency of the tendon as calculated in Table 4.18. This was done to ascertain if there will be any near-resonating TLP response.

4.8.1 Surge response

The results of the parametric study carried out for the TLP with constant significant wave height and varying increasing time periods are summarized in statistical values and presented in the form of a chart in Figure 4.88. After the transient path has been removed, an increase in wave period by 20% (10 secs to 12 secs) lead to an increase in maximum and RMS values by 9.2% and 3.2% respectively, while the minimum surge value decreased by 2.3%. Further increase in the wave period by 40% (10 secs to 14 secs) also increased the maximum, RMS and minimum by 20.8%, 12.5% and 4.3% respectively. The increase in wave period by 60% (10 secs to 16 secs) causes the maximum, RMS and minimum percentage increase to be 20.77%, 0.32% and 16.7% respectively. From the statistics, the increase in wave period increases RMS surge amplitudes up to 14 seconds and declined after this period. The reduction in the surge amplitude could be due to the fact that the increase in wave period increases the wavelength and this reduces the impact of the amplitude.

University of Malaya

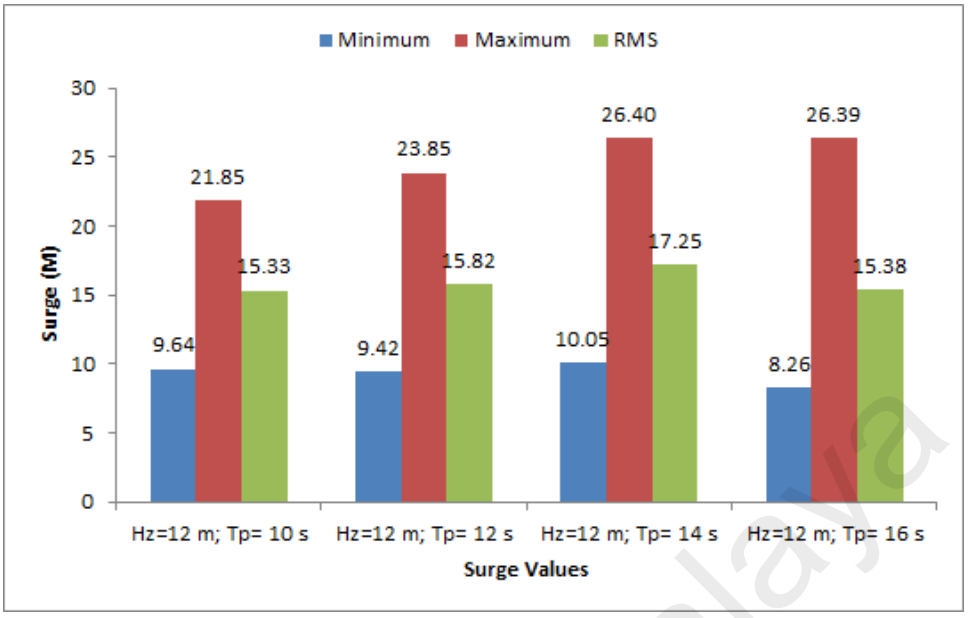

Figure 4.88: Surge statistical values for constant wave height with varying time periods

4.8.2 Heave response

The statistical values for heave response caused by hydrodynamic wave forces and coupling effect from other degrees of freedom are represented in Figure 4.89 with very small values for all the considered wave periods compared to surge responses. This was not unexpected as the platform is heave- restrained along the vertical direction due to the high stiffness of the tendons. Though the heave values are small, their effect may be significant if the wave of lower wave period occurs. The maximum and RMS responses reduced while the minimum amplitude increases in negative direction as the wave period increases. For 20%, 40% and 60% increased in wave period from (10 seconds to 12, 14 and 16 seconds) respectively, there are 26%, 43% and 57% increase in the minimum heave response. The percentage increase in RMS also increases with the increase in wave period of 10 to 12 seconds by 8.1%; 10 to 14 seconds by 29.73%; 10 to 16 seconds by 8.1%.

University of Malaya

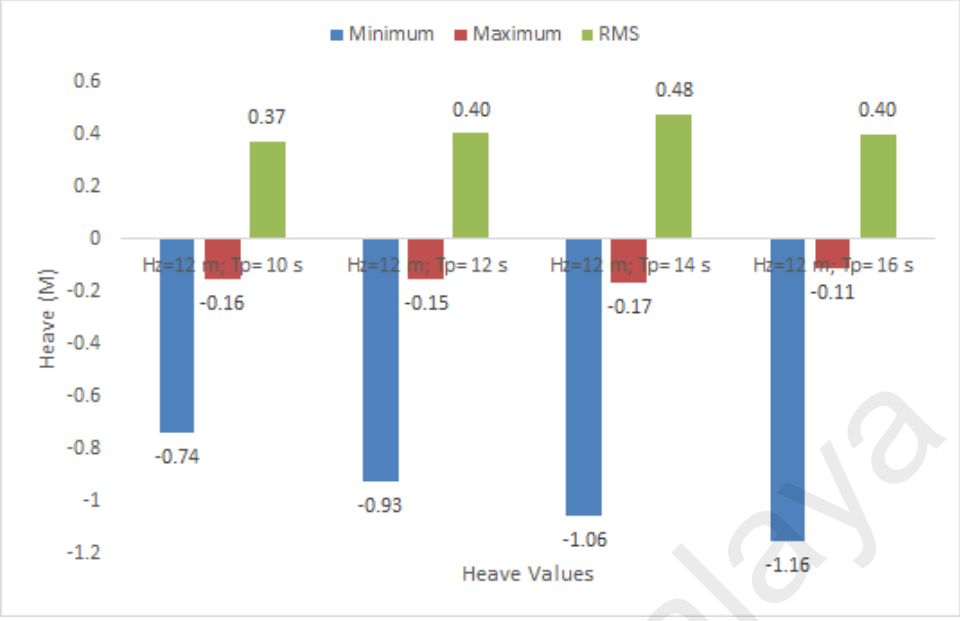

Figure 4.89: Heave statistical values for constant wave height- varying time periods

4.8.3 Pitch response

The pitch statistical values for all the wave periods are presented in Figure 4.90. Maximum, minimum and RMS values are small due to the restraints along the heave direction. Although the amplitude was small in both pitch and heave degrees of freedom, their effect was substantial and caused a high frequency of oscillation in the tendon tension. The discomfort on the platform deck was not expected for all the pertinent wave periods that were considered. With increase in wave period at constant wave height, there is an increase in the pitch responses.

University of Malaya

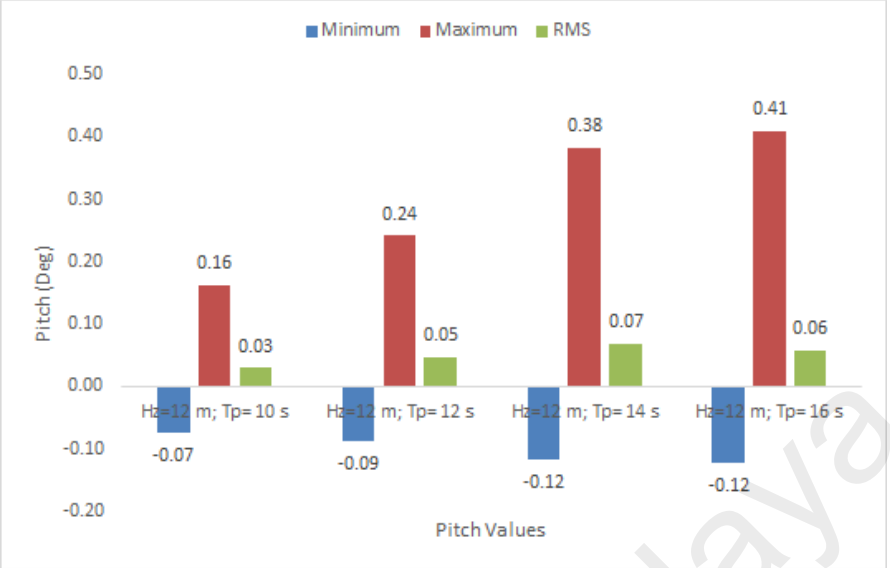

Figure 4.90: Pitch statistical values for constant wave height- varying time periods

4.8.4 Tendon tension response

This section studied the variation in tendon tension due to the combined effects of pretension, wave and current forces. The magnitude of the high frequency (Heave and Pitch) motions was small but their contribution was a key factor towards the high tension fluctuation. It was noticed that there was an unequal tension distribution in each tendon leg as represented by corner 1, 2, 3 and 4 (Figure 4.85) and this might have occurred due to the unequal set-down. The statistical tension parameter in corner, C1 is represented in Figure 4.91 for the parametric study. At constant wave height with increasing wave period, the minimum tension decreased, maximum tension values increased slightly and RMS remained almost unchanged for all the wave period increment. The variation within the tendon tension was within the limits and not susceptible to any unrealistic behaviours.

University of Malaya

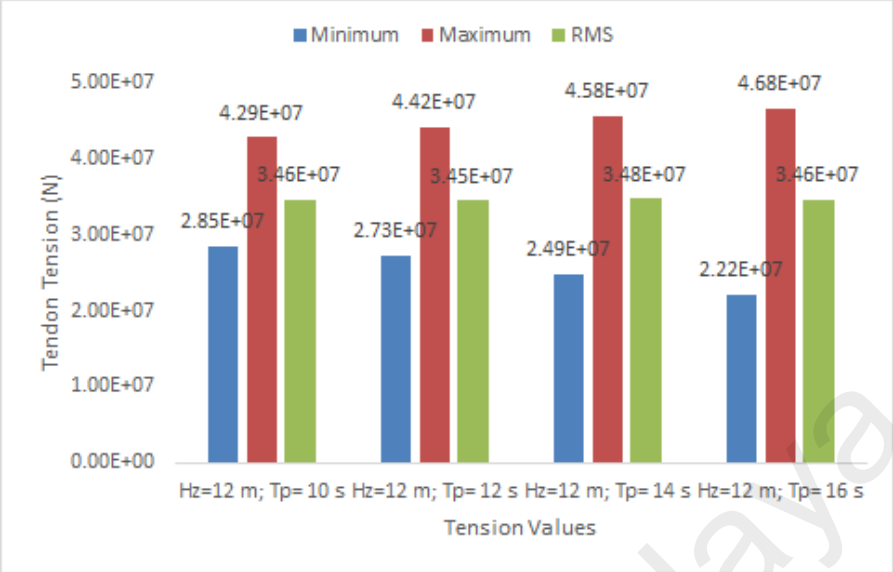

Figure 4.91: Tension statistical values for constant wave height- varying time periods

4.9 TLP response in varying wave height and constant wave period

Following the parametric study of constant wave height with varying wave period is the study of response of coupled ISSC TLP in random wave and current forces simulation for constant wave period of 10 seconds with increase in wave height varying from 10, 12, 14 and 16 metres. This was done to ascertain any near-resonating TLP response since the natural time period of tendon as calculated in Table 4.18 is around 10 seconds.

4.9.1 Surge response

The maximum, minimum and RMS values of the coupled surge response for constant wave period with increasing wave height are as shown in Figure 4.92. The increase in wave height increased the surge oscillation. The minimum, maximum and RMS surge responses increased as the wave height increased. For the increase in wave height by 20%, 40% and 60% respectively, the percentage increase in maximum responses were 0.64%, 38.97% and 58.22%. The RMS value increased by 9.58%, 27.23% and 44.10% and the minimum

University of Malaya

response by (4.78%, 7.93% and 3.04%) for 20%, 40% and 60% increase in wave heights respectively.

At the constant wave period, increase in wave height increased the surge response and it was believed that accompanying hydrodynamic damping prevented the surge response to be directly proportional to the percentage increase in wave height. The implication of an increase in surge response due to increasing wave height needs consideration since it is taking place near the tendon natural frequency.

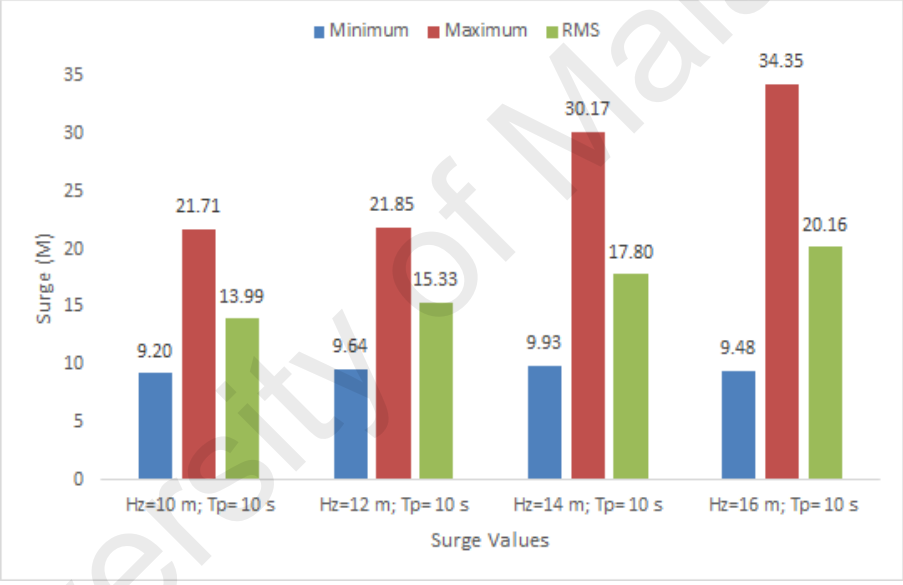

Figure 4.92: Surge statistical values for constant wave period with varying wave height

4.9.2 Heave response

The maximum heave amplitude was not affected by the increasing wave height but the minimum and RMS heave responses changed as the magnitude of wave height changes. As the wave height increased, the minimum heave response also increased in the negative direction. For 20%, 40% and 60% increase in wave height as shown in Figure 4.93, (10 m - 12 m; 10 m -14 m and 10 m – 16 m), the percentage increase in the negative direction were 4.23%, 130.99% and 225.35% respectively. The RMS was equally affected by the increase

University of Malaya

in wave height and for 20%, 40% and 60% increase in wave height, there was an increase of 15.63%, 68.75% and 121.88% in the RMS heave response. The most notable observation was the alarming increase in minimum heave response. As such, it calls for attention so as to prevent fatigue stresses in the tendon leg system.

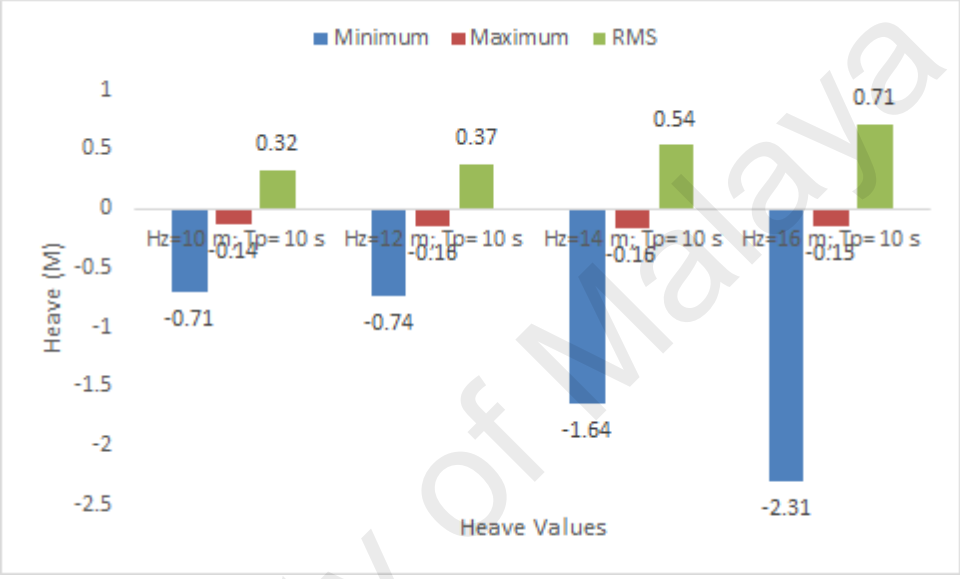

Figure 4.93: Heave statistical values for constant wave period with increasing wave height

4.9.3 Pitch response

Figure 4.94 shows the maximum, minimum and RMS for the coupled TLP pitch responses. The pitch response values are very small for all the increase in wave heights. When the wave height was increased by 20% (10 m – 12 m) the ratio of maximum, minimum and RMS pitch responses were 1:0.70; 1:1.17; 1:0.75. Also, with a further increase of 40% (10 m -14 m), the ratio of maximum, minimum and RMS pitch responses are 1:3.2; 1:2.5; 1:2.25. By increasing the wave height from 10m – 16m, the ratio of maximum, minimum and RMS pitch responses are (1:5.13; 1:3.3; 1:3.75). Although the RMS remained within the limits, the maximum pitch value needs to be looked into during the analysis.

University of Malaya

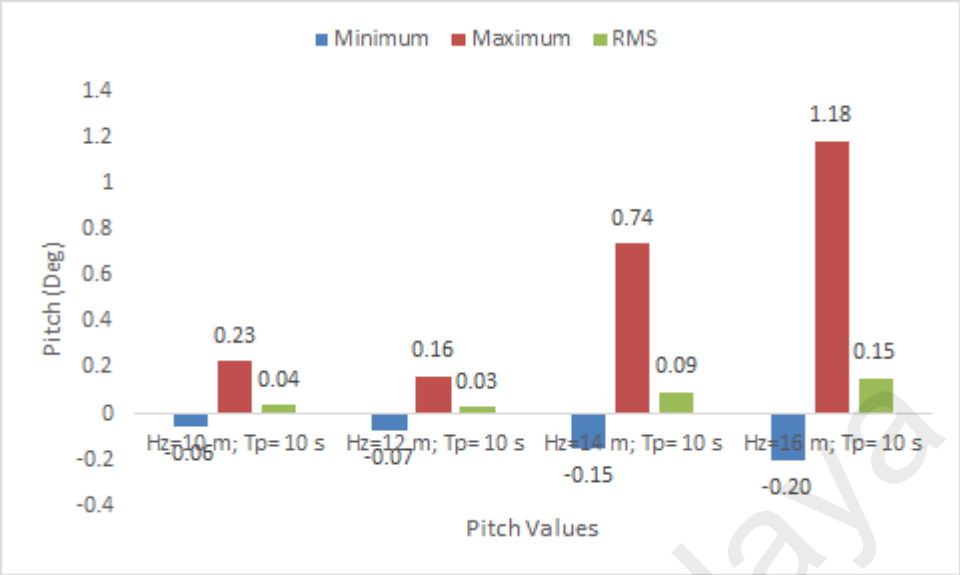

Figure 4.94: Pitch statistical values for constant wave period with increasing wave height

4.9.4 Tendon tension response

The cause of variation of tension in the tendons has been identified earlier to be as a result of large displacement, variable submergence, and pitch and heave motions. For a constant wave period with increasing wave height, there was a decrease in the minimum tension variation, an increase in maximum tension with slight variation in the RMS values. The trend of the variation is shown in Figure 4.95. The maximum and minimum tension values were positive for all increase in wave height.

University of Malaya

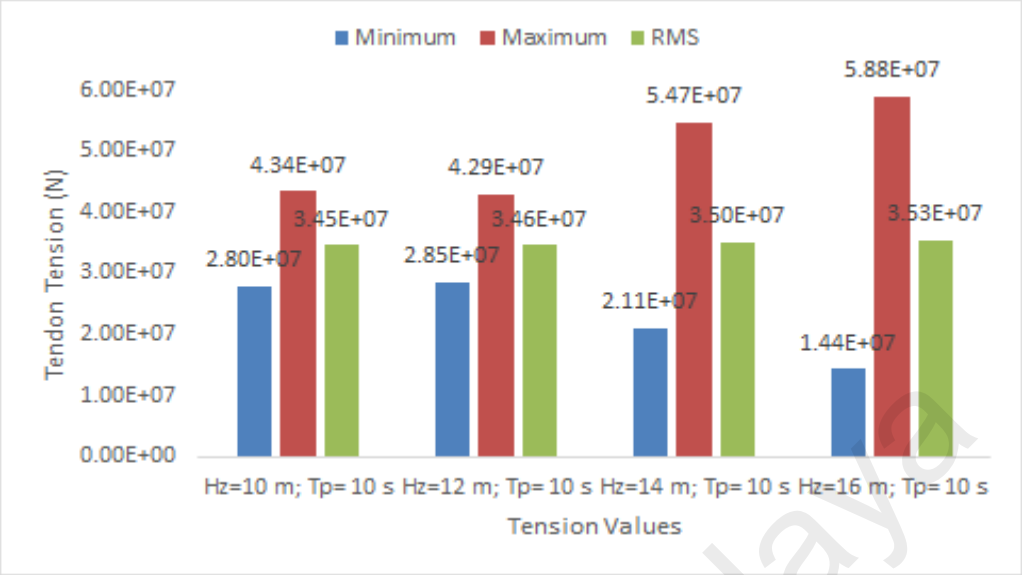

Figure 4.95: Tension statistical values for constant wave period with increasing wave height

University of Malaya

CHAPTER 5: CONCLUSIONS AND RECOMMENDATIONS

5.1 Conclusion

The present research was designed to investigate the dynamic response of tension leg platform and more specifically to examine the significance of coupling tendons with the platform. The platform governing equation of motion was formulated from the theory of structural engineering and idealized as rigid body approach. The tendon effect is considered and modelled as linearized spring stiffness in uncoupled TLP while the standard finite beam element was used to model tendons in the coupled TLP. Fluid-structure interaction is captured by applying linearized wave theory for regular wave, wave spectrum and modified Morison equations for the computation of the hydrodynamic forces on the structure. The time-variant, nonlinear and response-dependent second order equation of motion was solved numerically in time-domain.

Ocean characterization has great influence on the forces and corresponding motion of the TLP. Previous studies have idealized ocean waves as regular, which is not true of an ocean behaviour, while other works focused on unidirectional random wave without considering wave directionality. This work synthesized artificial sea states for regular and irregular sea states, hence, platform motion and tension variations in the tendons differ for regular, unidirectional and directional random wave forces and in different load cases. The other findings confirmed that results of simultaneous occurrence of wave, current and wind forces predicted highest response for an ideal TLP model due to the high velocities of wind and current for the chosen TLP and selected sea state. In addition, the effect of different sea state parameters, consequences of removal of one tendon from the group of tendon leg, and

University of Malaya

parametric study of different wave heights and wave periods on the TLP response are investigated.

The first objective of this research was to develop and solve platform equation of motion. This goal was achieved in Chapter Three for both coupled and uncoupled TLP models and the developed programs are included in Appendices A and B. These programs were used to achieve the second and third objectives which were to investigate the response of uncoupled and coupled TLP under the action of regular, unidirectional and directional random waves, current and wind forces. Further to this, the fourth objective on the significance of tendon dynamics was studied in Chapter Four by including tendon mass in the equation of motion, and applying hydrodynamic and damping forces on the tendons. The outcome of the dynamic analysis of TLP in different load cases of regular and irregular waves, current and wind forces was then analysed and interpreted in terms of their magnitude, frequency of vibration and statistical measures to fulfill the fifth objective.

The following inferences were drawn from the analysis carried out for ISSC TLP in GOM field. The motion response of the TLP was deduced to be a direct function of ocean wave characterization, therefore, directional random wave was recommended for ocean wave characterization. In addition, time histories, power spectral densities and statistical forms give useful insights into platform behaviour and frequency of vibration. The vibration of the platform predominantly occurred at the wave forcing frequency in regular wave simulation while platform oscillation occurred at surge natural frequency in random wave simulation, and is completely absent in regular sea wave representation. There is presence of other cluster of peaks around wave forcing frequency. This evidence suggests that random wave simulation represents an ideal ocean characterization and realistic TLP behaviours.

University of Malaya

The action of current drag force and low-frequency wind forces caused a steady offset and increased dynamic behaviour in all degrees of freedom. This behaviour suggests that ocean current, and mean and fluctuating wind forces should be included during the global motion analysis. The maximum and minimum tension values along the tendon length differed for different load combinations and these are reported for design of tendon leg system. The statistical motion responses and variations in tendon tension in different load cases are essential for decision making. Preferably, root mean square motion values are recommended for the purpose of TLP design since the probability of occurrence of RMS values proved that 99.7 percentage of their values lie around the mean value. The presence of prominent peaks in pitch and tendon tension PSD confirmed nonlinearities due to geometric nonlinearity, variable submergence and variable tendon tension. This fact established the need for stochastic dynamic analysis of the TLP against linear static analysis.

Lack of wave directionality in unidirectional random wave simulation led to higher motion and tendon forces response compared to directional wave simulation. Also, the difference between the maximum and minimum tension magnitude in directional seas was drastically reduced when compared to unidirectional random seas. This will prove economical during the design of strength requirement for tendons compared to regular and unidirectional sea modelling. Time histories of platform motion was governed by a combination of surge natural frequency of the platform as well as wave forcing frequency. As current and wind forces act with random wave, their effect was massive on the platform motion whereas variations in tendon forces due to these forces are not as large as motion responses.

The coupled TLP with tendon dynamics gave a true picture of platform response as compared to an uncoupled TLP. The analysis of the TLP as an uncoupled and coupled

University of Malaya

models has extended our understanding and confirmed the existing knowledge that surge motion response was fairly predicted by the two models but heave, pitch motions and variations in tendon tension differ significantly, hence the coupled model is recommended for analysis purpose. There was an unequal tension distribution in the platform tendons which could be due to result of unequal set-down, however, maximum tension variation in the linear spring models were higher and the minimum tension variation was lower compared to the beam elements with tendon dynamics and three out of four tendon legs were in compression. The overall effect of an increase in wave periods at constant wave height increased the surge, heave and pitch motion responses moderately. The increase in wave height at a constant wave period increased the surge, heave and pitch amplitudes but the accompanying increase in hydrodynamic damping force also damped the supposed escalating surge response.

To conclude, numerical programs for TLP models were formulated for uncoupled and coupled TLP models using theory of structural engineering and in an unconventional approach. With this, a single mathematical equation of motion for the solution of a fully-coupled TLP and tendons model that is time and cost effective, with potential to be fully developed into a standard software was developed and used to investigate nonlinear response of TLP to the stochastic wave and wind fields

5.2 Recommendation

The stochastic response of the tension leg platform was carried out numerically. The results are recommendable for preliminary decision making during TLP design. Due to the constraints of lack of laboratory facility, the following points would be recommended for future work:

University of Malaya

(1) Experimental analysis of the TLP should be carried in the standard laboratory with realistic scale models.

(2) The effects of potential theory for the simulation of low, high and wave frequency forces over the Morison equation should be established.

(3) The effects of vortex induced vibration on the tendons and risers and the corresponding influence on the platform should be analysed.

(4) The effects of inclusion of riser along with tendons and platform should also be carried out.

(5) The behaviour of the TLP in deep and ultra-deeper waters should also be accounted for.

(6) The stability and reliability analysis of platform and tendons for the purpose of fatigue analysis also need consideration.

(7) The numerical model formulated in FORTRAN should be expanded to include tendon dynamics and second order wave forces.

(8) The response of the TLP using different wave and wind spectra together with simulation of data local to the site of the study is recommended.

This research has modelled and solved a single mathematical equation of motion for a fully-coupled TLP platform and tendons model in Abaqus/Aqua software. With this, separate equations of motions for the platform model and the tendon leg system were avoided as it is a norm in some of the existing hydrodynamic software for offshore structures based on decoupled analysis such as AQWA, HOBEM, NBODY and NEPTUNE among others. Again, set of mathematical equations for an uncoupled TLP model was formulated in FORTRAN programming language from the existing literatures.

University of Malaya

Another contribution of this work is that Abaqus finite element tool that was not originally designed for the solution of offshore platforms was adapted for the platform model discretization. This was integrated with Abaqus/Aqua module for the application of hydrodynamic and aerodynamic loadings on the platform. The result of this approach is that offshore problem with high-level complexities is solved using knowledge of Civil Engineering.

By this research and with the validation that has been carried out, knowledge dissemination is enhanced and is made available to any researcher that want to go into analysis of offshore platform since the specialized software are expensive and require extensive time to comprehend. The numerical models have several practical applications such as assessment of different load cases for decision making. Various forms of environmental forces that the model was equipped with are regular wave, unidirectional and directional random waves, current and wind forces.

The analysis of the TLP as uncoupled and coupled model has extended our understanding to know that surge motion response can be taken to be fairly predicted by the two models but heave, pitch motions and variations in tendon tension differ significantly, hence coupled model is recommended. The findings from the ocean characterization suggest that ocean idealization influence forces and corresponding motions of the platform, however directional random wave idealization is recommended for a realistic sea. Taken together, TLP response in the combined action of wave, current and wind forces produce the largest response and simulating the model for all these loadings are recommended. Finally, the numerical models have proved to be valuable as a research tool and have potential to be developed as full-fledged software.

University of Malaya

REFERENCES

Abaqus, C. (2011). *Abaqus analysis user's manual* Velizy-Villacoublay, France: Dassault Systemes.

Abou-Rayan, A., Seleemah, A., & El-Gamal, A. R. (2012). Response of square tension leg platforms to hydrodynamic forces. *Ocean Systems Engineering, 2*(2), 115-135.

Abou-rayan, A. M., & Hussein, O. S. (2014). Dynamic Reponses of Square TLP's to Random Wave Forces. *International Journal of Civil Engineering, 3*(2), 103 -110.

Adamiec-Wojcik, I., Brzozowska, L., & Drag, L. (2015). An analysis of dynamics of risers during vessel motion by means of the rigid finite element method. *Ocean Engineering, 106*, 102-114. doi:10.1016/j.oceaneng.2015.06.053

Adrezin, R., Bar-Avi, P., & Benaroya, H. (1996). Dynamic Response of Compliant Offshore Structures- Review. *Journal of Aerospace Engineering, 9*.

Adrezin, R., & Benaroya, H. (1999a). Non-linear stochastic dynamics of tension leg platforms. *Journal of Sound and Vibration, 220*(1), 27-65. doi: 10.1006/jsvi.1998.1915

Adrezin, R., & Benaroya, H. (1999b). Response of a tension leg platform to stochastic wave forces. *Probabilistic Engineering Mechanics, 14*(1-2), 3-17. doi: 10.1016/S0266-8920(98)00012-5

Aguiar, L. L., Almeida, C. A., & Paulino, G. H. (2014). A three-dimensional multilayered pipe beam element: Nonlinear analysis. *Computers & Structures, 138*, 142-161. doi:10.1016/j.compstruc.2013.09.005

Ahmad, S. (1996). Stochastic TLP response under long crested random sea. *Computers & Structures, 61*(6), 975-993. doi:10.1016/0045-7949(96)00188-5

Ahmad, S., Islam, N., & Ali, A. (1997). Wind-induced response of a tension leg platform. *Journal of Wind Engineering and Industrial Aerodynamics, 72*(1-3), 225-240. doi:10.1016/S0167-6105(97)00238-9

Amanullah, M., Siddiqui, N. A., Umar, A., & Abbas, H. (2002). Fatigue reliability analysis of welded joints of a TLP tether system. *Steel & Composite Structures, 2*(5), 331-354.

University of Malaya

American Petroleum Institute. (1996). Recommended practice for design analysis of station-keeping systems for floating structure. *API-RP2SK*. Washington DC: American Petroleum Institute.

American Petroleum Institute. (2001). Recommended Practice for Planning, Designing, and Constructing Floating Production Systems *API Recommended Practice 2FPS*: API Publishing Services, 1220 L Street, N.W., Washington, D.C, 20005.

Ardakani, H. A., & Ketabdari, M. J. (2007). Experimental study on the response behaviour of seastar mini tension leg platform against random water waves. *Proceedings of the 26th International Conference on Offshore Mechanics and Arctic Engineering, Vol 1*, 767-776.

Astrup, O., Nestegård, A., Ronæss, M., & Sødahl, N. (2001). *Coupled analysis strategies for deepwater spar platforms.* Paper presented at the The Eleventh International Offshore and Polar Engineering Conference.

Bachynski, E. E., & Moan, T. (2012). Design considerations for tension leg platform wind turbines. *Marine Structures, 29*(1), 89-114. doi:10.1016/j.marstruc.2012.09.001

Bahtui, A., Alfano, G., Bahai, H., & Hosseini-Kordkheili, S. A. (2010). On the multi-scale computation of un-bonded flexible risers. *Engineering Structures, 32*(8), 2287-2299. doi:10.1016/j.engstruct.2010.04.003

Bar-Avi, P. (1999). Nonlinear Dynamic Response of a Tension Leg Platform. *Journal of Offshore Mechanics and Arctic Engineering, 121*(4), 219-226. doi:10.1115/1.2829571

Barranco-Cicilia, F., Lima, E. C. P., & Sagrilo, L. V. S. (2008). Reliability-based design criterion for TLP tendons. *Applied Ocean Research, 30*(1), 54-61. doi:10.1016/j.apor.2008.05.001

Bathe, K.-J. (1982). *Finite Element Procedures in Engineering Analysis*: Prentice-Hall, Inc., Englewood Cliffs, New Jersey 07632.

Benfratello, S., Di Paola, M., & Spanos, P. D. (1998). Stochastic Response of MDOF Wind-Excited Structures by means of Volterra series approach. *Journal of Wind Engineering and Industrial Aerodynamics*, 74—76.

University of Malaya

Bhattacharyya, S. K., Sreekumar, S., & Idichandy, V. G. (2003). Coupled dynamics of SeaStar mini tension leg platform. *Ocean Engineering, 30*(6), 709-737. doi:10.1016/S0029-8018(02)00061-6

Bisht, R. S., & Jain, A. K. (1997). Wind and wave induced behaviour of offshore guyed tower platforms. *Ocean Engineering, 25*(7), 501-519.

Borgman, L. E. (1967). Ocean wave simulation for engineering design *Wave research project*. Corps of Engineers, U.S Army.: Contract DA-49-055-CIV-ENG-64-4 Coastal Engineering research center.

Caire, M., & Schiller, R. (2012). The effect of coupled dynamic analysis of floater motions on the mooring and riser system response of an FPSO. *Marine Systems & Ocean Technology, 7*(2), 95-106.

Chakrabarti, S. (2005). *Handbook of Offshore Engineering* (2005 ed. Vol. 1). Elsevier, The Boulevard, Langford Lane, Kidlington, Oxford OX5 IGB, UK.

Chakrabarti, S. K. (1971). Discussion of Dynamics of Single Point Mooring in Deep Water by John H. Nath and Michael P. Felix. *Journal of the Waterways, Harbors and Coastal Engineering Division, 97*(3), 588-590.

Chakrabarti, S. K. (1987). *Hydrodynamics of offshore structures*: Computational Mechanics.

Chakrabarti, S. K. (2008). Challenges for a Total System Analysis on Deepwater Flaoting Systems. *The Open Mechanics Journal, 2*, 28-46.

Chandak, N. R., & Chandrasekaran, S. (2010). Structural Response of Triangular Tension Leg Platform Using Dynamic Morison Equation. *Iscm Ii and Epmesc Xii, Pts 1 and 2, 1233*, 1483-1488. doi:10.1063/1.3452127

Chandrasekaran, S., Chandak, N. R., & Anupam, G. (2006). Stability analysis of TLP tethers. *Ocean Engineering, 33*(3-4), 471-482. doi:10.1016/j.oceaneng.2005.04.015

Chandrasekaran, S., & Gaurav. (2008). Offshore triangular tension leg platform earthquake motion analysis under distinctly high sea waves. *Ships and Offshore Structures, 3*(3), 173 - 184. doi:10.1080/17445300802051681

University of Malaya

Chandrasekaran, S., & Jain, A. K. (2002a). Dynamic behaviour of square and triangular offshore tension leg platforms under regular wave loads. *Ocean Engineering, 29*(3), 279-313. doi:10.1016/S0029-8018(00)00076-7

Chandrasekaran, S., & Jain, A. K. (2002b). Triangular Configuration Tension Leg Platform behaviour under random sea wave loads. *Ocean Engineering, 29*(15), 1895-1928. doi:10.1016/S0029-8018(01)00111-1

Chandrasekaran, S., Jain, A. K., & Chandak, N. R. (2004). Influence of Hydrodynamic Coefficients in the Response Behavior of Triangular TLPs in Regular Waves. *Ocean Engineering, 31*, 2319–2342.

Chandrasekaran, S., Jain, A. K., & Chandak, N. R. (2006). Seismic analysis of offshore triangular tension leg platforms. *International Journal of Structural Stability and Dynamics, 6*(1), 97-120. doi:10.1142/S0219455406001848

Chandrasekaran, S., Jain, A. K., Gupta, A., & Srivastava, A. (2007). Response behavior of triangular tension leg platforms under impact loading. *Ocean Engineering, 34*, 45-53. doi:10.1016/j.oceaneng.2006.01.002

Chapra, S. C., & Canale, R. P. (2012). *Numerical methods for engineers* (Vol. 2): McGraw-Hill New York.

Chatterjee, P. C., Das, P. K., & Faulkner, D. (1996). A Hydro-structural Analysis Program for TLPs. *Ocean Engineering, 24*(4), 313-334.

Chen, J. M., Kong, X. Y., & Sun, Y. (2013). Hydrodynamic Responses Analysis for Tension Leg Platform. In X. H. Liu, K. F. Zhang, & M. Z. Li (Eds.), *Manufacturing Process and Equipment, Pts 1-4* (Vol. 694-697, pp. 27-30). Stafa-Zurich: Trans Tech Publications Ltd.

Chernetsov, V. A., & Karlinsky, S. L. (2006). Ice-resistant spar-type platform for middle sea depth. *Proceedings of the Sixteenth (2006) International Offshore and Polar Engineering Conference, Vol 1*, 614-619.

Chitrapu, A., & Ertekin, R. (1992). *Effect of nonlinear drag forces on the low-and high-frequency response of floating platforms*. Paper presented at the 11th Intl Conf on Offshore Mechanics & Arctic Engng, Calgary, Canada.

University of Malaya

Chitrapu, A., & Ertekin, R. (1993). *Nonlinear Effects in Floating Platform Response Using Time-Domain Simulation Methods*. Paper presented at the 12th Intl Conf on Offshore Mechanics & Arctic Engng, Glasgow, UK. .

Chitrapu, A. S., & Ertekin, R. C. (1995). Time-Domain Simulation of Large-Amplitude Response of Floating Platforms. *Ocean Engineering, 22*(4), 367-385. doi:10.1016/0029-8018(94)00013-W

Chitrapu, A. S., Ertekin, R. C., & Paulling, J. R. (1993). Viscous drift forces in regular and irregular waves. *Ocean Engineering, 20*(1), 33-55. doi:10.1016/0029-8018(93)90045-J

Clough, R. W., & Penzien, J. (1993). Dynamics of structures. 1993. *Copyright of Applied Mechanics & Materials*.

Correa, F. N., Jacob, B. P., & Mansur, W. J. (2010). Formulation of an efficient hybrid time–frequency domain solution procedure for linear structural dynamic problems. *Computers & Structures, 88*(5), 331-346.

Correa, F. N., Senra, S. F., Jacob, B. P., Masetti, I. Q., & Mourelle, M. M. (2002). *Towards the integration of analysis design of mooring systems risers, Parts I & II: Studies on a Dicas System.* Paper presented at the Proceedings of Offshore Mechanics Arctic Engineering Conference.

D'Souza, R., Aggarwal, R., & Basu, S. (2013). *The Tension Leg Platform-A Retrospective.* Paper presented at the Proceedings of the 18th SNAME Offshore Symposium,"Engineering the Future: The Arctic and Beyond," Houston, Texas.

Dassault, S. (2009). Abaqus Documentation Version 6.9. United States of America: Dassault System, Simulia Corp, Providence, RI, USA.

Dawson, T. H. (1983). *Offshore structural engineering* (illustrated ed.). The University of Michigan: Prentice-Hall.

Demirbilek, Z. (1990). Design Formulas for Offset, Set down and Tether Loads of a Tension Leg Platform (TLP). *Ocean Engineering, 17*(5), 517-523. doi:10.1016/0029-8018(90)90042-5

El-gamal, A. R., Essa, A., & Ismail, A. (2014). Effect of Tethers Tension Force on the Behaviour of Traiangular Tension Leg Platform. *American Journal of Civil Engineering and Architecture, 2*(3), 107 - 114. doi:10.12691/ajcea-2-3-3

University of Malaya

Elshafey, A. A., Haddara, M. R., & Marzouk, H. (2009). Dynamic response of offshore jacket structures under random loads. *Marine Structures, 22*(3), 504-521. doi:http://dx.doi.org/10.1016/j.marstruc.2009.01.001

Gadagi, M. M., & Benaroya, H. (2006). Dynamic response of an axially loaded tendon of a tension leg platform. *Journal of Sound and Vibration, 293*(1-2), 38-58. doi:10.1016/j.jsv.2005.09.027

Gao, Y. W., Li, C., & Cheng, X. (2013). Performance Research on Tension Leg Platform of Floating Offshore Wind turbine. In A. Wang, L. K. Che, R. Dong, & G. Zhao (Eds.), *Applied Energy Technology, Pts 1 and 2* (Vol. 724-725, pp. 645-648). Stafa-Zurich: Trans Tech Publications Ltd.

Garrett, D. L. (2005). Coupled analysis of floating production systems. *Ocean Engineering, 32*, 802 - 816. doi:10.1016/j.oceaneng.2004.10.010

Gie, T. S., & de Boom, W. (1981). *The wave induced motions of a tension leg platform in deep water.* Paper presented at the Offshore Technology Conference.

Giron, A. R. C., Correa, F. N., & Jacob, B. P. (2014). *An Evaluation of the Semi-Coupled Scheme for the Analysis of Floating Production Systems.* Paper presented at the Proceedings of the ASME 2014 33rd International Conference on Ocean, Offshore and Artic Engineering, OMAE2014, San Francisco, California, USA.

Goda, Y. (1970). Numerical experiments on wave statistics with spectral simulation. *Report of the Port and Harbour Research Institute, 9*(3), 3-57.

Guarga, F., Castells, M., Bosch, R., & Casals, P. (2014). Theorical and descriptive analysis of the wave energy in the "Barcelona World Race". *Journal of Maritime Research, 11*(2), 41-51.

Han, S. M., & Benaroya, H. (2002). Comparison of linear and nonlinear responses of a compliant tower to random wave forces. *Chaos, Solitons and Fractals*. doi:14 269-291.S0960-0779 (01) 00232-6

Hogben, N., & Standing, R. (1974). *Wave loads on large bodies.* Paper presented at the Proceedings of the International Symposium on the Dynamics of Marine Vehicles and Structures in Waves.

Horton, E. E., Brewer, J. H., Silcox, W. H., & Hudson, T. A. (1976). *"Means and methods for anchoring an offshore tension leg platform"*. (934,528). US.

University of Malaya

Islam, A., Jameel, M., Jumaat, M. Z., Shirazi, S. M., & Salman, F. A. (2012). Review of offshore energy in Malaysia and floating Spar platform for sustainable exploration. *Renewable & Sustainable Energy Reviews, 16*(8), 6268-6284. doi:10.1016/j.rser.2012.07.012

Islam, A. B. M. S., Jameel, M., Ahmad, S., Jumaat, M. Z., & Kurian, V. J. (2013). Structural Behaviour of Fully Coupled Spar-Mooring System under Extreme Wave Loading. *Journal of Civil Engineering and Management, 19*, S69-S77. doi:10.3846/13923730.2013.801899

Islam, A. B. M. S., Jameel, M., & Jumaat, M. Z. (2012). Oil and Gas Energy Potential at Malaysian Seabed and Spar Platform for Deepwater Installation. *International Journal of Green Energy, 9*(2), 111-120. doi:10.1080/15435075.2011.621493

Islam, A. B. M. S., Soeb, M. R., & Jumaat, M. Z. B. (2016). Floating spar platform as an ultra-deepwater structure in oil and gas exploration. *Ships and Offshore Structures*, 1-14. doi:10.1080/17445302.2015.1112179

Jain, A. K. (1997). Nonlinear coupled response of offshore tension leg platforms to regular wave forces. *Ocean Engineering, 24*(7), 577-592. doi:10.1016/0029-8018(95)00059-3

Jameel, M., Ahmad, S., Islam, A., & Jumaat, M. Z. (2013). Non-linear dynamic analysis of coupled Spar platform. *Journal of Civil Engineering and Management, 19*(4), 476-491. doi:10.3846/13923730.2013.768546

Jameel, M., Ahmad, S., Islam, A., & Jumaat, M. Z. (2014). *Wind Induced Nonlinear Response of Coupled SPAR Platform.* Paper presented at the Proceedings of the ASME 2014 33rd International Conference on Ocean, Offshore and Artic Engineering, OMAE2014, San Francisco, California, USA.

Jameel, M., Oyejobi, D. O., Siddiqui, N. A., & Ramli Sulong, N. H. (2016). Nonlinear dynamic response of tension leg platform under environmental loads. *KSCE Journal of Civil Engineering*, 1-9. doi:10.1007/s12205-016-1240-8

Jayalekshmi, R., Sundaravadivelu, R., & Idichandy, V. G. (2009). Hull-tether-riser dynamics of deep water tension leg platforms. *Fluid Structure Interaction V, 105*, 215-223. doi:10.2495/Fsi090201

Jayalekshmi, R., Sundaravadivelu, R., & Idichandy, V. G. (2010). Dynamic Analysis of Deep Water Tension Leg Platforms Under Random Waves. *Journal of Offshore*

University of Malaya

Mechanics and Arctic Engineering-Transactions of the Asme, 132(4), 4. doi:10.1115/1.4001432

Jefferys, E. R., & Patel, M. H. (1982). Dynamic Analysis Models of Tension Leg Platforms. *Journal of Energy Resources Technology, 104*(3), 217-223. doi:10.1115/1.3230406

Jensen, J. J., & Capul, J. (2006). Extreme response predictions for jack-up units in second order stochastic waves by FORM. *Probabilistic Engineering Mechanics, 21*(4), 330-337.

Jia, J. (2008). An efficient nonlinear dynamic approach for calculating wave induced fatigue damage of offshore structures and its industrial applications for lifetime extension. *Applied Ocean Research, 30*(3), 189-198.

Joseph, A., Mangal, L., & George, P. S. (2009). Coupled Dynamic Response of a Three-Column Mini TLP. *Journal of Naval Architecture and Marine Engineering, 6*, 52 - 61. doi:10.3329/jname.v6i2.2789

Kang, W.-H., Zhang, C., & Yu, J.-X. (2016). Stochastic extreme motion analysis of jack-up responses during wet towing. *Ocean Engineering, 111*, 56-66.

Kappos, A. J. (2002). *Dynamic Loading and Design of Structures*. London: Spons Press.

Kareem, A., & Li, Y. S. (1993). Wind-Excited Surge Response of Tension-Leg Platform - Frequency-Domain Approach. *Journal of Engineering Mechanics-Asce, 119*(1), 161-183. doi:10.1061/(Asce)0733-9399(1993)119:1(161)

Karlinsky, S. L., & Kuteynikov, M. A. (2008). *Damage Stability of Tension Leg Platform in Ice Environment.* Paper presented at the 8th International Conference on the stability of ships and Ocean Vehicles. Escuela Tecnica Superior de Ingenieros Navales.

Khan, R. A., Siddiqui, N. A., Naqvi, S. Q. A., & Ahmad, S. (2006). Reliability analysis of TLP tethers under impulsive loading. *Reliability Engineering & System Safety, 91*(1), 73-83. doi:10.1016/j.ress.2004.11.010

Kim, C. H., Lee, C. H., & Goo, J. S. (2007). A dynamic response analysis of tension leg platforms including hydrodynamic interaction in regular waves. *Ocean Engineering, 34*(11-12), 1680-1689. doi:10.1016/j.oceaneng.2006.10.011

University of Malaya

Kurian, V. J., Gasim, M. A., Narayanan, S. P., & Kalaikumar, V. (2008). *Parametric studies subjected to random waves.* Paper presented at the ICCBT 2008, Kuala Lumpur, Malaysia.

Le, C. H., Ding, H. Y., & Zhang, P. Y. (2014). Dynamic response analysis of a floating mooring system. *Journal of Ocean University of China, 13*(3), 381-389. doi:10.1007/s11802-014-2023-9

Lee, H. H., & Wang, P. W. (2000). Analytical solution on the surge motion of tension-leg twin platform structural systems. *Ocean Engineering, 27*(4), 393-415.

Lei, S., Zhang, W. S., Lin, J. H., Yue, Q. J., Kennedy, D., & Williams, F. W. (2014). Frequency domain response of a parametrically excited riser under random wave forces. *Journal of Sound and Vibration, 333*(2), 485-498. doi:10.1016/j.jsv.2013.09.025

Li, Y. S., & Kareem, A. (1990). Stochastic Response of Tension Leg Platforms to Wind and Wave Fields. *Journal of Wind Engineering and Industrial Aerodynamics, 36*(1-3), 915-926.

Liu, W. M. (2014). Research on Time-domain Dynamic Response of Tension Leg Platform in Regular Wave. *Applied Mechanics, Materials and Manufacturing Iv, 670-671*, 801-804. doi:10.4028/www.scientific.net/AMM.670-671.801

Low, Y. M. (2009). Frequency domain analysis of a tension leg platform with statistical linearization of the tendon restoring forces. *Marine Structures, 22*(3), 480-503. doi:10.1016/j.marstruc.2009.01.002

Low, Y. M., & Langley, R. S. (2006). Time and frequency domain coupled analysis of deepwater floating production systems. *Applied Ocean Research, 28*(6), 371-385. doi:10.1016/j.apor.2007.05.002

Lyons, G. J., & Patel, M. H. (1984). Comparisons of Theory With Model Test Data for Tensioned Buoyant Platforms. *Journal of Energy Resources Technology, 106*(4), 426-436. doi:10.1115/1.3231102

Mao, D., Zhong, C., Zhang, L., & Chu, G. (2015). Dynamic response of offshore jacket platform including foundation degradation under cyclic loadings. *Ocean Engineering, 100*, 35-45.

University of Malaya

Masciola, M., & Nahon, M. (2008). Modeling and Simulation of a Tension Leg Platform. *Proceedings of the Eighteenth (2008) International Offshore and Polar Engineering Conference, Vol 1*, 84-91.

Masciola, M., Nahon, M., & Driscoll, F. (2013). Preliminary Assessment of the Importance of Platform-Tendon Coupling in a Tension Leg Platform. *Journal of Offshore Mechanics and Arctic Engineering-Transactions of the Asme, 135*(3), 11. doi:10.1115/1.4023795

Mekha, B. B., Johson, C. P., & Roesset, J. M. (1996). Implications of Tendon Modeling on Nonlinear Response of TLP. *Journal of Structural Engineering, 122*, 142 - 149.

Mohd Zaki, N. I., Abu Hussain, M. K., & Najafian, G. (2014). Extreme structural response values from various methods of simulating wave kinematics. *Ships and Offshore Structures*. doi:10.1080/17445302.2014.987947

Morgan, J. R. (1983). *Dynamic analysis of tension-leg platforms*: ; Texas A and M Universty College Station, Texas.

Muhittin, S., & Oguz, Y. (2003). Hydrodynamic Design of a TLP type Offloading Platform. *Ocean Engineering, 30*, 1269–1282.

Naess, A., Gaidai, O., & Teigen, P. S. (2007). Extreme response prediction for nonlinear floating offshore structures by Monte Carlo simulation. *Applied Ocean Research, 29*(4), 221-230. doi:10.1016/j.apor.2007.12.001

Nallayarasu, S. (2008). *Offshore Structures (Analysis and Design)*. Department of Ocean Engineering, Indian Institute of Technology Madras, Chennais-600036. Indian.

Natvig, B. J., & Johnsen, O. (2000). *Coupled dynamics of tether and platform for a North Sea wellhead TLP.* Paper presented at the International Society of Offshore and Polar Engineers Conf (ISOPE 2000), .

Ng, C. Y., Kurian, V. J., & Liew, M. S. (2014). Dynamic responses of classic spar platform: Short crested waves vs long crested waves. *Applied Mechanics and Materials, 567*, 235-240. doi:10.4028/www.scientific.net/AMM.567.235

Nwogu, O., & Irani, M. (1990). *Numerical prediction of higher order wave induced loads on tethered platforms.* Paper presented at the The First ISOPE European Offshore Mechanics Symposium.

University of Malaya

Offshore Magazine. (2010). 2010 Worldwide Survey of TLPs, TLWPs. *Lindsey Wilhot and Chad Supan of Mustang Engineering*.

Ormberg, H., Baarholm, R., & Stansberg, C. T. (2003). *Time-domain coupled analysis of deepwater TLP, and verification against model tests.* Paper presented at the The Thirteenth International Offshore and Polar Engineering Conference.

Ormberg, H., & Larsen, K. (1998). Coupled analysis of floater motion and mooring dynamics for a turret-moored ship. *Applied Ocean Research, 20*(1), 55-67.

Paulling, J., & Webster, W. C. (1986). *A consistent, large-amplitude analysis of the coupled response of a TLP and tendon system*. Paper presented at the Proceedings of the Fifth International Symposium on Offshore Mechanics and Arctic Engineering, Tokyo.

Refat, H. M., & El-gamal, A. R. (2014). Influence of the Density of Water on the Dynamic Behaviour of Square Tension Lag Platform. *American Journal of Civil Engineering and Architecture, 2*(4), 122 - 129. doi:10.12691/ajcea-2-4-1

Rijken, O., & Leverette, S. (2007). Tension Leg Platform response to earthquake in Gulf of Mexico. *Proceedings of the Seventeenth (2007) International Offshore and Polar Engineering Conference, Vol 1- 4, Proceedings*, 190-193.

Rudman, M., & Cleary, P. W. (2013). Rogue wave impact on a tension leg platform: The effect of wave incidence angle and mooring line tension. *Ocean Engineering, 61*, 123-138. doi:10.1016/j.oceaneng.2013.01.006

Salpukas, A. (1994). Oil companies drawn to the deep. *The New York Times December, 7*, D1.

Sannasiraj, S., Sundar, V., & Sundaravadivelu, R. (1995). The hydrodynamic behaviour of long floating structures in directional seas. *Applied Ocean Research, 17*(4), 233-243.

Sen, D. (2002). *Time-domain simulation of large structures in nonlinear waves.* Paper presented at the Proceedings of 21st International Conference on Offshore Mechanics Arctic Engineering, OMAE 2002-28033, Oslo, Norway.

Senjanovic, I., Tomic, M., & Hadzic, N. (2013). Formulation of consistent nonlinear restoring stiffness for dynamic analysis of tension leg platform and its influence on response. *Marine Structures, 30*, 1-32. doi:10.1016/j.marstruc.2012.10.007

University of Malaya

Senjanovic, I., Tomic, M., & Rudan, S. (2013). Investigation of nonlinear restoring stiffness in dynamic analysis of tension leg platforms. *Engineering Structures, 56*, 117-125. doi:10.1016/j.engstruct.2013.04.020

Shehata, E., & Raheem, A. (2013). Nonlinear response of fixed jacket offshore platforn under structural and wave loads. *Coupled Systems Mechanics, 2*(1), 111 -126.

Siddiqui, N., & Ahmad, S. (2001). Fatigue and fracture reliability of TLP tethers under random loading. *Marine Structures, 14*(3), 331-352.

Siddiqui, N. A., & Ahmad, S. (2003). Dynamic behaviour of tension leg platform under impulsive loading. *Defence Science Journal, 53*(2), 205-210.

Simiu, E., & Leigh, S. D. (1984). Turbulent Wind and Tension Leg Platform Surge. *Journal of Structural Engineering-Asce, 110*(4), 785-802.

Spanos, P. D., & Agarwal, V. K. (1984). Response of a Simple Tension Leg Platform Model to Wave-Forces Calculated at Displaced Position. *Journal of Energy Resources Technology-Transactions of the Asme, 106*(4), 437-443.

Tabeshpour, M. R., Golafshani, A. A., & Seif, M. S. (2006). Second-order perturbation added mass fluctuation on vertical vibration of tension leg platforms. *Marine Structures, 19*(4), 271-283. doi:http://dx.doi.org/10.1016/j.marstruc.2007.02.001

Tabeshpour, M. R., & Shoghi, R. (2014). Nonlinear dynamic analysis of TLP surge motion using homotopy perturbation method. *Ships and Offshore Structures, 9*(6), 569-577. doi:10.1080/17445302.2014.912045

Taylor, R. E., & Jefferys, E. R. (1986). Variability of Hydrodynamic Load Predictions for a Tension Leg Platform. *Ocean Engineering, 13*(5), 449-490.

Veritas, B. (2012). Rules for the classification of tension leg platform (TLP). In V. Bureau (Ed.).

Veritas, D. N. (2007). *Environmental conditions and environmental loads*. Retrieved from Veritas-veien 1, NO -1322 Hovik, Norway:

Veritas, D. N. (2008). Structural Design of TLPS (LRFD METHOD). Veritasveien 1, NO-1322 Hovik, Norway.

University of Malaya

Vickery, P. J. (1995). Wind-Induced Response of Tension Leg Platform - Theory and Experiment. *Journal of Structural Engineering-Asce, 121*(4), 651-663. doi:10.1061/(Asce)0733-9445(1995)121:4(651)

Vlahos, G., Cassidy, M. J., & Martin, C. M. (2008). Experimental investigation of the system behaviour of a model three-legged jack-up on clay. *Applied Ocean Research, 30*(4), 323-337.

Wheeler, J. (1969). *Methods for calculating forces produced by irregular waves.* Paper presented at the Offshore Technology Conference.

Wilson, J. F. (2003). *Dynamics of Offshore Structures*. New Jersey: John Wiley & Sons, Inc.

Yang, M., Teng, B., Ning, D., & Shi, Z. (2012). Coupled dynamic analysis for wave interaction with a truss spar and its mooring line/riser system in time domain. *Ocean Engineering, 39*, 72-87. doi:10.1016/j.oceaneng.2011.11.002

Yang, M. D., Teng, B., Xiao, L. F., Ning, D. Z., Shi, Z. M., & Qu, Y. (2014). Full time-domain nonlinear coupled dynamic analysis of a truss spar and its mooring/riser system in irregular wave. *Science China-Physics Mechanics & Astronomy, 57*(1), 152-165. doi:10.1007/s11433-013-5273-4

Yilmaz, O., & Incecik, A. (1996a). Hydrodynamic design of moored floating platforms. *Marine Structures, 9*(5), 545-575.

Yilmaz, O., & Incecik, A. (1996b). Hydrodynamic Design of Moored Floating Platforms. *Marine Structures, 9*, 545 – 575. doi:0951-8339 (95) 00011-9

Yongjun, J., Jiemin, Z., & Qingyong, Z. (2008). Short crested wave-current forces around a large verical circular cylinder. *European Journal of Mechanics B/Fluids, 27*, 346 - 360. doi:10.1016/j.euromechflu.2007.08.001

Yoshida, K., Ozaki, M., & Oka, N. (1984). Structural Response Analysis of Tension Leg Platforms. *Journal of Energy Resources Technology, 106*(1), 10-17. doi:10.1115/1.3231005

Zaheer, M. M., & Islam, N. (2012). Stochastic response of a double hinged articulated leg platform under wind and waves. *Journal of Wind Engineering and Industrial Aerodynamics, 111*, 53-60. doi:10.1016/j.jweia.2012.08.005

University of Malaya

Zeng, X. H., Liu, J. Y., Liu, Y., & Wu, Y. X. (2007). Parametric studies of tension leg platform with large amplitude motions. *Proceedings of the Seventeenth (2007) International Offshore and Polar Engineering Conference, Vol 1- 4, Proceedings*, 202-209.

Zeng, X. H., Shen, X. P., & Wu, Y. X. (2007). Governing equations and numerical solutions of tension leg platform with finite amplitude motion. *Applied Mathematics and Mechanics-English Edition, 28*(1), 37-49. doi:10.1007/s10483-007-0105-1

Zou, J. (2003). *TLP Hull/ Tendon/Riser Coupled Dynamic Analysis in Deepwater.* Paper presented at the Proceedings of the Thirteeth (2003) International Offshore and Polar Engineering Conference, Honolulu, Hawaii, USA.

University of Malaya

LIST OF PUBLICATIONS AND PAPERS PRESENTED

1) M. Jameel, D.O. Oyejobi, N.A. Siddiqui & N.H Ramli Sulong (2016) Nonlinear Dynamic Response of Tension Leg Platform under Environmental Loads, KSCE Journal of Civil Engineering, doi 10.1007/s12205-016-1240-8, pISSN 1226-7988, eISSN 1976-3808
2) D.O. Oyejobi, M. Jameel, & N.H Ramli Sulong (2016) Nonlinear Response of Tension Leg Platform to Wave, Current and Wind Forces, International Journal of Civil Engineering, (IJCE), doi: 10.1007/s40999-016-0030-5
3) D.O. Oyejobi, M. Jameel, & N.H Ramli Sulong (2016) Stochastic response of intact and a removed tendon tension leg platform to random wave and current forces, The Arabian Journal of Science and Engineering, (AJSE), DOI: 10.1007/s13369-016-2282-4.
4) D.O. Oyejobi, M. Jameel, & N.H Ramli Sulong (2016) Dynamic behaviour of tension leg platform in short-crested directional seas, ICCOEE2016, International Conference on Civil, Offshore & Environmental Engineering, 15 – 17 August, Kuala Lumpur, Malaysia.

University of Malaya